



UNIVERSITÀ DEGLI STUDI DI MILANO

DIPARTIMENTO DI
SCIENZE FARMACEUTICHE

Ph.D in PHARMACEUTICAL SCIENCES

XXXI cycle

**Design and synthesis of novel molecular probes
targeting the alpha7 nicotinic acetylcholine
receptors: insight into the mechanisms of activation
and related therapeutic implications**

Dr. Maria Chiara Pismataro - R11241

Supervisor: Prof. Clelia DALLANOCE

Coordinator of the PhD course: Prof. Giancarlo ALDINI

ACADEMIC YEAR 2017/2018

Table of contents

CHAPTER I - Introduction.....	1
1.1 The nicotinic acetylcholine receptors	1
1.2 The $\alpha 7$ nAChR subtype.....	4
1.2.1 Localization and physiopatological roles.....	4
1.2.2 Structural features of $\alpha 7$ nAChR orthosteric binding site	5
1.2.3 Kinetic features and different conformations of $\alpha 7$ nAChR.....	7
1.2.4 Metabotropic-like activity of $\alpha 7$ nAChR	12
1.2.5 The colinergic anti-inflammatory pathway	15
1.3 Silent Agonism	17
1.3.1 The silent agonist NS6740	21
1.3.1.1 Electrophysiological profile of NS6740	21
1.3.1.2 Anti-inflammatory profile of NS6740	22
1.3.2 The silent pharmacophore model.....	27
1.3.3 The silent agonist KC-1	28
CHAPTER II - Aim of the thesis	31
2.1 SAR study on NS6740	33
2.1.1 Fragmentation of NS6740 molecular skeleton.....	34
2.1.2 Design and synthesis of novel NS6740 analogs	35
2.2 SAR study on KC-1	38
CHAPTER III - Chemistry.....	43
3.1 Synthetic approaches to NS6740 -related derivatives	43
3.1.1 Synthesis of 1,4-diazabicyclo[3.2.2]nonane dihydrochloride (16) and 1,3-diazabicyclo[3.2.2]nonane dihydrochloride (44)	43
3.1.2 Synthesis of (S,S) and (R,R)-2-benzyl-2,5-diazabicyclo[2.2.1]heptane (49 and 57)	44
3.1.3 Synthesis of aromatic acyl chlorides 97-110	46
3.1.4 Synthesis of NS6740 fragments 11-15	48
3.1.5 Synthesis of NS6740 and related derivatives 17-20	49
3.1.6 Reduction of the carbonyl group of NS6740	50
3.1.7 Synthesis of differently substituted NS6740 derivatives 22-33	51

3.2	Synthetic approaches to the KC-1 -related analogs	52
3.2.1	Synthesis of KC-1 derivatives 34-37	52
3.2.2	Synthesis of KC-1 derivatives 38-40	54
CHAPTER IV - Electrophysiological investigations		57
4.1	General pharmacological considerations	57
4.1.1	Pharmacological protocols for NS6740 and related derivatives	57
4.1.2	Pharmacological protocols for KC-1 -related derivatives	59
4.2	Electrophysiological profile of NS6740	60
4.3	Electrophysiological evaluation of NS6740 fragments 11-16	62
4.4	Electrophysiological evaluation of NS6740 derivatives 17-33	65
4.4.1	Basic nucleus modifications.....	65
4.4.2	Removal of hydrogen-bond acceptor group	68
4.4.3	Substitution of the <i>meta</i> -trifluoromethyl group.....	70
4.4.4	Introduction of different aromatic portions	74
4.5	Additional electrophysiological evaluation of 12 , 22-24 , 27 and 32 at different concentrations (1, 3, 30 μ M)	77
4.6	Recovery study for NS6740 and compound 27	88
4.7	Concentration-response curves for strong partial agonist 13 and 17	89
4.8	Electrophysiological investigation of NS6740 derivatives on the nicotinic heteromeric receptors $\alpha 4\beta 2$ and $\alpha 3\beta 4$	91
4.9	Electrophysiological evaluation for KC-1 derivatives	94
4.10	Electrophysiological investigation for KC-1 derivatives on the nicotinic heteromeric receptor $\alpha 4\beta 2$	97

CHAPTER V - <i>In silico</i> studies.....	101
5.1	Generale docking protocol101
5.2	Docking investigation of NS6740 and its derivatives103
5.2.1	Docking of NS6740, 12, 22-24, 27 and 32103
5.2.2	Docking of compound 28.....108
5.2.3	Docking of compound 33.....112
5.2.4	hc7S36V and hc7S36A116
5.3	Docking investigation of KC-1123
CHAPTER VI - Conclusions	126
6.1	Investigation of $\alpha 7$ nAChR silent activation.....126
6.1.1	NS6740-related analogs.....126
6.1.2	KC-1-related analogs129
CHAPTER VII - Experimental Section	131
7.1	CHEMISTRY131
7.1.1	Materials and methods.....131
7.1.2	Synthesis of NS6740 derivatives.....132
7.1.2.1	Synthesis of 1,4- and 1,3-diazabicycli[3.2.2]nonane dihydrochloride 15 and 43132
7.1.2.2	Synthesis of (1S,4S)-2-benzyl-2,5-diazabicyclo[2.2.1]heptane and (1R,4R)-2-benzyl-2,5-diazabicyclo[2.2.1]heptane135
7.1.2.3	Synthesis of differently substituted acyl chlorides 97-110146
7.1.2.3.1	General procedure for the preparation of compounds 71-82 of Suzuki-Miyaura reaction between methyl 5-bromofuran-2-carboxylate and the appropriate boronic acid146
7.1.2.3.2	General procedure for the hydrolysis of methyl ester intermediates 71-83153
7.1.2.3.3	General procedure for the chlorination of carboxylic acid intermediates 84-96 and commercially available 5-(3-nitrophenyl)furan-2-carboxylic acid.....160
7.1.2.4	Synthesis of NS6740 fragments 11-15.....168

7.1.2.4.1	General procedure for the acylation reaction between 1,4-diazabicyclo[3.2.2]nonane dihydrochloride (16) and the appropriate acyl chloride	168
7.1.2.5	Synthesis of NS6740 positively charged derivatives.....	172
7.1.2.5.1	General procedure for the synthesis of intermediates 111 and 112	175
7.1.2.5.2	General procedure for the synthesis of compounds 19 and 20	176
7.1.2.6	Synthesis of compound 21	179
7.1.2.7	Synthesis of NS6740 derivatives 22-33	180
7.1.3	Synthesis of KC-1 derivatives.....	191
7.1.3.1	Synthesis of the positively charged KC-1 derivatives 34-37	191
7.1.3.2	Synthesis of the meta-CF ₃ phenyl substituted KC-1 derivative 39	198
7.1.3.3	Synthesis of KC-1 derivatives 38 and 40	201
7.1.3.3.1	General procedure for the preparation of the intermediates 118 and 119 Suzuki-Miyaura reaction between 2-bromofuran and differently substituted phenyl boronic acids	201
7.2	Electrophysiological studies.....	208
7.2.1	Material and methods	208
7.3	<i>In silico</i> studies.....	210
7.3.1	Materials and methods.....	210
Abbreviations		212
References.....		215

CHAPTER I

Introduction

The cholinergic system is one of the most important nervous pathways. The neurotransmitter acetylcholine (ACh) is produced, stored and released by cholinergic neurons. [1] ACh plays its crucial role in the central nervous system (CNS) and peripheral nervous system (PNS) *via* muscarinic and nicotinic receptors. These two families of cholinergic receptors are modulated by muscarine and nicotine, respectively, [2] and the two alkaloids represent the key ligands which allowed the first historical sub-classification of ACh-mediated responses. [3]

1.1 The nicotinic acetylcholine receptors

Nicotinic Acetylcholine Receptors (nAChR) belong to the super family of Ligand Gated Ion Channel (LGIC), and specifically the Cys-loop receptor family, where also gamma aminobutyric acid receptor A (GABA_AR), glycine-receptor (GlyR) and serotonin 5HT₃ receptor are found. Among the conserved structural features shown by the members of this family, the most relevant is represented by a disulfide bridge between two cysteine residues, located in the extracellular portions, which are separated by fifteen amino acids. [3] [4] [5]

nAChRs display a pentameric architecture (**Figure 1**) incorporating different α and non- α subunits; α subunits (α 1- α 10) are characterized by the disulfide bridge, while the non- α types are represented by β 1- β 4, γ , δ , and ϵ subunits.

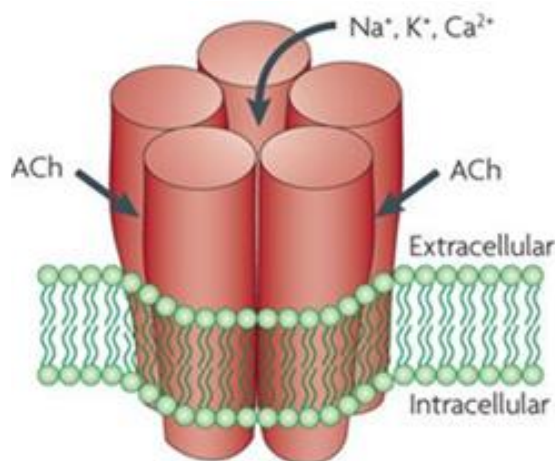


Figure 1: Models of pentameric arrangements of nAChRs in the cytoplasmic membrane (adapted from *Nat. Rev. Neurosci.* 2010, 11, 389-401). [6]

Various combinations of subunits generate an array of receptor subtypes possessing distinct structural and functional properties, such as different agonist affinities, different kinetics of activation, closure, desensitization, resensitization and internalization. Moreover, nAChR subtypes are associated with a variety of ligands characterized by a broad spectrum of pharmacological profiles.

Based on the type of assembled subunits, nAChRs are divided into homopentameric receptors, formed by α -type subunits only, and heteropentameric receptors, showing combinations of α and β subunits (Figure 2). [7] [8]

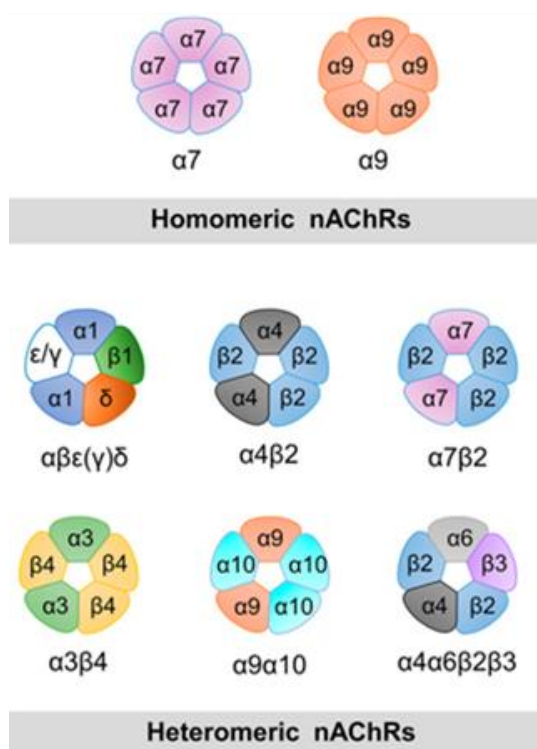


Figure 2: Models of pentameric arrangements of homomeric and some heteromeric nAChRs. Five different binding sites are present in the homopentameric structures, while only two sites are embedded in the heteropentameric receptors (adapted from Mol. Pharmacol. 2016, 90, 288-299). [8]

The key elements for ligand binding are found in α subunits that represent the primary surface of the orthosteric binding site, located at the interface of two different subunits. The complementary surface is represented by the close β , γ , δ , and ϵ subunits in heteropentameric architectures, whereas another α -type subunit is found in homopentameric receptors. [4] Thus, in the heteropentameric receptors, the

number of ligands that can be hosted is regulated by the ratio of α and non- α subunits, while the homopentameric channels can bind up to five different molecules of ACh.

All subunits display common structural features (**Figure 3**). They are composed by a relatively hydrophilic long *N*-terminal extracellular domain (ECD), which carries, in addition to the Cys-loop, the main immunogenic region (MIR) and several glycosylation sites. Then, a transmembrane portion is constituted by four transmembrane (TM) domains, named from 1 to 4. The TM2 of each subunit lines the central pore, controlling both, ion permeation (Na^+ , Ca^{2+} and K^+) and gating properties. The loop connecting TM2 and TM3 is part of the coupling region between ECD and TMD that is involved in the transmission of conformational changes between the two structural components.

Finally, the long cytoplasmic loop between TM3 and TM4 forms the intracellular domain (ICD) containing multiple phosphorylation sites that cover a crucial role in functional modulation. [9] [10]

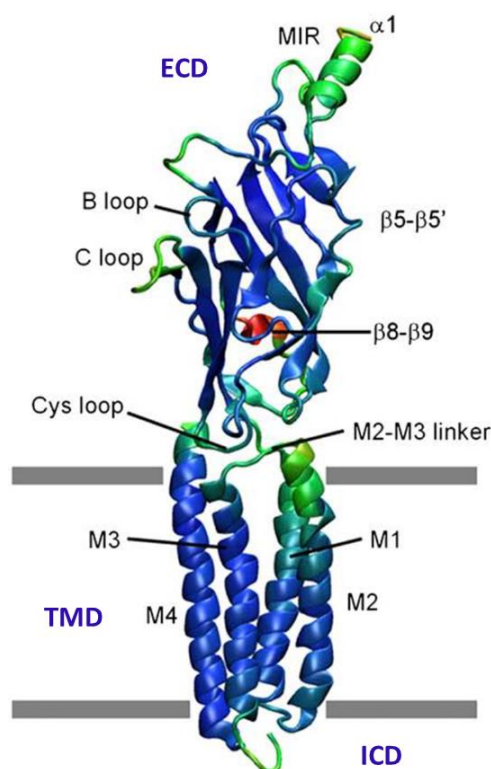


Figure 3: Models of subunits composition, showing the three main regions: extracellular domain, transmembrane domain and intracellular domain (adapted from *Biophys. J.* 2007, 2622-2634). [11]

1.2 The $\alpha 7$ nAChR subtype

1.2.1 Localization and physiopathological roles

The $\alpha 7$ receptor is a homopentameric nAChR highly permeable to Ca^{2+} and is one of the most abundant nAChR subtypes in the brain. It is mainly located in the prefrontal cortex, hippocampus, hypothalamus, dopaminergic and serotonergic neurons and it plays a crucial role in cognition processes, memory and sensory gating.

In the hippocampus, it has been identified in the presynaptic endings and somatodendritic sites on interneurons, where it controls the release of several neurotransmitters, such as γ -aminobutyric acid (GABA), glutamate, norepinephrine and dopamine. Upon activation triggered by agonist binding, an influx of Ca^{2+} and Na^{+} is stimulated that is relatively short in time, because of the rapid receptor desensitization, but it is sufficient to induce the Ca^{2+} release from the endoplasmic reticulum (Calcium-Induced Calcium Release CICR). Additionally, the membrane depolarization due to the ion conductance through $\alpha 7$ causes the activation of voltage-gated calcium channels (VGCC). Thus, the overall increase of cytosolic calcium levels modulates the release of neurotransmitters. [12] [13]

Given its localization in neuronal cells, this receptor subtype represents a promising target for diseases of the central nervous system (CNS) including Alzheimer's disease, Parkinson's disease, schizophrenia, autism, attention deficit hyperactivity disorder (ADHD), anxiety and depression, which have been addressed by $\alpha 7$ subtype-selective ligands. [1] [14] [15] [16] [17]

The $\alpha 7$ nAChR is also found in post-synaptic compartments, where it contributes to plasticity and neuronal excitability. [18] In addition to its localization in neuronal cells, $\alpha 7$ receptor is expressed in non-neuronal cells, such as skin, muscles, lymphoid and vascular tissues, astrocytes and macrophages. In these tissues, the $\alpha 7$ receptor is part of the cell-cell communication and also regulates various processes, e.g. proliferation, adhesion, migration, secretion, survival and apoptosis. In general, this receptor mediates the cellular responses to internal or external stimuli. [1]

Particularly interesting is the presence of $\alpha 7$ nAChRs in the immune cells, where they exert a central role in the so called "cholinergic anti-inflammatory pathway". The involvement of $\alpha 7$ nAChR in reduction of pro-inflammatory cytokines makes this receptor a promising therapeutic target for the treatment of acute and chronic inflammatory diseases, including autoimmune pathologies. [19]

The role of $\alpha 7$ nAChR in anti-inflammatory processes will be discussed in detail in the following paragraph 1.2.5.

1.2.2 Structural features of $\alpha 7$ nAChR orthosteric binding site

No high resolution structure is at present available for human $\alpha 7$ nAChR. The structural information achieved so far come from the acetylcholine receptor models of different species that provided general information for the class of nicotinic receptors. The earliest information about the structural features of nAChRs come from cryogenic electron microscopy (cryo-EM) of *Torpedo marmorata* acetylcholine receptor from post-synaptic membrane (17 Å). The presence of five subunits disposed around a central pore was revealed; the results obtained from a previous hydrophobicity analysis, that described each subunit as composed by ECD, TMD and ICD, were also confirmed. [20] Later on, the release of a better resolved structure of *Torpedo* (9 Å) provided deeper information on the ligand binding region. [21]

More recently, a membrane-associated *Torpedo* acetylcholine receptor at 4 Å resolution has been published. This model extended the analysis obtained from earlier models, also providing information on the channel opening process. This model, in fact, was imaged in the apo structure: after exposure to ACh and rotation of the ligand-binding subunits upon agonist binding, a concerted rearrangement of the TMD was observed. [22]

An important step in the structural investigation of $\alpha 7$ receptors was represented by the crystal structure obtained from *Lymnea stagnalis* acetylcholine binding protein (AChBP) (2.4 Å - PDB: 1I9D). [23] This molluscan model was considered a structural and functional homolog of the ECD of α subunits, although it lacked transmembrane and intracellular domains. This model confirmed the location of the ligand-binding site at the interface of two subunits as well as the position of the MIR in the ECD. Previous data on the residues forming the ligand-binding site, obtained by photo-affinity labelling and mutagenesis studies, were verified. This model provided the first description of the spatial arrangement of each residue. Showing 24% identity with $\alpha 7$ ECD and a homopentameric structure, AChBP represents a valuable template for modeling investigations of the $\alpha 7$ nAChR.

A more recent structure of AChBP has been obtained from *Aplysia californica*. The structure shared 33% of amino acid identity with the previous molluscan model, and it is also a homopentameric structure showing all the functional residues in the ligand binding site (LBS). [24]

In 2011, a chimera construct was built starting from the human $\alpha 7$ nAChR sequence and *Lymnaea stagnalis* AChBP, showing a 71% identity with the native $\alpha 7$ receptor. The crystal structure with epibatidine provided information on the molecular interactions involved in the agonist recognition process, where loops A-C as well as loops D-E play a central role. [25]

The orthosteric binding site

The orthosteric binding site is located at the interface of two different subunits. It is surrounded by six loops, named from A to F, that carry amino acid residues involved in the ligand-binding. Loops A-C belong to the positive subunit, while loops D-F belong to the negative one (**Figure 4**). The C-loop covered the orthosteric region and its closure and opening appeared to be related to the binding affinity of different kinds of ligands. [26]

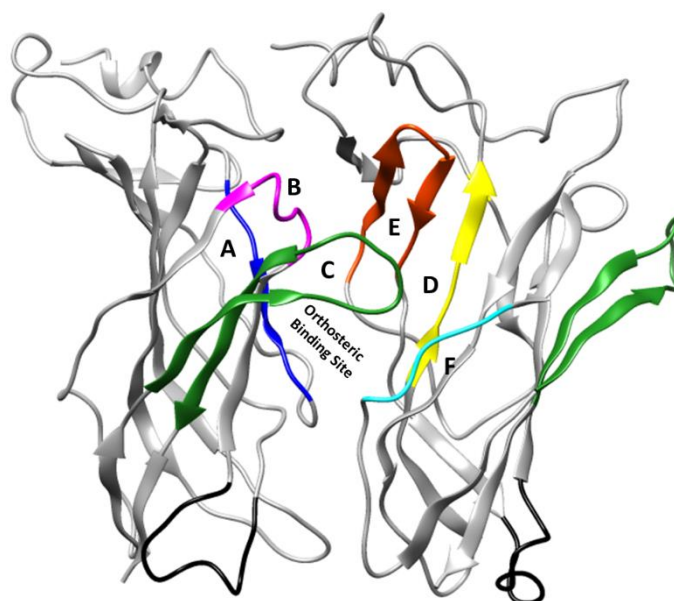


Figure 4: Homology model of the interface AB. The six loops A-F, highlighted in different colors, are positioned around the orthosteric binding site. The Cys-loop is shown in black. The figure was prepared in UCFS Chimera using the homology model 2 (HM2) previously built by Dr. Gulsevin, as reported in Chapter V.

The ligand-binding pocket of $\alpha 7$ nAChR shows an aromatic cage located under the C-loop, which is composed by essential residues such as Tyr91 (Tyr93 $\alpha 7$ numbering) from loop A, Trp145 (Trp149 $\alpha 7$ numbering) from loop B, Tyr184 and

Tyr191 (Tyr188 and Tyr195 $\alpha 7$ numbering) from loop C and Trp53 (Trp55 $\alpha 7$ numbering) from loop D (**Figure 5**). This aromatic nest has a central role in molecular recognition and binding stabilization, forming π -cation and van der Waals interactions with the ligands. Considering the binding pose of epibatidine in the $\alpha 7$ -nAChBP complex [25], the bridging nitrogen in the bicyclic structure interacted with the backbone carbonyl of Trp149 *via* hydrogen bonding, and also established a π -cation interaction with the side-chain indol ring of the same residue. This demonstrated the essential role of Trp149 within the aromatic cage. Additional residues located in the orthosteric binding site are Leu106, Gln114, and Leu116. [25]

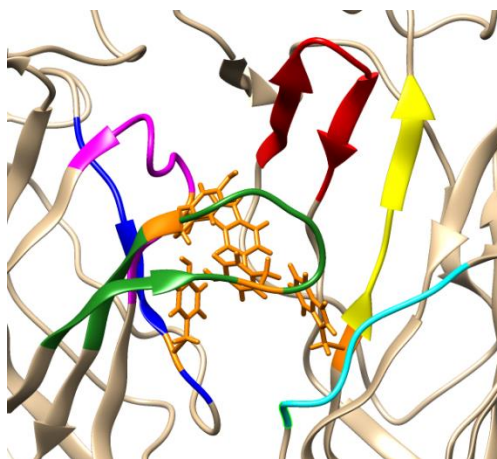


Figure 5: Homology model of the orthosteric binding site at the interface AB. The six loops A-F are highlighted in different colors; the amino acid residues that compose the aromatic cage are reported in orange. The figure was prepared in UCFS Chimera using the homology model 2 (HM2) previously built by Dr. Gulsevin, as reported in Chapter V.

1.2.3 Kinetic features and different conformations of $\alpha 7$ nAChR

The $\alpha 7$ nAChR is characterized by unique kinetic properties. It shows low channel opening probability during agonist evoked currents [27] and a very fast onset of receptor desensitization. Specifically, it displays a peculiar concentration-dependent rapid reversible desensitization. When a high agonist concentration is applied, i.e. sufficient to produce saturation of the agonist binding sites, a large peak current is initially obtained (that it is due to the receptor synchronization rather than to an

actual increase of the number of activated receptors), which is followed by faster stabilization of non-conducting states.

At high agonist concentration, the channel response is faster than the kinetics of the solution exchange and reaches the maximum peak current value well in advance the complete delivery of the agonist. The consequent rapid receptor desensitization determines the inability of additional application of agonist to produce channel opening. [28]

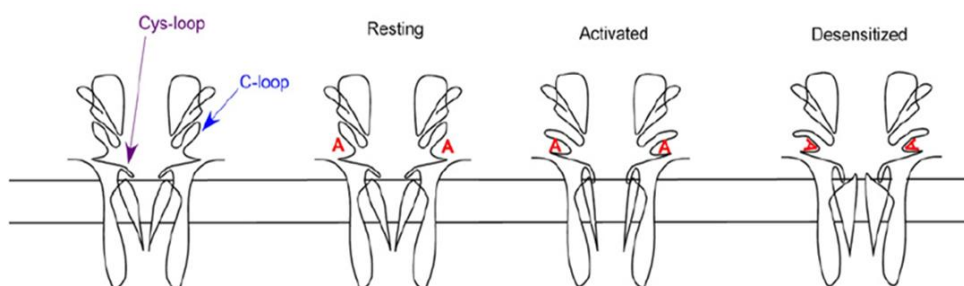
Receptor synchronization influences the peak current value without affecting the net charge. Considering the receptor activation given by ACh, the maximal $\alpha 7$ nAChR response is obtained at 300 μM ; applying a higher concentration than 300 μM , a progressive receptor synchronization takes place that leads to a larger peak current but not to a prolonged response. Thus, receptor desensitization induced by high agonist concentrations prevents the measurements of peak currents. [29] Therefore, the peak current occurs at low agonist concentrations, giving rise to sharp responses and over estimation of agonist concentrations associated to maximal channel activation. [30]

On the contrary, net charge represents the time integration (i.e. peak area) of all the channel activation that occurs in response to a drug application, and thus net charge values depend on the total amount of receptors that are activated by an agonist and are not affected by the synchronization processes. The comparison between the values of peak current and net charge at 30 μM and 3 mM ACh supported this concept. The peak response, given by 3 mM, was 16 fold greater than the peak value obtained after application of 30 μM , while the net charge was just 2 fold larger. With the application of high agonist concentration, the synchronized activation (i.e. the peak current) occurs well in advance the time when the full concentration of the drug is present in the chamber. [29] Net charge is thus considered a more reliable value to be taken into account in the analysis and comparison of electrophysiological data.

As already described, the $\alpha 7$ nAChR presents a strong tendency to desensitize. Non-conducting forms, in fact, are part of the interconvertible and functionally distinct states assumed by the receptor, as depicted in **Figure 6** [31]:

- a resting closed state (C), populated in absence of agonist, in which no ion influx through the channel can be detected; it presents lower probability of spontaneous opening;

- an active open state (O^*), transiently stabilized by the presence of an agonist; it is a very short-lasting cation-permeable open state where ion fluxes through the receptor channel are observed;
- desensitized closed states (D), stabilized by the sustained presence of the agonist but with no ion fluxes detected.



A = agonist

Figure 6: Representation of different conformational states of nAChRs (adapted from *Biochem. Pharmacol.* 2014, 89, 1-11). [4]

Upon complete washout and based on the nature of the agonist, the nAChR can rapidly recover from desensitization, thus converting again to a closed resting state or show a residual inhibition or desensitization. [32]

Two different types of non-conducting states can be assumed by the $\alpha 7$ nAChR. D_s is a non-conducting state that is sensitive to the application of type II positive allosteric modulators (PAM). Due to the possibility to be destabilized and converted into an open state, it is considered a reversible desensitized receptor form. Conversely, D_i is a non-conducting state that is completely insensitive to type II PAMs and promoted by higher ligand concentration. [33] Type II PAMs are ligands that bind nAChRs without triggering any channel response when applied alone, but giving response potentiation in presence of an orthosteric ligand. [34] Type II PAMs affect energy transitions between different states by reducing the energy barrier between the closed and open states. Thus, after agonist application, in presence of a type II PAM, the channel opening probability is enhanced. Moreover, type II PAMs destabilize the desensitized states, favoring a prolonged activation of previously non-conducting receptors.

While type II PAMs are able to alter the receptor kinetics, type I PAMs lower the energy barrier into the open state but do not affect the equilibrium between desensitized and open state. [35] The binding sites of the positive allosteric modulators are mainly located in the TMD. [36]

The dynamic nature of the $\alpha 7$ receptors is strictly related to the equilibria and the rate of transition between two conformational states that reproduce the differences in the free energy values of the various states. [4] Moreover, the conformational transition is regulated by the type of ligand and the level of occupancy of the binding site.

The most recent description of the hypothetical energy landscapes of $\alpha 7$ receptors is reported in **Figure 7** [37] and is based on a number of studies. [38] [33] [39] [40] This model is related to activation, desensitization and modulation of the $\alpha 7$ receptor in presence of classical agonists, silent agonists and type II PAM.

Silent agonists, which will be discussed more in detail later on, are $\alpha 7$ receptor ligands able to bind the receptor with low channel opening and strong stabilization of D_s states that can be converted into the open form by applying a type II PAM. At higher concentrations, silent agonists mainly prefer the stabilization of D_i conformations. As depicted in **Figure 7**, the putative ligand binding site for silent agonist (S) is proximal and considered an extension of the orthosteric binding site (A). The reported direct allosteric activation (DAA) binding site (D) is an additional binding pocket found on the vestibular site of the receptor; it has been described after the discovery of a new type of modulators called “ago-PAM”. [38] Finally, the positive allosteric modulator sites (P) are located in the TMD.

In absence of ligands, the resting-closed state (C) is the most energetically favoured conformation with low channel opening probability typical of $\alpha 7$ receptors. [4] [41] The ligand binding causes the decrease of the energy barrier between the closed state (C) and the short-lived open state (O^*). The transition from closed to open state is a rapid and transient process leading to channel opening and subsequent ion flux. The O^* state is achieved in presence of intermediate agonist occupancy, before saturation of the agonist binding sites. [33] Upon ligand binding, the energy differences between the closed (C) and desensitized states are very small and this reflects the fast onset of desensitization displayed by the $\alpha 7$ receptor. The stability of D_s and D_i increases with agonist occupancy, with deeper stabilization of D_i at higher agonist concentrations. When a silent agonist is bound to the receptor, the induction of the non-conducting states is more intense. Although also the energy barrier to enter

the short-lived open state (O^*) is lower, the receptor desensitization is strongly preferred and this is in accordance with the low channel opening detected for a silent compound. As already described for the classical agonists, D_i is favored over D_s in presence of high ligand concentrations. [37]

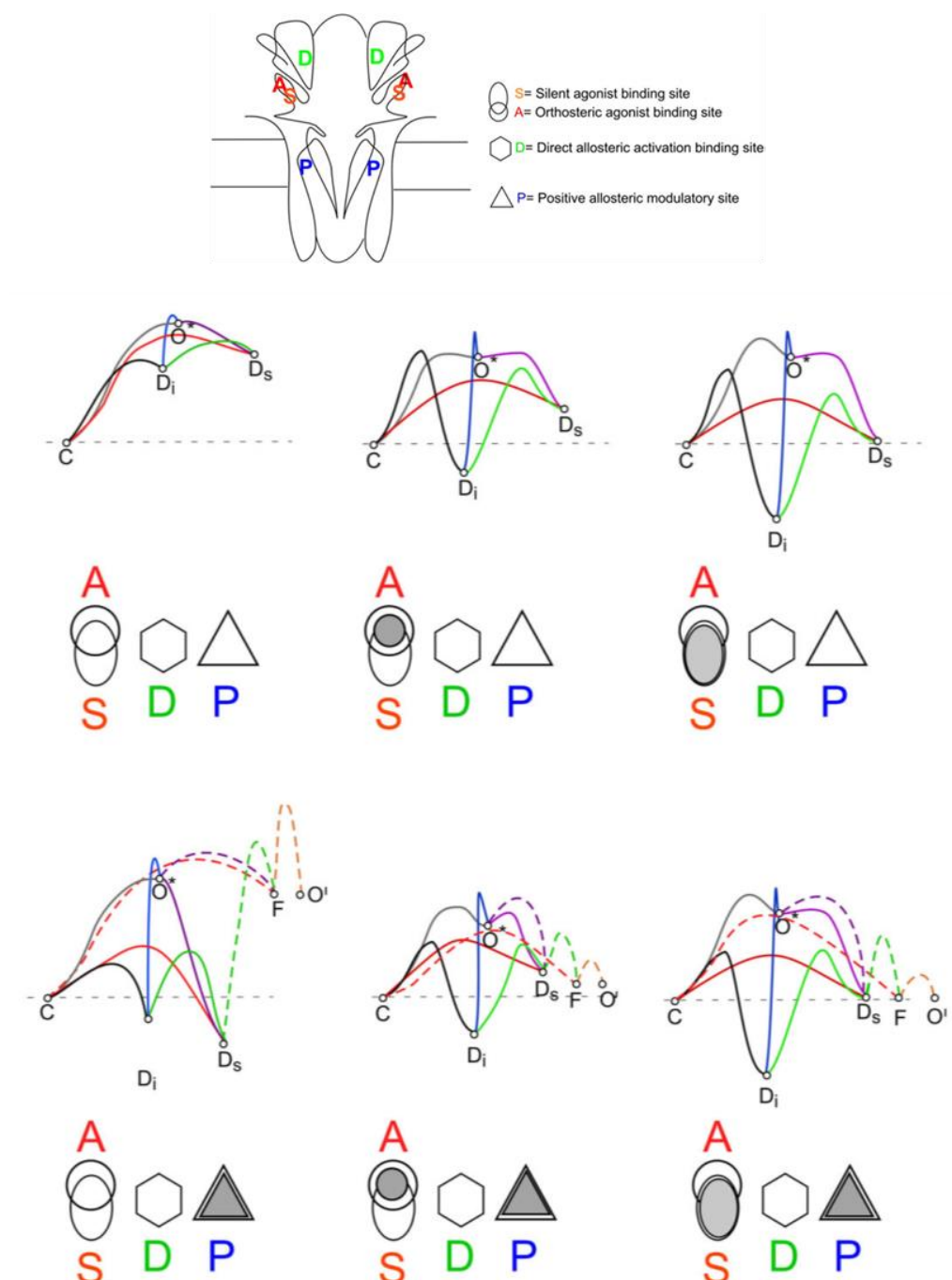


Figure 7: Hypothetical energy landscapes for conformational state transitions based on occupancy of A, S and P sites (adapted from Br. J. Pharmacol. 2018, 175, 1838-1854). [37]

The lower part of **Figure 7** reports the energy landscapes in presence of type II PAMs. When a type II PAM is applied alone, no ion flux is detected through the channel; however, a type II PAM is able to induce the D_s state. When the A/S site is occupied, type II PAMs promote the conversion of D_s state into a new long-lived open state (O'); intraburst closed state (F) is the “flip” state proposed to precede channel activation. [42] With high concentrations of both agonist and type II PAM, the D_i state is induced, thus demonstrating that a low-intermediate level of occupancy is required to reach the maximal potentiation. [33]

Recently, computational investigations have been focused on the $\alpha 7$ nAChR desensitized states. Chiodo et al. explored the structural descriptors of a putative $\alpha 7$ desensitized homology model after 200 ns of dynamic simulation. At variance with the V-like conformation observed in the open form, the ligand bound non-conducting model displayed the M2 helices disposed in parallel to each other. This particular conformation was related to the twisting motion of the LBD relative to TMD in the open-to-desensitized transition.

Analyzing the LBD and the TMD, a series of hydrogen bonds were detected, both intra- and inter-subunits. The number of hydrogen bonds was much higher than that of the open form and they were also more persistent during the trajectory time. Moreover, the Cys-loop was moved farther from the M2-M3 loop at the LBD/TMD interface compared to the open conformation. Finally, the interactions involved in the epibatidine binding were considered. The contribution of the van der Waals interactions was stronger in the desensitized structure than in the open conformation and this might be consistent with the higher ligand affinity characteristic of the desensitized state. [43]

Although not related to ionotropic activity, the desensitized states are functionally relevant. The receptor desensitization, in fact, has been found to be pivotal in the metabotropic-like activity of $\alpha 7$ nAChRs. [44] Therefore, the identification of compounds able to preferentially stabilize the desensitized states represents a quite interesting approach for a deeper understanding of the peculiar modulation of $\alpha 7$ receptor response and for the development of novel therapeutics.

1.2.4 Metabotropic-like activity of $\alpha 7$ nAChR

The physiological involvement of the $\alpha 7$ receptor in the increase of Ca^{2+} levels in presynaptic compartments has been previously described in paragraph 1.2.1. Upon agonist binding, the short-lived channel opening is obtained, with subsequent Ca^{2+} and Na^{+} influx. The ion conductance through the $\alpha 7$ channel activates CICR from ER and produces membrane depolarization that leads to the opening of VGCCs. [13] Agonist stimulation, however, promotes the rapid conformational transition of $\alpha 7$ receptor from open to non-conducting state. Since the observed transient Ca^{2+} extends beyond the timecourse of Ca^{2+} flux *via* the $\alpha 7$ receptor open form, the contribution of the long-lasting receptor desensitization has been suggested (Figure 8). [44]

As already well known, the interaction of $\alpha 7$ nAChRs with GTP-binding proteins (G proteins) produces a metabotropic component of the channel response that extends the temporal and spatial activation of the $\alpha 7$ signaling beyond the ionotropic response. [44] [45] The strong association between nAChRs and G proteins was found in several advanced proteomic analyses [46] [47] [48]; an extensive description of the nAChR interactomes in neuronal, immune and epithelial cells was provided [49] [50], which was subsequently confirmed in different rodent tissues. [51] [52]

Recent discoveries have suggested a central role of ICD in the channel-independent activity of the $\alpha 7$ receptor.

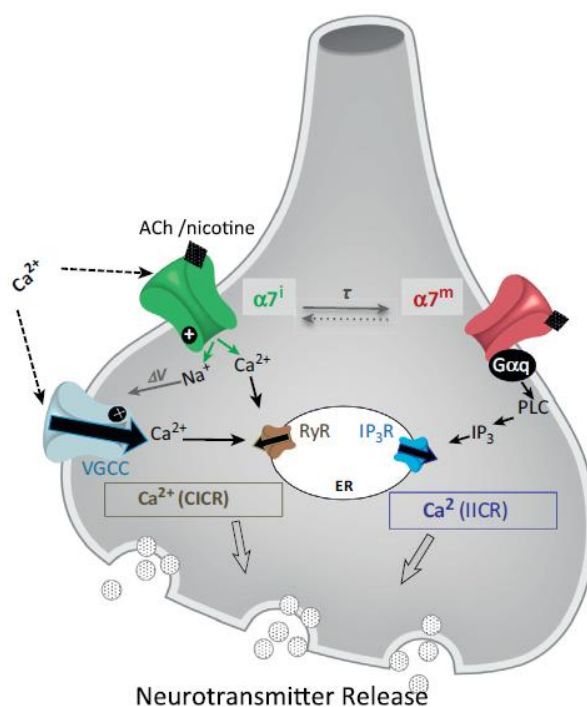


Figure 8: Synaptic $\alpha 7$ -induced Ca^{2+} release. The brief $\alpha 7$ opening enables sufficient membrane depolarization that activates VGCCs and Ca^{2+} influx that leads to CICR from the endoplasmic reticulum (ER) in the presynaptic terminal. The transition (τ) of the $\alpha 7$ nAChR into the desensitized state supports a metabotropic response via G protein activation of PLC, inositol trisphosphate (IP_3) production, and final IP_3 -induced calcium release (IICR) (adapted from Trends Pharmacol. Sci. 2018, 34, 2, 354-366). [44]

The ICD of $\alpha 7$ nAChR is a well-conserved structure that was investigated through specific sequence and hydrophobicity analyses, comparing all human nAChR subunits with a sequence alignment. The perimembrane portions (after TM3 and before TM4) are characterized by some relatively well-conserved charged amino acids; the central part of the intracellular loop is highly variable and structurally disordered. Functional sites, such as -SH2 and -SH3, in the $\alpha 7$ domain sequences have been discovered by the Eukaryotic Linear Motif resource for Functional Site in Proteins (ELM) and ProSite. They are mainly localized in the central variable part of ICD and could be involved in receptor assembly and disassembly, positioning and participation in cell signaling cascades. [53]

Particularly relevant to the coupling between G proteins and $\alpha 7$ receptors is a conserved sequence of four amino acid residues in the ICD, depicted in **Figure 9**, which has been identified as the G-protein binding cluster (GPBC). [52] The direct

binding of G proteins at this site was confirmed through the mutation of the four amino acids involved and the subsequent loss of G-protein interaction.

Previous studies of nicotinic modulation of presynaptic Ca^{2+} signal demonstrated the role of PLC in nicotine-induced CICR *via* the IP_3 receptor of endoplasmic reticulum [54]; in light of the new information provided for the G-protein coupling of $\alpha 7$ receptors, the involvement of $G_{\alpha q}$ in $\alpha 7$ channel-independent activity has been suggested. As depicted in **Figure 8**, the increase of intracellular Ca^{2+} levels relies on the initial short-lasting $\alpha 7$ ionotropic activation and the subsequent persistent metabotropic signaling that appears to coincide with the timing of receptor desensitization. [44]

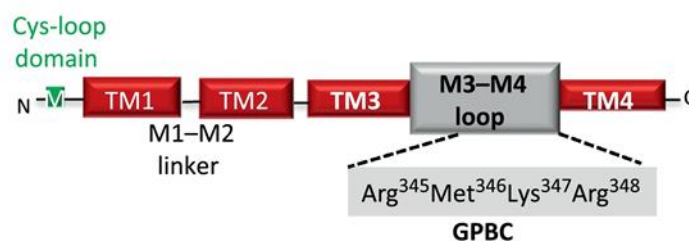


Figure 9: Schematic representation of the location of TMDs and, in particular, the ICD containing the G-protein binding cluster (GPBC) (adapted from *Trends Pharmacol. Sci.* 2018, 34, 2, 354-366). [44]

1.2.5 The cholinergic anti-inflammatory pathway

The metabotropic signaling is now considered a key functional aspect of the $\alpha 7$ receptor activation in different cell types. Especially in immune cells, the anti-inflammatory activity of $\alpha 7$ nAChR seems to be strictly related to the ion-independent metabotropic signal transduction during channel desensitization, even if it's still uncertain which desensitized states, D_s or D_i or others, are involved in the metabotropic mode of action. The role of ACh in the regulation of pro-inflammatory cytokines release was discovered by Borovikova et al. in 2000, [55] which demonstrated that the stimulation of the vagus nerve reduced the systemic inflammatory response. In particular, the ability of ACh to suppress the release of $\text{IL-1}\beta$, IL-6 , IL-18 and $\text{TNF-}\alpha$ *via* post-transcriptional mechanisms was proven. Although the role of nicotinic rather than muscarinic receptors had already been clarified, later

on the $\alpha 7$ subtype was identified as the receptor expressed on the surface of human macrophages and involved in the cholinergic inhibition of TNF. To assess the critical role of the $\alpha 7$ receptor, antisense oligonucleotides specific for this subunit were prepared. Macrophages exposed to these antisense oligonucleotides showed a lower sensitivity towards inhibition of TNF release after nicotine administration. [56] Moreover, alpha7 knockout mice were characterized by higher serum levels of TNF- α , IL-1 β and IL-6 after administration of bacterial endotoxin compared to wild-type animals, confirming the central role of the $\alpha 7$ subunit in the cholinergic anti-inflammatory pathway. [57] [58]

In response to an inflammatory stimulus, ACh is released in organs of the reticuloendothelial system, including lungs, spleen, liver, kidneys, and the gastrointestinal tract. [59] Upon release, ACh interacts with the $\alpha 7$ nAChRs expressed on cells of both innate and adaptive immunity, including T and B lymphocytes, macrophages, neutrophils, monocytes, dendritic cells, and microglia, thus suppressing the release of TNF- α , down-regulating pro-inflammatory cytokines synthesis and preventing tissue damage. [60]

Activation of the $\alpha 7$ receptor, in macrophages and other inflammatory cells *in vitro* and *in vivo*, reduces pro-inflammatory cytokine release by JAK/STAT signaling, inhibition of NF- κ B activation and phosphoinositol-3-kinase (PI3K)/Akt/Nrf-2 pathway (**Figure 10**). [61]

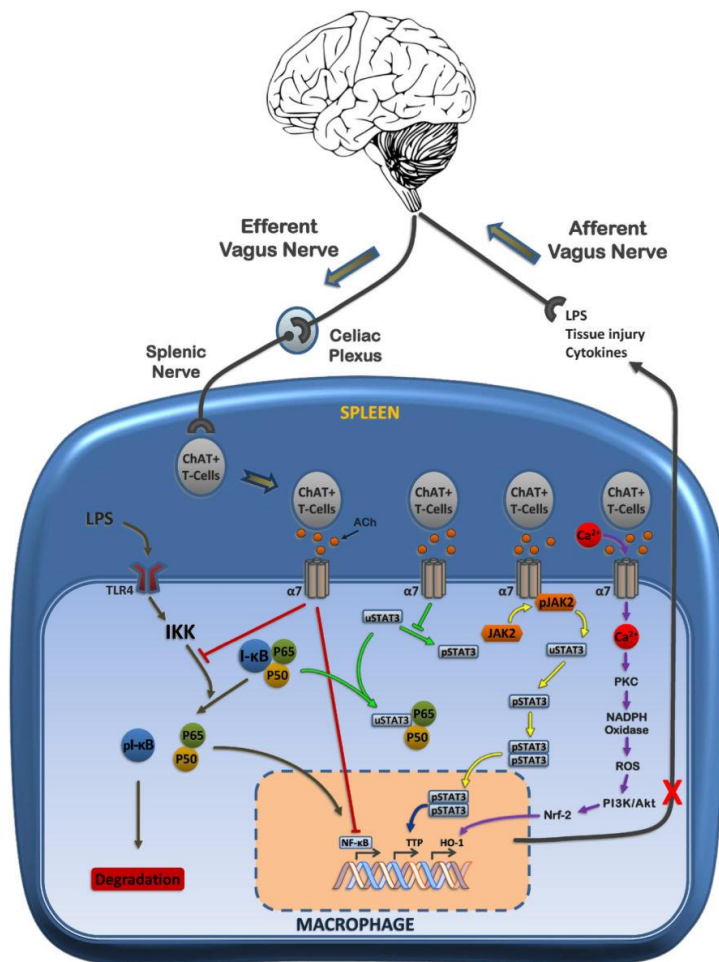


Figure 10: Schematic representation of $\alpha 7$ nAChR-related pathways involved in cholinergic anti-inflammatory activity. Activation of the vagus nerve leads to ACh release and binding to alpha7 receptors on cytokine producing cells, affecting different intracellular signaling pathways involved in the anti-inflammatory responses (adapted from J. Neuroimmune Pharmacol. 2015, 10, 468-476). [61]

Upon pro-inflammatory stimulation and ACh binding, the $\alpha 7$ receptor triggers Jak2 phosphorylation that in turn leads to STAT3 recruitment to the receptor complex, and STAT3 phosphorylation. Phosphorylated STAT3 then forms dimers that translocate into the cell nucleus and negatively regulate the production and release of pro-inflammatory cytokines. [62]

NF- κ B is the second signaling pathway involved in the anti-inflammatory activity of $\alpha 7$ receptors. Under inflammatory conditions, I- κ B, which forms an inactive complex with NF- κ B in the cellular cytoplasm, is phosphorylated and degraded; thus, NF- κ B is released and allowed to translocate into the cell nucleus where it evokes the production of pro-inflammatory cytokines; the $\alpha 7$ -related signaling pathway inhibits the phosphorylation of I- κ B, thereby preventing activation of NF- κ B. [60]

Furthermore, activation of the $\alpha 7$ receptor has been proposed to inhibit STAT3 phosphorylation, leaving STAT3 available to bind NF- κ B subunits avoiding their nuclear translocation. [62]

An alternative mechanism for the anti-inflammatory activity of the $\alpha 7$ receptor is mediated by Ca^{2+} -dependent activation of PLC and subsequent activation of the (PI3K)/Akt/Nrf-2 pathway that leads to the upregulation of heme-oxygenase-1 (HO-1). [63] [64]

The $\alpha 7$ nAChR covers a central role in the cholinergic anti-inflammatory pathway, a signaling transduction pathway that involves both nervous and immune systems and regulates pro-inflammatory responses. Thus, the $\alpha 7$ receptor represents a potential therapeutic target for various inflammatory-related diseases and pathological conditions, like asthma, sepsis, osteoarthritis, obesity, type 2 diabetes and chronic pain, through the modulation of pro-inflammatory cytokines. [60]

1.3 Silent agonism

The direct $\alpha 7$ receptor modulation of signal transduction independent of channel activation is strongly supported by recent evidence showing that some efficacious $\alpha 7$ anti-inflammatory modulators act as silent agonists. Silent modulators are very weak partial agonists that bind the receptor with no apparent or very low channel opening and show ACh inhibition properties.

The most interesting aspect of silent agonism is the ability to promote the stabilization of the D_s state, which for the $\alpha 7$ receptor subtype is detectable by co-application with type II PAMs, such as PNU-120596. Type II PAMs represent a valuable tool to convert the desensitized receptor into an ion-conductive state that can be detected and quantified employing the two electrode voltage-clamping technique.

The non-conducting receptor desensitized states are considered pharmacologically active in the metabotropic sense; therefore, a silent agonist is relatively silent for the ionotropic activity, but it behaves as an agonist for the $\alpha 7$ -mediated metabotropic-like activity. [65] Some compounds acting as $\alpha 7$ nAChR silent agonists show promising anti-inflammatory and antinociceptive activities in both *in vitro* and *in vivo* tests, thus representing a new approach to target this receptor subtype in view of putative therapeutic applications. [66] [67] [68]

Several different structures have been identified as silent agonists, displaying stabilization of receptor desensitization in lieu of channel opening (**Figure 11**).

The recent study performed on the archetypal silent agonist **NS6740** (**Figure 11**) and the ago-PAM GAT107 evidenced different channel-related activity profiles for the two compounds in the oocyte expression system. **NS6740** may induce the desensitized state D_i in preference of D_s , whereas with GAT107 the balance between D_s and D_i is shifted toward D_s . However, the two derivatives show similar anti-inflammatory and analgesic activity in animal models. [66] [69] Thus, the anti-inflammatory effects of these drugs are likely not to depend on channel activity, rather to a metabotropic signaling transduction of the $\alpha 7$ receptor, but which desensitized state is connected with the metabotropic function is not completely clear yet. [37]

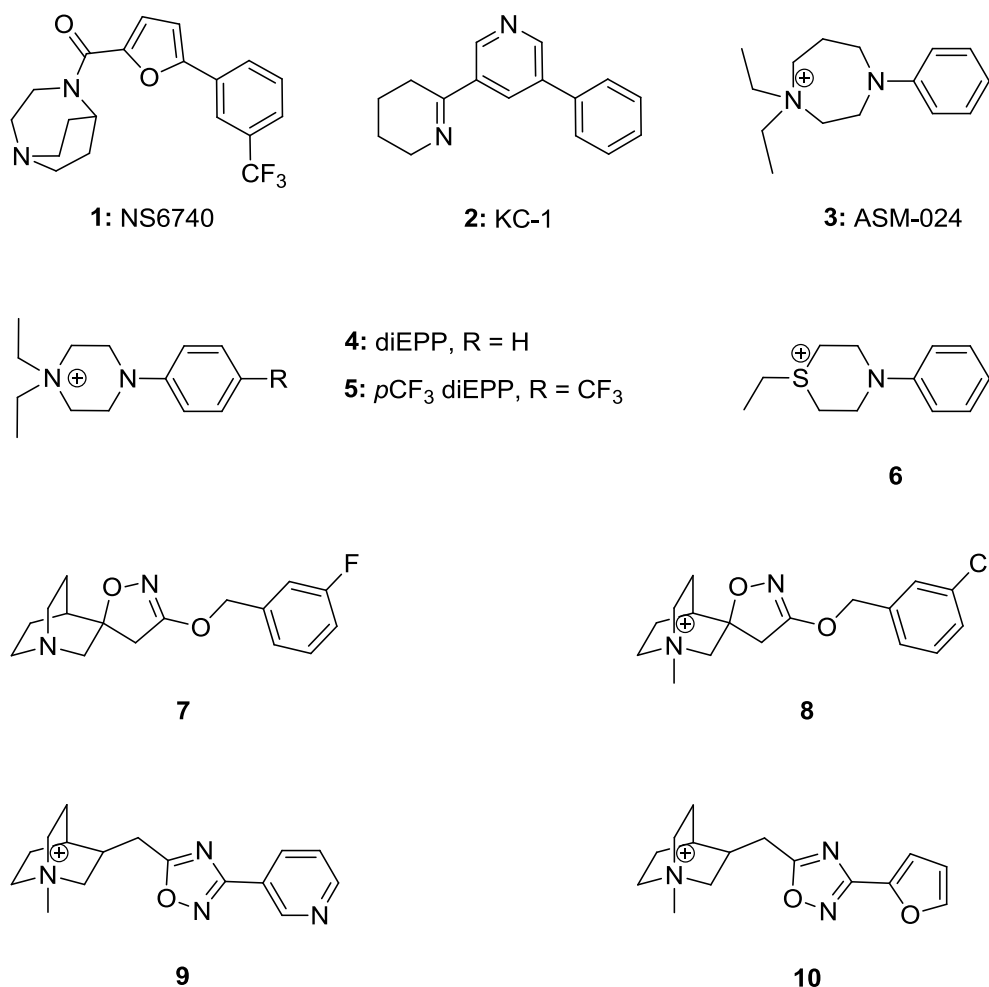


Figure 11: Structures of selected silent agonists 1-10.

The main common feature of all silent agonists has been identified in the positive charge, as either a permanent quaternary ammonium nitrogen or a tertiary nitrogen that is protonated at physiological pH. [65] The minimum pharmacophore for silent agonism was proven to be the tetraethylammonium cation (TEA), in a study in which several quaternary ammonium salts were prepared, which showed a systematic modification of the size of the alkyl substituents around the central nitrogen. This observation derived from the analysis performed on diethyldimethylammonium (diEdiMA, the minimal structure needed for a selective activation of $\alpha 7$ nAChRs), whose methyl groups were progressively replaced with ethyl groups, affording first triethylmethylammonium (triEMA), a partial agonist of the $\alpha 7$ receptor, then TEA, an $\alpha 7$ silent agonist (Figure 12).

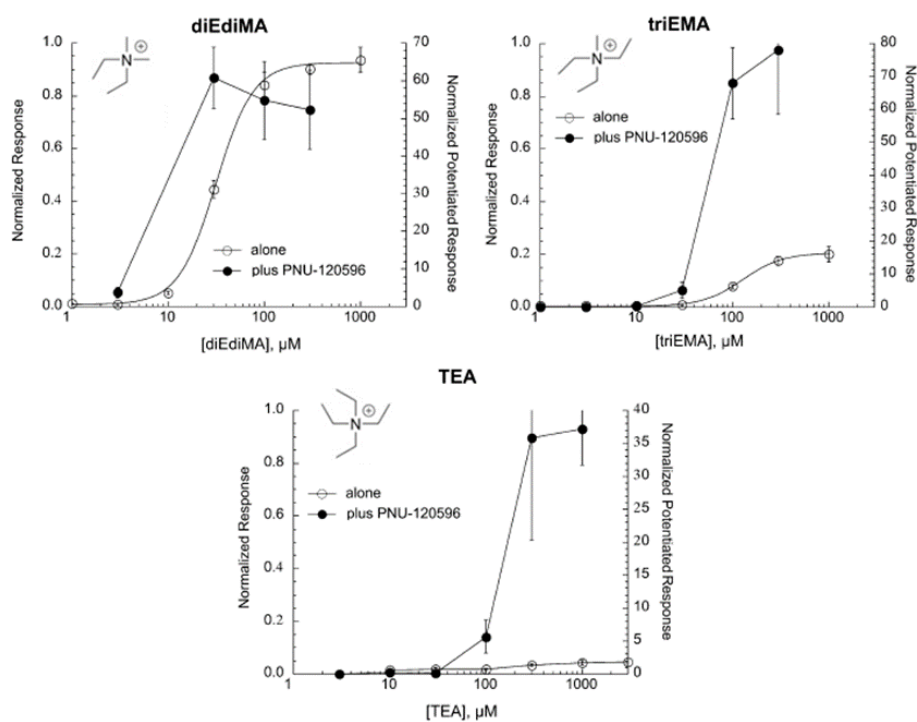


Figure 12: Structures and relative electrophysiological profiles of **diEdiMA**, **triEMA** and **TEA**. Concentration-response studies reported the orthosteric (drug applied alone) and allosterically potentiated (drug co-applied with 10 μM PNU-120596) activation of $\alpha 7$ nAChR (adapted from *J. Pharmacol. Exp. Ther.* 2014, 35, 665–680). [40]

The data proved a correlation between the stabilization of a specific receptor conformation and the molecular volume surrounding the central nitrogen: a steric bulk around the positive charge leads to decrease the channel opening in favor of a stronger stabilization of the non-conducting states. [40]

According to the TEA minimal pharmacophore for silent agonism, the *N,N*-diethyl-*N'*-phenylpiperazinium (**diEPP**) was designed starting from the *N,N*-dimethyl-*N'*-phenylpiperazinium (**diMPP**), which is a ganglionic agonist. **diEPP** (**4**) showed inability to channel opening when tested alone, but acquired an agonist profile in co-application with PNU-120596. The silent activity found for **diEPP** confirmed the previously described correlation. [40] Subsequent introduction of a *para*-trifluoromethyl group on the phenyl ring of **diEPP** gave the potent silent agonist **CF₃ diEPP** (**5**), indicating that potential interactions between the receptor protein and suitable substituents apart from the charged nitrogen atom may evoke or modulate the silent agonist profile. [70] **CF₃-diEPP** (**5**) was proven to be active in *in vivo* mouse models of hyperalgesia and edema and its activity could be ascribed to α 7-signaling pathways independent of channel activation. [67]

Quite recently, the sulfonium group was investigated as an alternative moiety to the classical ammonium group of **diEPP** in giving π -cation recognition inside the α 7 receptor. When compared to **diEPP**, compound **6** displayed decreased channel opening associated to enhanced desensitization. [71]

In the medicinal chemistry research laboratory where I performed my PhD thesis, new interesting silent scaffolds have been identified, possessing both tertiary amine and quaternary ammonium functions. Compounds **7** and **8** are characterized by a 3-benzyloxy substituted group on the α 7-agonist quinuclidinyl- Δ^2 -isoxazoline core that confers a low agonist activity and a noticeable desensitizing profile. [72] The 5-(quinuclidin-3-ylmethyl)-1,2,4-oxadiazole skeleton, including either a 3-substituted pyridine (**9**) or a furan ring (**10**), also imparted a significant silent agonist profile. [73] Lastly, the homopiperazinium derivative **ASM-024** (**3**) showed silent agonist activity and is currently in phase II clinical trials for the treatment of asthma and chronic obstructive pulmonary disease (COPD). [68]

1.3.1 The silent agonist NS6740

1.3.1.1 Electrophysiological profile of NS6740

NS6740 is a silent agonist, a member of the diazabicyclononane chemical series, characterized by a strong desensitizing profile. It exhibited high-affinity binding to the $\alpha 7$ nAChR sites in rat brain membranes, displacing the $\alpha 7$ -selective agonist [3 H]A-585539 with a K_i value of 1.1 nM. [74] Its silent behavior has been investigated employing homomeric $\alpha 7$ nAChRs expressed in *Xenopus laevis* oocytes and two-electrode voltage clamping [75], where it showed very weak partial agonism activity, when applied alone, but intense PNU-related potentiation. [66] In the same study, the authors investigated the competitive antagonism of silent agonist NS6740, by evaluating the inhibition of 60 μ M ACh in co-application with several test drug concentrations (Figure 13). NS6740 inhibited the net-charge responses evoked by 60 μ M ACh with an IC_{50} value of $4.0 \pm 0.7 \mu$ M. The reduction of the following ACh post-control responses (especially after the application of NS6740 $\geq 10 \mu$ M) demonstrated the persistent presence of NS6740 in the binding site after the washout and the stabilization of the desensitized states.

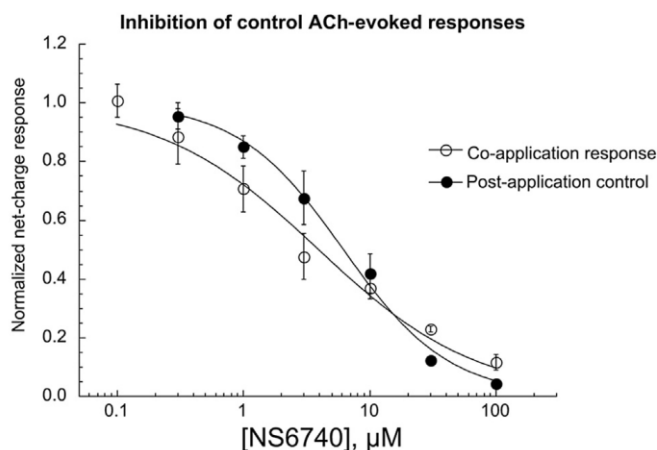


Figure 13: Inhibition of control ACh-evoked response. The open circles show the channel responses after co-application of NS6740 and ACh; the filled circles show the ACh control responses obtained after a 4 min washout (adapted from *Neuropharmacology* 2015, 91, 34-42). [66]

The peculiar prolonged binding and the consequent induction of a sustained receptor desensitization are the most relevant characteristics of NS6740. The ability of NS6740 to remain in the binding site was proven as shown in Figure 14. After the delivery of 30 μ M of NS6740, a receptor washout 6 min long was carried out. The

following application of 60 μM ACh was strongly reduced, compared to the ACh pre-control, demonstrating that the receptor was still deeply desensitized (Figure 14, panel A). Panel B of Figure 14 reports the values of PNU-related channel responses recorded at different time points after the initial 12s application of 30 μM NS6740. Interestingly, after 87 minutes, the channel activation promoted by PNU-120596 application was still detected. [37]

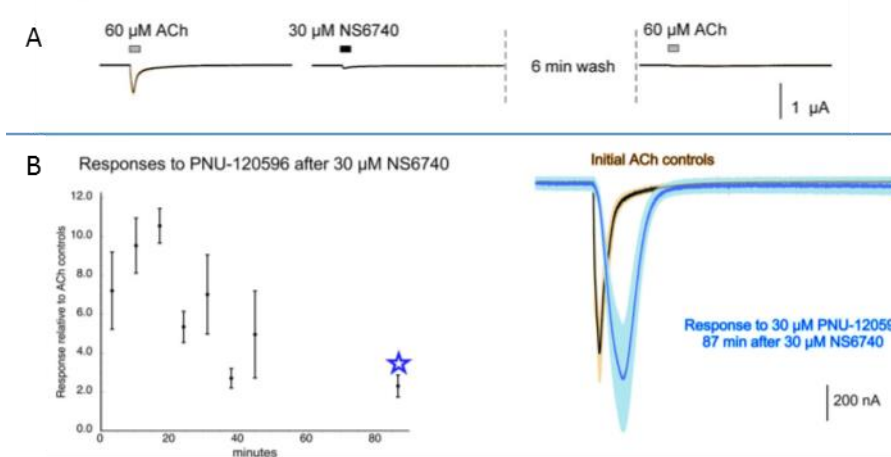


Figure 14: (A) Data showing the receptor response to 30 μM NS6740 and, following a 6 min washout, the inhibition of 60 μM ACh control; (B) Data showing PNU-related responses at different time points after the initial application of 30 μM NS6740 (adapted from Br. J. Pharmacol. 2018, 175, 1838-1854). [37]

1.3.1.2 Anti-inflammatory profile of NS6740

Although NS6740 failed in giving enhanced cognitive performance in mouse inhibitory avoidance (IA) memory retention, [74] a very interesting anti-inflammatory profile was delineated. Pharmacological studies on the inflammatory function of the microglia proved that NS6740 is a better modulator of the inflammatory processes compared to classical nAChR agonists (including choline), suppressing lipopolysaccharide (LPS)-stimulated secretion of TNF- α in rat cultured microglia, with some effects at 25 μM and complete inhibition at 50 and 100 μM (Figure 15).

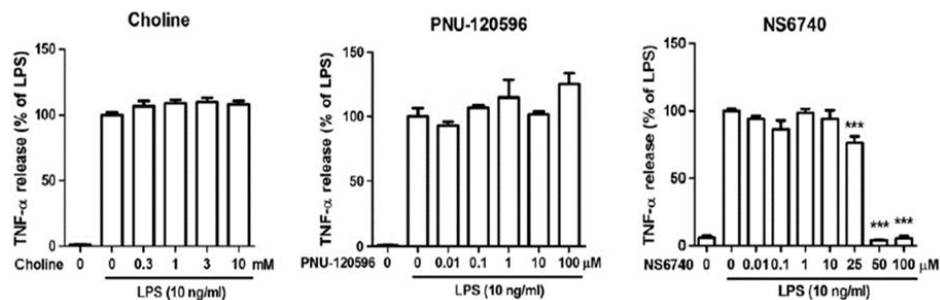


Figure 15: Effects of the $\alpha 7$ agonist choline, PAM PNU-120596 and silent agonist NS6740 on LPS-induced TNF- α release in rat microglia enriched cultures. Rat microglia enriched cultures were exposed to 0.3–10 μ M choline, 0.01–100 μ M PNU-120596 or 0.01–100 μ M NS6740 for 30 min before adding 10 ng/mL LPS for another 4h, after which the culture media were collected and submitted to an ELISA for TNF- α (adapted from J. Neuroimmunol., 2012, 251, 65-72). [76]

Considering the absence of this inhibitory effect in presence of choline (an $\alpha 7$ -selective orthosteric agonist) or PNU-120596 (an $\alpha 7$ -selective PAM), the involvement of receptor non-conducting states in the modulation of inflammatory processes was further confirmed. Nicotine was also able to reduce the release of pro-inflammatory cytokines induced by LPS and this effect was observed only at high concentrations (10 – 100 μ M), at which nicotine induced receptor desensitization. Therefore, the neuroprotective and anti-inflammatory effects of nicotine were hypothesized to depend on the conformational state associated to metabotropic signaling of the $\alpha 7$ nAChR. [66]

Further studies demonstrated that NS6740 is effective in the treatment of inflammatory and neuropathic pain in mouse (i.e. chronic pain and peripheral neuropathy). NS6740 was tested in several *in vivo* mouse pain models. Data recorded revealed that this compound is able to induce significant dose- and time-dependent antinociceptive activity in formalin- and acetic acid-induced nociceptive behaviors as well as in the chronic constrictive nerve injury (CCI) model for neuropathic pain. [66]

Formalin test

The formalin test can be divided into two distinct phases:

- phase I, immediately after formalin injection,
- phase II, known as the inflammatory phase, which starts later after formalin injection.

NS6740 was efficacious in exerting an anti-edema effect, as revealed by the difference in the ipsilateral paw diameter (Δ PD) before and after injection of the

compound (**Figure 16**, panel B). Furthermore, **NS6740** reduced inflammation both in the early and the late phases (**Figure 16**, panel A) and pretreatment with methyllycaconitine (MLA, a selective nicotinic $\alpha 7$ antagonist) totally blocked the observed anti-nociceptive effects, thus proving the $\alpha 7$ mediation (confirmed also by a genetic approach, using $\alpha 7$ receptor KO mice).

The upper left panel of the **Figure 16** (panel A) reports the anti-nociceptive effects of **NS6740** after administration of various doses (0.1, 1, 3, and 9 mg/kg, intraperitoneally) on formalin-induced pain behavior in the mouse. The cumulative pain response of time of licking was measured during the period of 0-5 min (first phase) and 20-40 min (second phase). In the upper right panel of **Figure 16** (panel A) is shown blockage of **NS6740** antinociceptive effects in the formalin test by the $\alpha 7$ antagonist MLA (10 mg/kg, subcutaneously) given 15 min before an active dose of 3 mg/kg of **NS6740** or vehicle. Fifteen min later, mice were injected with formalin and then observed for pain behaviors.

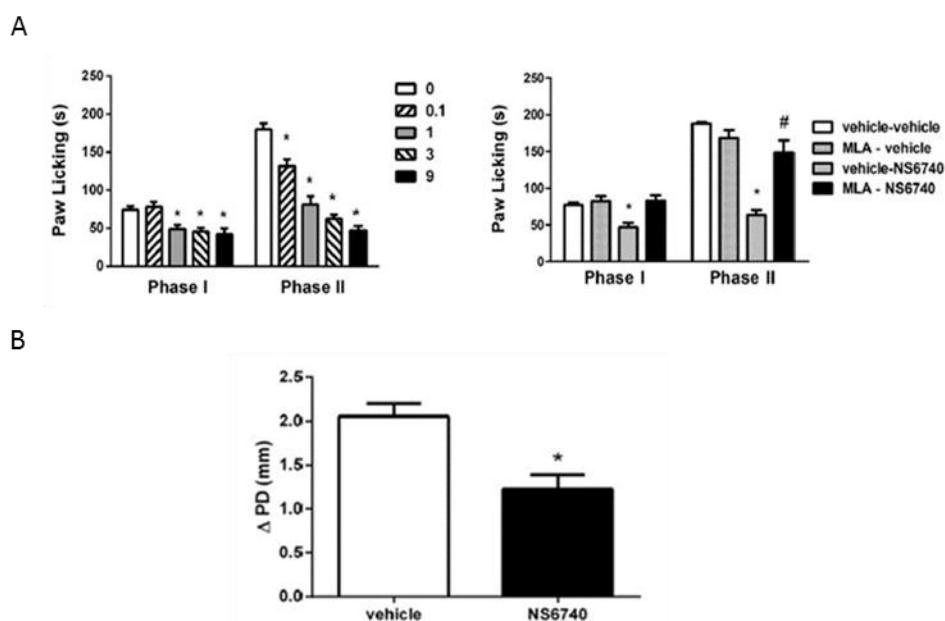


Figure 16: The anti-nociceptive effects of **NS6740** in *in vivo* mouse models of chronic pain. The anti-nociceptive effects of **NS6740** after administration of various doses on formalin-induced pain behavior in the mouse. The cumulative pain response of time of licking is shown in upper left panel A. In upper right panel A is reported the blockage of **NS6740** antinociceptive effects in the formalin test by the $\alpha 7$ selective antagonist MLA. Panel B. Anti-edema effect of **NS6740** (9 mg/kg) in the formalin test, as measured by the difference in the ipsilateral paw diameter before and after injection (Δ PD) (adapted from *Neuropharmacology* 2015, 91, 34-42). [66]

Acetic acid test

To measure the acetic acid-induced nociceptive behavior, each mouse was given an intraperitoneally (i.p.) injection of either vehicle or **NS6740** (1 and 3 mg/kg) and 15 min later they received acetic acid (1%, i.p.). For a total of 60 min, the number of typical writhing behaviors induced after acetic acid injection was recorded together with the number of stretches (a contraction of the abdomen followed by an extension of the hind limbs) (**Figure 17**). The number of writhings decreases as the dose of **NS6740** rises, suggesting that the compound is able to block in a dose-related manner the noxious visceral stimulus induced by i.p. administration of acetic acid in the mouse.

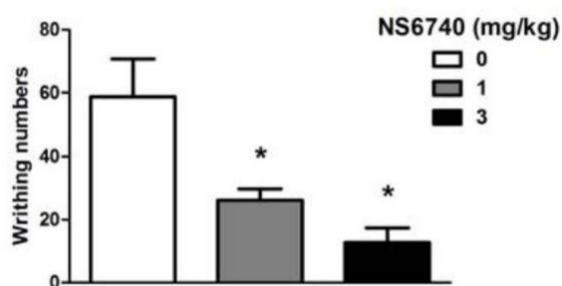


Figure 17: Intraperitoneal injection of **NS6740** (1 or 3 mg/kg) attenuated acetic acid-induced writhing behavior (adapted from *Neuropharmacology* 2015, 91, 34-42). [66]

CCI model

In addition to the effects observed in the formalin and acetic acid tests, **NS6740** significantly attenuated the pain associated with CCI-induced mechanical allodynia in a dose- and time-dependent way. The anti-allodynic effects of **NS6740** were mediated by the $\alpha 7$ receptor since they were totally blocked by pretreatment with the nicotinic antagonist methyllycaconitine MLA (**Figure 18**).

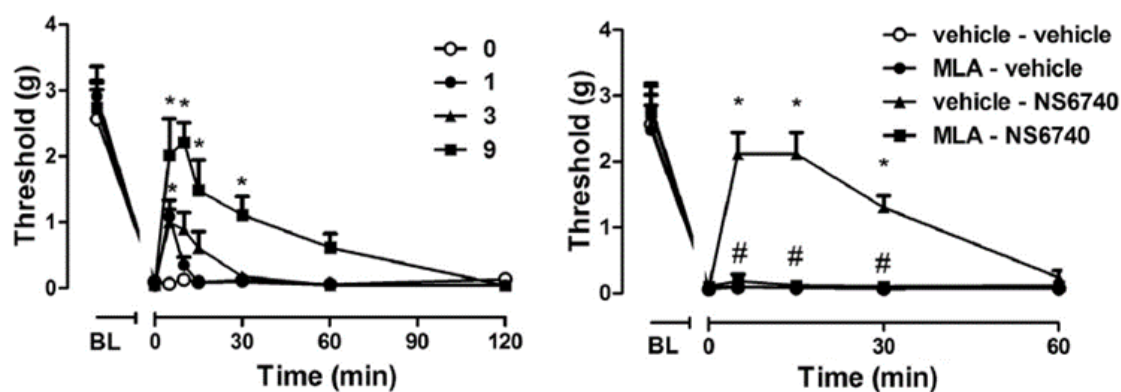


Figure 18: The antiallodynic effects of **NS6740** in chronic constrictive injury (CCI) neuropathic model are dose-dependent (left panel) and mediated by the $\alpha 7$ nAChR, since blocked by methyllycaconitine (MLA) (right panel). **NS6740** (1, 3, and 9 mg/kg, *i.p.*) significantly attenuated CCI-induced mechanical allodynia in a dose-related manner (left panel). Blockade of the antiallodynic effect of **NS6740** in the CCI test by MLA (10 mg/kg, *s.c.*) given 15 min before an active dose of 9 mg/kg of **NS6740** or vehicle proved mediation of the $\alpha 7$ receptor subtype (adapted from *Neuropharmacology* 2015, 91, 34-42). [66]

According to time and concentration dependence, the observed effects were consistent with the $\alpha 7$ desensitized state induced by **NS6740**, supporting the thesis that analgesia can be achieved through non-conducting states of $\alpha 7$ nAChR signal transduction. Overall, these results underlined the therapeutic potential of $\alpha 7$ selective silent agonists in mouse models of tonic and chronic pain and in the treatment of diseases characterized by a strong inflammatory component. However, although **NS6740** resulted to be efficacious in *in vivo* mouse models of chronic pain and inflammation, it appeared to be inactive in a $\alpha 7$ -sensitive cognitive improvement mouse model. The explanation of such a discordant behavior lies in the nature of the $\alpha 7$ nAChR itself, which can function in different modes in distinct cell types. For example, $\alpha 7$ nAChRs expressed in non-excitable immune cells that are involved in inflammation are not conductive in response to the endogenous ligand acetylcholine, meanwhile in neuronal cells involved in cognitive and learning signaling the $\alpha 7$

receptors act as classical ion channels. These evidences support the selective induction of $\alpha 7$ desensitized states promoted by **NS6740**, which may exert disparate effects on different cell types, such as the cells involved in inflammatory processes and the neuronal cells involved in cognition. Besides, the lack of cognitive activity of **NS6740** in the mouse may be explained by the poor penetrability of the compound into the brain. [66] [74] [77]

1.3.2 The silent pharmacophore model

Given the intriguing profiles displayed by silent agonists, a preliminary pharmacophore model was proposed starting from the chemical structure of the archetypal $\alpha 7$ silent agonist **NS6740** (Figure 19).

In detail:

- a positively charged center, represented by the tertiary amine embedded in the diazabicyclic structures;
- a central portion capable of forming hydrogen bond, represented by the amide carbonyl;
- an aryl group, potentially suitable for a wide range of structural modifications.

All the elements of this pharmacophore model are in specific angular relationships.

In order to test the validity of this proposed model, **KC-1** (Figure 19) was designed as a simpler analog of **NS6740**, containing the three pharmacophore features described above. [78]

The silent agonism displayed by **KC-1** when tested in the electrophysiological assays (results described in detail in the following paragraph 1.3.3), demonstrated the reliability of this preliminary pharmacophore model and **KC-1** was considered a successful test ligand of the model.

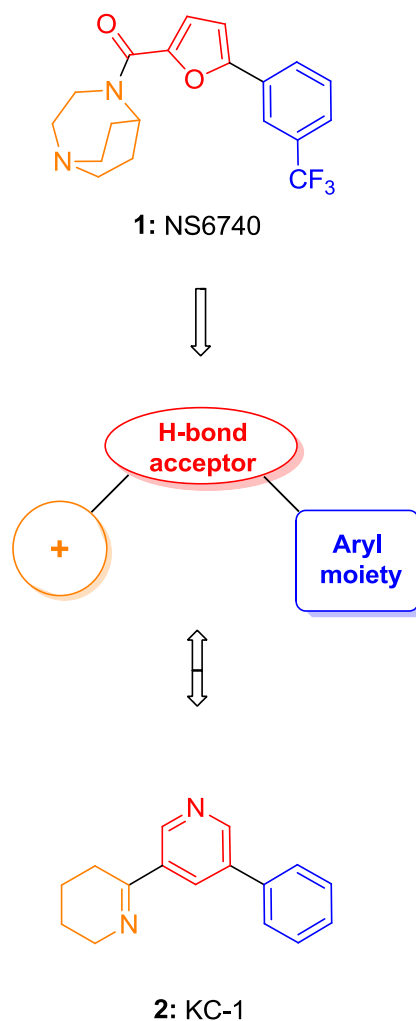


Figure 19: General pharmacophoric features of silent agonists.

1.3.3 The silent agonist KC-1

KC-1 is a derivative of the non-selective nAChR agonist anabaseine, where the introduction of an additional phenyl ring in position 5 of pyridine provided an $\alpha 7$ selective silent agonist. [78] **KC-1** was tested on human $\alpha 7$ nAChRs expressed in *Xenopus laevis* oocytes and employing two-electrode voltage clamping. **KC-1** was assayed alone at 100 μM , in order to test its agonist profile; then, 100 μM **KC-1** was co-applied with 60 μM of ACh control to investigate the ability of inducing ACh control inhibition. Finally, 100 μM **KC-1** was co-applied with the type II PAM PNU-120596 to detect receptor desensitization. The results are shown in **Figure 20**.

When tested alone at 100 μM (Figure 20, panel A), **KC-1** did not show agonist behavior, with no channel opening observed (peak current 0.004 ± 0.001 , net charge 0.083 ± 0.009). When 100 μM **KC-1** was co-applied with 60 μM ACh control (Figure 20, panel B), a strong decrease in ACh response was detected, thus demonstrating the control inhibitory activity of **KC-1** (peak current 0.17 ± 0.08 , net charge 0.29 ± 0.06). The final co-application of 100 μM **KC-1** and 10 μM PNU-120596 (Figure 20, panel C) gave an intense potentiated response (peak current 4.10 ± 0.68 , net charge 17.8 ± 2.4), revealing the stabilization of D_s state by **KC-1**.

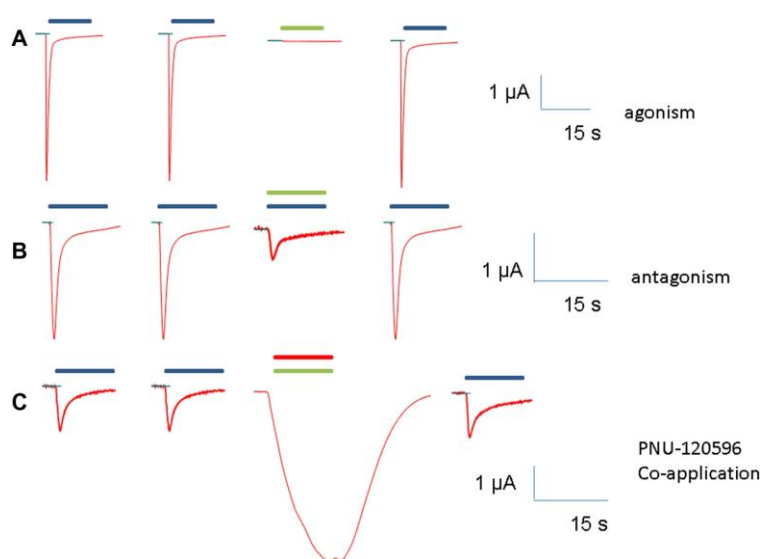


Figure 20: Representative traces of the *ha7* nAChR response to applications of **KC-1**. Blue bars represent duration of ACh applications, green bars the **KC-1** application, and the red bar represents PNU-120596 application. A) Application of 100 μM **KC-1**; B) Application of 100 μM **KC-1** plus 60 μM ACh; C) Application of 100 μM **KC-1** plus 10 μM PNU-120596 (adapted from *Bioorg. Med. Chem. Lett.* 2013, 23, 4145-4149). [78]

Moreover, **KC-1** inhibited the responses evoked by 60 μM ACh control with an IC_{50} value of 41 ± 5 μM . The selectivity conferred by the additional phenyl group was proven in a control experiment in which the $\alpha 7$ selective antagonist methyllycaconitine (MLA) (100 nM) totally blocked the response to 100 μM **KC-1** co-applied with 10 μM PNU-120596.

CHAPTER II

Aims of the thesis

The current PhD research project aimed at investigating the $\alpha 7$ nAChR signal transduction mediated by compounds characterized by the silent agonism profile. The attention to the $\alpha 7$ nAChR silent agonism is emerging in the last few years, since growing evidence supports the implication of this new type of $\alpha 7$ receptor modulation in anti-inflammatory processes, *via* metabotropic activation, and, as previously mentioned, the metabotropic-like activity seems to be related to $\alpha 7$ receptor desensitization. [66] [67] [65] [76] Silent agonists are compounds that do not show an intense ionotropic activity, but induce the non-conducting receptor states and promote receptor desensitization over activation. The $\alpha 7$ silent ligands represent not only significant probes for the mechanistic investigation of the $\alpha 7$ receptor, but appear to be also interesting potential therapeutic tools mainly for peripheral pain and inflammatory diseases.

In this context, my PhD research focused on in depth study of the alternative metabotropic modulation of the $\alpha 7$ nAChRs, in particular through the synthesis of new analogs of the two well-known silent agonists **NS6740** and **KC-1** and their electrophysiological investigations. This project aimed at giving a further contribution to clarifying the mechanistic complexity surrounding the $\alpha 7$ nAChR activation/function, and at better defining the structural requirements that promote and tune the silent activity profile. Indeed, the investigation of the $\alpha 7$ silent activation may allow to achieve additional insights on $\alpha 7$ receptor desensitization.

NS6740 and **KC-1** were taken as model compounds because of their ability to promote the $\alpha 7$ receptor desensitization and given the presence in their skeleton of common structural pharmacophoric features (**Figure 19**). Thus, both compounds appeared useful pharmacological tools to further clarify some aspects of the ligand-receptor interaction able to induce the $\alpha 7$ silent modulation. Moreover, **NS6740** shows *in vivo* efficacy in mouse models of chronic pain and inflammation and this effect is related to its ability to induce non-conducting ligand-bound conformational states. Thus, **NS6740** and other related $\alpha 7$ silent agonists may represent putative therapeutic agents in the treatment of chronic inflammatory and neuropathic pain.

On this basis, with the purpose (I) to elucidate the pharmacophore features for silent agonists, (II) to shed light on the ligand-receptor interactions that are able to induce the $\alpha 7$ desensitized states, (III) to discover new silent agonists, and besides aiming also (IV) at a better understanding of the receptor desensitized states and their dynamic balance, which are responsible for the metabotropic function, we planned:

- to synthesize **NS6740** fragments (compounds **11-16**) and **NS6740** and **KC-1** analogs (compounds **17-33** and **34-40**, respectively) (**Table 1**)
- to establish the electrophysiological profile of the new compounds by employing human $\alpha 7$ nAChRs expressed in *Xenopus laevis* oocytes and two electrode voltage clamping. In this electrophysiological investigation, to evidence and evaluate the silent properties of the new compounds, we determined (i) channel activation, (ii) inhibition of ACh responses, (iii) responses potentiated by the PAM PNU-120596.
- to deduce the structure-activity relationships associated with the electrophysiological properties.
- to perform preliminary investigations about silent ligand-receptor molecular interactions through molecular modeling study of the most interesting compounds by docking them into a homology model of the $\alpha 7$ receptor and also by using $\alpha 7$ receptor mutants.

My PhD research activity started by considering the preliminary silent pharmacophore model which has been obtained from the scaffolds of the silent agonists **NS6740** and **KC-1**, as described in Paragraph 1.3.3. of the Introduction Section (**Figure 19**). [78] This model is characterized by a positively charged center, a central hydrogen bond acceptor and an aryl moiety, and represents an initial definition of the structural features required to induce the silent activation of the $\alpha 7$ receptor.

In order to provide a deeper pharmacophoric description and achieve a better understanding of steric and electronic features able to promote silent agonism through induction of non-conducting ligand-bound conformational states, a variety of structural modifications have been planned and performed on the three key pharmacophoric portions in the skeleton of the model silent compounds **NS6740** and **KC-1** (**Figure 19**):

- basic nucleus, represented by the 1,4-diazabicyclo[3.2.2]nonane system and the 3,4,5,6-tetrahydropyridine ring in **NS6740** and **KC-1**, respectively;
- hydrogen bond acceptor moiety, represented by the amide carbonyl group and the central pyridine ring in **NS6740** and **KC-1**, respectively;
- aryl fragment, represented by the *meta*-trifluoromethyl phenyl group and the unsubstituted phenyl ring in **NS6740** and **KC-1**, respectively.

In particular, with the aim to evaluate the importance of the distance between the positive charged center and the hydrogen bond acceptor portion, the original basic nucleus of the two lead compounds was replaced by new bicyclic and monocyclic moieties with the basic nitrogen in different positions, thus obtaining shorter or longer distances between the two key pharmacophoric features. Then, the hydrogen bond acceptor portion was deleted or modified by the insertion of a different hydrogen bond acceptor moiety, whereas the aromatic portion was substituted in *meta* position by chemical groups displaying different electrostatic and polar properties, and, in the **NS6740** skeleton, also replaced by different aromatic and heteroaromatic moieties.

The chemical modifications planned on **NS6740** and **KC-1** were carried out not only for structure-activity relationship studies to better delineate the silent pharmacophoric features but also aimed at developing new chemical entities worthy to be considered for further *in vitro* and *in vivo* anti-inflammatory investigations. Preliminary *in silico* studies were also carried out on the lead compounds and the most interesting newly synthesized analogs, with the purpose to shed light on the relationships between their observed functional profile and their binding to the $\alpha 7$ receptor subtype.

2.1 SAR study on NS6740

Firstly, the silent agonist **NS6740** was taken as a model compound due to its peculiar ability to induce prolonged desensitized activity. To identify the essential structural features able to promote the silent agonist behavior, two different chemical modification approaches were applied to its scaffold:

- i. fragmentation of **NS6740** molecular skeleton: synthesis of fragments to highlight the role of each structural portion in inducing the $\alpha 7$ silent activation and the peculiar prolonged receptor binding exhibited by the lead;
- ii. design and synthesis of novel **NS6740** analogs: the structure of this model compound was dissected into three major fragments corresponding to the key pharmacophoric regions and a number of chemical modifications were introduced on the three portions.

2.1.1 Fragmentation of NS6740 molecular skeleton

To identify the molecular fragments of NS6740 responsible for inducing non-ionotropic activation of the $\alpha 7$ receptor by promoting and stabilizing its desensitized conformations, a fragmentation of the NS6740 molecular scaffold (Figure 21) was planned through a progressive deletion of its structural portions. The new chemical entities should allow to clarify which key structural elements are still able to preserve the silent agonist profile.

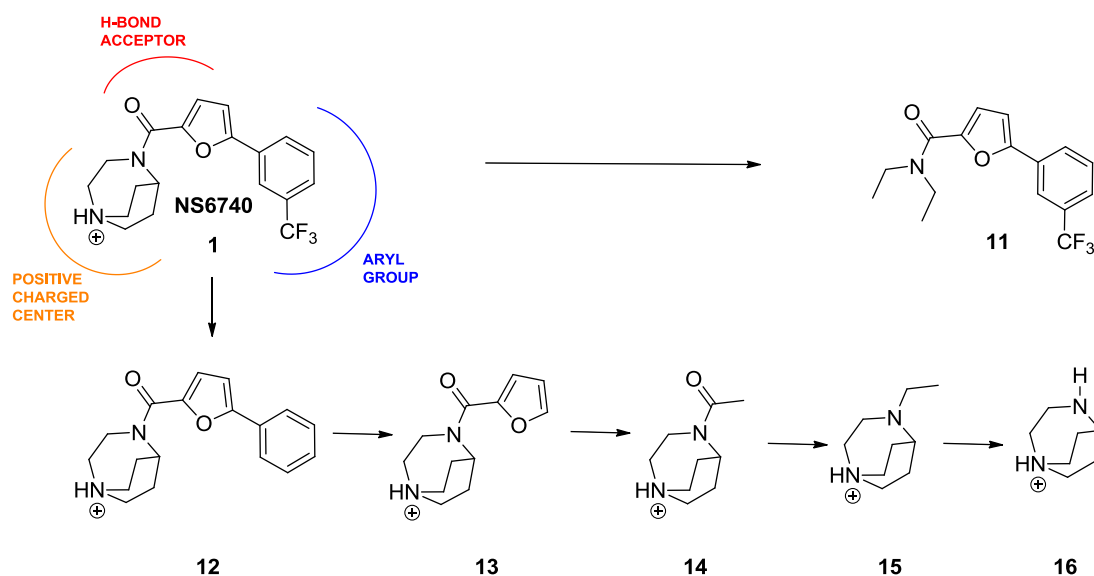


Figure 21: Fragmentation of the NS6740 molecular skeleton.

First of all, in order to evaluate the influence of the basic nitrogen into the diazabicyclic nucleus for receptor interaction and stabilization of non-conducting states, derivative **11** was designed by removing the diazabicyclic system while maintaining a diethyl amide group. At the opposite side of the lead molecular skeleton, the *meta*-trifluoromethyl group on the phenyl ring was removed (**12**) to investigate its role in generating silent agonism. Then, compound **13** was planned by deleting the phenyl ring and preserving only two out of three pharmacophoric features, i.e. the basic diazabicyclic moiety and the bridge carbonyl connected with the furan ring, i.e. the positively charged center and the hydrogen bond acceptor, respectively.

The NS6740 scaffold was further reduced by progressive removal of the furan ring (**14**) and the carbonyl group (**15**). Finally, in compound **16** only the azabicyclic

nucleus is preserved. Therefore, the two smallest fragments, **15** and **16**, exhibit the positively charged center as the sole pharmacophoric feature.

2.1.2 Design and synthesis of novel NS6740 analogs

To further shed light on the pharmacophore characteristics and to identify novel compounds characterized by the peculiar pharmacological profile of silent agonists, three series of NS6740 derivatives were also designed and synthesized.

The structural modifications were planned and performed on the three portions of the NS6740 skeleton, i.e. the diazabicyclic nucleus, the central carbonyl group and the *m*-trifluoromethyl phenyl moiety, corresponding to the three pharmacophoric features (Figures 22, 23, 24).

With regard to the positively charged center of the above illustrated pharmacophore, the 1,4-diazabicyclo[3.2.2]nonane system of NS6740 has been variously modified to investigate if the new basic portion are still able to maintain the electrostatic interactions promoting and stabilizing the non-conducting desensitized $\alpha 7$ receptor states (Figure 22). Firstly, the original 1,4-diazabicyclo[3.2.2]nonane nucleus was converted into the corresponding quaternary methyl ammonium salt (**17**). Indeed, the positive charge center can be either a protonatable nitrogen or a permanently positively charged ion, i.e. a quaternary ammonium head. However, a permanent charge could generate strong ionic interactions that may lead to conformational receptor changes and induce different desensitization states, which would result in a different electrophysiological profile than that of the corresponding protonated salt. Then, the 1,4-diazabicyclo[3.2.2]nonane nucleus was substituted by the regioisomer 1,3-diazabicyclo[3.2.2]nonane (**18**) to evaluate the importance of the distance between the positive charged nitrogen atom and the hydrogen bond acceptor carbonyl moiety in preserving the suitable orientation in the ligand binding receptor site able to promote the silent activation. Finally, the enantiomeric derivatives **19** and **20**, characterized by the presence of the (*S,S*)- and the (*R,R*)-2,5-diazabicyclo[2.2.1]heptane nucleus respectively, were planned and synthesized. The novel basic diazabicyclic ring has smaller dimension than the 1,4-diazabicyclo[3.2.2]nonane system of NS6740 and includes a secondary amine instead of the tertiary amine of the parent compound. These structural modifications could give rise to different electrostatic and spatial interactions within the receptor binding pocket, which could lead to a variation of the electrophysiological profile.

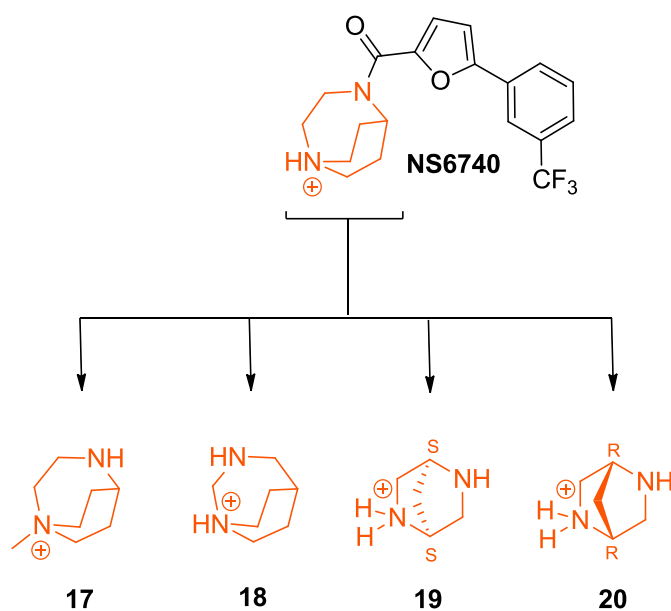


Figure 22: Modified target compounds at the azabicyclic nucleus of NS6740.

In order to investigate the potential influence of hydrogen-bond interactions over the silent agonist activity of the model compound, derivative **21** was designed by removing the carbonyl group (**Figure 23**). Compound **21** lacks the amide bond and is characterized by a second protonatable nitrogen atom in the bicyclic system and by a more flexible structure due to the methylene bridge connecting the diazabicyclic nucleus and the furan ring. These structural differences with respect to the parent compound might deeply influence the ligand-receptor interactions.

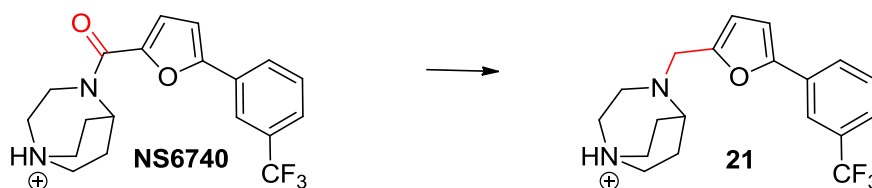


Figure 23: Structure of the target NS6740-related derivative without the carbonyl group.

Finally, as illustrated in **Figure 24**, a series of structural variations were planned at the aryl moiety of NS6740. In particular, preserving the diazabicyclic-carbonyl-furan scaffold as the key element, the novel derivatives **22-27** and **32-33** arose by introduction of different substituents in *meta* position of the phenyl ring, in analogy

to the parent compound. The substituents were chosen according to their different chemical nature, electrostatic properties and steric bulkiness, which would allow to establish different bonding interactions in the $\alpha 7$ receptor binding site.

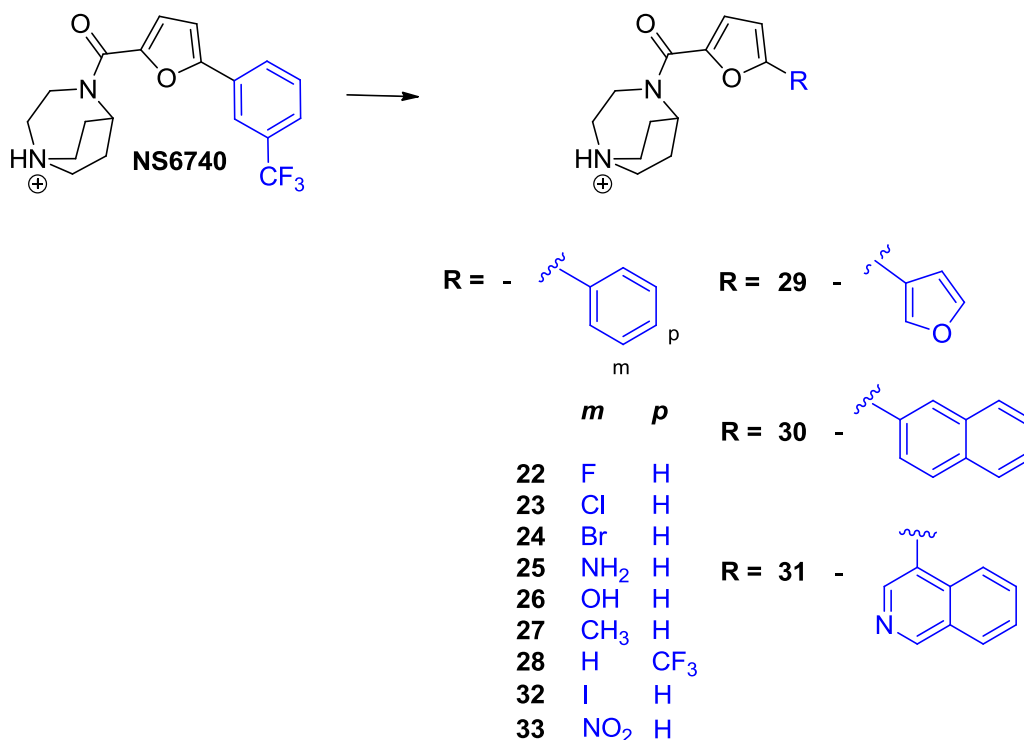


Figure 24: Structures of the target NS6740-related derivatives modified at the aryl group.

To evaluate the influence of halogen bonding interactions over the silent agonist activity of NS6740, a set of derivatives was designed by inserting the halogen atoms of increasing size, i.e. fluorine (**22**), chloride (**23**), bromine (**24**) and iodine (**32**), in the *meta* position of the aromatic moiety. Then, amino (**25**), hydroxyl (**26**) and nitro (**33**) groups as polar substituents with hydrogen-bond electron-donor or acceptor properties and a methyl group (**27**), as a isosteric replacement of the trifluoromethyl group, were introduced. Furthermore, the trifluoromethyl group was moved from the *meta* to the *para* position of the phenyl ring (**28**). The shift of this substituent could lead to a relocation of the aryl portion conferring a different grade of interaction capability, which might affect the interactions within the receptor binding pocket. Finally, the influence of a different side aromatic portion was investigated by replacing the phenyl moiety with the heteroaromatic furan ring (**29**) a naphthalene (**30**) and an isoquinoline (**31**) group to estimate whether the receptor binding pocket would bear a greater steric hindrance and still preserve the silent agonist activity.

2.2 SAR study on KC-1

The experimental work on **KC-1** derivatives described in this thesis has been carried out in the Department of Chemistry at the University of Florida under the supervision of Dr. Nicole A. Horenstein during my one year stay in Gainesville (Florida - USA) as a visiting researcher.

Still focusing the attention on the investigation of $\alpha 7$ nAChR signal transduction mediated by compounds characterized by the silent agonism profile, the silent agonist **KC-1** was taken as model compound to further explore the previously described silent pharmacophore model. As reported in the introduction section, **KC-1** binds in the same $\alpha 7$ binding site as ACh but favors the D_s state without channel opening, and thus acts as a silent agonist; however the stabilization of non-conducting receptor states promoted by **KC-1** is shorter than that induced by **NS6740**. [78]

To add further information to the pharmacophore requirements for $\alpha 7$ silent agonism and also aiming at identifying new compounds characterized by a silent profile, a series of structural modifications were planned on the three pharmacophoric portions of the **KC-1** skeleton by applying a similar approach to that used for **NS6740**.

Firstly, the cyclic imine nucleus of **KC-1** was modified to evaluate the relevance of the distance between the basic imine nitrogen and the pyridine nitrogen atom with hydrogen bond properties. In particular, the secondary amine **34** and the corresponding methyl tertiary amine **35** and dimethyl ammonium quaternary salt **36**, were designed and synthesized (**Figure 25**). The novel derivatives differ in terms of electrostatic properties and bulky features with respect to the parent compound and might establish different interactions within the bonding pocket.

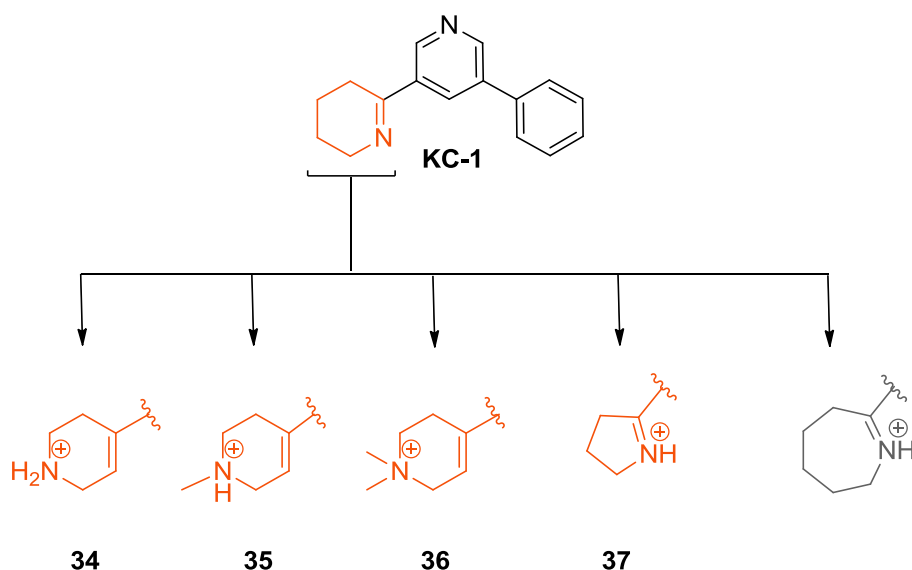


Figure 25: Structures of target compounds related to **KC-1** cyclic imine nucleus modifications.

Furthermore, the pyrroline ring (**37**) as lower cyclic homologue of the tetrahydropyridine nucleus was introduced. Conversely, the derivative with the corresponding cyclic upper homologue, 3,4,5,6-tetrahydro-2*H*-azepine, in grey in **Figure 26**, was not obtained because the equilibrium towards the open chain is strongly favored with respect to the closed cyclic imine.

Then, the hydrogen-bond acceptor pharmacophoric region was investigated by isosteric replacement of the pyridine ring with the furan ring (**38**), which is present in the structure of **NS6740** (**Figure 26**).

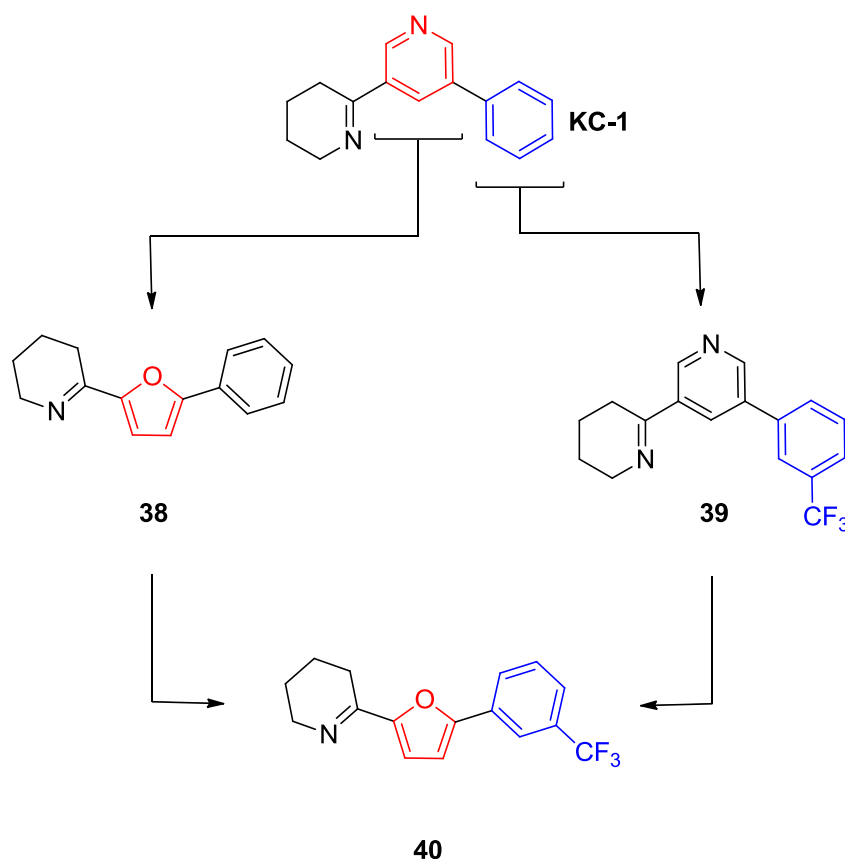


Figure 26: Structures of target compounds related to **KC-1**: modifications of the central hydrogen-bond acceptor and aromatic portions.

Noteworthy, always according to the structural and spatial determinants of the silent agonist **NS6740**, the phenyl moiety of **KC-1** skeleton was modified in *meta* position by introduction of a trifluoromethyl group (**39**), which is present also in the structures of the silent agonist **TFM-diEPP**, as reported in the introduction section (**Figure 11**). Finally, derivative **40** was designed and synthesized by applying the molecular hybridization approach, which is a structural modification tool to design new molecules with improved bioactivity. Hybrid **39** displays the basic cyclic imine of **KC-1**, as positively charged center, combined with the furan and *p*-trifluoromethyl phenyl moieties of **NS6740**, as hydrogen-bond acceptor and aryl portions. The electrophysiological investigation of **40** could help to achieve additional information to better define the silent pharmacophore features.

In this thesis, I will illustrate the synthetic routes to the designed derivatives (**Table 1**) and discuss the pharmacological results and the docking studies. The new compounds were assayed in electrophysiological experiments to determine their functional activation of the target $\alpha 7$ nAChR.

	Cmp	Structure	Cmp	Structure	
NS6740 derivatives	NS6740		22		
	11		23		
	12		24		
	13		25		
	14		26		
	15		27		
	16		28		
	17		29		
	18		30		
	19		31		
	20		32		
	21		33		
	KC-1 derivatives	KC-1		37	
		34		38	
		35		39	
		36		40	

Table 1: Structures of the lead compounds NS6740 and KC-1 and their related target compounds.

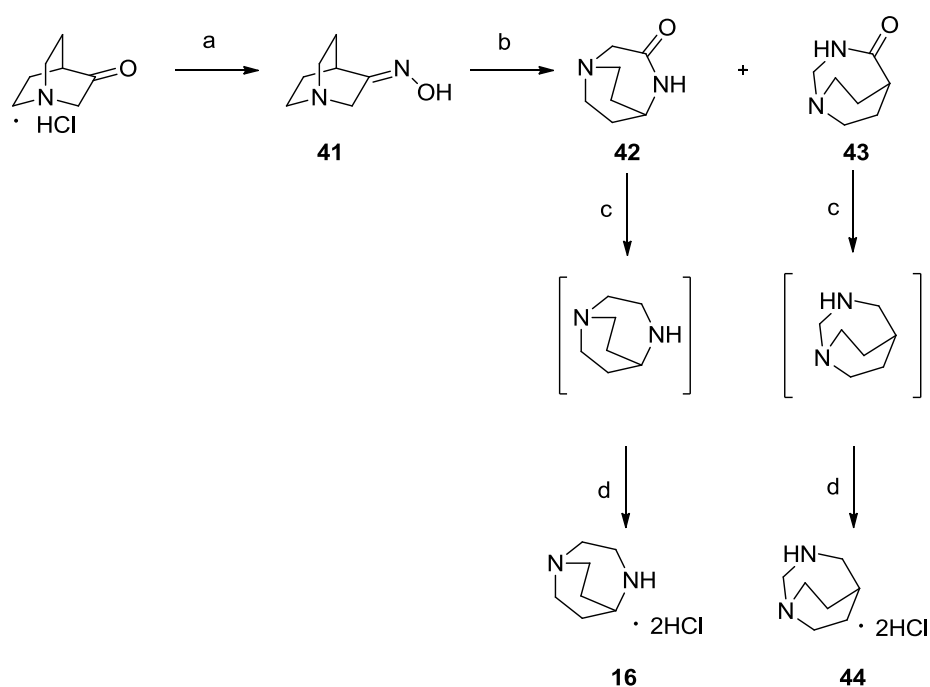
CHAPTER III

Chemistry

3.1 Synthetic approaches to NS6740-related derivatives

3.1.1 Synthesis of 1,4-diazabicyclo[3.2.2]nonane hydrochloride (16) and 1,3-diazabicyclo[3.2.2]nonane hydrochloride (44)

Compounds **16** and **44** were prepared partially following a patented procedure [79], showed in **Scheme 1**.



Scheme 1: Synthesis of 1,4-diazabicyclo[3.2.2]nonane dihydrochloride and 1,3-diazabicyclo[3.2.2]nonane dihydrochloride. Reagents and conditions: a) $\text{NH}_2\text{OH} \cdot \text{HCl}$ (1.15 equiv), CH_3COONa (3 equiv), H_2O , 70 °C, 1 h; b) $\text{H}_{n+2}\text{P}_n\text{O}_{3n+1}$, 130 °C, 20h; c) 1 M LiAlH_4 in THF (1.2 equiv), 0 °C to reflux, overnight; d) 4 M HCl in dioxane (2 equiv), r.t., overnight.

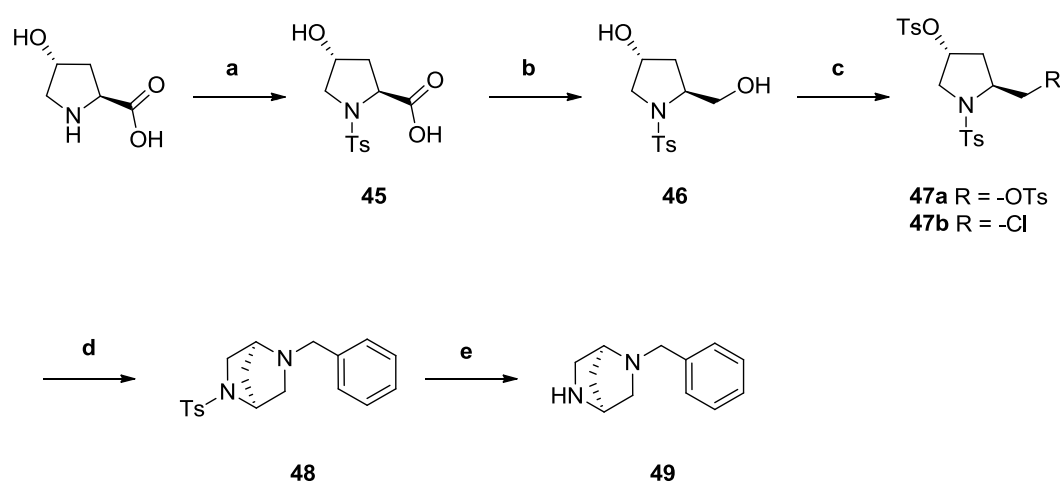
The carbonyl group of the commercially available quinuclidine-3-one hydrochloride was converted into the corresponding oxime **41** by reaction with hydroxylamine hydrochloride and sodium acetate in water. The subsequent Beckmann rearrangement allowed the transformation of the oxime group into the amide, giving the enlargement of the original ring. Polyphosphoric acid at 130° was employed and the ring expansion led to the two corresponding lactam regioisomers, with a prevalence of **42** over **43** (6:1). Silica gel column chromatography allowed the separation of two regioisomers, and the following reduction, in the presence of

lithium aluminum hydride, led to 1,4-diazabicyclo[3.2.2]nonane and 1,3-diazabicyclo[3.2.2]nonane free bases. Given their high volatility, the crude free bases were reacted with a 4M hydrochloric acid and **16** and **44** were finally isolated as their corresponding dihydrochlorides by recrystallization from MeOH and Et₂O.

3.1.2 Synthesis of (*S,S*) and (*R,R*)-2-benzyl-2,5-diazabicyclo[2.2.1]heptane (**49** and **57**)

The preparation of the pair of enantiomers **49** and **57** was achieved partially following a procedure reported in literature. [80]

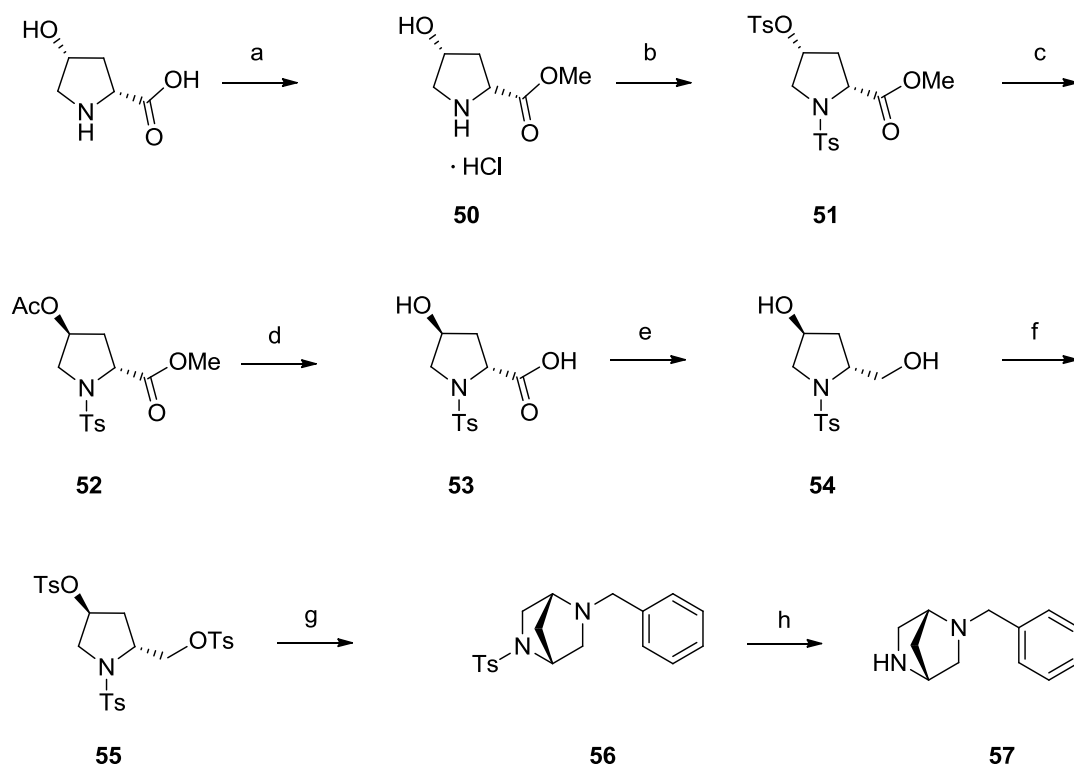
Compound **49** was synthesized starting from the commercially available *trans*-4-hydroxy-L-proline (**Scheme 2**), whose secondary amine was initially protected with the tosyl group using *p*-toluensulfonyl chloride and sodium carbonate as a base. The following reduction of the *N*-tosylated hydroxyproline **45** was carried under mild conditions given by the employment of BH₃ in THF, at variance with a procedure reported in the literature.



Scheme 2: Synthesis of (*1S,4S*)-2-benzyl-2,5-diazabicyclo[2.2.1]heptane. Reagents and conditions: a) TsCl (1.2 equiv), Na₂CO₃ (2.10 equiv), water, 0 °C to r.t., 48 h; b) 1 M BH₃ dry THF complex (2 equiv), 0 °C to r.t., overnight; c) TsCl (5 equiv), dry pyridine (4.8 equiv), DMAP (0.2 equiv), dry DCM, 0 °C to r.t., overnight; d) benzylamine (10 equiv), MeOH, 95 °C, overnight; e) 33% HBr/AcOH, 60 °C, 2h.

The resulting diol **46** was then bis-tosylated in pyridine and in the presence of DMAP, giving the key tritosylated intermediate **47a**. From the same reaction, even the chloro intermediate **47b** was isolated. Since compound **47b** resulted to be less reactive under the following cyclization conditions, after separation by silica gel chromatography, only compound **47a** was used for the reaction in the presence of benzylamine in MeOH, leading to the cyclized compound **48**. The final cleavage of tosyl group was achieved using 30% hydrogen bromide and acetic acid at 50 °C. The precipitated dihydrobromide was treated with saturated aqueous solution of Na₂CO₃ and extracted with a mixture of DCM and *i*-PrOH giving the free amine **49**.

Compound **57** was synthesized starting from commercially available *cis*-4-hydroxy-D-proline (**Scheme 3**).



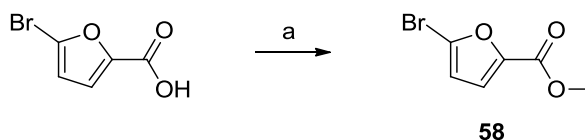
Scheme 3: Synthesis of (1R,4R)-2-benzyl-2,5-diazabicyclo[2.2.1]heptane. Reagents and conditions: a) 1.25 M HCl in MeOH, 0 °C to reflux, 6 h; b) TsCl (6.6 equiv), pyridine, Et₃N (3 equiv), 0 °C, 15 h; c) tetraethylammonium acetate (1.3 equiv), dry toluene, reflux, 4 h; d) KOH (5 equiv), *r.t.*, 3 h; e) 1 M BH₃ dry THF complex (3 equiv), 0 °C to *r.t.*, 6 h; f) TsCl (2 equiv), dry pyridine (4.8 equiv), DMAP (0.2 equiv), dry DCM, argon, 0 °C, 27 h; g) benzylamine (10 equiv), MeOH, 95 °C, overnight; h) 33% HBr/AcOH, 60 °C, 5 h.

Esterification of the carboxylic moiety was carried out in MeOH in the presence of hydrochloric acid, achieving the corresponding methyl ester **50** as hydrochloride. The following reaction in the presence of *p*-toluensulfonyl chloride, pyridine and triethylamine provided compound **51** showing both *O*- and *N*-tosylation. The inversion of the configuration relative to the substituent on position 4 was obtained employing tetraethyl ammonium acetate at 110 °C, giving acetyl derivative **52**. The subsequent de-acylation as well as hydrolysis of methyl ester were carried out in KOH at room temperature, affording compound **53**, the corresponding enantiomer of **45**. Intermediate **53** underwent the same synthetic steps described for its enantiomer **45**, *via* the tritosylated intermediate **55**, cyclization in the presence of benzylamine (*N*-tosyl derivative **56**) and final conversion to the free base **57**.

3.1.3 Synthesis of the aromatic acyl chlorides 97-110

The synthetic procedure for the preparation of aromatic chains started from a Suzuki-Miyaura coupling, employing methyl 5-bromofuran-2-carboxylate **58**, simply prepared from the commercially available 5-bromofuran-2-carboxylic acid (**Scheme 4**), and then differently substituted commercially available boronic acids (**59-70**) (**Scheme 5**).

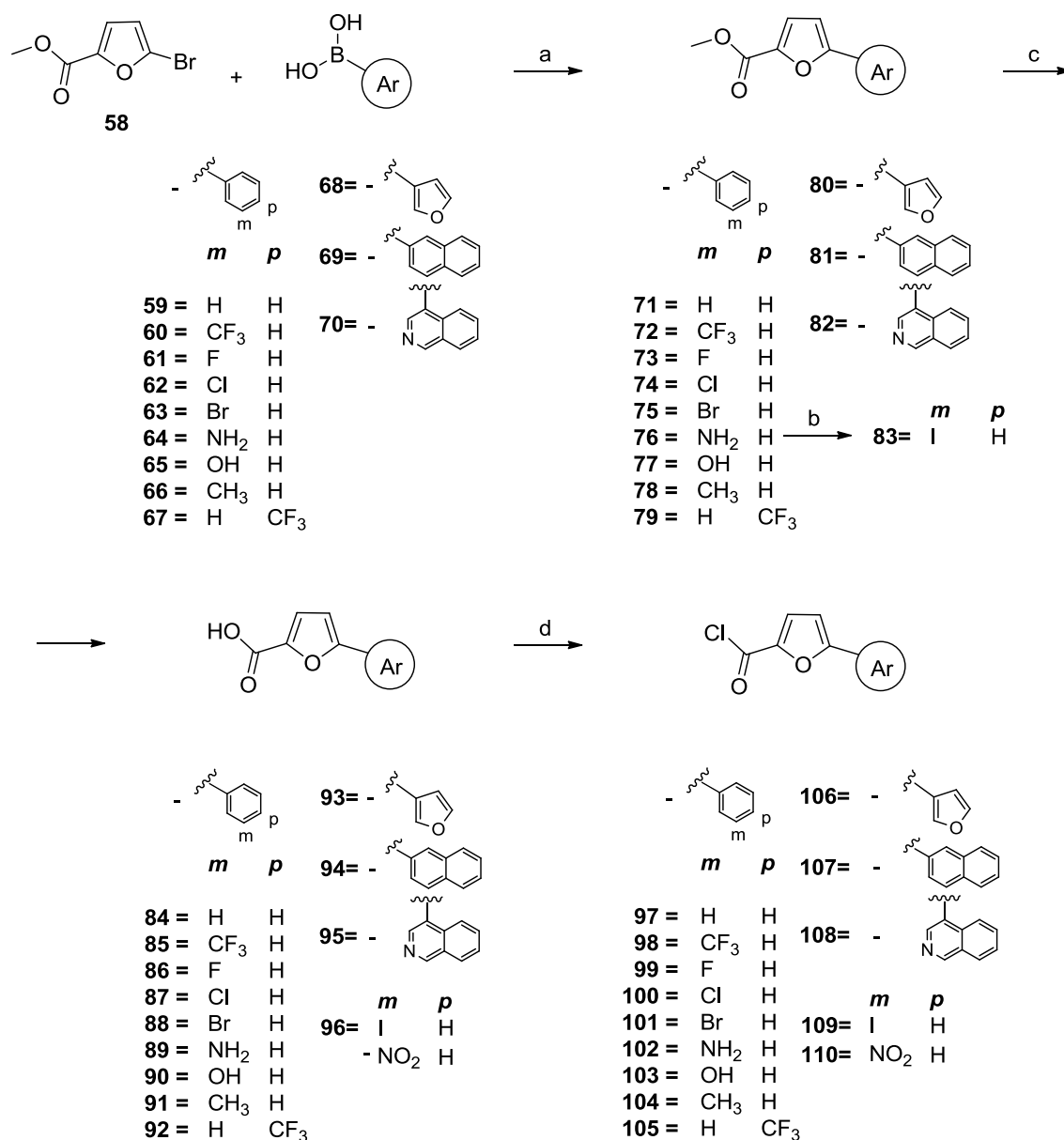
The reactions were carried out in inert conditions in the presence of 2M Na₂CO₃ in DME and tetrakis (triphenylphosphine)palladium(0) Pd(PPh₃)₄ as the catalyst; due to solubility issues, DMF was instead used as solvent with the isoquinoline boronic acid **70**. The ester intermediates **71-82** were obtained in high yields, between 60 and 90%. Considering the issues due to the reactivity of iodine in Suzuki conditions, derivative **83** was prepared from the corresponding amino derivative **76** *via* diazonium salt and subsequent substitution with potassium iodide.



Scheme 4: Synthesis of methyl 5-bromofuran-2-carboxylate. Reagents and conditions:
a) Conc. H₂SO₄ (0.2 mL/mmol), MeOH, reflux, overnight.

The subsequent saponification, conducted in presence of NaOH in THF at room temperature, provided the corresponding carboxylic acids **84-89** and **91-96**.

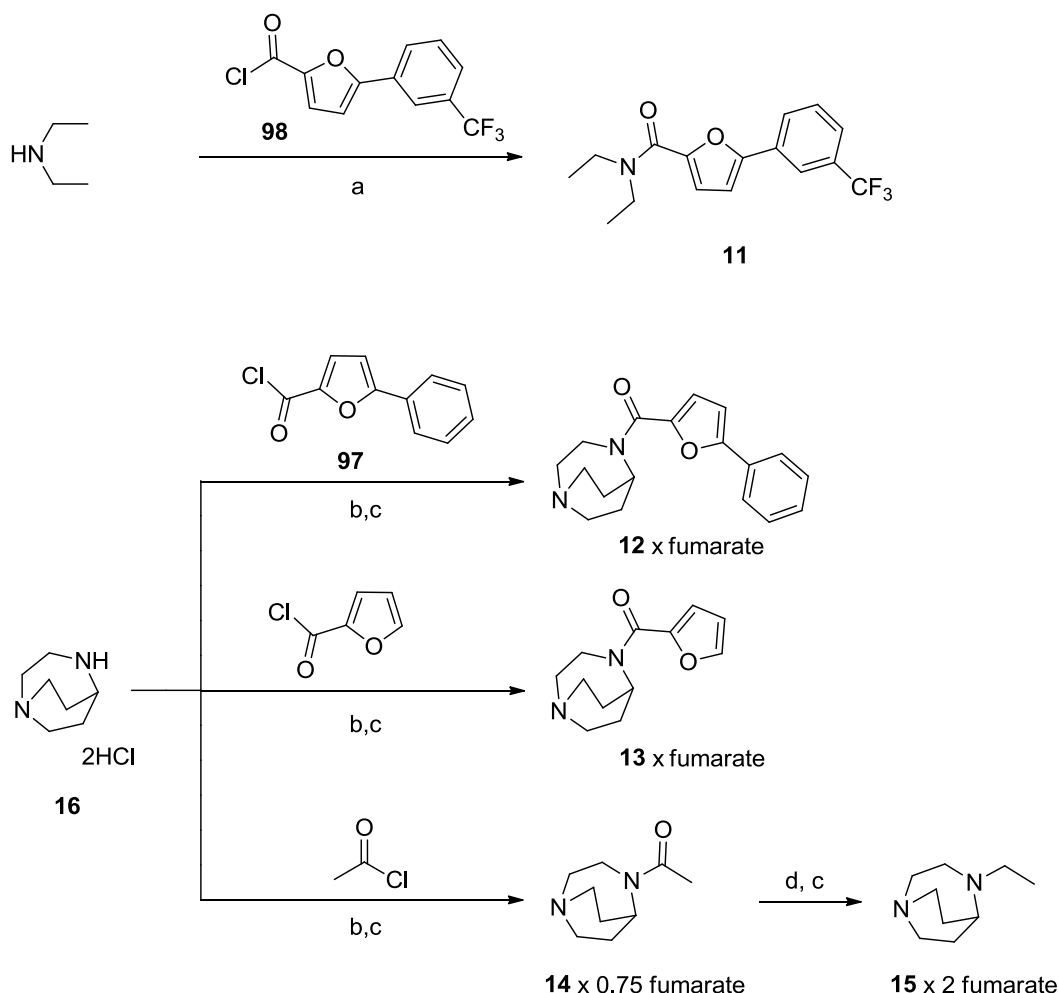
Derivative **90** required the employment of LiOH as base to give the hydrolysis of methyl ester (**77**). Finally, all the carboxylic acid intermediates were reacted with thionyl chloride at reflux in neat conditions, affording the corresponding acyl chlorides **97-109**. The commercially available 3-nitrophenyl furoic acid was also introduced in this pool of compounds and reacted with thionyl chloride, giving compound **110**.



Scheme 5: Synthesis of aryl-furoyl acyl chlorides moieties. Reagents and conditions: a) Pd(PPh₃)₄ (0.05 equiv), Na₂CO₃ (4.20 equiv), DME or DMF, argon, reflux, 3-12 h; b) NaNO₂ (1.05 equiv), conc. H₂SO₄ (0.2 mL/mmol), KI (1.50 equiv), 0 °C, 6 h; c) 1.5 M NaOH (1.5 equiv), THF, r.t., overnight or 2.5 M LiOH (2 equiv), THF, r.t., 72 h; d) SOCl₂ (2 mL/mmol), reflux, 2-4 h.

3.1.4 Synthesis of NS6740 fragments 11-15

As reported in **Scheme 6**, fragment **11** was prepared from the previously synthesized acyl chloride **98** reacted with diethylamine in presence of TEA. After purification by silica gel column chromatography, the final compound **11** was isolated with 50% yield. Fragments **12**, **13** and **14** were synthesized through nucleophilic substitution of 1,4-diazabicyclo[3.2.2]nonane dihydrochloride **16** with the appropriate acyl chloride. The acylation reactions were conducted in anhydrous and inert conditions, in the presence of cesium carbonate, used as base, and DMF at room temperature with final yields between 50-60%. Reduction of compound **14**, under anhydrous and inert environment, with lithium aluminum hydride in dry diethyl ether, produced fragment **15**.

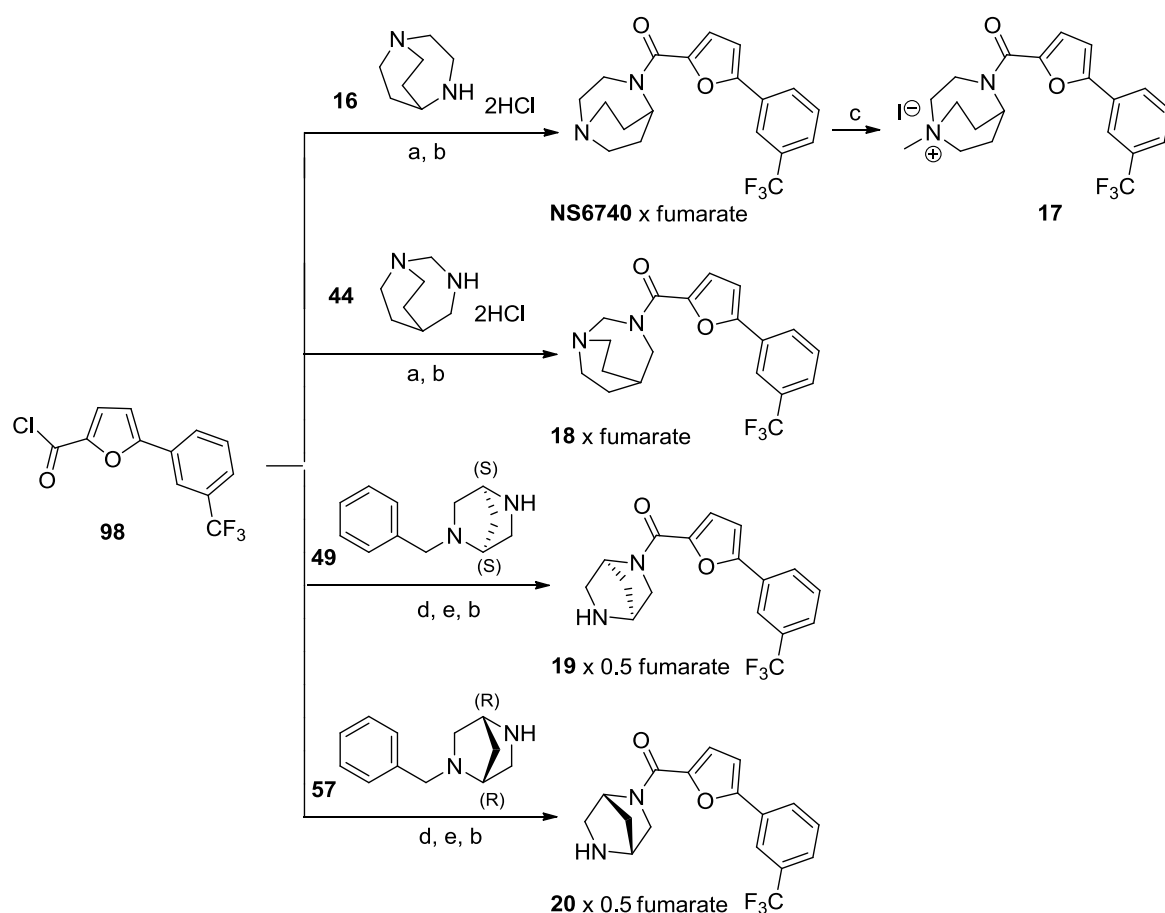


Scheme 6: Synthesis of the fragments of NS6740. Reagents and conditions: a) TEA (1 equiv), dry DCM, r.t., 1.5 h; b) Cs₂CO₃ (5 equiv), dry DMF, r.t., overnight; c) fumaric acid (1 equiv), MeOH, r.t., overnight; d) LiAlH₄ (2.25 equiv), dry Et₂O, 0 °C to reflux, 3 h.

3.1.5 Synthesis of NS6740 and related derivatives 17-20

Scheme 7 reports the synthetic steps employed for the preparation of **NS6740** and some related analogs. The preparation of the lead compound **NS6740** was achieved through the acylation of 1,4-diazabicyclo[3.2.2]nonane dihydrochloride **16** with 5-(3-trifluoromethyl)phenyl)furan-2-carbonyl chloride **98**, employing the same conditions previously described for compounds **12-14**. Pure final compound **1** was obtained by crystallization from MeOH as fumaric acid salt. The corresponding **NS6740** free base was methylated with MeI in MeOH affording the corresponding quaternary ammonium salt **17**, crystallized from *i*-PrOH/MeOH.

The acyl chloride **98** was also reacted with the regioisomer 1,3-diazabicyclo[3.2.2]nonane dihydrochloride **44**, providing the final fumarate **18**, crystallized from EtOH/Et₂O.

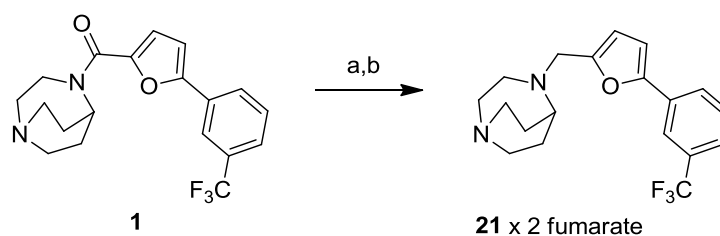


Scheme 7: Synthesis of NS6740-related analogs. Reagents and conditions: *a*) Cs₂CO₃ (5 equiv), dry DMF, r.t., overnight; *b*) fumaric acid (1 equiv), MeOH, r.t., overnight; *c*) MeI, MeOH, r.t., overnight; *d*) TEA (1.10 equiv), dry 1,4-dioxane, r.t., overnight; *e*) H₂, Pd/C (10%), r.t., overnight.

Finally, the enantiomers **49** and **57** were acylated with **98** in dry 1,4-dioxane, then submitted to catalytic hydrogenation (H_2 over 10% Pd/C) to cleave the protecting benzyl groups. The resulting free amines were treated with fumaric acid and crystallized from EtOH/*i*-PrOH/Et₂O, giving the final salts **19** and **20**.

3.1.6 Reduction of the carbonyl group of NS6740

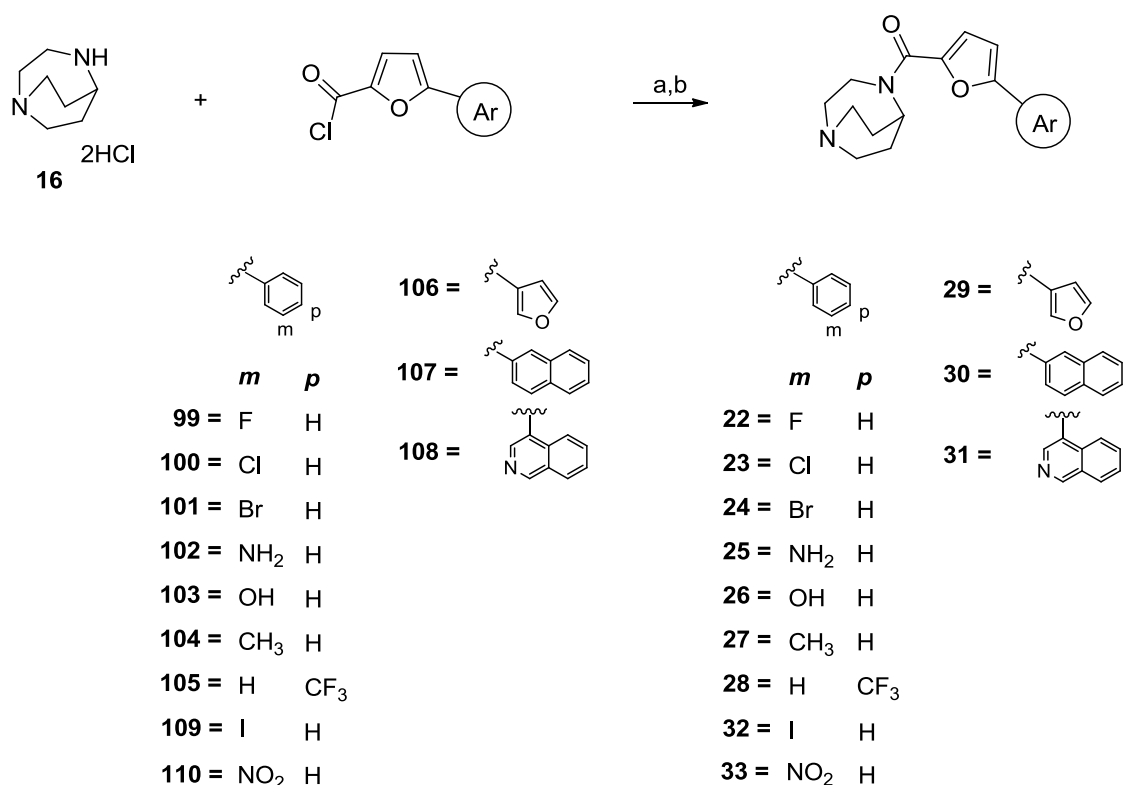
The free base of **NS6740** was also treated with lithium aluminium hydride in diethyl ether under anhydrous and inert atmosphere, affording **21**, the reduced analog of our model compound, which was purified as fumaric acid salt (**Scheme 8**).



Scheme 8: Synthesis of compound 21. Reagents and conditions: a) LiAlH_4 (2.25 equiv), dry Et_2O , 0°C to reflux, 2 h; b) fumaric acid (1 equiv), MeOH, r.t., overnight.

3.1.7 Synthesis of NS6740 derivatives 22-33

Newly designed compounds **22-33** were prepared *via* acylation of 1,4-diazabicyclo[3.2.2]nonane **16** with the previously described aromatic acyl chlorides **99-110**, using cesium carbonate as base and dry DMF (**Scheme 9**). After workup and extraction, the corresponding free bases were reacted with fumaric acid: the final salts were purified through recrystallization from appropriate solvent mixtures.

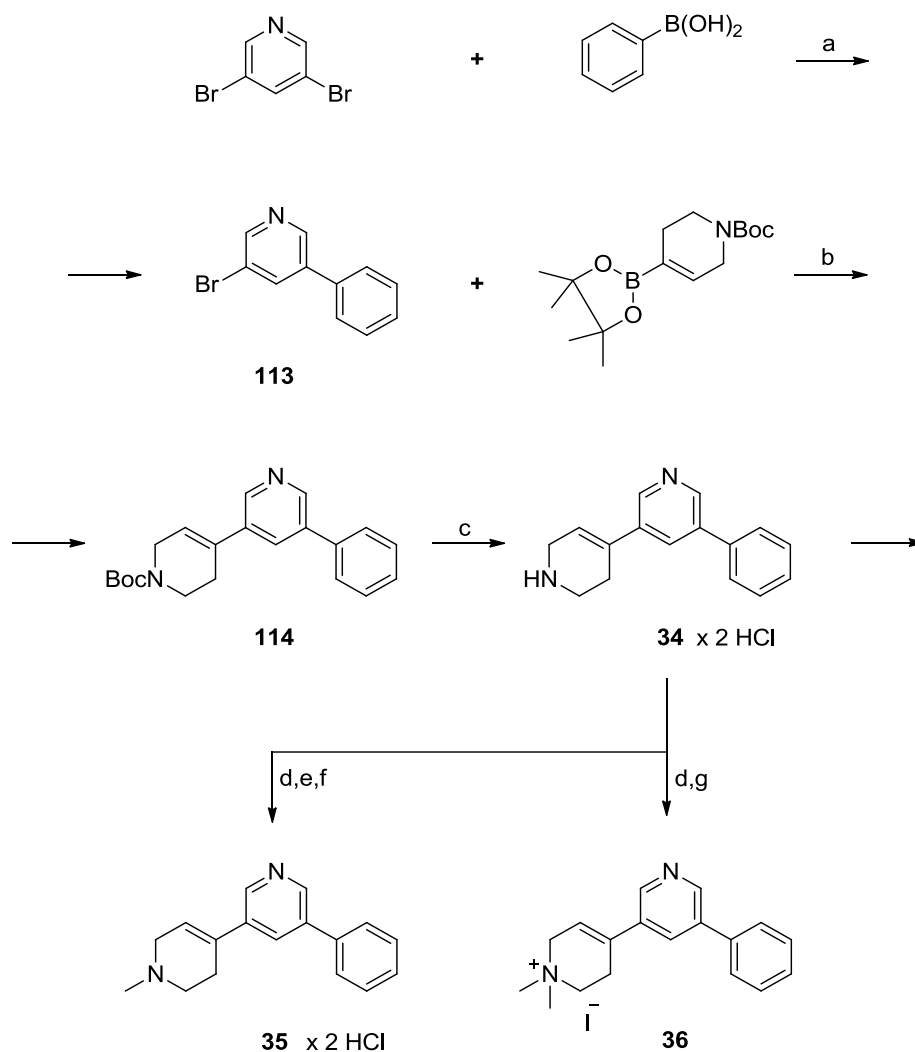


Scheme 9: Synthesis of differently substituted NS6740 analogs. Reagents and conditions: a) Cs₂CO₃ (5 equiv), dry DMF, r.t., overnight; b) fumaric acid (1 equiv), MeOH, r.t., overnight.

3.2 Synthetic approaches to the KC-1-related analogs

3.2.1 Synthesis of KC-1 derivatives 34-37

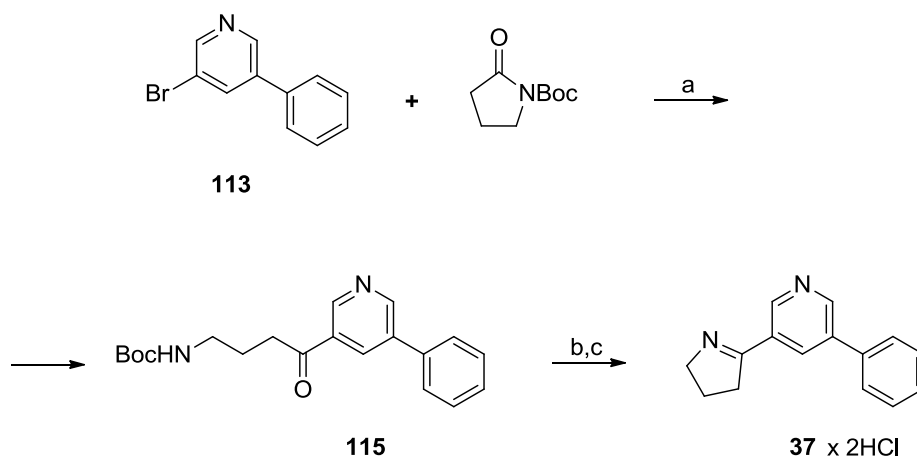
The synthetic procedure leading to derivatives **34-37** is depicted in **Scheme 10**. Compound **34** was prepared through a three step sequence starting from a Suzuki-Miyaura coupling between commercially available 3,5-dibromopyridine and phenyl boronic acid, in the presence of $\text{Pd}(\text{PPh}_3)_4$ and 2 M K_2CO_3 in DME.



Scheme 10: Synthesis of KC-1-related analogs **34-36**. Reagents and conditions: a) $\text{Pd}(\text{PPh}_3)_4$ (0.02 equiv), 2 M K_2CO_3 (3.35 equiv), DME/ H_2O , reflux, 4 h; b) $\text{Pd}(\text{PPh}_3)_4$ (0.05 equiv), 2 M Na_2CO_3 (4.20 equiv), DMF, 110 °C, 24 h; c) HCl/MeOH (10 equiv), r.t., 12 h; d) 1 M NaOH (1.3 equiv) e) 37% HCHO (10 equiv), NaBH_3CN (1.5 equiv), HCl, CH_3CN , r.t., 18h, NaOH; f) HCl/MeOH (2 equiv), r.t.; g) MeI (2 equiv), NaHCO_3 (1 equiv), MeOH, 0 °C, 7h.

The resulting coupled compound **113** was then reacted in a second Suzuki-Miyaura reaction with commercially available *tert*-butyl 4-(4,4,5,5-tetramethyl-1,3,2-dioxaborolan-2-yl)-5,6-dihydropyridine-1(2H) carboxylate, affording the Boc-protected intermediate **114**. Both Suzuki-Miyaura reactions were characterized by \approx 80% yields. The protecting group of **114** was cleaved with a methanol solution of hydrochloric acid and the wanted final base **34** was recrystallized as the corresponding hydrochloride. Next, **34** was reacted with an aqueous formaldehyde solution (37%) in the presence of NaBH₃CN and HCl, giving the monomethylated amine **35**, which was recrystallized as hydrochloride. Alternatively, **34** was reacted with MeI in MeOH at 0° giving the quaternary ammonium salt **36**.

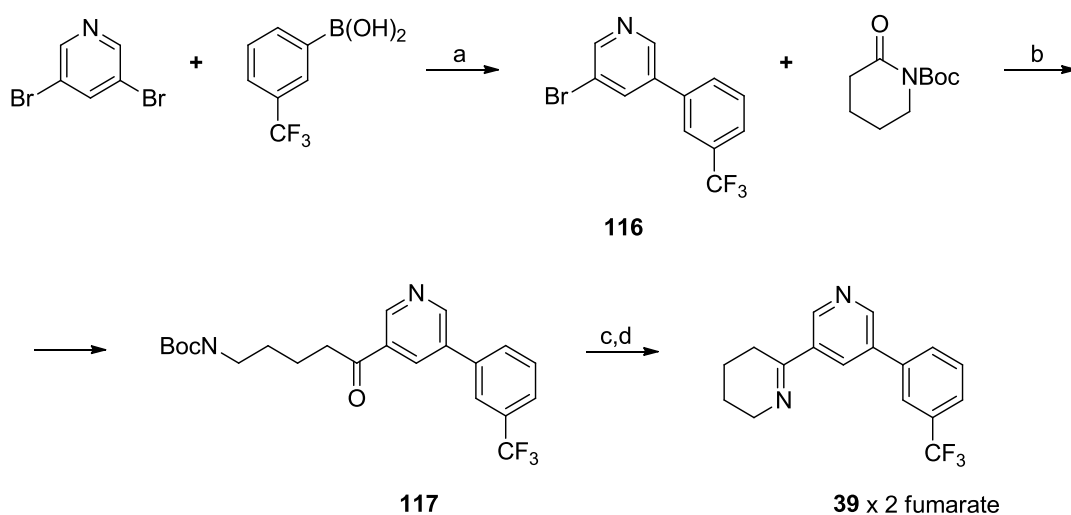
Compound **37** (**Scheme 11**) was prepared starting from intermediate **113** *via* transmetallation [81] in the presence of *n*BuLi at -78 °C and *N*-Boc-2-pyrrolidinone, which gave the open compound **115** in 60% yield. The latter was deprotected and cyclized with trifluoroacetic acid and then, after quenching with 5 M NaOH, was isolated as the free base **37**. This compound was purified as the related hydrochloride upon recrystallization from EtOH.



Scheme 11: Synthesis of KC-1 derivative **37**. Reagents and conditions: a) 1.6 M *n*BuLi (1 equiv), dry Et₂O, -78 °C; b) TFA (3 mL/mmol), DCM, 0-5°C, 2 h, 5 M NaOH; c) HCl/MeOH (2 equiv).

3.2.2 Synthesis of KC-1 derivatives 38-40

Scheme 12 reports the synthetic pathway leading to derivative **39**, which was prepared starting from a Suzuki-Miyaura coupling between commercially available 3,5-dibromopyridine and 3-trifluorophenyl boronic acid that gave **116**, under the same conditions employed to obtain the previous intermediate **113**. Reaction of **116** with *n*BuLi at $-78\text{ }^{\circ}\text{C}$ and treatment with commercially available *N*-Boc-2-piperidone gave the intermediate open form **117**, which was treated with trifluoroacetic acid to provide the cyclized compound **39**. Upon quenching with 5 M NaOH, the free base **39** was reacted with fumaric acid and recrystallized as the corresponding salt. Isolation of this derivative was characterized by low yield due to the moderate instability under several recrystallization conditions.

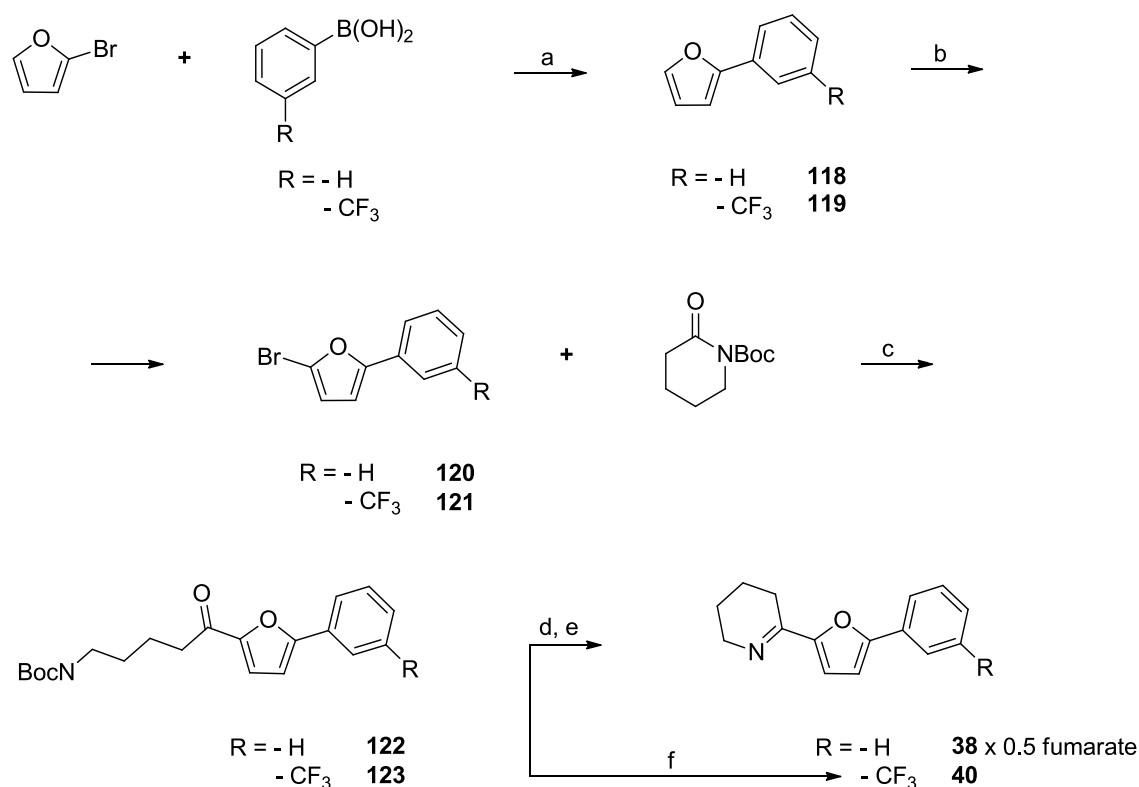


Scheme 12: Synthesis of compound 39. Reagents and conditions: a) $\text{Pd}(\text{PPh}_3)_4$ (0.02 equiv), 2 M K_2CO_3 (3.35 equiv), DME/ H_2O , reflux, 4 h; b) 1.6 M *n*BuLi (1 equiv), dry Et_2O , $-78\text{ }^{\circ}\text{C}$, 2 h; c) TFA (3.4 mL/mmol), DCM, $0-5\text{ }^{\circ}\text{C}$, 2 h, 5 M NaOH; d) fumaric acid (1 equiv), MeOH, r.t..

Newly designed compounds **38** and **40** were prepared as shown in **Scheme 13**, starting from a Suzuki-Miyaura coupling reaction between commercially available 2-bromofuran and either phenyl boronic acid or 3-trifluoromethyl phenyl boronic acid, using $\text{Pd}(\text{PPh}_3)_4$ and 2 M Na_2CO_3 in DME/ H_2O .

Coupled intermediates **118** and **119** were obtained in 60-80% yield. Then, they were reacted in the presence of *N*-bromosuccinimide at $0\text{ }^{\circ}\text{C}$ that allowed the selective bromination on position 2 of the furan ring. Intermediates **120** and **121** were isolated

via silica gel column chromatography. Both compounds **120** and **121** displayed the typical NMR signals of a 2,4-disubstituted furan ring, represented by two doublet signals with coupling constant $J = 3.4$ Hz, as well as the correct proton integration of phenyl portions, thus demonstrating that selective bromination on position 2 of the furan ring occurred. The transmetalation of compounds **120** and **121** was carried out in presence of *n*BuLi at -78 °C, followed by reaction with *N*-Boc-2-piperidone. The pure isolated protected open chain intermediates **122** and **123** were treated with trifluoroacetic acid, obtaining the cleavage of the protecting group coupled with a cyclization reaction. After quenching with 5 M NaOH, the free bases **38** and **40** were reacted with fumaric acid; compound **38** was easily recrystallized from MeOH/EtOH, while compound **40** gave a non crystalline precipitate under several conditions; hence it was characterized and tested as free imine.



Scheme 13: Synthesis of compound **38** and **40**. Reagents and conditions: a) $\text{Pd}(\text{PPh}_3)_4$ (0.03 equiv), 2 M Na_2CO_3 (4.2 equiv), DME/ H_2O , 60 °C, 6 h; b) NBS (1 equiv), DMF, 0 °C, 1 h; c) 1.6 M *n*BuLi (1 equiv), dry Et_2O , -78 °C, 2 h; d) TFA (3.6 mL/mmol), DCM, 0-5 °C, 2 h; e) fumaric acid (1 equiv), MeOH, *r.t.*; f) 5 M NaOH.

CHAPTER IV

Electrophysiological investigations

4.1 General pharmacological considerations

The newly synthesized compounds were tested for silent agonist activity in two-electrode voltage clamping experiments on human $\alpha 7$ nAChRs expressed in *Xenopus laevis* oocytes. [75] The assays were performed in the research group led by Prof. Roger L. Papke at the Department of Pharmacology and Therapeutics, College of Medicine, University of Florida, Gainesville.

The responses evoked at the $\alpha 7$ nAChR by the tested derivatives can be reported as peak current or net charge values measured at a holding potential of -60 mV. During drug application, the $\alpha 7$ receptors could be subjected to channel synchronization, a phenomenon reported in 1.2.3 paragraph. As already described, since the net charge values are less affected by channel synchronization than peak currents, the first ones are characterized by greater physiological relevance and scientific validity. [29] [82] Therefore, we took into account net charge values to analyze and compare our results.

Noteworthy, high levels of agonist binding site occupancy induce concentration-dependent desensitization of the $\alpha 7$ receptor subtype, which affects the relationship between peak current and net charge.

For each tested derivative, the net charge values represent the average of the responses from at least four different oocytes. For each oocyte, the test response was normalized for the average of the first two ACh pre-controls. The electrophysiological data are illustrated in **Figures 27-41** and in **Tables 2-11**. In **Figures 27-41** only the net charge responses are reported on vertical axis of bar graphs, whereas **Tables 2-11** display both the net charge and the peak current values evoked by compounds.

4.1.1 Pharmacological protocols for NS6740 and related derivatives

As reported in the Introduction, **NS6740** displays peculiar prolonged receptor binding and strong ability to stabilize the desensitized states of $\alpha 7$ nAChR. Several experiments have demonstrated its interesting behavior, as shown in **Figure 13** [66] and **Figure 14** [37] (Chapter I). Due to its characteristic electrophysical profile, for the screening of **NS6740** we employed a particular protocol named “**two-shot experiment**”: after two applications of 60 μ M ACh pre-control, used to normalize the

channel responses, 10 μM test drug was delivered in order to test its ability to promote channel opening. Then, 60 μM ACh post-control was delivered to verify the ability of the test drug to remain in the binding site and induce a prolonged desensitized state. Next, the application of 10 μM of type II PAM PNU-120596 aimed at revealing the residual desensitized states induced by the test drug. The interesting aspect of this procedure is that **NS6740** was given to the cell only at the beginning of the experiment, but its inhibiting effect for ACh control and the response potentiation given by PNU-120596 were still detected after several minutes and repeated washouts (as described in detail in the following Paragraph 4.2), thus verifying the previous results (**Figure 13** [66] and **Figure 14** [37]). Finally, 60 μM ACh post-control at the end of the test aimed at determining the desensitization or rundown of the $\alpha 7$ receptor or residual potentiation following the application of the PAM.

The newly synthesized **NS6740** derivatives **11-33** were initially tested employing the two-shot experiment as well, in order to highlight the presence of long-lasting desensitizers among the novel set of compounds.

A second protocol named “**one-shot experiment**” was then followed: after two applications of 60 μM ACh pre-control, used to normalize the channel responses, 10 μM test drug was delivered in co-application with 10 μM type II PAM PNU-120596. Finally, the delivery of 60 μM ACh post-control at the end of the test aimed at determining the residual desensitization or potentiation of the $\alpha 7$ receptor. Differently from the two-shot experiment, this protocol helped us to highlight the presence of short-lasting desensitizers in our pool of new **NS6740**-related derivatives. Short-lasting silent agonists do not give either channel activation or prolonged desensitization when tested alone, but they give channel potentiation only in co-application with PNU-120596.

We will comment on the one-shot data only for those compounds which are relevant to the discussion. In the following paragraphs of this and the next chapter, residual PAM-potentiation refers to PNU-120596 potentiated responses observed in two-shot experiments, while direct PAM-potentiation identifies PNU-120596 potentiated responses detected in one-shot experiments.

After these initial experiments, the most interesting desensitizing agents identified among the newly synthesized **NS6740** derivatives were additionally tested at different concentrations and/or in recovery studies. Depending on the specific aim of the investigation, the following protocols were applied:

- **Two-shot and one-shot procedures carried out at 1, 3, 30 μM :** besides the different test drug concentration, the protocols consisted of the same subsequential steps reported above.
- **Recovery study:** after two 60 μM ACh pre-controls, used to normalize the subsequent responses, 10 μM of test drug was applied, followed by six shots of 60 μM ACh post-controls given at six different increasing time points; final shot of 10 μM PNU-120596 to evaluate the residual channel potentiation.

Finally, the potency (EC_{50}) of the strongest partial agonists evidenced among the new derivatives was determined through the **concentration-response curves (CRCs)**, by measuring the responses evoked by test drug at different concentrations. In addition to the electrophysiological investigations at the $\alpha 7$ subtype, the best desensitizers and strongest partial agonists of the series were also assayed on heteromeric $\alpha 4\beta 2$ and $\alpha 3\beta 4$ nAChRs.

To compare the results for different compounds and different concentrations, statistical analyses were performed. We applied two-tailed t-tests and calculated the corresponding P values. By conventional criteria, the differences were considered statistically significant if the P value was lower than 0.05.

4.1.2 Pharmacological protocols for KC-1-related derivatives

Differently from the electrophysiological investigation of **NS6740**, in the procedure employed for **KC-1** and its derivatives **34-40**, the inhibition of ACh control and the receptor potentiation given by PNU-120596 were evaluated in co-application with the tested drug. This was due to the shorter residence time displayed by the lead compound **KC-1**.

The newly synthesized **KC-1** derivatives were assayed in order to evaluate three different behaviors:

- **Agonist activity:** after two 60 μM ACh pre-controls, used to normalize the channel responses, 100 μM test drug alone was applied, to estimate the channel opening. Finally, 60 μM ACh post-control was delivered.
- **ACh inhibition:** after two 60 μM ACh pre-controls, used to normalize the channel responses, 100 μM test drug was co-applied with 60 μM ACh, to

estimate the control inhibiting ability. Finally, 60 μM ACh post-control was delivered.

- **Agonist response potentiation:** after two 60 μM ACh pre-controls, used to normalize the channel responses, 100 μM test drug was co-applied with 10 μM PNU-120596, to estimate the potentiated response. Finally, 60 μM ACh post-control was delivered.

The newly synthesized **KC-1** derivatives **34-37** were also tested on heteromeric $\alpha 4\beta 2$ nAChRs (**Table 10**).

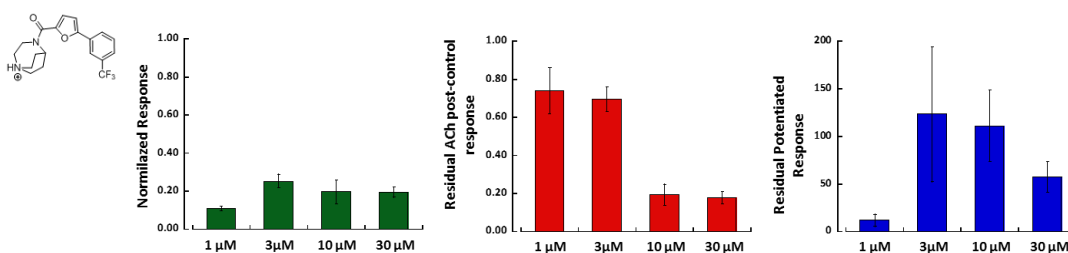
4.2 Electrophysiological profile of NS6740

The nAChR profile of **NS6740** was defined following the previously described two-shot and one-shot experiments, and the most recent results we obtained are reported in **Figure 27** and **Table 7**.

NS6740 presented a very weak partial agonist behavior at all four different concentrations tested (**Figure 27**). In particular, 1 and 3 μM concentration did not show strong ACh post-control inhibition, but the following application of PNU-120596 gave a remarkably potentiated response, especially at 3 μM (net charge 123 ± 71). We hypothesized that low concentrations of **NS6740** were able to bind only a small fraction of the $\alpha 7$ receptors, and out of these only a limited number of the available binding sites were actually affected by the compound. This low binding rate was not enough to give receptor desensitization, thus allowing the subsequent ACh post-control to bind the still accessible binding sites and give channel opening. The 181 s wash-out after the post-control effectively removed the ACh without affecting the binding of **NS6740**, as evidenced by the following application of the type II PAM. Indeed, in the two-shot experiment PNU-120596 produced intense receptor potentiation, revealing the prolonged residence time of **NS6740** in the $\alpha 7$ subtype.

NS6740

(1) A Two shot EXPERIMENT



B One shot EXPERIMENT

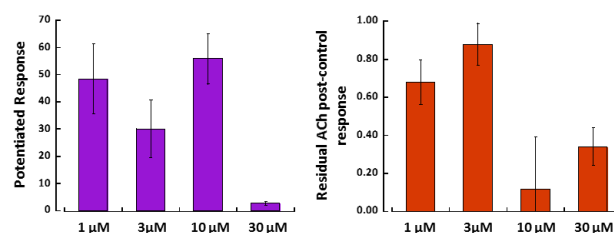


Figure 27: Electrophysiological profile of NS6740 assayed at 1, 3, 10 and 30 μM. (A) green bars: agonist response when NS6740 is applied alone; red bars: following residual 60 μM ACh post-control activation; blue bars: residual receptor potentiation after final application of 10 μM type II PAM PNU-120596. (B) violet bars: receptor potentiation given by co-application of 10 μM NS6740 and 10 μM type II PAM PNU-120596; orange bars: following residual 60 μM ACh post-control activation.

Higher concentrations (10 and 30 μM) of NS6740 produced a very good inhibition of ACh post-control (net charges 0.2 ± 0.06 and 0.18 ± 0.04 residual ACh post-control responses, respectively) due to the ability of the compound to promote deeper receptor desensitization. 10 μM NS6740 showed very significant residual PAM-potentiated response (net charge 111 ± 37), while 30 μM gave strongless response (net charge 55 ± 16). The direct potentiated responses obtained for 10 and 30 μM (net charges 56 ± 9 and 3 ± 0.7 , respectively) were much less intense than the corresponding residual ones. The ability of higher concentrations of NS6740 to mainly favor the faster stabilization of D_i over D_s accounts for this observed phenomenon, which was detectable when PNU-120596 was co-applied (one-shot experiment). Indeed, when the positive allosteric modulator was delivered few minutes after NS6740 in the two-shot experiment, the $\alpha 7$ receptor had enough time to allow the transition from the D_i to the D_s state so that higher potentiation was observed. This behavior confirmed what was previously described by Papke et al. [66]

Finally, the reduced ACh post-control response after co-application of 10 and 30 μM and PNU-120596 verified the sustained receptor desensitization, already observed in the two-shot experiment.

4.3 Electrophysiological evaluation of NS6740 fragments 11-16

The different profiles of the new NS6740 fragments 11-16 at the $\alpha 7$ nAChR were characterized by means of the previously described one-shot and two-shot experiment protocols (4.1.1), and the results obtained are reported in **Figure 28** and **Table 2**.

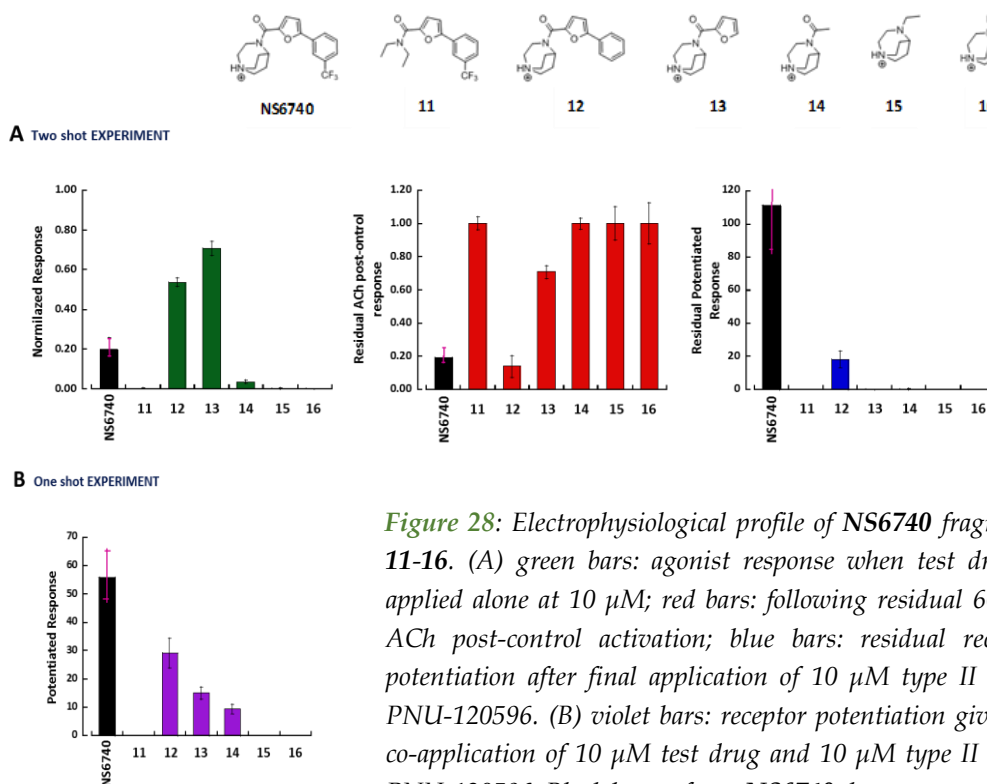


Figure 28: Electrophysiological profile of NS6740 fragments 11-16. (A) green bars: agonist response when test drug is applied alone at 10 μM ; red bars: following residual 60 μM ACh post-control activation; blue bars: residual receptor potentiation after final application of 10 μM type II PAM PNU-120596. (B) violet bars: receptor potentiation given by co-application of 10 μM test drug and 10 μM type II PAM PNU-120596. Black bars refer to NS6740 data.

The removal of the basic nucleus as pharmacophore feature in compound 11 led to complete loss of activity. Indeed, this compound did not show agonist responses neither when applied alone (two-shot experiment) nor in co-application with PNU-120596 (one-shot experiment). Moreover, neither ACh post-control inhibition nor residual PAM-potentiated response by PNU-120596 applied alone (two-shot experiment) were observed for compound 11. These results demonstrated that the interactions between the positive charge and the aromatic cage in the orthosteric binding site are crucial for retaining the activity of NS6740.

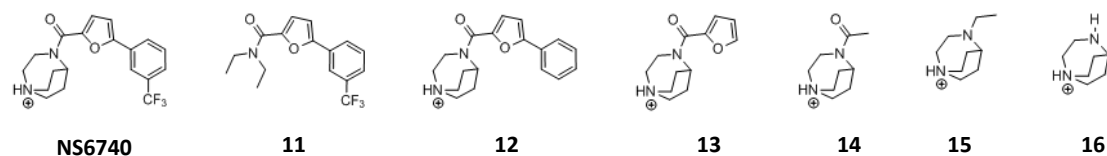
Derivative **12**, which lacks the *meta* trifluoromethyl group of **NS6740**, presented increased partial agonist properties (net charge 0.5 ± 0.02) compared to its parent compound (net charge 0.2 ± 0.06). The most interesting finding for derivative **12** was its ability to strongly inhibit ACh post-control (net charge 0.14 ± 0.07) while producing a good residual potentiated response (net charge 18 ± 5), thus proving to be an effective receptor desensitizer. In light of these results, the role of the trifluoromethyl group appeared to be relevant in silencing the agonist response, but this substituent is not strictly required to stabilize the desensitized states.

In compound **13**, a furan ring represents the aromatic part of the **NS6740** pharmacophore. This derivative showed a very good partial agonist behavior with a net charge of 0.7 ± 0.04 ($\approx 70\%$ of ACh response), and in co-application with PNU-120596 (one-shot experiment) it displayed a direct PAM-potentiation, in line with what is expected for a partial agonist. In spite of these results, compound **13** failed to remain in the receptor long enough to stabilize a prolonged non-conductive state, as evidenced by the lack of residual potentiated response to PNU-120596 in the two-shot experiment.

Fragment **14** retains the hydrogen bond acceptor group and positive center of the **NS6740** pharmacophore, and exhibited short-lasting silent agonist characteristics. Indeed, **14** did not give channel opening when tested alone (two-shot experiment) while induced potentiation in co-application with PNU-120596 (one-shot experiment), thus proving its silent behavior. The absence of the aromatic portion of the **NS6740** pharmacophore determined a short-lasting interaction with the binding site, that is evidenced by the full ACh post-control response (no inhibition) and by the lack of residual PNU-potentiated response (two-shot experiment).

Finally, the simplest fragments of **NS6740**, namely **15** and **16**, were completely inactive. This was surprising by considering the similar bicyclic structure that compounds **15** and **16** share with quinuclidine and some of its derivatives, which proved to be effective $\alpha 7$ agonists. [82] To account for this outcome, we hypothesized that in our compounds the presence of two protonatable centers did not allow them to adopt a correct orientation inside the aromatic cage of the receptor binding domain.

Altogether, these results highlighted the structural specificity required to maintain the peculiar activity of **NS6740**. The basic nucleus along with the hydrogen bond acceptor and the aromatic portion are associated with the ability to engender a good desensitization, while the presence of the trifluoromethyl group seems to be related to the low channel opening typical of **NS6740**.



Compound	Two-shot experiment ^a						One-shot experiment ^b	
	Agonist response		Residual 60 μM ACh response		Residual potentiated response		Agonist potentiated response	
	peak current	net charge	peak current	net charge	peak current	net charge	peak current	net charge
NS6740 (1)	0.071 ± 0.025	0.197 ± 0.062	0.100 ± 0.035	0.194 ± 0.055	21.400 ± 5.1	111.059 ± 37.179	19.953 ± 8.327	55.819 ± 9.232
11	0.006 ± 0.003	0.000 ± 0.007	0.874 ± 0.083	1.212 ± 0.039	0.007 ± 0.003	0.000 ± 0.009	0.006 ± 0.002	0.023 ± 0.018
12	0.624 ± 0.111	0.536 ± 0.020	0.047 ± 0.011	0.140 ± 0.067	4.783 ± 0.721	18.334 ± 5.132	9.074 ± 1.907	29.122 ± 5.262
13	1.862 ± 0.228	0.707 ± 0.036	1.018 ± 0.042	0.741 ± 0.066	0.067 ± 0.062	0.251 ± 0.253	4.323 ± 0.586	14.995 ± 2.135
14	0.014 ± 0.002	0.034 ± 0.008	0.949 ± 0.109	1.014 ± 0.033	0.053 ± 0.029	0.424 ± 0.273	2.416 ± 0.252	9.472 ± 1.599
15	0.010 ± 0.004	0.005 ± 0.003	1.073 ± 0.226	1.426 ± 0.366	0.033 ± 0.026	0.062 ± 0.039	2.449 ± 1.368	0.002 ± 0.008
16	0.003 ± 0.001	0.002 ± 0.002	1.199 ± 0.183	1.257 ± 0.122	0.005 ± 0.001	0.008 ± 0.001	0.041 ± 0.011	0.093 ± 0.021

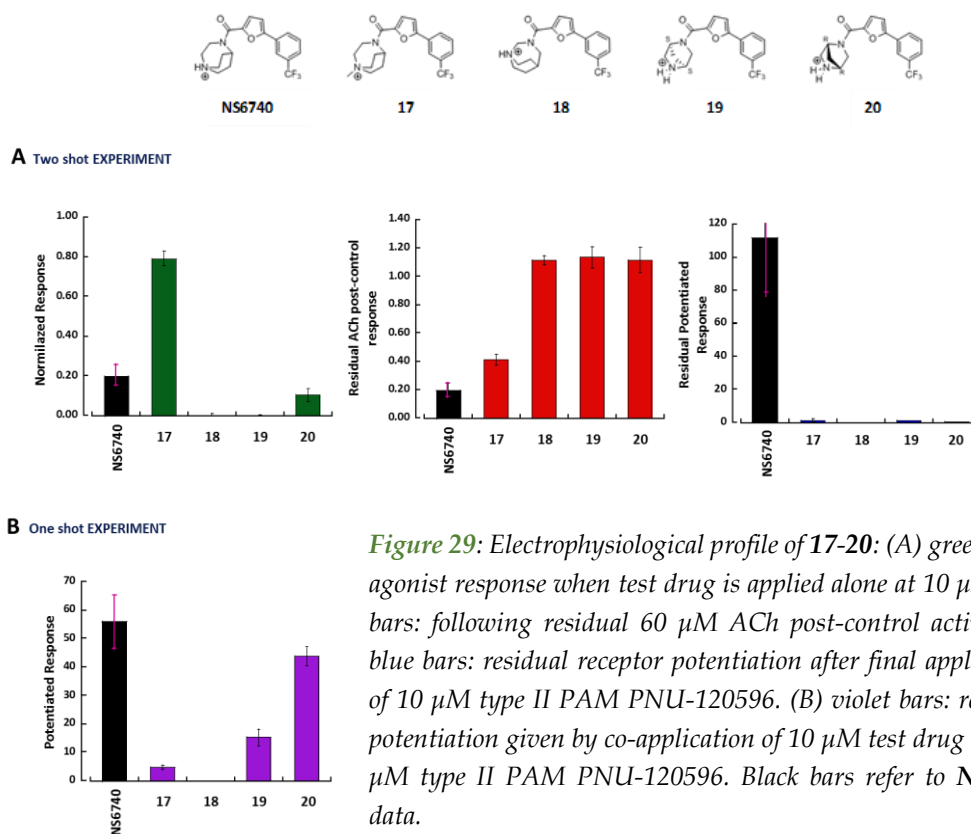
Table 2: Electrophysiological data of NS6740 fragments 11-16 on human alpha7 nAChRs expressed in *Xenopus* oocytes. Data are reported as mean ± SEM (standard error of mean) and relative to two 60 μM ACh pre-controls. (a) Two-shot experiment: Agonist response refers to receptor response to 10 μM application of test compound, residual ACh response refers to receptor response to 60 μM application of control and residual potentiated response refers to receptor response to 10 μM application of type-II PAM PNU-120596. (b) One-shot experiment: Agonist potentiated response refers to receptor response to 10 μM test compound in co-application with 10 μM of type-II PAM PNU-120596.

4.4 Electrophysiological evaluation of NS6740 derivatives 17-33

4.4.1 Basic nucleus modifications

The profiles of compounds **17-20** at the $\alpha 7$ nAChR were outlined in one-shot and two-shot experiments as previously described in the general pharmacological considerations 4.1.1.

The collected set of data is reported in **Figure 29** and **Table 3**, and suggest that even small structural modifications of the basic bicyclic ring of **NS6740** lead to loss of the prolonged receptor desensitization typical of the parent compound.

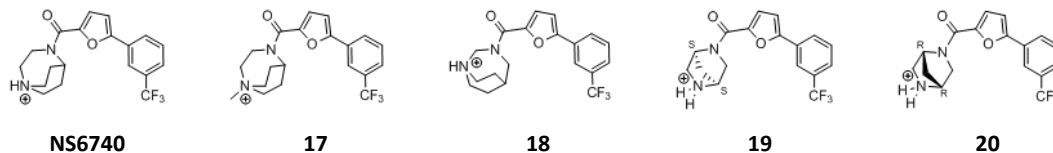


The corresponding quaternary ammonium salt of **NS6740**, compound **17**, displayed a very good partial agonist behavior with a net charge of 0.8 ± 0.03 ($\approx 80\%$ ACh response). This derivative was not able to stabilize a prolonged non-conductive state and displayed a very small residual potentiated response (net charge 1.4 ± 0.9 two-shot experiment). Although not strongly, it induced a PAM-potentiation in line with what is expected for a partial agonist in co-application with PNU-120596 (one-shot experiment). In conclusion, the methylation of the tertiary amine of **NS6740** increased the channel opening ability of the new derivative **17**, reduced the time **17**

remains bound to the receptor, and also reduced its effectiveness in stabilizing the $\alpha 7$ desensitized state.

Derivative **18** represents the 1,3-diazabicyclo[3.2.2]nonane regioisomer of **NS6740**, with the bicyclic secondary amine shifted of one position compared to the parent compound. This minor structural difference caused, however, derivative **18** to be completely inactive. These results suggest that the distance between the two nitrogens in the basic nucleus and the distance between the positive charge and the hydrogen bond acceptor group are essential for **NS6740** activity. Indeed, reduction of those distances from **NS6740** to **18** was detrimental to the correct binding of the compound in the receptor and its orientation in the aromatic cage.

Regarding the couple of enantiomers **19** (*S,S*) and **20** (*R,R*), interesting results were obtained from one-shot experiments, where they exhibited good potentiated responses in co-application with PNU-120596 (15 ± 3 and 44 ± 3 , respectively). Given the absence of agonist responses as well as the absence of ACh post-control inhibitions and residual potentiations, we could conclude that, compared to **NS6740**, the introduction of a smaller bicyclic ring with a secondary amine as protonable center conferred short lasting silent characteristics to both **19** and **20**.



<i>Compound</i>	Two-shot experiment^a						One-shot experiment^b	
	Agonist response		Residual 60 μM ACh response		Residual potentiated response		Agonist potentiated response	
	<i>peak current</i>	<i>net charge</i>	<i>peak current</i>	<i>net charge</i>	<i>peak current</i>	<i>net charge</i>	<i>peak current</i>	<i>net charge</i>
NS6740(1)	0.071 \pm 0.025	0.197 \pm 0.062	0.100 \pm 0.035	0.194 \pm 0.055	21.400 \pm 5.1	111.059 \pm 37.179	19.953 \pm 8.327	55.819 \pm 9.232
17	2.266 \pm 0.554	0.790 \pm 0.034	0.897 \pm 0.101	0.411 \pm 0.036	0.323 \pm 0.227	1.392 \pm 0.856	1.970 \pm 0.142	4.722 \pm 0.665
18	0.008 \pm 0.003	0.000 \pm 0.011	1.087 \pm 0.143	1.112 \pm 0.030	0.012 \pm 0.004	0.037 \pm 0.010	0.026 \pm 0.008	0.022 \pm 0.006
19	0.004 \pm 0.001	0.001 \pm 0.004	1.040 \pm 0.192	1.131 \pm 0.074	0.935 \pm 0.108	1.045 \pm 0.013	2.822 \pm 0.393	15.224 \pm 2.946
20	0.032 \pm 0.006	0.103 \pm 0.032	0.923 \pm 0.063	1.114 \pm 0.090	0.083 \pm 0.062	0.299 \pm 0.299	7.937 \pm 1.345	43.705 \pm 3.305

Table 3: Electrophysiological data of NS6740 derivatives 17-20 on human α 7 nAChRs expressed in *Xenopus* oocytes. Data are reported as mean \pm SEM (standard error of mean) and relative to two 60 μ M ACh pre-controls. (a) Two-shot experiment: Agonist response refers to receptor response to 10 μ M application of test compound, residual ACh response refers to receptor response to 60 μ M application of control and residual potentiated response refers to receptor response to 10 μ M application of type-II PAM PNU-120596. (b) One-shot experiment: Agonist potentiated response refers to receptor response to 10 μ M test compound in co-application with 10 μ M of type-II PAM PNU-120596.

4.4.2 Removal of the hydrogen-bond acceptor group

The profile of compound **21** at the $\alpha 7$ nAChR was defined in one-shot and two-shot experiments following the previously described protocols in 4.1.1 (Figure 30 and Table 4).

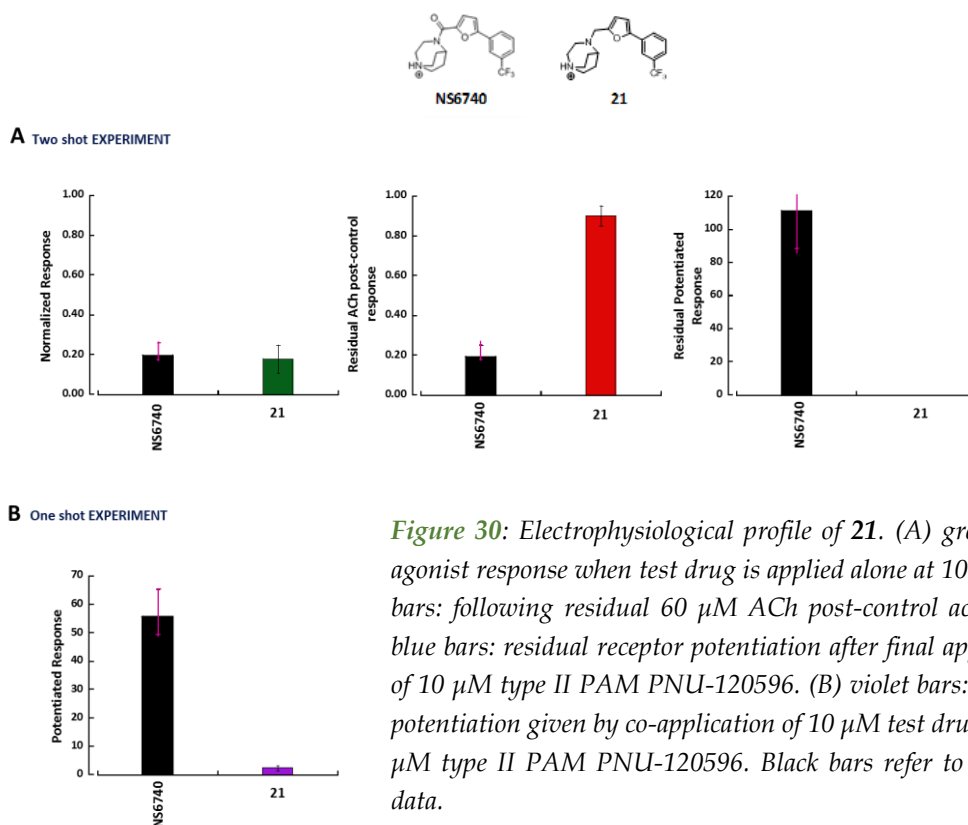
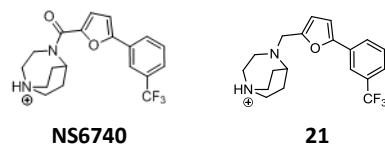


Figure 30: Electrophysiological profile of **21**. (A) green bars: agonist response when test drug is applied alone at 10 μM ; red bars: following residual 60 μM ACh post-control activation; blue bars: residual receptor potentiation after final application of 10 μM type II PAM PNU-120596. (B) violet bars: receptor potentiation given by co-application of 10 μM test drug and 10 μM type II PAM PNU-120596. Black bars refer to NS6740 data.

The deletion of the pharmacophoric carbonyl group was detrimental to the activity of compound **21**. Only in the one-shot experiment, **21** showed a very small PNU-potentiation which is of minor significance. By converting the carbonyl group to a methylene, not only the hydrogen bond acceptor group was removed but also a second protonatable center was introduced, associated with a new rotatable center in the molecule. Thus, the loss of activity could be due to:

- lack of hydrogen bond established between the molecule and the receptor;
- different orientation of basic nucleus in the aromatic cage, due to the competition between the two protonated amine nitrogen atoms;
- increased flexibility of the new analog.

Thus, we cannot assert with any certainty if the data obtained for **21** are due to one or a combination of the three effects related to the acquired structural features of **21**.



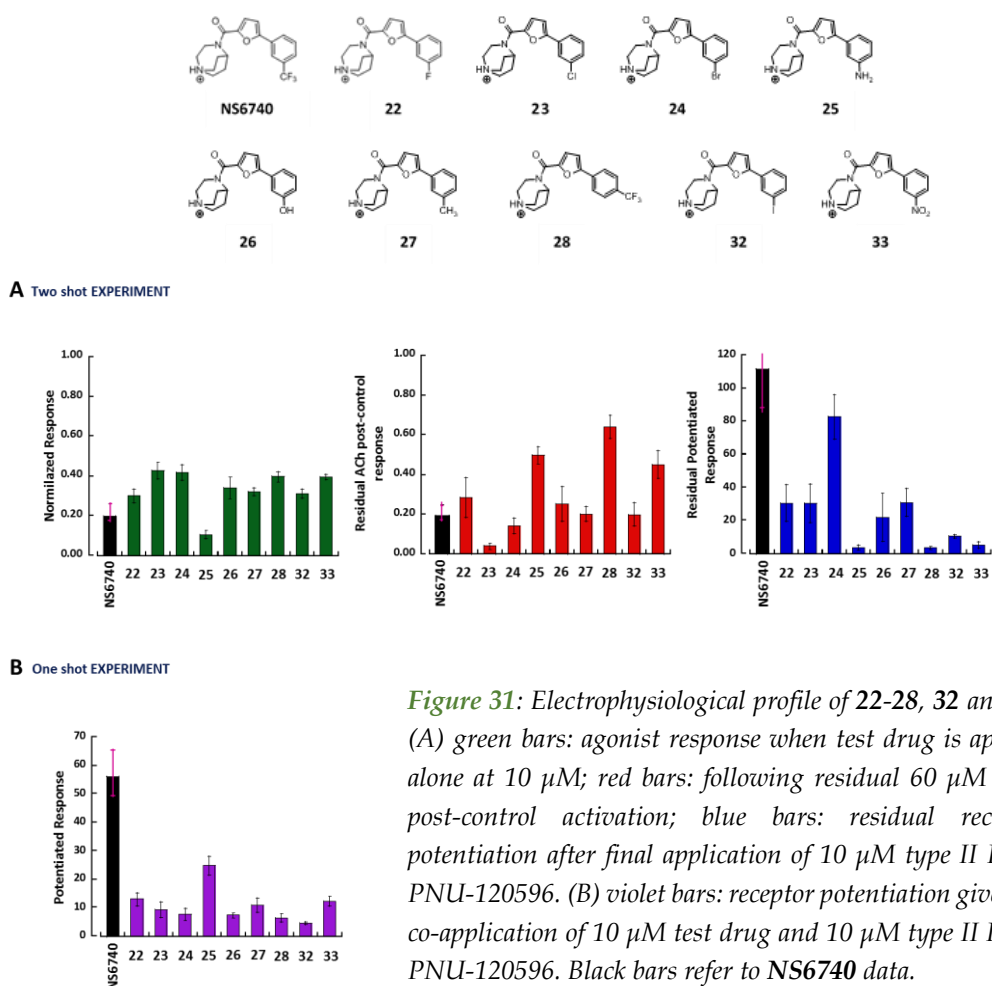
<i>Compound</i>	Two-shot experiment^a						One-shot experiment^b	
	Agonist response		Residual 60 μM ACh response		Residual potentiated response		Agonist potentiated response	
	<i>peak current</i>	<i>net charge</i>	<i>peak current</i>	<i>net charge</i>	<i>peak current</i>	<i>net charge</i>	<i>peak current</i>	<i>net charge</i>
NS6740 (1)	0.071 ± 0.025	0.197 ± 0.062	0.100 ± 0.035	0.194 ± 0.055	21.400 ± 5.1	111.059 ± 37.179	19.953 ± 8.327	55.819 ± 9.232
21	0.057 ± 0.019	0.176 ± 0.070	0.780 ± 0.091	0.899 ± 0.050	0.082 ± 0.035	0.144 ± 0.060	0.992 ± 0.385	2.299 ± 0.873

Table 4: Electrophysiological data of NS6740 derivative **21** on human $\alpha 7$ nAChRs expressed in *Xenopus* oocytes. Data are reported as mean \pm SEM (standard error of mean) and relative to two 60 μ M ACh pre-controls. (a) Two-shot experiment: Agonist response refers to receptor response to 10 μ M application of test compound, residual ACh response refers to receptor response to 60 μ M application of control and residual potentiated response refers to receptor response to 10 μ M application of type-II PAM PNU-120596. (b) One-shot experiment: Agonist potentiated response refers to receptor response to 10 μ M test compound in co-application with 10 μ M of type-II PAM PNU-120596.

4.4.3 Substitutions of the *meta*-trifluoromethyl group

The profiles of compounds **22-29**, **32** and **33** at the $\alpha 7$ nAChR were characterized in one-shot and two-shot experiments following the previously described protocols in 4.1.1.

The corresponding data set (Figure 31 and Table 5) suggested that the replacement of the original *meta* trifluoromethyl group on the aromatic ring conferred partial agonist activity, associated with a more likely channel opening than the parent **NS6740**. Moreover, the PNU-related response was generally higher for the parent compound than for its derivatives **22-29**, **32** and **33**.



The introduction of halogen atoms with increasing size, i.e. fluorine (**22**), chlorine (**23**), bromine (**24**) and iodine (**32**) in the *meta* position of the phenyl ring gave agonist responses ranging from 25% to 50% of ACh control. The channel opening induced by compound **22** was not significantly different from that of **NS6740** (P value of 0.059).

The weak partial agonists **23**, **24** and **32** induced a significantly greater channel opening than **NS6740**.

For the halogen-containing derivatives, interesting findings arose from the ACh post-control inhibition data. While all halogen derivatives showed ACh post-control inhibition, the highest residual ACh response belonged to the fluorine derivative **22** (net charge 0.3 ± 0.1), and the strongest ACh inhibition was observed with the chlorine-containing compound **23** (residual ACh response net charge 0.04 ± 0.01).

The high residual PAM-potentiated responses in the two-shot experiments suggested that halogen derivatives induced prolonged $\alpha 7$ desensitization. Interestingly, the halogen compounds displayed good channel potentiation in co-application with PNU-120596 (one-shot experiments), albeit lower than the residual PAM-potentiation observed in two-shot experiments. Most likely, as previously reported for the parent compound **NS6740**, derivatives **22-24** and **32** favored the faster stabilization of D_i over D_s . Indeed, in two-shot experiments, the lapse of time between test drug application and PNU-120596 delivery allowed the receptor to transition from D_i to D_s state, thus favoring the activation by type II PAM.

In light of the results observed for **22**, **23**, **24**, and **32** we can conclude that the presence of a halogen atom on the *meta* position of the phenyl ring is required to obtain prolonged permanence of compound in the receptor binding site, and therefore good stabilization of desensitized states.

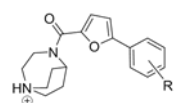
While different halogens mainly provided similar data, the insertion of different polar substituents in **25**, **26**, and **33** gave a variety of results. To derivative **25**, with its *meta* amino group, a typical short-lasting silent agonist behavior was associated, with very low agonist response (net charge 0.1 ± 0.02) and low ACh post-control inhibition (net charge 0.5 ± 0.04). Moreover, for **25** PAM-potentiation was observed only in co-application with PNU-120596 (net charge 25 ± 3 , one-shot experiment). Interestingly, compound **26**, with a hydroxyl substituent, displayed weak partial agonist response and inhibition of ACh post-control comparable with halogen derivatives data. The residual PAM-potentiation (two-shot experiment) obtained for **26** appeared to be remarkable at first, but unfortunately this result was characterized by a high standard error of the mean.

Conversely, the nitro-containing group (derivative **33**) behaved as a weak partial agonist with weak ACh-post control inhibition. The residual observed channel PNU-potentiation (two shot experiment) was relatively low (net charge 5 ± 2), while the

direct one reflected what is expected for a partial agonist (net charge 12 ± 2 , one-shot experiment).

Derivative **27**, characterized by a bioisosteric replacement of the trifluoromethyl group of **NS6740** with a methyl, showed an increased channel opening compared to **NS6740**, making it a weak partial agonist. Moreover, very good ACh post-control inhibition (net charge 0.2 ± 0.04) and residual potentiated response (net charge 31 ± 9) were displayed by **27**. As already observed for compounds **22-24** and **32**, the direct potentiation given by co-application with PNU-120596 (one-shot experiment) was lower than the residual one (two-shot experiment). The results obtained for **27** showed that the bioisosteric methyl group maintained the overall prolonged receptor desensitization of **NS6740**.

Finally, derivative **28** with a *para* trifluoromethyl group was assayed. Shifting the trifluoromethyl group from *meta* to *para* position caused the loss of the typical **NS6740** characteristics. In detail, **28** gave a channel opening (net charge 0.4 ± 0.03) approximately 2-folds greater than the agonist activity of **NS6740**. Moreover, **28** did not show strong inhibition of ACh post-control, (net charge 0.7 ± 0.06) with residual (two-shot experiment) and direct (one-shot experiment) potentiation (net charges 3 ± 0.6 and 6 ± 1.4 , respectively) much lower than **NS6740**. Considering these results, we concluded that moving the trifluoromethyl group from its original *meta* to the *para* position was detrimental to the prolonged binding time showed by the parent compound **NS6740**. We hypothesized that this modification could affect the profile of **28** directly by promoting the interaction with a different group of amino acidic residues. Alternatively, the shift of the trifluoromethyl group could indirectly induce the phenyl ring in the binding domain to rearrange and therefore affect the binding time of the new ligand.



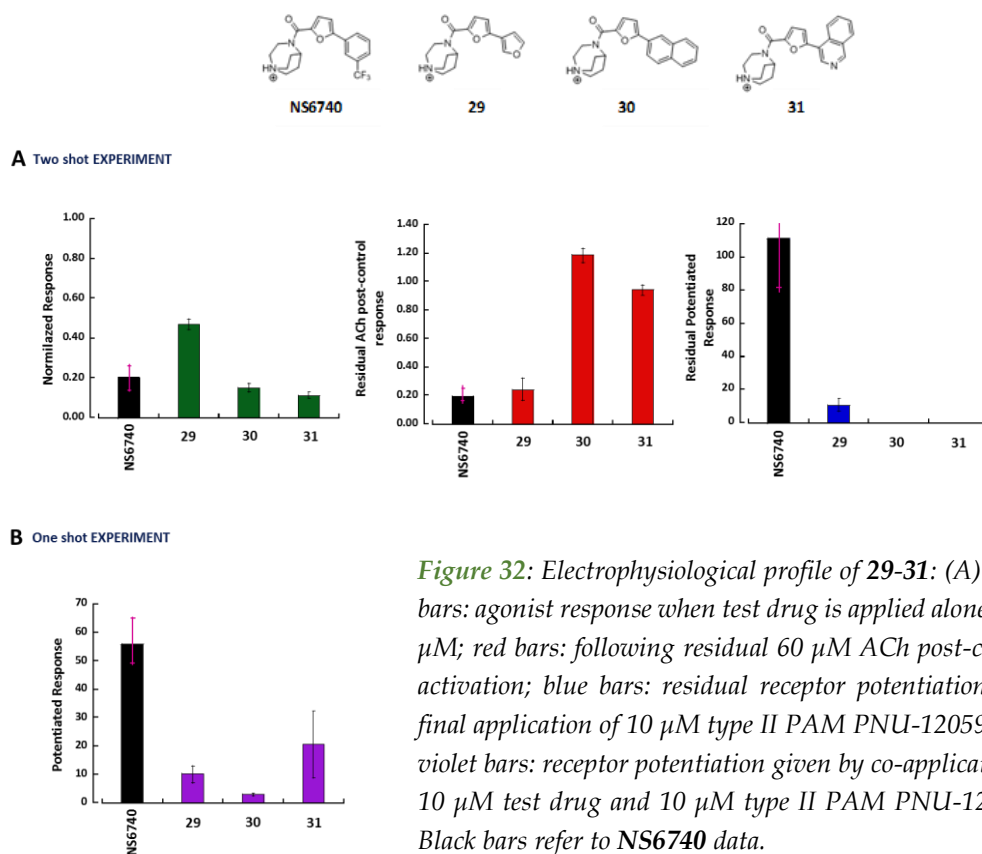
Compound	Agonist response		Two-shot experiment^a				One-shot experiment^b	
	<i>peak current</i>	<i>net charge</i>	Residual 60 μM ACh response		Residual potentiated response		Agonist potentiated response	
			<i>peak current</i>	<i>net charge</i>	<i>peak current</i>	<i>net charge</i>	<i>peak current</i>	<i>net charge</i>
NS6740 (1)	0.071 \pm 0.025	0.197 \pm 0.062	0.100 \pm 0.035	0.194 \pm 0.055	21.400 \pm 5.1	111.059 \pm 37.179	19.953 \pm 8.327	55.819 \pm 9.232
22 R= <i>m</i> -F	0.215 \pm 0.050	0.298 \pm 0.034	0.390 \pm 0.194	0.284 \pm 0.100	3.233 \pm 0.870	30.357 \pm 11.104	3.374 \pm 0.417	12.849 \pm 2.205
23 R= <i>m</i> -Cl	0.469 \pm 0.081	0.425 \pm 0.041	0.060 \pm 0.014	0.039 \pm 0.014	6.054 \pm 1.404	30.312 \pm 11.732	3.480 \pm 0.373	9.287 \pm 2.809
24 R= <i>m</i> -Br	0.417 \pm 0.084	0.416 \pm 0.040	0.061 \pm 0.032	0.142 \pm 0.038	10.762 \pm 0.991	82.398 \pm 13.3878	2.290 \pm 0.651	7.499 \pm 2.077
25 R= <i>m</i> -NH ₂	0.020 \pm 0.005	0.104 \pm 0.021	0.633 \pm 0.115	0.498 \pm 0.044	0.506 \pm 0.259	3.384 \pm 1.329	4.855 \pm 0.820	24.616 \pm 3.300
26 R= <i>m</i> -OH	0.263 \pm 0.014	0.339 \pm 0.052	0.538 \pm 0.121	0.252 \pm 0.087	3.809 \pm 2.093	21.811 \pm 14.398	2.542 \pm 0.214	7.219 \pm 0.891
27 R= <i>m</i> -CH ₃	0.240 \pm 0.037	0.319 \pm 0.019	0.124 \pm 0.040	0.201 \pm 0.038	5.502 \pm 0.497	30.739 \pm 8.769	3.336 \pm 0.349	10.740 \pm 2.472
28 R= <i>p</i> -CF ₃	0.227 \pm 0.034	0.395 \pm 0.025	0.768 \pm 0.135	0.639 \pm 0.058	0.828 \pm 0.306	3.234 \pm 0.646	2.589 \pm 0.802	6.250 \pm 1.399
32 R= <i>m</i> -I	0.290 \pm 0.036	0.309 \pm 0.022	0.050 \pm 0.012	0.200 \pm 0.058	3.002 \pm 0.387	10.319 \pm 1.138	1.842 \pm 0.308	4.414 \pm 0.525
33 R= <i>m</i> -NO ₂	0.231 \pm 0.033	0.392 \pm 0.014	0.529 \pm 0.170	0.449 \pm 0.071	1.514 \pm 0.831	4.776 \pm 2.071	4.592 \pm 0.545	12.187 \pm 1.682

Table 5: Electrophysiological data of NS6740 derivatives 22-28, 32 and 33 on human α 7 nAChRs expressed in *Xenopus* oocytes. Data are reported as mean \pm SEM (standard error of mean) and relative to two 60 μ M ACh pre-controls. (a) Two-shot experiment: Agonist response refers to receptor response to 10 μ M application of test compound, residual ACh response refers to receptor response to 60 μ M application of control and residual potentiated response refers to receptor response to 10 μ M application of type-II PAM PNU-120596. (b) One-shot experiment: Agonist potentiated response refers to receptor response to 10 μ M test compound in co-application with 10 μ M of type-II PAM PNU-120596.

4.4.4 Introduction of different aromatic portions

The profiles of compounds **29-31** at the $\alpha 7$ nAChR were defined in one-shot and two-shot experiments following the previously described protocols in 4.1.1 paragraph (**Figure 32** and **Table 6**).

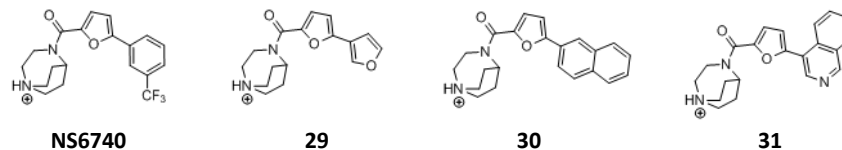
The final group of **NS6740** derivatives analyzed displayed different aromatic and heteroaromatic moieties, which replaced the original *meta* trifluoromethyl phenyl ring of the parent compound.



Compound **29**, with two furan rings embedded in its structure, behaved as partial agonist with almost 50% of ACh response. The most interesting feature of **29** was its relatively long binding to the receptor, which determined considerable ACh post-control inhibition and good residual PAM-potentiated response.

Regarding the wider naphthalene (**30**) and isoquinoline (**31**) derivatives, they both displayed low agonist activity (net charges 0.15 ± 0.02 and 0.1 ± 0.02 , respectively) and low ACh post-control inhibition (net charges 0.05 ± 0.02 and 0.01 ± 0.002 , respectively). The residual potentiation (two-shot experiments) was completely absent in **30** and **31**, as we expected considering their results on ACh inhibition.

Surprisingly, in co-application with PNU-120596 (one-shot experiment), **30** did not show any direct potentiated response, while compound **31** gave a noticeable response (net charge 20 ± 12). According to these results, the introduction of bulkier aromatic portions led to large steric hindrance which did not permit **30** and **31** to bind the receptor for a prolonged time. Anyway, the aromatic amino group of isoquinoline together with the different orientation of the bicyclic ring in **31** conferred to this derivative short lasting silent agonist properties.



Compound	Two-shot experiment^a						One-shot experiment^b	
	Agonist response		Residual 60 μM ACh response		Residual potentiated response		Agonist potentiated response	
	<i>peak current</i>	<i>net charge</i>	<i>peak current</i>	<i>net charge</i>	<i>peak current</i>	<i>net charge</i>	<i>peak current</i>	<i>net charge</i>
NS6740 (1)	0.071 \pm 0.025	0.197 \pm 0.062	0.100 \pm 0.035	0.194 \pm 0.055	21.400 \pm 5.100	111.059 \pm 37.179	19.953 \pm 8.327	55.819 \pm 9.232
29	0.626 \pm 0.062	0.467 \pm 0.025	0.373 \pm 0.099	0.242 \pm 0.078	1.224 \pm 0.249	10.675 \pm 3.714	3.871 \pm 0.412	10.036 \pm 2.898
30	0.093 \pm 0.022	0.149 \pm 0.022	1.009 \pm 0.285	1.182 \pm 0.049	0.025 \pm 0.008	0.050 \pm 0.016	1.310 \pm 0.394	2.854 \pm 0.425
31	0.063 \pm 0.016	0.112 \pm 0.016	1.054 \pm 0.089	0.939 \pm 0.035	0.006 \pm 0.001	0.011 \pm 0.002	5.904 \pm 2.022	20.438 \pm 11.774

Table 6: Electrophysiological data of NS6740 derivatives **29-31** on human $\alpha 7$ nAChRs expressed in *Xenopus* oocytes. Data are reported as mean \pm SEM (standard error of mean) and relative to two 60 μ M ACh pre-controls. (a) Two-shot experiment: Agonist response refers to receptor response to 10 μ M application of test compound, residual ACh response refers to receptor response to 60 μ M application of control and residual potentiated response refers to receptor response to 10 μ M application of type-II PAM PNU-120596. (b) One-shot experiment: Agonist potentiated response refers to receptor response to 10 μ M test compound in co-application with 10 μ M of type-II PAM PNU-120596.

4.5 Additional electrophysiological evaluation of **12**, **22-24**, **27** and **32** at different concentrations (1, 3 and 30 μ M)

Within the new class of **NS6740**-related derivatives, the most interesting $\alpha 7$ receptor desensitizers emerged in the one- and two-shot experiments at 10 μ M (**12**, **22-24**, **27** and **32**) were additionally tested in similar protocols at 1, 3 and 30 μ M. **Figures 33-37** and **Table 7** report these results for compound **12**, **22-24**, **27** and **32**.

Overall, at 1, 3 and 30 μ M concentrations, all the new derivatives **12**, **22-24**, **27** and **32** showed very weak or weak partial agonism, similarly to what already observed at 10 μ M. Moreover, derivatives **12**, **22-24**, **27** and **32** displayed the strongest 60 μ M ACh inhibition when applied at 10 and 30 μ M.

In one-shot experiments, the co-application of 10 μ M PNU-120596 with different concentrations of **12**, **22-24**, **27** or **32** gave potentiated responses, which were generally lower than those measured for **NS6740**. The same experiments highlighted that lower potentiated responses were obtained with increasing concentrations of test drugs. Indeed, with the exception of compound **12** and **27**, all the other **NS6740** analogs here investigated favored the stabilization of D_i state over D_s state at 30 μ M.

The electrophysiological data obtained at the different concentrations are described in details for each compound (**12**, **22-24**, **27** and **32**) (**Figures 33-37** and **Table 7**).

1 and 3 μM concentrations of compound **12** (Figure 33) led to low inhibition of ACh post-controls, which were not significantly different from the corresponding values of **NS6740** (P values of 0.65 and 0.56, respectively). Outstanding results were observed for ACh post-control inhibition at 10 and 30 μM of **12**, when residual responses of only 0.14 ± 0.07 and 0.01 ± 0.00 were respectively detected. In particular, 30 μM of **12** induced an ACh response reduction significantly greater than 30 μM **NS6740** (P value of 0.001). These data, together with good residual PNU-potentiated responses, highlighted prolonged stabilization of non-conductive states promoted by compound **12**. In one-shot experiments, for **12** we observed intense PNU-related responses also at 30 μM , differently from **NS6740**. To account for this responses, we hypothesized that compound **12** maintains favorable stabilization of D_s over D_i even at higher concentrations. However, after the co-application of concentrations of $\mathbf{12} \geq 3 \mu\text{M}$, the ACh post-control responses were interestingly reduced, demonstrating the sustained receptor desensitization.

Compound **12**

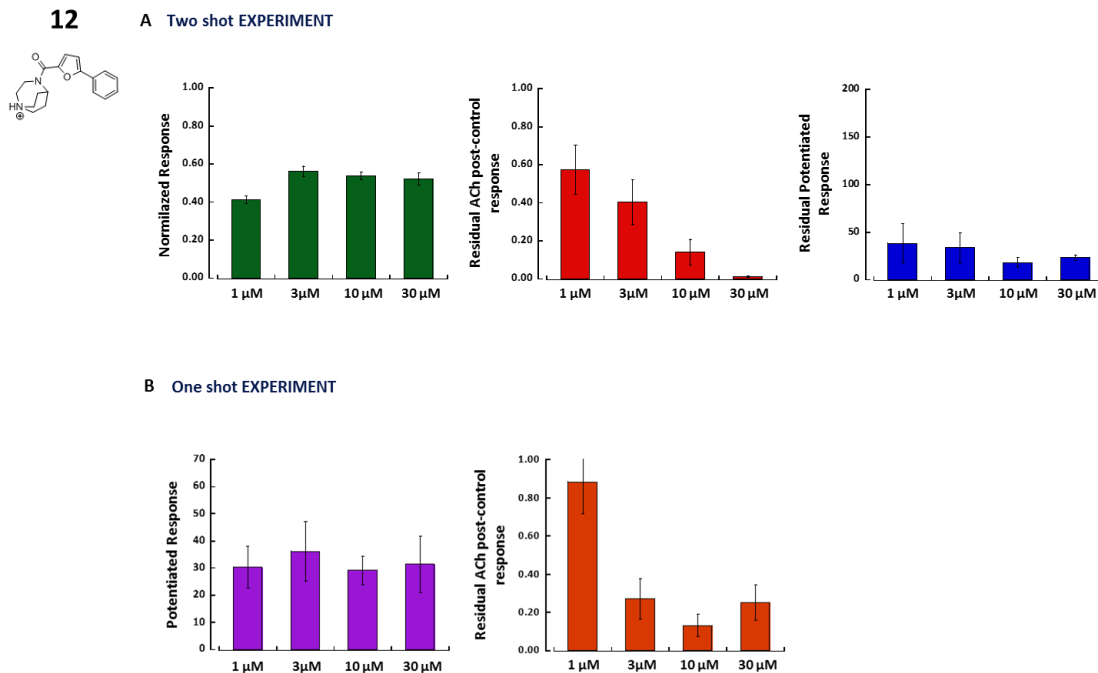
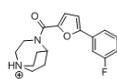


Figure 33: Electrophysiological profile of **12** assayed at 1, 3, 10 and 30 μM . (A) green bars: agonist response when **12** is applied alone at 10 μM ; red bars: following residual 60 μM ACh post-control activation; blue bars: residual receptor potentiation after final application of 10 μM type II PAM PNU-120596. (B) violet bars: receptor potentiation given by co-application of 10 μM **12** and 10 μM type II PAM PNU-120596; orange bars: following residual 60 μM ACh post-control activation.

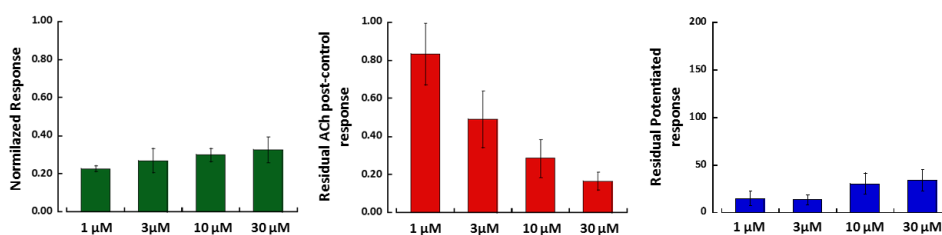
Compound **22** (Figure 34), tested at low concentration, displayed a very similar behavior to NS6740, with low ACh post-control inhibition, but PNU-related response, which is probably due to the persistent binding. At higher concentrations ($\geq 3 \mu\text{M}$), **22** reduced ACh post-control responses related to the stabilization of desensitized states induced by test drug. This was confirmed by the subsequent PNU-dependent receptor activations in the two-shot experiment. In co-application with PNU-120596 (one-shot experiment), **22** showed potentiated responses that decreased when the test drug concentration increased, thus suggesting the favorable stabilization of D_i over D_s , as already observed for NS6740. The final response of ACh post-control resulted to be interestingly affected after application of 10 and 30 μM of **22** in co-application with PNU-120596, demonstrating the persistent receptor desensitization.

Compound

22



A Two shot EXPERIMENT



B One shot EXPERIMENT

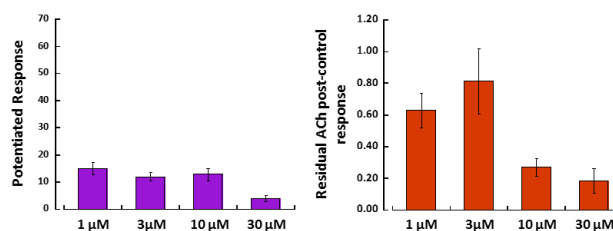


Figure 34: Electrophysiological profile of **22** assayed at 1, 3, 10 and 30 μM . (A) green bars: agonist response when **22** is applied alone at 10 μM ; red bars: following residual 60 μM ACh post-control activation; blue bars: residual receptor potentiation after final application of 10 μM type II PAM PNU-120596. (B) violet bars: receptor potentiation given by co-application of 10 μM **22** and 10 μM type II PAM PNU-120596; orange bars: following residual 60 μM ACh post-control activation.

Similarly to NS6740, derivative **23** (Figure 35) presented low reduction of ACh post-control channel activation when tested at 1 and 3 μM . On the other hand, the residual ACh post-control responses associated with 10 and 30 μM (net charges 0.04 ± 0.01 and 0.08 ± 0.05 , respectively) were remarkably affected and reduced, thus showing a significantly stronger inhibiting profile of **23** compared to NS6740 (P value equals 0.01 and 0.005, respectively). The final application of PNU-120596 gave receptor potentiation and this accounted for the long permanence of **23** in the receptor binding site. The one-shot experiment proved the favorable stabilization of D_i over D_s at higher concentration of **23**. The following residual ACh responses were interestingly reduced after application of **23** (at concentration $\geq 3 \mu\text{M}$), confirming that **23** produced intense receptor desensitization.

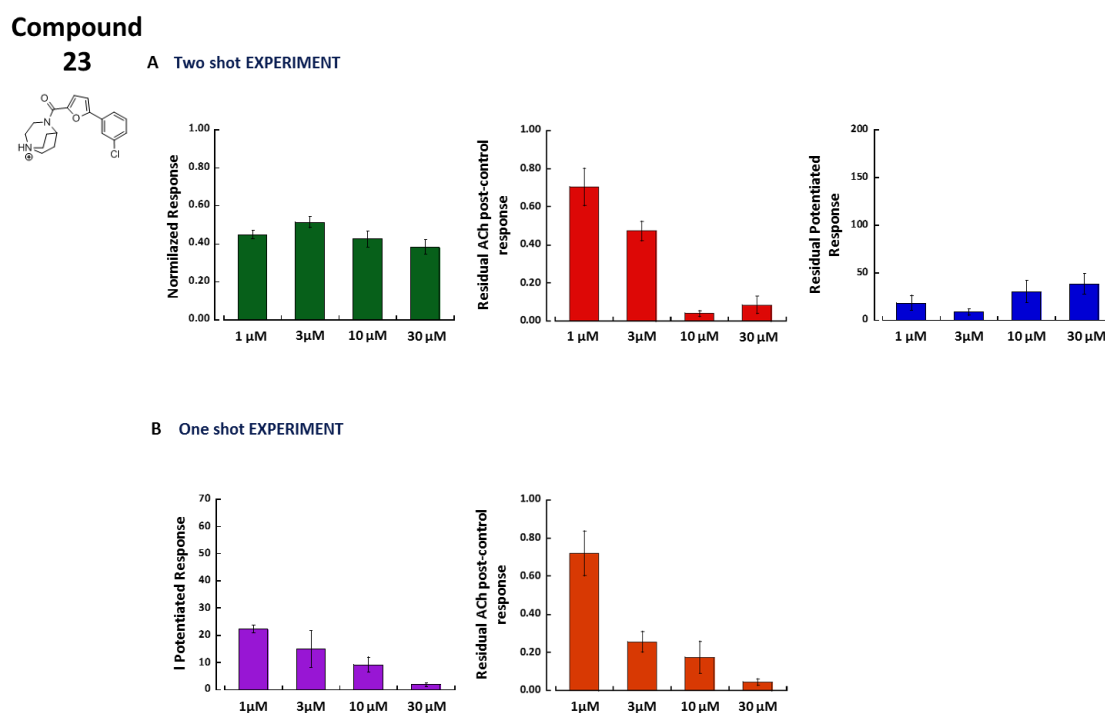


Figure 35: Electrophysiological profile of **23** assayed at 1, 3, 10 and 30 μM . (A) green bars: agonist response when **23** is applied alone at 10 μM ; red bars: following residual 60 μM ACh post-control activation; blue bars: residual receptor potentiation after final application of 10 μM type II PAM PNU-120596. (B) violet bars: receptor potentiation given by co-application of 10 μM **23** and 10 μM type II PAM PNU-120596; orange bars: following residual 60 μM ACh post-control activation.

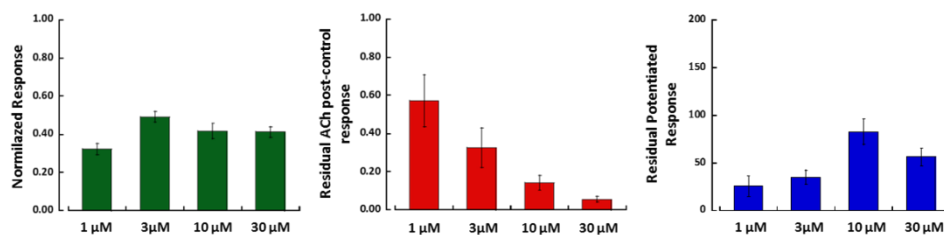
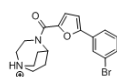
The inhibition of residual ACh post-control responses was progressively intensified by increasing concentrations of compound **24** (Figure 36). In particular, notable results were obtained at 10 and 30 μM of **24** (net charges 0.14 ± 0.04 and 0.06 ± 0.02 , respectively). Good residual PAM-potentiated responses were observed for all four concentrations tested, proving the long receptor binding and the ability of **24** to induce receptor desensitization.

The channel potentiation given by the co-application of **24** and PNU-120596 decreased at higher concentration of the test drug (30 μM); interestingly, the following ACh post-control responses were strongly affected also after the application of lower concentrations of **24**. These low channel openings produced by the post-control confirmed the prolonged receptor binding of **24** and the consequent stabilization of the non-conducting receptor states.

Compound

24

A Two shot EXPERIMENT



B One shot EXPERIMENT

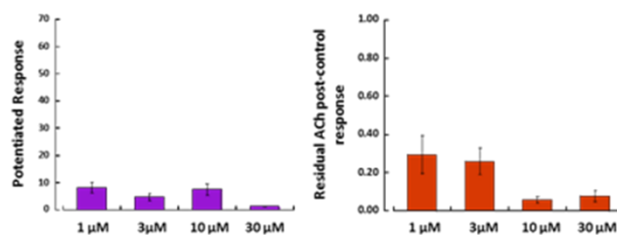


Figure 36: Electrophysiological profile of **24** assayed at 1, 3, 10 and 30 μM . (A) green bars: agonist response when **24** is applied alone at 10 μM ; red bars: following residual 60 μM ACh post-control activation; blue bars: residual receptor potentiation after final application of 10 μM type II PAM PNU-120596. (B) violet bars: receptor potentiation given by co-application of 10 μM **24** and 10 μM type II PAM PNU-120596; orange bars: following residual 60 μM ACh post-control activation.

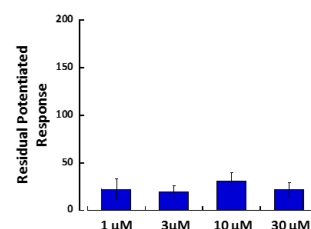
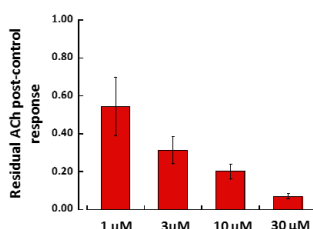
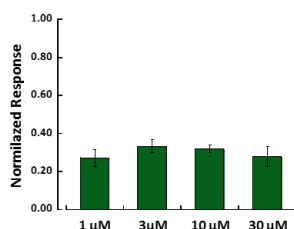
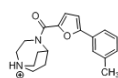
Finally, **27** (Figure 37) presented ACh post-control inhibition associated with all four different concentrations, with a remarkable decrease in ACh channel opening at 30 μM (net charge 0.07 ± 0.02) that was significantly deeper than **NS6740** (P value of 0.01). Prolonged receptor desensitization was highlighted by application of PNU-120596 and related potentiated responses.

When tested in co-application with 10 μM PNU-120596, differently from the previous compounds, this derivative did not display lower potentiation at higher concentration of test drug; however, **27** produced inhibition of post control responses, especially after application of $> 3 \mu\text{M}$ concentrations.

Compound

27

A Two shot EXPERIMENT



B One shot EXPERIMENT

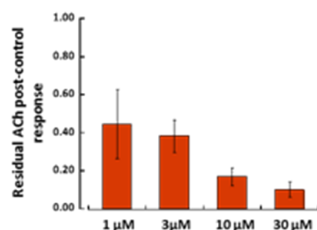
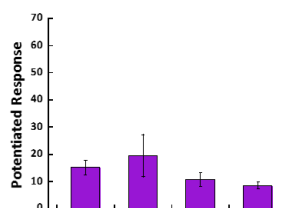
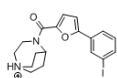


Figure 37: Electrophysiological profile of **27** assayed at 1, 3, 10 and 30 μM . (A) green bars: agonist response when **27** is applied alone at 10 μM ; red bars: following residual 60 μM ACh post-control activation; blue bars: residual receptor potentiation after final application of 10 μM type II PAM PNU-120596. (B) violet bars: receptor potentiation given by co-application of 10 μM **27** and 10 μM type II PAM PNU-120596; orange bars: following residual 60 μM ACh post-control activation.

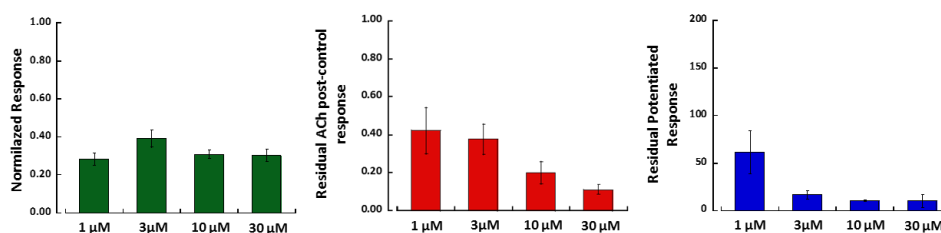
Compound **32** (Figure 38) exhibited inhibiting activities of ACh post-controls at all tested concentrations, with effects gradually deepening with increasing concentrations of **32**. The PNU-related responses proved the prolonged binding of **32** and its ability to produce receptor desensitization. The results obtained in the one-shot experiment suggested a favorable stabilization of D_i over D_s associated with higher concentration of **32**. The following inhibition of post-control responses proved a sustained desensitization of the receptor.

Compound

32



A Two shot EXPERIMENT



B One shot EXPERIMENT

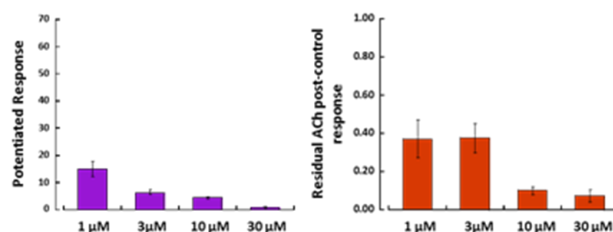
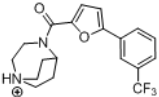


Figure 38: Electrophysiological profile of **31** assayed at 1, 3, 10 and 30 μM . (A) green bars: agonist response when **31** is applied alone at 10 μM ; red bars: following residual 60 μM ACh post-control activation; blue bars: residual receptor potentiation after final application of 10 μM type II PAM PNU-120596. (B) violet bars: receptor potentiation given by co-application of 10 μM **31** and 10 μM type II PAM PNU-120596; orange bars: following residual 60 μM ACh post-control activation.

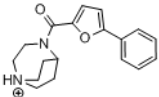
Taken together, the electrophysiological results obtained for the new differently *meta* substituted derivatives **12**, **22-24**, **32** and **27** demonstrated their ability to trigger remarkable prolonged and deep $\alpha 7$ receptor desensitization, which is a subject of great interest in the current thesis work.

NS6740
(1)



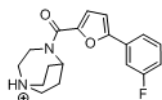
<i>[conc]</i>	Agonist response		Residual 60 μM ACh response		Residual potentiated response		Agonist potentiated response	
	<i>peak current</i>	<i>net charge</i>	<i>peak current</i>	<i>net charge</i>	<i>peak current</i>	<i>net charge</i>	<i>peak current</i>	<i>net charge</i>
1 μM	0.042 \pm 0.010	0.108 \pm 0.012	0.690 \pm 0.243	0.739 \pm 0.120	1.518 \pm 0.499	11.927 \pm 6.290	9.739 \pm 1.383	48.483 \pm 12.872
3 μM	0.084 \pm 0.034	0.253 \pm 0.035	0.357 \pm 0.139	0.695 \pm 0.065	14.585 \pm 4.047	123.211 \pm 71.011	8.936 \pm 1.561	30.089 \pm 10.548
10 μM	0.071 \pm 0.025	0.197 \pm 0.062	0.100 \pm 0.035	0.194 \pm 0.055	21.400 \pm 5.100	111.059 \pm 37.179	19.953 \pm 8.327	55.819 \pm 9.232
30 μM	0.052 \pm 0.013	0.195 \pm 0.028	0.059 \pm 0.011	0.177 \pm 0.034	22.528 \pm 7.145	57.411 \pm 15.718	0.790 \pm 0.274	2.734 \pm 0.729

Compound
12



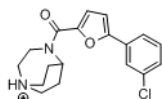
<i>[conc]</i>	Agonist response		Residual 60 μM ACh response		Residual potentiated response		Agonist potentiated response	
	<i>peak current</i>	<i>net charge</i>	<i>peak current</i>	<i>net charge</i>	<i>peak current</i>	<i>net charge</i>	<i>peak current</i>	<i>net charge</i>
1 μM	0.335 \pm 0.029	0.412 \pm 0.020	0.541 \pm 0.196	0.572 \pm 0.131	3.168 \pm 1.479	38.581 \pm 20.262	6.123 \pm 1.031	30.423 \pm 7.581
3 μM	0.672 \pm 0.046	0.561 \pm 0.027	0.478 \pm 0.158	0.403 \pm 0.116	6.098 \pm 1.999	33.522 \pm 15.832	12.599 \pm 2.911	36.262 \pm 11.038
10 μM	0.624 \pm 0.111	0.536 \pm 0.020	0.047 \pm 0.011	0.140 \pm 0.067	4.783 \pm 0.721	18.334 \pm 5.132	9.074 \pm 1.907	29.122 \pm 5.262
30 μM	0.615 \pm 0.085	0.522 \pm 0.032	0.016 \pm 0.009	0.014 \pm 0.004	6.606 \pm 0.665	23.415 \pm 2.925	7.667 \pm 2.256	31.447 \pm 10.480

**Compound
22**



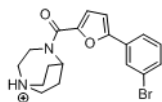
[conc]	Agonist response		Two-shot experiment ^a				One-shot experiment ^b	
	peak current	net charge	Residual 60 μ M ACh response		Residual potentiated response		Agonist potentiated response	
			peak current	net charge	peak current	net charge	peak current	net charge
1 μM	0.132 \pm 0.017	0.226 \pm 0.015	0.766 \pm 0.153	0.832 \pm 0.161	1.877 \pm 0.642	15.044 \pm 7.841	3.786 \pm 0.252	14.970 \pm 2.242
3 μM	0.250 \pm 0.083	0.268 \pm 0.063	0.595 \pm 0.231	0.490 \pm 0.146	1.653 \pm 0.500	13.429 \pm 5.256	3.481 \pm 0.846	12.010 \pm 1.721
10 μM	0.215 \pm 0.050	0.298 \pm 0.034	0.390 \pm 0.194	0.284 \pm 0.100	3.233 \pm 0.870	30.357 \pm 11.104	3.374 \pm 0.417	12.849 \pm 2.205
30 μM	0.252 \pm 0.068	0.326 \pm 0.068	0.076 \pm 0.039	0.165 \pm 0.048	4.555 \pm 0.906	33.705 \pm 11.077	1.776 \pm 0.489	3.974 \pm 1.181

**Compound
23**



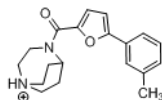
[conc]	Agonist response		Two-shot experiment ^a				One-shot experiment ^b	
	peak current	net charge	Residual 60 μ M ACh response		Residual potentiated response		Agonist potentiated response	
			peak current	net charge	peak current	net charge	peak current	net charge
1 μM	0.281 \pm 0.021	0.448 \pm 0.021	0.729 \pm 0.127	0.704 \pm 0.097	3.057 \pm 1.076	18.452 \pm 7.595	8.314 \pm 0.750	22.299 \pm 1.372
3 μM	0.328 \pm 0.032	0.515 \pm 0.028	0.426 \pm 0.103	0.474 \pm 0.051	1.563 \pm 0.225	8.887 \pm 3.165	4.248 \pm 1.262	14.984 \pm 6.766
10 μM	0.469 \pm 0.081	0.425 \pm 0.041	0.060 \pm 0.014	0.039 \pm 0.014	6.054 \pm 1.404	30.312 \pm 11.732	3.480 \pm 0.373	9.287 \pm 2.809
30 μM	0.330 \pm 0.049	0.384 \pm 0.038	0.024 \pm 0.009	0.085 \pm 0.045	5.072 \pm 0.921	38.242 \pm 10.995	0.623 \pm 0.136	1.982 \pm 0.681

**Compound
24**



[conc]	Agonist response		Residual 60 μ M ACh response		Residual potentiated response		Agonist potentiated response	
	peak current	net charge	peak current	net charge	peak current	net charge	peak current	net charge
1 μM	0.239 \pm 0.039	0.323 \pm 0.030	0.552 \pm 0.157	0.572 \pm 0.136	3.273 \pm 1.207	25.338 \pm 10.801	2.778 \pm 0.613	8.309 \pm 1.856
3 μM	0.370 \pm 0.037	0.491 \pm 0.028	0.240 \pm 0.155	0.326 \pm 0.105	5.865 \pm 0.539	34.931 \pm 7.531	1.133 \pm 0.225	4.716 \pm 1.147
10 μM	0.417 \pm 0.084	0.416 \pm 0.040	0.061 \pm 0.032	0.142 \pm 0.038	10.762 \pm 0.991	82.398 \pm 13.387	2.290 \pm 0.651	7.499 \pm 2.077
30 μM	0.471 \pm 0.044	0.412 \pm 0.029	0.079 \pm 0.024	0.055 \pm 0.016	8.482 \pm 1.376	56.192 \pm 9.074	0.609 \pm 0.124	1.374 \pm 0.112

**Compound
27**



[conc]	Agonist response		Residual 60 μ M ACh response		Residual potentiated response		Agonist potentiated response	
	peak current	net charge	peak current	net charge	peak current	net charge	peak current	net charge
1 μM	0.140 \pm 0.030	0.271 \pm 0.046	0.512 \pm 0.140	0.543 \pm 0.153	2.248 \pm 0.581	22.473 \pm 10.159	4.561 \pm 0.671	15.176 \pm 2.668
3 μM	0.301 \pm 0.033	0.331 \pm 0.033	0.265 \pm 0.093	0.314 \pm 0.071	4.127 \pm 1.044	19.493 \pm 5.889	4.093 \pm 0.721	19.463 \pm 7.808
10 μM	0.240 \pm 0.037	0.319 \pm 0.019	0.124 \pm 0.040	0.201 \pm 0.038	5.502 \pm 0.497	30.739 \pm 8.769	3.336 \pm 0.349	10.740 \pm 2.472
30 μM	0.228 \pm 0.054	0.279 \pm 0.053	0.034 \pm 0.013	0.072 \pm 0.015	3.066 \pm 0.523	21.771 \pm 7.435	2.307 \pm 0.265	8.582 \pm 1.291

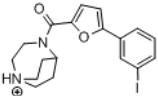
Compound 32 	Two-shot experiment ^a						One-shot experiment ^b	
	Agonist response		Residual 60 μM ACh response		Residual potentiated response		Agonist potentiated response	
[conc]	peak current	net charge	peak current	net charge	peak current	net charge	peak current	net charge
1 μM	0.225 ± 0.057	0.283 ± 0.031	0.457 ± 0.139	0.421 ± 0.124	7.844 ± 2.711	61.351 ± 22.487	4.217 ± 1.001	15.026 ± 2.904
3 μM	0.220 ± 0.016	0.391 ± 0.047	0.340 ± 0.102	0.376 ± 0.079	3.743 ± 0.890	16.641 ± 4.439	2.581 ± 0.462	6.470 ± 0.754
10 μM	0.290 ± 0.036	0.309 ± 0.022	0.050 ± 0.012	0.200 ± 0.058	3.002 ± 0.387	10.319 ± 1.138	1.842 ± 0.308	4.414 ± 0.525
30 μM	0.314 ± 0.016	0.304 ± 0.032	0.110 ± 0.045	0.112 ± 0.025	4.232 ± 2.476	10.323 ± 6.777	0.538 ± 0.101	0.942 ± 0.155

Table 7: Electrophysiological data of 1, 3, 10, 30 μM of **12**, **22-24**, **27** and **32** on human $\alpha 7$ nAChRs expressed in *Xenopus* oocytes. Data are reported as mean ± SEM (standard error of mean) and relative to two 60 μM ACh pre-controls. (a) Two-shot experiment: Agonist response refers to receptor response to 1, 3, 10 and 30 μM application of test compound, residual ACh response refers to receptor response to 60 μM application of control and residual potentiated response refers to receptor response to 1, 3, 10 and 30 μM application of type-II PAM PNU-120596. (b) One-shot experiment: Agonist potentiated response refers to receptor response to 1, 3, 10 and 30 μM test compound in co-application with 10 μM of type-II PAM PNU-120596.

4.6 Recovery study for NS6740 and compound 27

Due to their long-lasting effects of **NS6740** and its bioisosteric analog **27**, recovery studies were performed on the two compounds, aimed at investigating the time-dependent residual $\alpha 7$ nAChR desensitization triggered by application of 10 μM test drug. To this end, after 10 μM of drug (**NS6740** or **27**), six subsequent 60 μM ACh post-control applications at different increasing time points were delivered and the corresponding evoked responses were measured. Finally, we applied 10 μM PNU-120596 to further verify the persistent presence of test drug in the receptor binding site. The degree of ACh post-control inhibition and PNU-120596 potentiation allowed us to estimate the extent of desensitization induced by each specific **NS6740** derivative. In other words, the recovery studies aimed at determining how long it takes for the $\alpha 7$ subtype to transition from the non-conductive D_s to the closed state, and therefore recover from the desensitization induced by each specific derivative. **Figure 39** reports the net charge data corresponding to each single shot of ACh and PNU-120596.

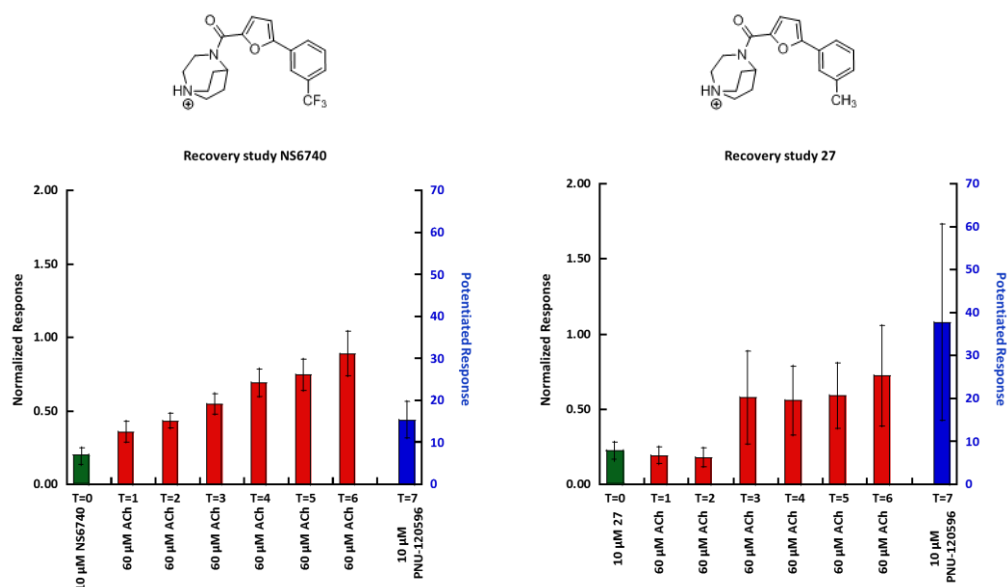


Figure 39: Recovery study of **NS6740** and compound **27**: 10 μM drug, six 60 μM ACh controls given at different increasing time points, 10 μM type II PAM PNU-120596.

In the case of **NS6740**, the six ACh post-control responses gradually recovered from desensitization and were up to full channel activation within the last ACh shot. Good inhibiting results characterized the first two shots of ACh, with receptor

activations lower than 50% of full pre-control responses (net charges 0.36 ± 0.07 and 0.43 ± 0.05 , respectively).

The final delivery of 10 μM PNU-120596 highlighted the prolonged receptor binding of **NS6740**. In fact, residual PAM-potentiation was still detected after an extended period of time between **NS6740** shot and PNU-120596 application, longer than the one in a simple two-shot experiment.

Compound **27** displayed a less gradual inhibition of ACh post-controls, partially due to the higher variability of the net charge values affecting ACh shots three to six. Interestingly, the residual ACh channel activations observed for the first two post-controls (net charges 0.2 ± 0.06 and 0.18 ± 0.06 , respectively) were lower than the corresponding ones for **NS6740**. The ACh inhibition induced by **27** for shots three to six was comparable to the **NS6740** data set.

Finally, as already observed for **NS6740**, 10 μM PNU-120596 gave remarkable residual channel potentiation, demonstrating the persistent presence of compound **27** within the binding domain.

4.7 Concentration-response curves for strong partial agonists **13** and **17**

The newly synthesized compounds **13** and **17** demonstrated strong partial agonist behavior with channel opening responses respectively of 0.70 ± 0.04 ($\approx 70\%$ of ACh response) and 0.8 ± 0.03 ($\approx 80\%$ ACh response) when tested at 10 μM on the $\alpha 7$ nAChR. Therefore, we generated the concentration-response curves (CRCs) (**Figure 40**) in order to obtain the I_{MAX} and EC_{50} values for **13** and **17**. Derivatives **13** and **17** were tested at different concentrations (0.1, 0.3, 1, 3, 10, and 30 μM) and the corresponding evoked net charge values were measured. The two CRCs highlighted greater receptor responses evoked by **17** compared to **13** for all the concentrations tested and this was particularly evident for concentrations equal to or lower than 1 μM . The CRCs data were fit to the Hill equation using the Levenberg-Marquardt algorithm. I_{MAX} and EC_{50} values were then extrapolated:

- Compound **13** showed $I_{\text{MAX}} = 0.71 \pm 0.02$ and $EC_{50} = 764 \pm 52$ nM;
- Compound **17** showed $I_{\text{MAX}} = 0.81 \pm 0.01$ and $EC_{50} = 322 \pm 18$ nM.

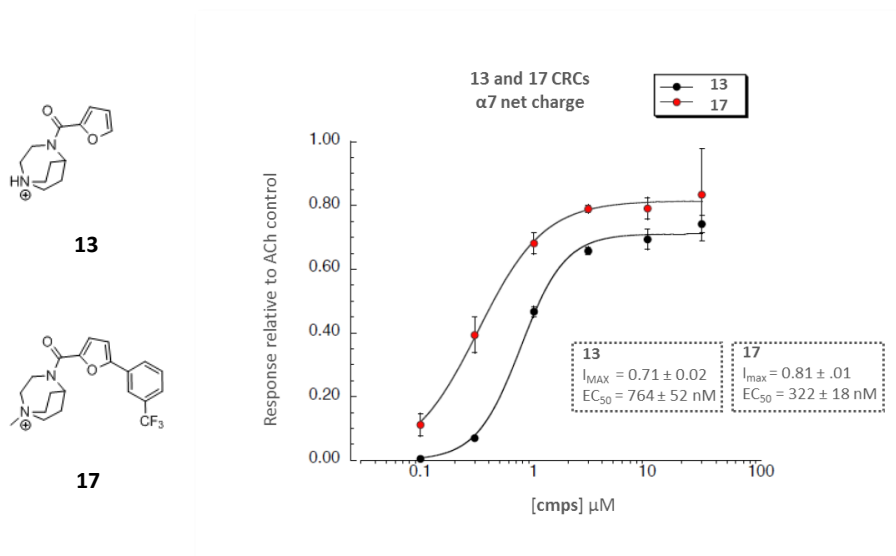


Figure 40: Concentration-response curves for partial agonists 13 and 17.

Despite the differences in their molecular structures, both **13** and **17** proved to be very good partial agonists. The removal of the substituted phenyl ring in **13** as well as the methylation of bicyclic tertiary amine in **17** was detrimental to the original silent activity of **NS6740**, but favorable for partial agonist activation. Considering the results obtained for **13** and **17**, we could conclude that both the free tertiary amine and the phenyl ring are mandatory requirements to stabilize the prolonged desensitization of **NS6740**.

4.8 Electrophysiological investigation for NS6740 derivatives on the nicotinic heteromeric receptors $\alpha 4\beta 2$ and $\alpha 3\beta 4$

In order to evaluate their selectivity for $\alpha 7$ nAChR, the selected most interesting NS6740 derivatives **12**, **13**, **17**, **22-24**, **27**, and **32** were tested on the nicotinic heteromeric receptors $\alpha 4\beta 2$ and $\alpha 3\beta 4$.

Depending on the data collected on the $\alpha 7$ receptor, two different protocols were applied on both heteromeric receptors:

- Good partial agonist **13** and **17**. After two shots of 100 ($\alpha 3\beta 4$) or 30 ($\alpha 4\beta 2$) μM ACh pre-control, used to normalize the data set, 100 μM of test drug was applied, followed by 30 ($\alpha 3\beta 4$) or 100 ($\alpha 4\beta 2$) μM ACh post-control.
- Weak partial agonists and good desensitizers **12**, **22-24**, **27**, and **32**. Two different protocols were followed to evaluate the agonist (1) or the antagonist (2) profile at the heteromeric nAChRs. Briefly, the protocols consisted in the following subsequential steps: (1) after two shots of 100 ($\alpha 3\beta 4$) or 30 ($\alpha 4\beta 2$) μM ACh pre-control, used to normalize the data set, 30 μM of test drug was applied, followed by 100 ($\alpha 3\beta 4$) or 30 ($\alpha 4\beta 2$) μM ACh post-control; (2) after two shots of 100 ($\alpha 3\beta 4$) or 30 ($\alpha 4\beta 2$) μM ACh pre-control, used to normalize the data set, 30 μM of test drug was applied in co-application with 100 ($\alpha 3\beta 4$) or 30 ($\alpha 4\beta 2$) μM ACh, followed by 100 μM ACh post-control.

As depicted in [Table 8](#), **13** and **17** were completely inactive on both heteromeric receptors $\alpha 4\beta 2$ and $\alpha 3\beta 4$. They did not show neither agonist activity when tested alone nor residual inhibition of ACh post-control.

$\alpha 4\beta 2$				
Compound	100 μM test drug		30 μM ACh post-control response	
	peak current	net charge	peak current	net charge
13	0.007 \pm 0.002	0.002 \pm 0.001	1.115 \pm 0.035	1.255 \pm 0.053
17	0.003 \pm 0.001	0.000 \pm 0.000	1.160 \pm 0.059	1.066 \pm 0.051

$\alpha 3\beta 4$				
Compound	100 μM test drug		100 μM ACh post-control response	
	peak current	net charge	peak current	net charge
13	0.004 \pm 0.001	0.002 \pm 0.001	0.990 \pm 0.025	0.933 \pm 0.036
17	0.019 \pm 0.005	0.014 \pm 0.004	0.906 \pm 0.040	0.722 \pm 0.058

Table 8: Electrophysiological results on heteromeric receptors $\alpha 4\beta 2$ and $\alpha 3\beta 4$ for **13** and **17**: the responses were normalized on two 100 ($\alpha 3\beta 4$) or 30 ($\alpha 4\beta 2$) μM ACh pre-controls (data not shown); 100 μM of test drug was applied in order to evaluate the agonist activity; finally, in order to study the residual post-control activation, 100 ($\alpha 3\beta 4$) or 30 ($\alpha 4\beta 2$) μM ACh was given to the receptor.

Table 9 reports the data set for **12**, **22-24**, **27** and **31** tested on the heteromeric receptors $\alpha 4\beta 2$ and $\alpha 3\beta 4$. None of the tested derivatives displayed agonist activity on either $\alpha 4\beta 2$ or $\alpha 3\beta 4$. However, in co-application with ACh all of the tested compounds presented reversible antagonist behavior, as evidenced by the decreased ACh responses compared to the controls (net charge values lower than 1). The inhibition of ACh and therefore the antagonism profile of the derivatives was particularly strong on the $\alpha 3\beta 4$, with residual ACh responses never greater than 30% of the pre-control.

$\alpha 4\beta 2$								
<i>Compound</i>	30 μM test drug (1)		30 μM ACh post-control response (1)		30 μM test drug + 30 μM ACh (2)		30 μM ACh post-control response (2)	
	<i>peak current</i>	<i>net charge</i>	<i>peak current</i>	<i>net charge</i>	<i>peak current</i>	<i>net charge</i>	<i>peak current</i>	<i>net charge</i>
12	0.003 \pm 0.001	0.000 \pm 0.000	1.136 \pm 0.067	1.102 \pm 0.059	0.840 \pm 0.051	0.704 \pm 0.038	1.204 \pm 0.029	1.019 \pm 0.034
22	0.061 \pm 0.016	0.020 \pm 0.013	1.046 \pm 0.051	1.143 \pm 0.095	0.811 \pm 0.036	0.652 \pm 0.034	1.127 \pm 0.028	1.038 \pm 0.023
23	0.003 \pm 0.000	0.001 \pm 0.084	0.957 \pm 0.097	0.914 \pm 0.084	0.788 \pm 0.080	0.693 \pm 0.052	0.985 \pm 0.075	0.869 \pm 0.064
24	0.025 \pm 0.008	0.003 \pm 0.001	1.165 \pm 0.108	1.181 \pm 0.103	0.514 \pm 0.019	0.414 \pm 0.067	0.849 \pm 0.034	0.716 \pm 0.071
27	0.004 \pm 0.002	0.002 \pm 0.001	1.160 \pm 0.061	1.235 \pm 0.070	0.622 \pm 0.076	0.509 \pm 0.079	1.119 \pm 0.074	0.928 \pm 0.052
32	0.024 \pm 0.008	0.004 \pm 0.001	1.046 \pm 0.067	1.087 \pm 0.068	0.471 \pm 0.040	0.433 \pm 0.066	0.788 \pm 0.069	0.698 \pm 0.065

$\alpha 3\beta 4$								
<i>Compound</i>	30 μM test drug (1)		100 μM ACh post-control response (1)		30 μM test drug + 100 μM ACh (2)		30 μM ACh post-control response (2)	
	<i>peak current</i>	<i>net charge</i>	<i>peak current</i>	<i>net charge</i>	<i>peak current</i>	<i>net charge</i>	<i>peak current</i>	<i>net charge</i>
12	0.003 \pm 0.001	0.001 \pm 0.000	0.984 \pm 0.031	0.855 \pm 0.066	0.161 \pm 0.018	0.213 \pm 0.024	0.933 \pm 0.040	0.812 \pm 0.042
22	0.005 \pm 0.001	0.003 \pm 0.002	1.032 \pm 0.066	1.015 \pm 0.067	0.304 \pm 0.049	0.302 \pm 0.043	0.985 \pm 0.049	0.873 \pm 0.038
23	0.013 \pm 0.009	0.006 \pm 0.004	0.917 \pm 0.044	0.901 \pm 0.063	0.128 \pm 0.014	0.201 \pm 0.034	0.854 \pm 0.033	0.845 \pm 0.045
24	0.003 \pm 0.001	0.001 \pm 0.000	0.972 \pm 0.045	1.092 \pm 0.134	0.141 \pm 0.031	0.218 \pm 0.040	0.744 \pm 0.062	0.685 \pm 0.065
27	0.019 \pm 0.008	0.009 \pm 0.005	1.178 \pm 0.089	1.209 \pm 0.151	0.096 \pm 0.027	0.138 \pm 0.045	0.825 \pm 0.034	0.752 \pm 0.046
32	0.004 \pm 0.002	0.001 \pm 0.001	0.899 \pm 0.032	0.886 \pm 0.047	0.156 \pm 0.021	0.244 \pm 0.048	0.832 \pm 0.086	0.819 \pm 0.081

Table 9: Electrophysiological results on heteromeric receptors $\alpha 4\beta 2$ and $\alpha 3\beta 4$ for **12, 22-24, 27** and **32**: All responses were normalized on two 100 ($\alpha 3\beta 4$) or 30 ($\alpha 4\beta 2$) μM ACh pre-controls (data not shown), **(1)** 30 μM of test drug was applied alone, followed by 100 ($\alpha 3\beta 4$) or 30 ($\alpha 4\beta 2$) μM ACh post-control; **(2)** co-application of 30 μM test drug with 100 ($\alpha 3\beta 4$) or 30 ($\alpha 4\beta 2$) μM ACh, followed by 100 ($\alpha 3\beta 4$) or 30 ($\alpha 4\beta 2$) μM ACh.

4.9 Electrophysiological evaluation for KC-1 derivatives

The profiles of compounds **34-37** at the $\alpha 7$ nAChR were defined following the protocols previously described in 4.2.1. The corresponding data are reported in **Figure 41** and **Table 10**.

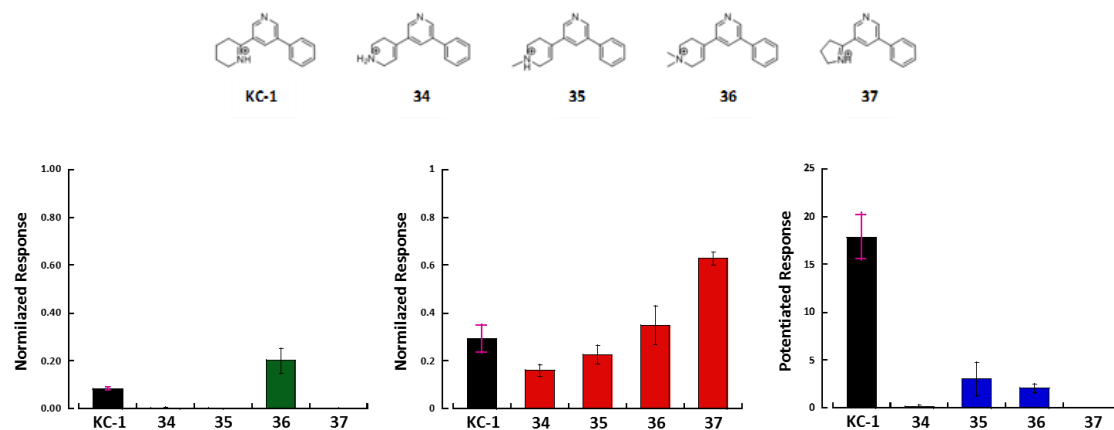


Figure 41: Electrophysiological data of 100 μ M **34-37** on human $\alpha 7$ nAChRs expressed in *Xenopus* oocytes. Green bars: agonist response when **34-37** are applied alone at 100 μ M; red bars: inhibition of 60 μ M ACh control in co-application with 100 μ M **34-37**; blue bars: receptor potentiation given by co-application of 100 μ M **34-37** and 10 μ M type II PAM PNU-120596. Black bars refer to **KC-1** data.

The modification of the original anabaseine portion in derivatives **34-37** by introducing a different basic nucleus compromised the **KC-1** silent behavior.

When tested alone, **34** showed no agonist activity (net charge 0.004 ± 0.001) and a full recovered ACh post-control response (data not shown). The ACh inhibition (residual response net charge 0.16 ± 0.02) given by **34** co-applied with 60 μ M ACh, and the absence of PNU-related potentiation confirmed the reversible antagonist activity associated with derivative **34**.

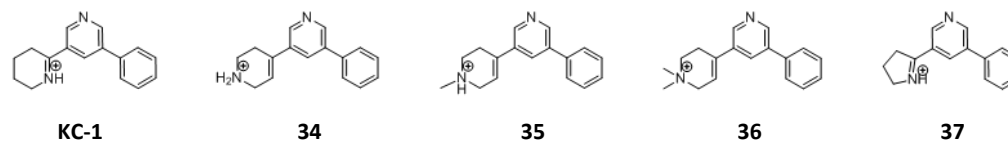
Compound **35** was not able to evoke channel opening when tested alone (net charge 0.003 ± 0.002) and in the same experiment the ACh post-control response was not affected (data not shown). The lack of ACh inhibition demonstrated the inability of **35** to stabilize the desensitized state. When co-applied with 60 μ M ACh, the ACh response was strongly inhibited (0.23 ± 0.04) but no residual post-control inhibition was observed (data not shown). Finally, the co-application of **35** with 10 μ M PNU-120596 induced very low potentiated activation (3 ± 1.8), thus making **35** a reversible very weak silent agonist.

The results collected for **34** and **35** demonstrated that modifications on the nitrogen position in the basic ring, which led to an increased distance between the positive charge and the hydrogen bond acceptor, were completely detrimental for the stabilization of $\alpha 7$ nAChR non-conductive states associated with **KC-1**.

On the other hand, compound **36**, bearing a permanent positive charge, resulted to be a weak partial agonist, with channel activation $\approx 20\%$ of ACh response.

Finally, the smaller dimensions of basic nucleus in **37** determined a weak reversible antagonism, characterized by no channel opening, fully recovered receptor after application of test drug alone (data not shown), medium-low ACh inhibition (net charge 0.63 ± 0.03) and absence of PNU-related response.

The modification of the original anabaseine portion, with the introduction of a different basic nucleus, compromised the **KC-1** silent behavior.



Compound	Agonist response		60 μ M ACh response inhibition		Agonist potentiated response	
	peak current	net charge	peak current	net charge	peak current	net charge
KC-1 (2)	0.004 \pm 0.001	0.083 \pm 0.009	0.170 \pm 0.080	0.290 \pm 0.060	4.100 \pm 0.680	17.800 \pm 2.400
34	0.002 \pm 0.000	0.004 \pm 0.001	0.131 \pm 0.021	0.160 \pm 0.024	0.062 \pm 0.036	0.199 \pm 0.151
35	0.016 \pm 0.007	0.003 \pm 0.002	0.198 \pm 0.106	0.226 \pm 0.038	1.980 \pm 1.273	3.019 \pm 1.792
36	0.120 \pm 0.036	0.201 \pm 0.052	0.545 \pm 0.095	0.350 \pm 0.080	0.732 \pm 0.165	2.067 \pm 0.458
37	0.006 \pm 0.002	0.000 \pm 0.005	0.526 \pm 0.065	0.628 \pm 0.026	0.031 \pm 0.010	0.001 \pm 0.004

Table 10: Electrophysiological data of **KC-1** derivatives **34-37** on human $\alpha 7$ nAChRs expressed in *Xenopus* oocytes. Data are reported as mean \pm SEM (standard error of mean) and relative to two 60 μ M ACh pre-controls. Agonist response refers to receptor response to 100 μ M application of test compound, ACh inhibition refers to receptor response to 60 μ M application of control co-applied with 100 μ M test drug and residual potentiated response refers to receptor response to 100 μ M test drug co-applied with 10 μ M type-II PAM PNU-120596.

4.10 Electrophysiological investigation for KC-1 derivatives on the nicotinic heteromeric receptor $\alpha 4\beta 2$

In order to evaluate their selectivity for $\alpha 7$ nAChR, **34**, **35**, **36** and **37** were tested on heteromeric receptor $\alpha 4\beta 2$.

Compound	100 μ M test drug (1)		100 μ M test drug + 30 μ M ACh (2)	
	peak current	net charge	peak current	net charge
34	0.068 \pm 0.011	0.044 \pm 0.008	0.433 \pm 0.041	0.487 \pm 0.029
35	0.091 \pm 0.021	0.088 \pm 0.016	0.402 \pm 0.034	0.409 \pm 0.031
36	0.034 \pm 0.006	0.050 \pm 0.011	0.050 \pm 0.006	0.040 \pm 0.009
37	0.013 \pm 0.006	0.004 \pm 0.005	0.752 \pm 0.027	0.692 \pm 0.031

Table 11: Electrophysiological results on heteromeric receptor $\alpha 4\beta 2$ for **34**, **35**, **36** and **37**: the responses were normalized on two 100 μ M ACh pre-controls (data not shown); (1) 100 μ M of test drug was applied in order to evaluate the agonist activity; finally, in order to study the residual post-control activation, 30 μ M ACh was given to the receptor.

The data reported in **Table 11** demonstrated the antagonist activity characterizing compounds **34-37**. While no channel opening was detected when the compounds were tested alone at 100 μ M, **34-37** were able to reduce the ACh responses evoked when 100 μ M of test drug was co-applied with 100 μ M ACh. The strongest ACh inhibition was observed for compound **36** (net charge 0.04 \pm 0.01).

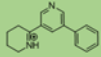
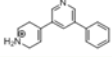
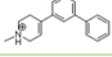
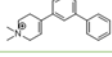
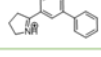
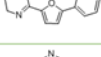


The following **Table 12** summarizes all the electrophysiological results obtained for the lead compounds **NS6740** and **KC-1** and their corresponding derivatives **11-33** and **34-40** respectively, on $\alpha 7$ nAChR.

Table 12: Summary of the electrophysiological profiles of the lead compounds NS6740 and KC-1 and their related target compounds.

NS6740 derivatives

Cmp	Structure	Electrophysiological profile
NS6740		<ul style="list-style-type: none"> ❖ Very weak partial agonist ❖ Long term desensitization
11		<ul style="list-style-type: none"> ❖ No agonist activity ❖ No desensitizing properties
12		<ul style="list-style-type: none"> ❖ Weak partial agonist ❖ Long term desensitization
13		<ul style="list-style-type: none"> ❖ Strong partial agonist ❖ No desensitizing properties
14		<ul style="list-style-type: none"> ❖ No agonist activity ❖ Short lasting silent agonist
15		<ul style="list-style-type: none"> ❖ No agonist activity ❖ No desensitizing properties
16		<ul style="list-style-type: none"> ❖ No agonist activity ❖ No desensitizing properties
17		<ul style="list-style-type: none"> ❖ Strong partial agonist ❖ No long term desensitization
18		<ul style="list-style-type: none"> ❖ No agonist activity ❖ No desensitizing properties
19		<ul style="list-style-type: none"> ❖ No agonist activity ❖ Short lasting silent agonist
20		<ul style="list-style-type: none"> ❖ Very weak partial agonist ❖ Short lasting silent agonist
21		<ul style="list-style-type: none"> ❖ Very weak partial agonist ❖ No desensitizing properties
22		<ul style="list-style-type: none"> ❖ Very weak partial agonist ❖ Long term desensitization
23		<ul style="list-style-type: none"> ❖ Weak partial agonist ❖ Long term desensitization
24		<ul style="list-style-type: none"> ❖ Weak partial agonist ❖ Long term desensitization
25		<ul style="list-style-type: none"> ❖ Very weak partial agonist ❖ Short lasting silent agonist
26		<ul style="list-style-type: none"> ❖ Weak partial agonist ❖ Long term desensitization
27		<ul style="list-style-type: none"> ❖ Weak partial agonist ❖ Long term desensitization
28		<ul style="list-style-type: none"> ❖ Weak partial agonist ❖ No long term desensitization
29		<ul style="list-style-type: none"> ❖ Weak partial agonist ❖ Long term desensitization
30		<ul style="list-style-type: none"> ❖ Very weak partial agonist ❖ No desensitizing properties
31		<ul style="list-style-type: none"> ❖ Very weak partial agonist ❖ Short lasting silent agonist
32		<ul style="list-style-type: none"> ❖ Weak partial agonist ❖ Long term desensitization
33		<ul style="list-style-type: none"> ❖ Weak partial agonist ❖ No long term desensitization

Table 12: Summary of the electrophysiological profiles of the lead compounds **NS6740** and **KC-1** and their related target compounds.

KC-1 derivatives	Cmp	Structure	Electrophysiological profile
	KC-1		❖ Short lasting silent agonist
	34		❖ Reversible antagonist
	35		❖ Very weak silent agonist
	36		❖ Weak partial agonist
	37		❖ Weak reversible antagonist
	38		❖ To be tested
	39		❖ To be tested
40		❖ To be tested	

CHAPTER V

In silico studies

5.1 General docking protocol

Docking studies were carried out to analyze the binding modes of the two classes of silent agonists. As already discussed, the $\alpha 7$ nAChR is composed by five alpha identical subunits, which implies five binding sites available for the molecular recognition of ligand compounds.

Docking investigations started from non-symmetry-enforced homology model 2 (HM2), previously built by Dr. Aican Gulsevin, in the Dr. Horenstein's lab at the Chemistry Department of the University of Florida. This homology model was generated by employing the epibatidine- $\alpha 7$ -AChBP chimera complex [25] and considering CHRNA7 (UniProt Identifier: P36544-1) as the target sequence. Initially, the h $\alpha 7$ nAChR subunit was cropped to fit the starting crystal structure, resulting to be composed by 204 amino acids. Then, the non-homologous residues were substituted and optimized by energy minimization. The modeling process was performed without imposing fivefold symmetry, thus obtaining an asymmetric final homology structure composed by 1020 total amino acids, uniformly distributed in the five subunits A, B, C, D and E named in a counter-clockwise direction and viewed from the top of the channel. The binding pocket was localized at the interface between two different subunits; these interfaces were identified as I_{AB}, I_{BC}, I_{CD}, I_{DE} and I_{EA}, where the first letter represented the positive face, while the second letter the negative one. Any resulting five binding pocket contained one molecule of epibatidine. Given the nature of a non-symmetric model, docking calculations were run at all five interfaces.

Initially, ligand structures were drawn using Molview (MolView.org) and then Molden 5.0 [83] was used to optimize the bond lengths and to introduce the protonation on the basic nitrogen. The final ensuing structures were then optimized in their geometry employing a two-step procedure: HF/6-31G* optimization followed by B3LYP/6-31G** optimization (Gaussian 09).

Once completed the geometry optimization, the resulting structures, converted into .mol2 files, were prepared for the following docking investigation using the LigPrep program (Schrödinger Suite 2014-2). Regarding the ionization, the possible states at target pH = 7 ± 2 were generated.

Glide XP, belonging to Schrödinger Suite 2014-2 [84], was employed to run the docking analysis. Ligand sampling flexibility was permitted during calculations, the

planarity of conjugated pi atom was enhanced, intramolecular hydrogen bonds were rewarded and post-docking minimization was applied.

Two different grids were built to run the calculation:

- a small grid covered the orthosteric binding site and was related to the original epibatidine position in the $\alpha 7$ -AChBP crystal structure used as template;
- a large grid covered a wider portion of each subunit that also included the DAA (Direct Allosteric Activation) site.

GlideScore was taken into account to analyze single results. It is an empirical scoring function that approximates the ligand binding free energy and allows classifying compounds based on their binding affinity.

GlideScore includes the terms occurring in the binding process, such as:

- lipophilic-lipophilic term
- hydrogen bonds
- rotatable bond penalty
- protein-ligand coulomb-vdW energies
- hydrophobic enclosure

For a correct interpretation of the docking results obtained from these investigations, some points have to be considered. As mentioned above, the used $\alpha 7$ extracellular domain structure is a homology model since an actual experimental structure of extracellular domain is not available. Moreover, the $\alpha 7$ receptor desensitization likely involves cooperativity between subunits, and surely involves conformational changes in the transmembrane region, which are not part of the model. Thus, it's difficult to correlate desensitization with particular extracellular domain poses of the various bound compounds. Besides, the static model employed in docking analysis and the followed procedure, which use one interface at a time, can't reproduce the physiological reciprocal influence of ligand binding at the five already cited receptor interfaces I_{AB} , I_{BC} , I_{CD} , I_{DE} and I_{EA} . Because of these limits, sometimes compounds might show similar binding mode despite different electrophysiological results. Finally, poses associated with GlideScore values 3 kcal/mol lower than the best one were not considered in the analysis. The necessity of setting up a cutoff value might exclude some poses which could turn out to be physiologically relevant.

Therefore, the docking data here reported represent important preliminary studies that lead to predictions about point to point interactions of the ligands with the receptor side chains. However, due to uncertainty associated to these modeling

investigations, molecular dynamic simulations and targeted future mutagenesis experiments will have to be performed to support and complete these preliminary results and shed light on the molecular interactions that promote the silent agonism profile and the related metabotropic $\alpha 7$ receptor function.

5.2 Docking investigation of NS6740 and its derivatives

NS6740 and its analogs were docked following the previously described procedure. Analyzing the obtained results, only protonated forms were considered, given the high pK_a value for the tertiary amine embedded in the diazabicyclic structure and the consideration that active nicotinic orthosteric ligands require a positive charge. At physiological $pH=7$, in fact, the studied ligands are mainly positively charged. In addition, poses associated with GlideScore values 3 kcal/mol lower than the best one were not considered for this analysis.

Selected derivatives **12**, **22-24**, **27** and **32** were docked because they showed a desensitizing profile similar to that of NS6740. Then, the docking investigation of derivative **28** was aimed at highlighting putative differences in the binding process between *meta* and *para* position of the CF_3 substituent. Finally, compound **33** was studied to evaluate the possible interactions given by the more polar nitro group.

5.2.1 Docking of NS6740, 12, 22-24, 27 and 32

The following **Table 13** reports the binding site, GlideScore and number of acceptable poses on WT $\alpha 7$ nAChR calculated by docking with the large grid.

Interface AB showed low values for GlideScore, that, as already reported in the general protocol description, approximates ligand binding free energy. Moreover, all docked compounds were located in the orthosteric site, showing a similar binding mode, also in terms of ligand-receptor interactions. The same uniformity of results was not found for I_{BC} and I_{CD} , where docking poses in both orthosteric and DAA sites were found. Furthermore, the GlideScore associated with interfaces I_{BC} and I_{CD} was higher than that found for I_{AB} , thus describing a less favorable binding process.

Interface DE favored the binding in the DAA site for all compounds; although sharing the same binding pocket and orientation, the specific ligand-receptor interactions were not uniform. The GlideScore associated with I_{DE} was the highest found in this docking investigation.

	INTERFACES				
	AB	BC	CD	DE	EA
NS6740					
SITE	ORTHOSTERIC	ORTHOSTERIC	DAA	DAA	ORTHOSTERIC
GLIDE SCORE	-14.315	-6.864 / -8.860	-8.756, -7.502	-6.861 / -5.308	-10.006/-8.780
n° OF POSES	1	4	2	3	4
compound 12					
SITE	ORTHOSTERIC	ORTHOSTERIC	DAA	DAA	ORTHOSTERIC
GLIDE SCORE	-13.289, -12.520	-7.954 / -6.091	-7.473 / -6.781	-5.723 / -4.654	-12.715 / -10.734
n° OF POSES	2	3	3	3	3
compound 22					
SITE	ORTHOSTERIC	ORTHOSTERIC	DAA	DAA	ORTHOSTERIC
GLIDE SCORE	-13.551	-10.089 / -7.356	-7.174 / -5.275	-6.064 / -4.378	-9.432/-9.270
n° OF POSES	1	3	3	4	4
compound 23					
SITE	ORTHOSTERIC	ORTHOSTERIC	DAA	DAA	ORTHOSTERIC
GLIDE SCORE	-13.482	-8.890 / -6.081	-7.948	-6.212 / -4.592	-10.746
n° OF POSES	1	4	1	4	1
compound 24					
SITE	ORTHOSTERIC	DAA	ORTHOSTERIC	DAA	ORTHOSTERIC
GLIDE SCORE	-13.338	-6.037	-9.478 / -8.277	-5.616 -5.115	-4.596 -3.429
n° OF POSES	1	1	4	2	2
compound 27					
SITE	ORTHOSTERIC	ORTHOSTERIC	DAA	DAA	ORTHOSTERIC
GLIDE SCORE	-13.664 / -12.652	-6.522	-10.722	-6.581 / -5.105	-12.687, -12.205
n° OF POSES	4	1	1	3	2
compound 32					
SITE	ORTHOSTERIC	ORTHOSTERIC	ORTHOSTERIC	DAA	ORTHOSTERIC
GLIDE SCORE	-13.400, -12.605	-8.757, -7.175	-10.285 / -9.946	-5.593 / -5.389	-9.705 / -9.675
n° OF POSES	2	2	3	3	3

Table 13: Summary of sites, GlideScore and number of poses found for NS6740 and 12, 22-24, 27 and 32 for each interface. When one or two poses were found, GlideScore is reported specifically for each pose; when more possible poses were identified, the range of GlideScore is reported.

Finally, the interaction at I_{EA} gave rise to similar results for all compounds in terms of binding site, and the orthosteric portion of the receptor protein emerged as the favorite one, with a general, very good GlideScore. Surprisingly, compound **24** was associated with a much lower value of GlideScore and this was explicable with its different orientation within the orthosteric site. While all the other compounds placed the basic nucleus in the so called aromatic cage, compound **24** was upside down, with the phenyl portion interacting with Trp E149. Most likely, the absence of interactions between the positive charge and the residues located in the aromatic region under the C-loop determined the higher value of GlideScore.

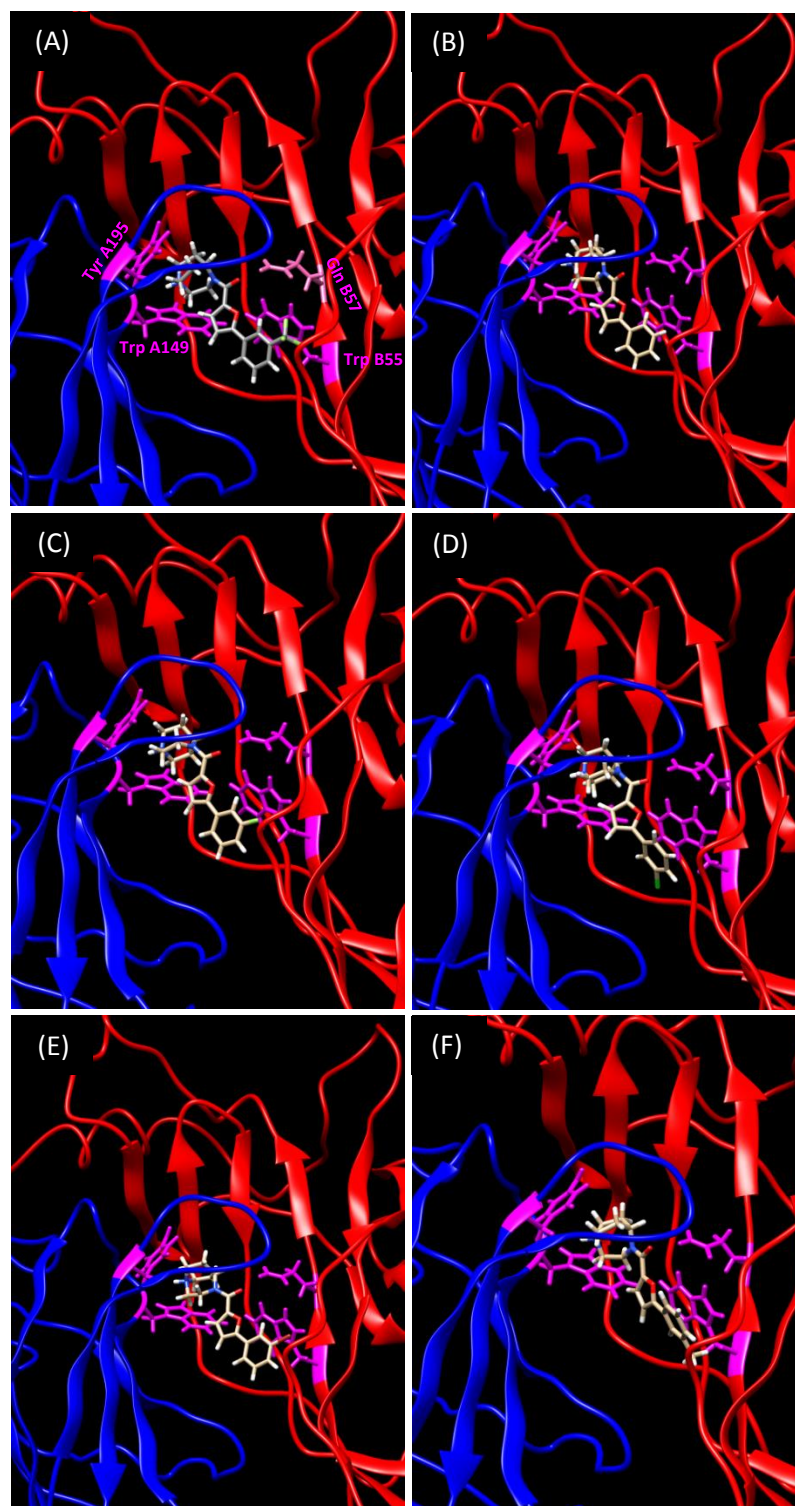
From the analysis and comparison of docking results, we concluded that I_{AB} better described the potential binding mode of **NS6740** and its derivatives. This interface, in fact, not only displayed the best GlideScore and similar binding poses among these good desensitizing agents, but also the interactions found for each compound were consistent with the typical interactions for partial agonists reported in literature [85].

The results found for I_{AB} showed that **NS6740** and its analogs are placed in the orthosteric site, with the positively charged diazabicyclic structure embedded in the aromatic cage.

Specifically, the typical partial agonist interactions were exhibited:

- Hydrogen bond with oxygen of Trp A149 backbone
- Two π -cation interactions with Trp A149 sidechain
- One π -cation interaction with Tyr A195 sidechain

Moreover, the carbonyl group, that represented the hydrogen bond acceptor moiety in the pharmacophore model, established a hydrogen bond with Gln B57 sidechain, with a bond-distance of 2.08 Å. The aromatic portions pointed under the C-loop, and the furan and phenyl rings were at a suitable position for face-to-face π - π stacking with Trp B55. While the previously described interactions in the aromatic cage and the hydrogen bond with Gln B57 were established by all compounds, the aromatic interaction with Trp B55 were observed depending on the specific compound. The best poses for each compound on the I_{AB} are shown in **Figure 42**.



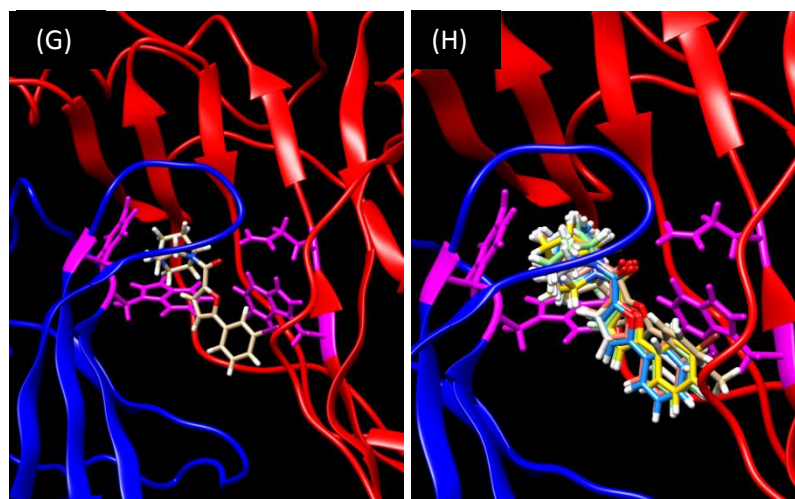


Figure 42: Best poses for NS6740, 12, 22, 23, 24, 27 and 32 in the orthosteric binding site of I_{AB} (subunit A blue, subunit B red). Interacting residues highlighted in magenta. (A): Best pose of NS6740; (B): Best pose of 12; (C): Best pose of 22; (D): Best pose of 23; (E): Best pose of 24; (F): Best pose of 27; (G): Best pose of 32; (H): all best poses superimposed.

As already discussed in Chapter 4, NS6740 showed a very weak partial agonist response, that was $\leq 20\%$ of ACh activation. The most interesting aspect about NS6740 behavior was the ability to promote and stabilize different receptor desensitized states over a long period. As a consequence, it strongly inhibited the ACh post-control response and the intense PNU-related potentiated channel opening. Compound 12, 22-24, 27 and 32 showed similar strong desensitizing properties, with a very weak partial agonism.

Keeping this in mind, it is not surprising to obtain similar binding poses from docking analysis and this supported our conclusion that I_{AB} better described the behavior of these compounds in the orthosteric domain of the $\alpha 7$ nAChR.

5.2.2 Docking of compound 28

Docking investigations of compound **28** were carried out following the same protocol previously described.

Although **28** showed a little structural modification, represented by the shifting of $-CF_3$ from *meta* to *para* position, it gave interestingly different results, especially in terms of ACh post-control inhibition and PNU-related response. Derivative **28**, in fact, was characterized by lower ability in stabilizing the desensitized states of $\alpha 7$ nAChRs, possibly due to the shorter binding time. Derivative **28** was docked on all interfaces, with the aim to highlight a possible reason for the loss of prolonged binding and receptor desensitization associated with the presence of the substituent in *para* position.

	INTERFACES				
	AB	BC	CD	DE	EA
NS6740					
SITE	ORTHOSTERIC	ORTHOSTERIC	DAA	DAA	ORTHOSTERIC
GLIDE SCORE	-14.315	-8.860 / -6.864	-8.756, -7.502	-6.861 / -5.308	-10.006/-8.780
n° OF POSES	1	4	2	3	4
compound 28					
SITE	ORTHOSTERIC	ORTHOSTERIC	DAA	DAA	ORTHOSTERIC
GLIDE SCORE	-15.047	-10.880	-6.979, -5.622	-6.750	-11.458, -11.245
n° OF POSES	1	1	2	1	2

Table 14: Summary of sites, GlideScore and number of poses found for NS6740 and 28 for each interface. When one or two poses were found, GlideScore is reported specifically for each pose; when more possible poses were identified, the range of GlideScore is reported.

Comparing the docking results for **NS6740** and **28**, similarities in terms of binding site and GlideScore for each interface were found (**Table 14**).

As already seen for **NS6740**, also **28** gave the best GlideScore in I_{AB} . Here, **28** established the typical partial agonist interactions in the aromatic cage (**Figure 43 A**):

- Hydrogen bond with oxygen of Trp A149 backbone
- π -cation interaction with Trp A149 sidechain
- π -cation interaction with Tyr A195 sidechain

In addition, the carbonyl group, that represented the hydrogen bond acceptor in the pharmacophore model, established an hydrogen bond with B Gln57 sidechain. Similarly to **NS6740**, the aromatic chain pointed under the C-loop and interacted with Trp B55 through a π - π staking interaction.

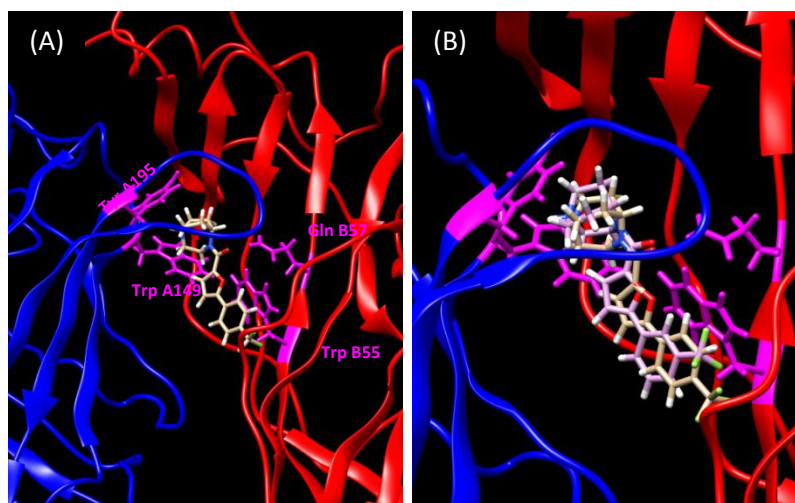


Figure 43: (A) Best pose for **28** in the orthosteric binding site of I_{AB} (subunit A blue, subunit B red). Interacting residues highlighted in magenta; (B) Structure overlapping of **NS6740** (lilac) and **28** (dove-grey) best poses.

The only difference observed overlapping the two structures was the shifted positions of furan and phenyl rings of **28** compared to those associated to **NS6740** pose (**Figure 43 B**).

Several hypothesis might be proposed:

- the shifted position of phenyl ring of **28** did not allow the establishment of a long lasting π - π stacking interaction, decreasing the residence time in the binding site;

- the *para* substitution determined electrostatic effects that negatively affected the formation and stabilization of π - π stacking interaction;
- the shifting of CF_3 from *meta* to *para* position would favor the interaction with a different interface.

Taking into account the last assumption, good alternative interfaces for **28** binding are represented by I_{BC} and I_{EA} . The docking results for I_{BC} (Figure 44 A) showed the basic nucleus of **28** placed in the aromatic cage of the orthosteric domain, with an hydrogen bond interaction between its protonated nitrogen and Trp B149 backbone. Additionally, a face-to-face π - π interaction between the furan portion and Tyr B93 sidechain was displayed. Finally, an hydrogen bond type interaction between CF_3 and nitrogen on the backbone of Ile C123 was established.

Docking results for I_{EA} (Figure 44 B) also showed the positively charged portion embedded in the aromatic cage, forming π -cation interactions with Trp E149 and with Tyr E188 and an hydrogen bond with the protonated nitrogen and Ser E148 backbone. An additional hydrogen bond was formed between the amide carbonyl group and Lys E145 sidechain, and, finally, an edge-to-face π - π stacking interaction with the furan moiety and Trp A55 sidechain was present.

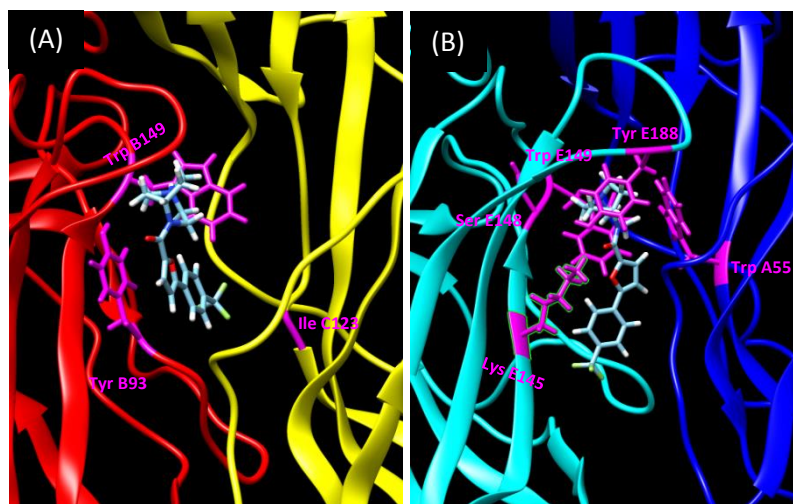


Figure 44: (A) Best pose for **28** in the orthosteric binding site of I_{BC} (subunit B red, subunit C yellow). (B) Best pose for **28** in the orthosteric binding site of I_{EA} (subunit E cyano, subunit A blue). Interacting residues highlighted in magenta.

5.2.3 Docking of compound **33**

Docking investigations of compound **33** were carried out following the same protocol previously described.

The replacement of original CF₃ with NO₂ group increased the partial agonist behavior in channel opening and allowed a faster receptor recovery and thus higher ACh post-control response. Losing the ability to persistently bind the receptor, the residual PNU-potentiated response was much lower than the one showed by **NS6740**.

In order to understand the role of the more polar nitro group in interacting with the binding site, **33** was docked on all interfaces.

	INTERFACES				
	AB	BC	CD	DE	EA
NS6740					
SITE	ORTHOSTERIC	ORTHOSTERIC	DAA	DAA	ORTHOSTERIC
GLIDE SCORE	-14.315	-8.860 / -6.864	-8.756, -7.502	-6.861 / -5.308	-10.006/-8.780
n° OF POSES	1	4	2	3	4
compound 33					
SITE	ORTHOSTERIC	ORTHOSTERIC	DAA	DAA	ORTHOSTERIC
GLIDE SCORE	-13.580, -13.571	-9.510 / -8.524	-9.182	-5.780 / -5.378	-11.032
n° OF POSES	2	3	1	4	1

Table 15: Summary of sites, GlideScore and number of poses found for NS6740 and 33 for each interface. When one or two poses were found, GlideScore is reported specifically for each pose; when more possible poses were identified, the range of GlideScore is reported.

Comparing the docking results for **NS6740** and **33**, similarities in terms of binding site interactions and GlideScore for each interface were found (**Table 15**). Interface AB was associated with the best GlideScore. The positively charged nitrogen of **33** interacted with Trp A149, via hydrogen bond with oxygen backbone and π -cation interaction with sidechain, and Tyr A195 through π -cation interaction. The amide carbonyl exhibited an hydrogen bond with Glu B57 and the *meta* nitro group produced electrostatic interactions with Asp B164 sidechain; part of the phenyl ring was exposed to solvent. (**Figure 45 A**)

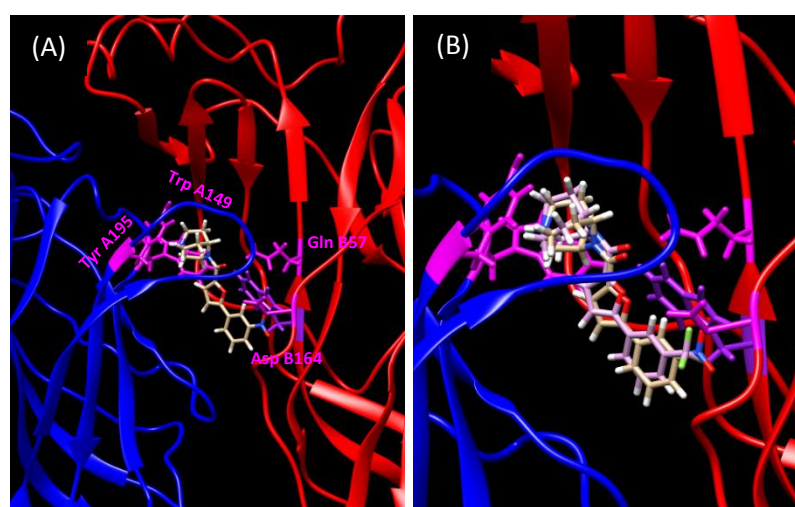


Figure 45: (A) Best pose for **33** in the orthosteric binding site of I_{AB} (subunit A blue, subunit B red). Interacting residues highlighted in magenta; Trp B55 is highlighted in darker violet; (B) Structure overlapping of **NS6740** (lilac) and **33** (dove-grey) best poses.

The superimposition of **NS6740** and **33** in the binding domain of AB interface is reported in **Figure 45 B**. The phenyl portions of both compounds seemed to occupy a similar region in the binding space, but, differently from **NS6740**, **33** did not stack Trp B55 by π - π interaction. Different hypothesis might be proposed:

- the increased polarity of the nitro group could affect the electronic properties of the phenyl ring, thus compromising the stabilization of π - π interaction;
- the formation of electrostatic interactions with the Asp B164 could modify the arrangement of vicinal residues in the binding region, bringing to lose the π - π interaction or, in general, the correct binding to favor the non-conductive receptor states;

- the introduction of the nitro group favored the interaction with a different interface.

Considering the last assumption, a valid alternative interface was represented by I_{EA}. Protonated nitrogen of diazabicyclic ring stacked with Trp E149 and Tyr E188, and bound Ser E148 backbone via hydrogen bond. Finally, the amide carbonyl group formed an hydrogen bond with Lys E145 sidechain (**Figure 46**).

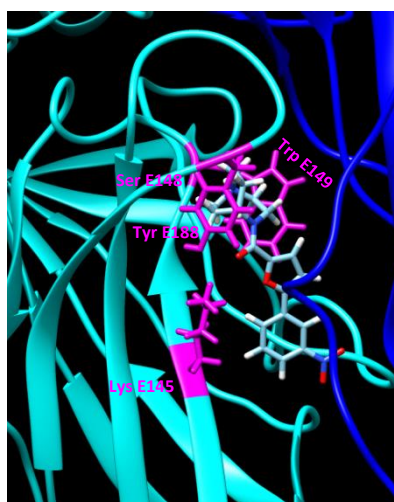


Figure 46: Best pose for **33** in the orthosteric binding site of I_{EA} (subunit E cyano, subunit A blue). Interacting residues highlighted in magenta.

5.2.4 hc7S36V and hc7S36A

The docking pose of **NS6740** in the orthosteric binding site of I_{AB} showed the *meta* CF₃ substituent located near the -OH group of residue Ser B36. Although in the static model system no interaction was highlighted, in a dynamic simulation the two residues may be able to get in closer contact and establish a non-covalent interaction. Potentially, this interaction could explain the difference observed in electrophysiological results for **NS6740** and **28**, since the *para* position of CF₃ did not point towards residue Ser B36 (**Figure 47**).

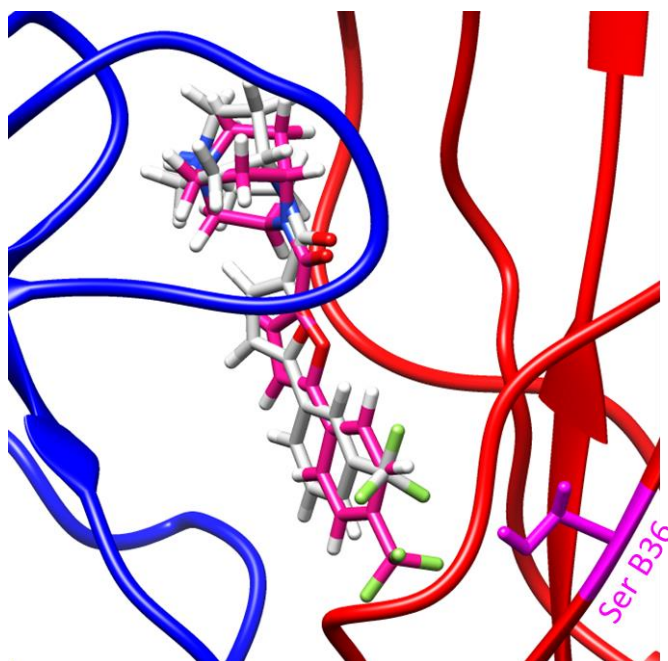


Figure 47: Best pose for **NS6740** (silver) and **28** (magenta) in the orthosteric binding site of I_{AB} (subunit A blue, subunit B red). Different orientations of the -CF₃ groups, related to Ser B36 position, are shown.

Thus, site-directed mutagenesis was applied to generate the functional $\alpha 7$ mutants:

- hc7S36V
- hc7S36A

Together with **NS6740** and **28**, derivative **33** was also assayed on S36V and S36A. The electrophysiological investigations were carried out according to the general procedure for two- and one-shot experiments described in Chapter 4. The

concentration of test drug used was 30 μM and the results are reported in **Figure 48**, **49**, **50**, and **Table 16**, respectively.

When tested on ha7S36V, **NS6740** showed a significantly reduced partial receptor activation relative to WT (net charges 0.04 ± 0.01 on ha7S36V and 0.2 ± 0.03 on WT, P value 0.004) (**Figure 48**). Furthermore, the residual ACh post-control response was completely unaffected by the previous application of test drug (net charge 1.3 ± 0.09), while on the WT the ACh post-control gave a receptor <20% activation (net charge 0.12 ± 0.03). When the final application of PNU-120596 was given, no potentiation was observed, thus showing that **NS6740** completely lost the ability to strongly bind the receptor and stabilize any type of desensitized state with this mutant. The co-application of **NS6740** and PNU-120596 (net charge 0.37 ± 0.18) confirmed the weaker binding of **NS6740** with the substitution of Ser 36 in the orthosteric site, compared to WT (P value 0.011).

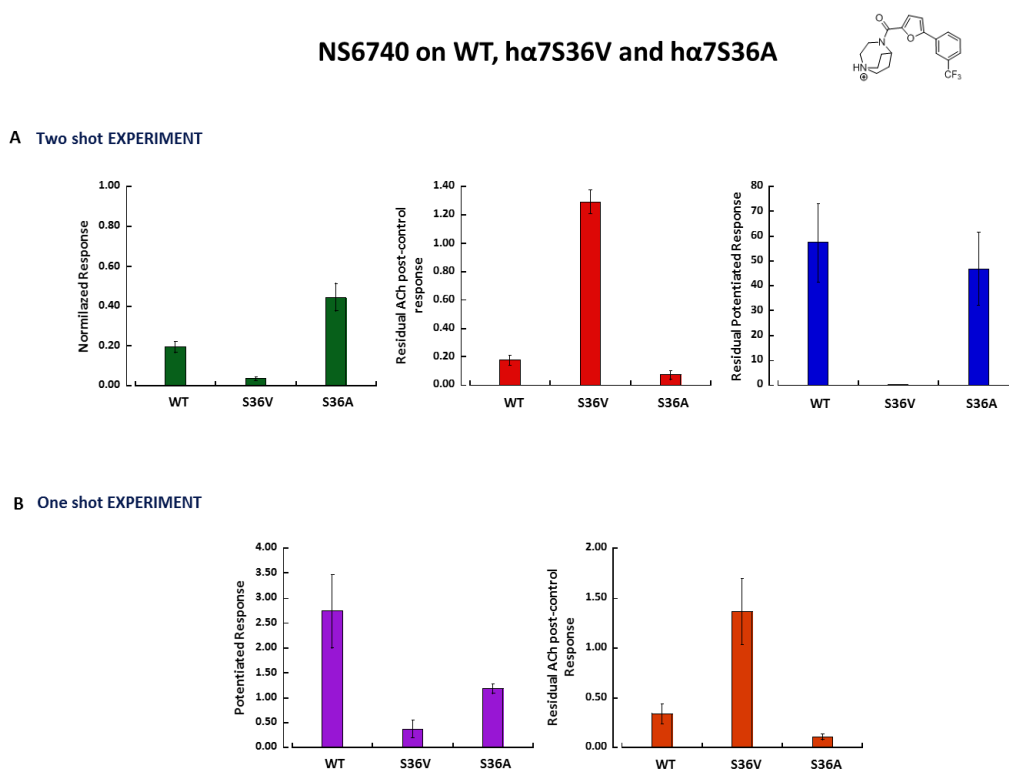


Figure 48: Comparison of the electrophysiological profiles of **NS6740** assayed at 30 μM on WT, ha7S36V and ha7S36A: (A) green bars represent the agonist response when **NS6740** is applied alone at 30 μM ; red bars represent the following residual 60 μM ACh post-control activation; blue bars represent the residual receptor potentiation after final application of 10 μM type II PAM PNU-120596. (B) violet bars represent the receptor potentiation given by co-application of 30 μM **NS6740** and 10 μM type II PAM PNU-120596; orange bars represent the following residual 60 μM ACh post-control activation.

NS6740, assayed on $\alpha 7S36A$, showed stronger partial agonism (net charges 0.44 ± 0.07 on $\alpha 7S36A$ and 0.2 ± 0.03 on WT, P value 0.008), while maintaining comparable values in terms of post-control inhibition and potentiated responses in both two- and one-shot experiments. Interestingly, after PNU-120596 applications, the receptor remained in a non-conductive state revealed by the following ACh responses:

- net charge 0.17 ± 0.05 in two-shot experiment (data not shown);
- net charge 0.1 ± 0.03 in one-shot experiment

Compound **28** (**Figure 49**) exhibited a significantly decreased partial agonist activity on $\alpha 7S36V$ (P value 0.0009), compared with the WT (net charge 0.06 ± 0.01 on $\alpha 7S36V$, 0.25 ± 0.03 on WT), associated with a recovered post-control response (net charges 0.94 ± 0.12 on $\alpha 7S36V$, 0.56 ± 0.06 on WT). Regarding PNU-related responses, **28** on $\alpha 7S36V$ did not present any potentiated responses in both two-shot and one-shot experiments.

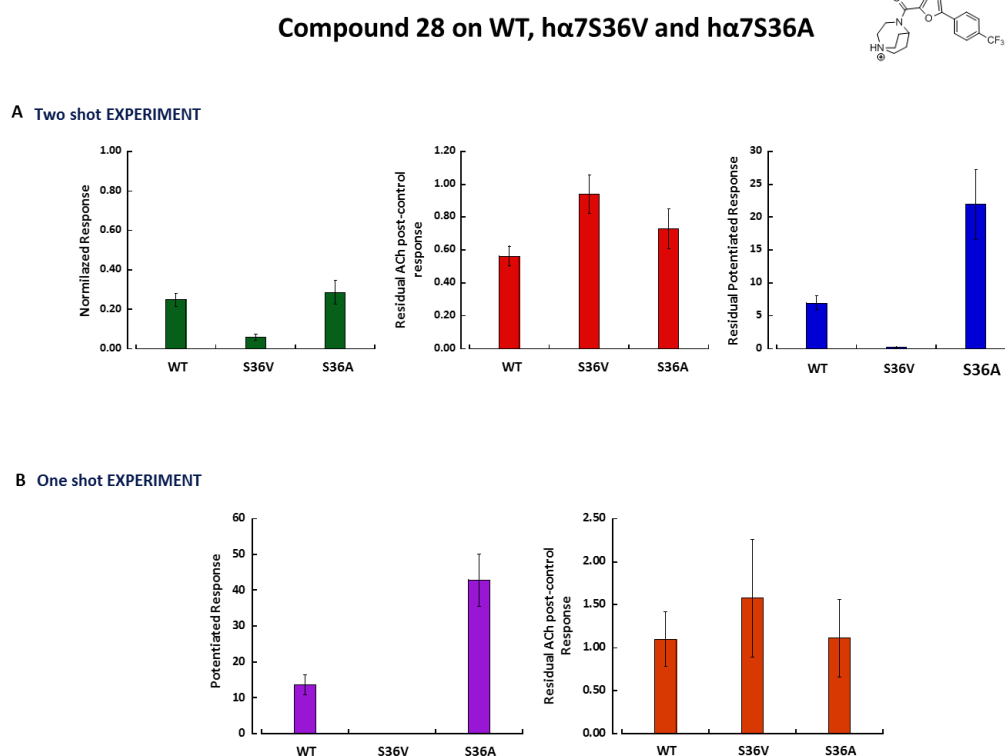


Figure 49: Comparison of the electrophysiological profiles of **28** assayed at $30 \mu M$ on WT, $\alpha 7S36V$ and $\alpha 7S36A$: (A) green bars represent the agonist response when **28** is applied alone at $30 \mu M$; red bars represent the following residual $60 \mu M$ ACh post-control activation; blue bars represent the residual receptor potentiation after final application of $10 \mu M$ type II PAM PNU-120596. (B) violet bars represent the receptor potentiation given by co-application of $30 \mu M$ **28** and $10 \mu M$ type II PAM PNU-120596; orange bars represent the following residual $60 \mu M$ ACh post-control activation.

Regarding the mutant $ha7S36A$, derivative **28** displayed partial channel activation and post-control response comparable with the WT. The PNU-related activation was intense, but not significantly different from the response on the WT (P value 0.71). The co-application with PNU-120596 gave strong channel potentiation that was not statistically different from the response on the WT (P value 0.068).

The partial activation observed for **33** (Figure 50) on the WT was significantly decreased when tested on $ha7S36V$ (P value 0.027). In addition, although **33** did not intensively inhibit the post-control response on the WT (net charge 0.457 ± 0.090), for the valine mutant the ACh activation was fully recovered (net charge 1.23 ± 0.11). Residual PNU-related response was completely absent on the mutant (net charge 0.07 ± 0.04), while medium-low potentiation was observed on the WT. Interestingly, when co-applied with PNU-120596 (one-shot experiment), **33** showed an intense potentiated receptor activation; however, the subsequent application of ACh gave a full response, meaning that no sustained receptor desensitization was obtained.

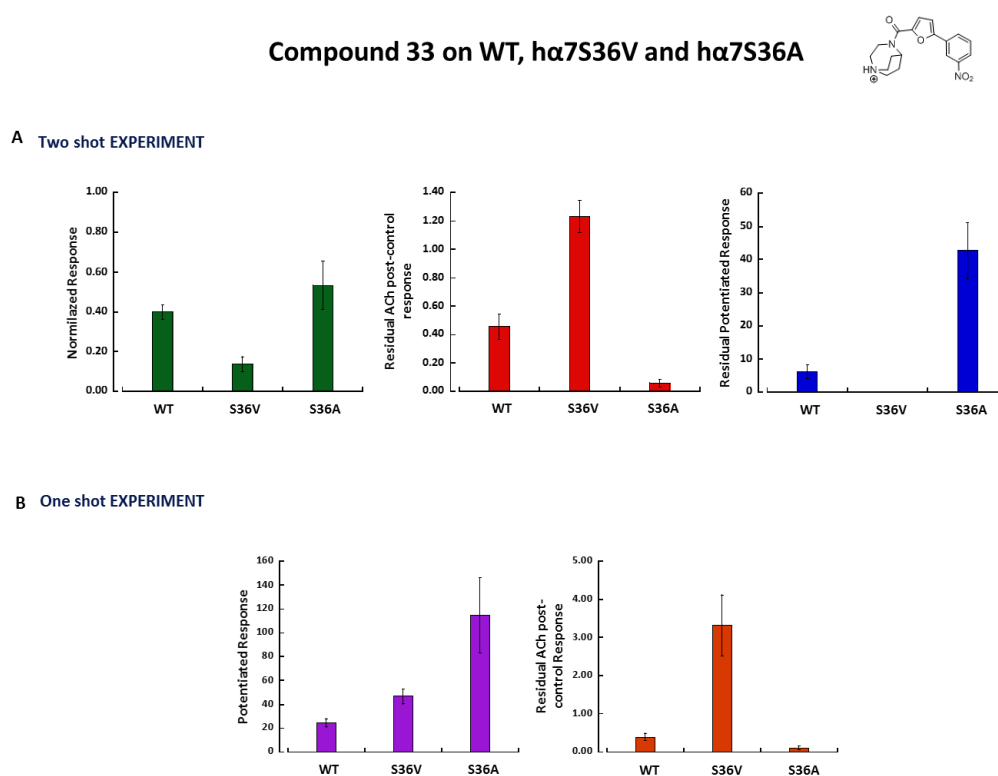


Figure 50: Comparison of the electrophysiological profiles of **33** assayed at $30 \mu\text{M}$ on WT, $ha7S36V$ and $ha7S36A$: (A) green bars represent the agonist response when **33** is applied alone at $30 \mu\text{M}$; red bars represent the following residual $60 \mu\text{M}$ ACh post-control activation; blue bars represent the residual receptor potentiation after final application of $10 \mu\text{M}$ type II PAM PNU-120596. (B) violet bars represent the receptor potentiation given by co-application of $30 \mu\text{M}$ **33** and $10 \mu\text{M}$ type II PAM PNU-120596; orange bars represent the following residual $60 \mu\text{M}$ ACh post-control activation.

In light of the behavior demonstrated on hα7S36V, **33** could be classified as short-lasting silent agonist with this substitution of residue Ser 36.

Finally, **33** preserved the partial agonist properties already observed for the WT receptor when tested on the hα7S36A, but the ACh post-control activity was extremely reduced (net charge 0.06 ± 0.03 on hα7S36A), thus suggesting prolonged binding and stabilization of the receptor desensitized state, deeper than the one gained on the WT (net charge 0.46 ± 0.09). The ability to favor a non-conductive receptor form was confirmed by PNU-related responses which, in both two- and one-shot experiments, were intense (net charges 43 ± 9 and 115 ± 31 , respectively), although, from a statistical point of view, these responses were not different from that on the WT (P values 0.18 and 0.41, respectively). In the one-shot experiment, the final ACh application gave a very low channel opening (net charge 0.11 ± 0.04), thus demonstrating that the receptor was still profoundly desensitized.

We might conclude that, the replacement of Ser 36 with a valine residue in the orthosteric binding site affected the **NS6740** and **28** activities; both compounds, showing the $-CF_3$ substituent on the phenyl ring, in a similar manner compromised the receptor binding. The presence of the more polar nitro group on the phenyl ring allowed **33** to acquire silent characteristics, although shortening the residence time. The side chain of valine residue, most likely, determined a general rearrangement of the binding site that led to loss of proper binding for **NS6740** and **28**; the same modification conferred lower channel opening ability to **33** associated with the faster but not prolonged stabilization of the D_s state.

The replacement of Ser 36 with the smaller alanine residue in the orthosteric binding site preserved the desensitizing properties of **NS6740**, while increasing its partial agonist characteristics; this mutant maintained similar stabilization of non-conductive PNU-responsive receptor forms for **28** and **33** compared to WT.

Since the potentiated response given by co-application with PNU-120596 (one-shot experiment) was lower than the residual one (two-shot experiment) for **NS6740**, we could speculate that the preferred stabilization of D_i over D_s was allowed by the receptor mutant, as already highlighted on the WT.

A favorable equilibrium toward D_s , instead, was revealed by responses related to **28** and **33**, since they were characterized by potentiated response given by co-application with PNU-120596 (one-shot experiment) higher than the residual one (two-shot experiment).

Table 16: Electrophysiological results of **NS6740**, **28** and **33** on *ha7S36V* (A) and *ha7S36A* (B). Data are reported as mean \pm SEM (standard error of mean) and relative to two 60 μ M ACh pre-controls. (a) Two-shot experiment: Agonist response refers to receptor response to 30 μ M application of test compound, ACh post-control refers to receptor response to 60 μ M application of control and residual potentiated response refers to receptor response to 10 μ M application of type-II PAM PNU-120596. (b) Agonist potentiated response refers to receptor response to 30 μ M test compound in co-application with 10 μ M of type-II PAM PNU-120596 and residual ACh response refers to receptor response to 60 μ M application of control.

A	ha7S36V		WT	
	<i>peak current</i>	<i>net charge</i>	<i>peak current</i>	<i>net charge</i>
NS6740				
Two-shot experiment (a)				
30 nM test drug	0.025 \pm 0.004	0.038 \pm 0.010	0.052 \pm 0.013	0.195 \pm 0.028
60 nM ACh post-control	1.070 \pm 0.211	1.292 \pm 0.087	0.059 \pm 0.011	0.117 \pm 0.034
10 nM PNU-120596	0.045 \pm 0.014	0.199 \pm 0.097	22.528 \pm 7.145	57.411 \pm 15.718
One-shot experiment (b)				
30 nM test drug +10 nM PNU-120596	0.268 \pm 0.111	0.372 \pm 0.175	0.790 \pm 0.274	2.734 \pm 0.729
60 nM ACh post-control	1.433 \pm 0.507	1.366 \pm 0.331	0.070 \pm 0.013	0.340 \pm 0.099
28				
Two-shot experiment (a)				
30 nM test drug	0.043 \pm 0.009	0.058 \pm 0.014	0.154 \pm 0.022	0.248 \pm 0.034
60 nM ACh post-control	0.759 \pm 0.108	0.939 \pm 0.117	0.474 \pm 0.110	0.563 \pm 0.061
10 nM PNU-120596	0.101 \pm 0.024	0.169 \pm 0.102	3.007 \pm 0.641	6.997 \pm 1.076
One-shot experiment (b)				
30 nM test drug +10 nM PNU-120596	0.072 \pm 0.017	0.086 \pm 0.024	6.035 \pm 1.328	13.735 \pm 2.786
60 nM ACh post-control	1.010 \pm 0.227	1.575 \pm 0.682	0.638 \pm 0.105	1.103 \pm 0.312
33				
Two-shot experiment (a)				
30 nM test drug	0.119 \pm 0.048	0.138 \pm 0.037	0.193 \pm 0.018	0.398 \pm 0.037
60 nM ACh post-control	0.891 \pm 0.138	1.231 \pm 0.112	0.422 \pm 0.119	0.457 \pm 0.090
10 nM PNU-120596	0.104 \pm 0.045	0.068 \pm 0.036	2.485 \pm 0.730	6.275 \pm 2.009
One-shot experiment (b)				
30 nM test drug +10 nM PNU-120596	11.089 \pm 1.829	46.512 \pm 5.996	12.697 \pm 3.799	24.383 \pm 3.594
60 nM ACh post-control	1.864 \pm 0.342	3.317 \pm 0.795	0.488 \pm 0.089	0.391 \pm 0.096

B	ha7S36A		WT	
	<i>peak current</i>	<i>net charge</i>	<i>peak current</i>	<i>net charge</i>
NS6740				
Two-shot experiment (a)				
30 nM test drug	0.272 ± 0.049	0.444 ± 0.068	0.052 ± 0.013	0.195 ± 0.028
60 nM ACh post-control	0.111 ± 0.030	0.074 ± 0.031	0.059 ± 0.011	0.117 ± 0.034
10 nM PNU-120596	8.764 ± 1.579	46.833 ± 14.608	22.528 ± 7.145	57.411 ± 15.718
One-shot experiment (b)				
30 nM test drug +10 nM PNU-120596	0.475 ± 0.143	1.179 ± 0.091	0.790 ± 0.274	2.734 ± 0.729
60 nM ACh post-control	0.069 ± 0.016	0.107 ± 0.027	0.070 ± 0.013	0.340 ± 0.099
28	<i>peak current</i>	<i>net charge</i>	<i>peak current</i>	<i>net charge</i>
Two-shot experiment (a)				
30 nM test drug	0.127 ± 0.021	0.286 ± 0.060	0.154 ± 0.022	0.248 ± 0.034
60 nM ACh post-control	0.592 ± 0.164	0.729 ± 0.121	0.474 ± 0.110	0.563 ± 0.061
10 nM PNU-120596	2.597 ± 0.681	21.925 ± 5.327	3.007 ± 0.641	6.997 ± 1.076
One-shot experiment (b)				
30 nM test drug +10 nM PNU-120596	5.569 ± 0.420	42.880 ± 7.270	6.035 ± 1.328	13.735 ± 2.786
60 nM ACh post-control	0.316 ± 0.051	1.113 ± 0.682	0.638 ± 0.105	1.103 ± 0.312
33	<i>peak current</i>	<i>net charge</i>	<i>peak current</i>	<i>net charge</i>
Two-shot experiment (a)				
30 nM test drug	0.870 ± 0.191	0.533 ± 0.121	0.193 ± 0.018	0.398 ± 0.037
60 nM ACh post-control	0.034 ± 0.018	0.060 ± 0.026	0.422 ± 0.119	0.457 ± 0.090
10 nM PNU-120596	4.483 ± 0.584	42.717 ± 8.500	2.485 ± 0.730	6.275 ± 2.009
One-shot experiment (b)				
30 nM test drug +10 nM PNU-120596	9.481 ± 1.377	114.776 ± 31.317	12.697 ± 3.799	24.383 ± 3.594
60 nM ACh post-control	0.037 ± 0.010	0.107 ± 0.042	0.488 ± 0.089	0.391 ± 0.096

5.3 Docking investigation of KC-1

The silent agonist **KC-1** was docked following the previously described procedure (paragraph 5.1). Analyzing the obtained results, only protonated forms were considered, given the pK_a value for the cyclic imine. In addition, poses associated with GlideScore values 3 kcal/mol lower than the best one for that analysis were not considered. As already observed for the docking results on **NS6740**, based on GlideScore values, I_{AB} and I_{EA} seemed to be the interfaces that better described possible binding modes for **KC-1**. The other interfaces, in fact, were characterized by worse values of docking score, especially I_{CD} and I_{DE} were particularly high and thus not considered to be favorable docking sites (**Table 17**).

Figure 50 A shows the best pose found for **KC-1** when docked on I_{AB} . The charged iminium group was buried in the aromatic cage, interacting with Trp A149, Tyr A188, Tyr A195 *via* π -cation interactions. The pyridine ring established π - π stacking interaction with Tyr A188, and the pyridine nitrogen formed a hydrogen bond with Gln B57 sidechain. The phenyl ring stacked with Phe B104 and Tyr A93.

Figure 50 B shows the best pose found for **KC-1** when docked on I_{EA} . The charged iminium group was embedded in the aromatic pocket interacting with Trp E149 and Tyr E188 by π -cation interactions; the positive charge of residue Lys E145 sidechain was stabilized by π -cation interactions with both pyridine and phenyl rings.

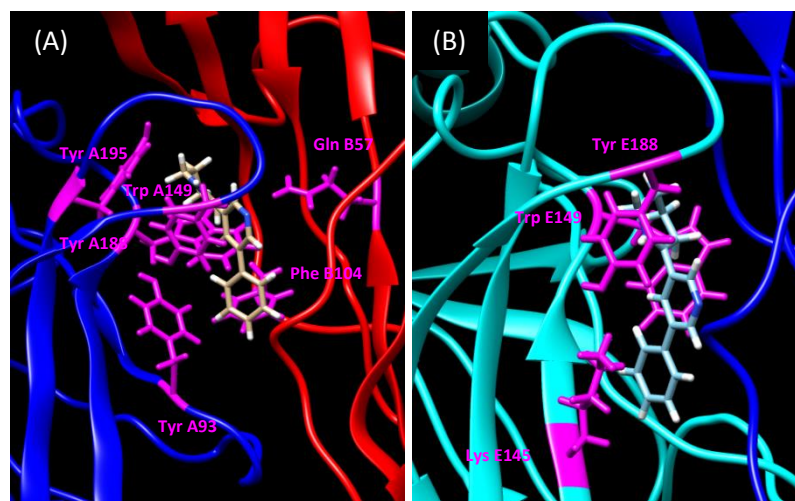


Figure 50: (A) Best pose for **KC-1** in the orthosteric binding site of I_{AB} (subunit A blue, subunit B red). (B) Best pose for **KC-1** in the orthosteric binding site of I_{EA} (subunit E cyan, subunit A blue). Interacting residues highlighted in magenta.

KC-1 SITE	INTERFACES				
	AB	BC	CD	DE	EA
GLIDE SCORE	ORTHOSTERIC -12.272 / -9.609	ORTHOSTERIC -6.103 / -5.225	DAA -2.951, -1.623	DAA -3.966 / -3.955	ORTHOSTERIC -9.803/-9.426
n° OF POSES	3	3	2	2	2

Table 17: Summary of sites, GlideScore and number of poses found for **KC-1** for each interface. When one or two poses were found, GlideScore is reported specifically for each pose; when more possible poses were identified, the range of GlideScore is reported.

CHAPTER VI

Conclusions

6.1 Investigation of $\alpha 7$ nAChR silent activation

The experimental activity performed in this PhD thesis focused on the investigation of structure-activity relationships (SARs) of the two well-known $\alpha 7$ nAChR silent agonists **NS6740** and **KC-1**. The project aimed at fulfilling the lack of information on the molecular ligand-receptor interactions responsible for the silent activation mechanism related to the $\alpha 7$ metabotropic mode of action. The receptor desensitization induced by silent agonists appears to be associated to analgesic and anti-inflammatory effects.

As far as the study on the lead compound **NS6740** is taken into account, a group of new derivatives was designed, synthesized and tested, following two general approaches: (i) the structural fragmentation of the original molecular skeleton, and (ii) the modification of **NS6740** structural moieties corresponding to the three pharmacophoric component parts, i.e. the positively charged nucleus, the hydrogen bond acceptor moiety and the aromatic portion.

The second approach was also followed to design new **KC-1**-related analogs.

To investigate the silent agonist profile, the newly synthesized **NS6740** and **KC-1** derivatives, **11-33** and **34-40** respectively, were tested on $\alpha 7$ nAChRs expressed in *Xenopus laevis* oocytes in two-electrode voltage clamping experiments (**Table 12**). The lead compounds and the most interesting derivatives were submitted to preliminary *in silico* studies, performed on an $\alpha 7$ nAChR homology model, and additionally analyzed in targeted mutagenesis experiments.

6.1.1 NS6740-related analogs

The SARs on **NS6740** represent the core data of the experimental activity performed in this thesis. The main results are summarized in the following.

- The fragmentation analysis demonstrated the structural specificity of **NS6740** in engendering its silent behavior. The crucial role of the positive ionizable group, the central hydrogen-bond acceptor and the aromatic moiety in the prolonged receptor binding and in the induction of the $\alpha 7$ desensitized PAM-sensitive state was confirmed.
- The modifications of the basic nucleus, such as a) the methylation of the tertiary amine, b) the variation in the distance between the positive charge and hydrogen

bond acceptor and c) the reduction of the azabicyclic nucleus dimensions, led to the loss of the peculiar activity profile of **NS6740**.

- The deletion of the hydrogen bond acceptor, *via* amide carbonyl reduction, was detrimental to the stabilization of the receptor binding, and thus to the sustained induction of receptor desensitization.
- The *meta*-CF₃ substitution on the phenyl ring was found to be favored over the *para*-substituted analog; the introduction of halogen atoms generally increased the partial agonist behavior while maintaining the prolonged receptor binding and the sustained desensitization. Similar results were found for the *meta*-CH₃-substituted derivative. When more polar groups were inserted, shorter residence time and weaker stabilization of non-conducting states were generally observed.
- The introduction of bulkier aromatic portions decreased the binding stability, thus abolishing the prolonged stabilization of the receptor desensitization.

Concerning the results obtained from the *in silico* studies on **NS6740** and the good desensitizing analogs **12**, **22-24**, **27** and **32**, we propose a binding mode highlighting the role of the aromatic cage in the stabilization of the positive charge *via* π -cation interactions and hydrogen bonding. Moreover, the amide carbonyl group was predicted to interact with Gln 57 through hydrogen bonding and the aromatic chain was located below the C-loop, establishing π - π interactions with Trp 55. This proposed binding mode would be additionally supported by considering the electrophysiological behavior of other **NS6740** derivatives.

Concerning the electrophysiological results obtained for compound **17**, which is the corresponding quaternary ammonium salt of **NS6740**, the inability of establishing a hydrogen bond with Trp 149 would be the reason for its shorter binding time and weaker receptor desensitization. Furthermore, the different position of the tertiary amine, like in compound **18**, and the smaller dimensions of the basic nucleus, characterizing both compounds **19** and **20**, compromise the correct placement of the ligand in the aromatic nest, thus determining lower stabilization of receptor binding.

Considering the hydrogen bond between the bridge carbonyl group and Gln 57, loss of the prolonged receptor binding of compound **21**, whose carbonyl moiety was replaced by a methylene group, confirms the central role of this ligand-receptor interaction.

Finally, the crucial role of the aromatic interaction with the Trp 55 was confirmed by analyzing the results of compounds **13** and **14**. Indeed, the short activity observed

for **13**, showing only the furan ring, and **14**, with the absence of the aromatic portion, is likely due to the lack of this specific interaction with the receptor counterpart.

The docking results obtained for analogs **28** and **33**, with the *para*-CF₃ and *meta*-NO₂ groups, respectively, showed a binding mode similar to that of **NS6740**. Conversely, compounds **28** and **33** displayed electrophysiological profiles different from that associated to **NS6740**, in terms of both, residence time and stabilization of the non-conducting receptor states. The static model used in the docking investigation did not allow to account for the weaker receptor binding of **28** and **33** and a more accurate dynamic investigation would be required.

The results obtained on the two mutants $\alpha 7S36V$ and $\alpha 7S36A$ demonstrated that the residue Ser 36 was not associated to a specific interaction with the *meta* trifluoromethyl group of **NS6740**, since its mutations affected also the activity of compounds **28** and **33**. Especially, the substitution with the valine residue gave interestingly different data for all compounds compared with the relative WT data. These results could be related with a general rearrangement of the binding site upon replacement of the original serine with the valine residue.

Noteworthy, the molecular docking studies carried out on **NS6740** and related derivatives led to predictions about point to point contacts between ligands and receptor side chains. However, these preliminary results should be completed by performing molecular dynamics (MD) investigations and by targeted mutagenesis experiments. The MD computational approach would help to better understand the induction of desensitized states and the ligand-residence time as well as the effect of PAM co-application.

In conclusion, the SARs on **NS6740** and the related *in silico* studies provided deeper insights on the **NS6740** structural features able to promote the $\alpha 7$ nAChR silent activation. Moreover, among the new compounds under study, we identified interesting good receptor desensitizers (**12**, **22-24**, **27** and **32**) as well as good partial agonists (**13** and **17**).

Compounds **12**, **22-24**, **27** and **32** in general displayed a partial agonist activity higher than that shown by **NS6740**, but still associated with a prolonged receptor binding and strong desensitization. Therefore, these novel derivatives would be worthy of further analysis to prove the metabotropic function of the receptor, for

instance by measuring G-protein coupling or downstream activation. Moreover, *in vitro* and *in vivo* studies should be performed on **12**, **22-24**, **27** and **32** to investigate their potential analgesic properties and also to verify how their increased partial agonism may affect or not the anti-inflammatory effects.

6.1.2 KC-1-related analogs

The electrophysiological data so far available allowed to conclude that the modifications introduced on the **KC-1** cyclic imine nucleus, such as a different position of the basic nitrogen and a smaller ring, compromised the silent activity of the parent compound. At present, we cannot comment on the SARs related to the modifications carried out on the pyridine ring as well as the aromatic portion of **KC-1** since analogs **38-40** are still under pharmacological investigation.

The *in silico* analysis of **KC-1** provided potential interaction modes. However, **KC-1**-related analogs endowed with a silent profile similar to that of the parent compound are still unavailable and, as a consequence, we are unable to identify the most relevant among the proposed binding interactions.

CHAPTER VII

Experimental Section

7.1 CHEMISTRY

7.1.1 Materials and methods

^1H and ^{13}C NMR spectra were recorded on a Varian Mercury-300 (300 and 75 MHz, respectively) or Varian Inova-500 (500 and 126 MHz) instruments. Chemical shifts (δ scale) are reported in parts-per-million (*ppm*) and coupling constants (*J*) in hertz (*Hz*). For each compound analyzed, the specific deuterated solvent (CDCl_3 , CD_3OD , $(\text{CD}_3)_2\text{CO}$, or $(\text{CD}_3)_2\text{SO}$) used is reported. Chemical shifts (δ scale) are reported in parts per million (*ppm*) relative to the peak of the internal standard TMS ($\delta = 0.00$ ppm) for CDCl_3 , CD_3OD , $(\text{CD}_3)_2\text{CO}$ or relative to the central peak of the solvent ($\delta = 2.50$ ppm for $(\text{CD}_3)_2\text{SO}$) in ^1H NMR and relative to the central peak of the solvent ($\delta = 77.16$ ppm for CDCl_3 , 49.00 for CD_3OD , 39.52 for $(\text{CD}_3)_2\text{SO}$ (DMSO-*d*6), and 29.84 for $(\text{CD}_3)_2\text{CO}$) in ^{13}C NMR. Processing of the spectra was performed with MestReNova 8.1.1. The optical rotation measurements were carried out with Jasco P1010 polarimeter. High resolution mass spectra (HRMS) were registered with Fourier Transform Ion Cyclotron Resonance (FT-ICR) Mass Spectrometer APEX II & Xmass software (Bruker Daltonics) – 4.7 T Magnet (Magnex). Concentration Data are reported as mass/charge ratio (*M/Z*) for the final title compounds **1** and **11-33**. Mass spectrometry was carried out with Agilent 6220 Time-of-Flight (TOF), Gas temperature – 350°C, Drying gas (N_2) – 8.0 L/min, Nebulizer – 30 p for the final title compounds **34-40**.

Melting points were recorded on a Büchi Mod. B 540 instrument or on an MFB-595010M Gallenkamp apparatus equipped with a digital thermometer, and were not corrected.

Reactions were monitored by TLC analyses performed on commercial silica gel 60 F254 aluminium sheets/glass plates (Merck or EMD Millipore) or neutral alumina TLC plates (Fluka). Unless otherwise noted, the TLC analyses were performed on silica gel sheets/glass plates. Spots were observed with UV-lamp ($\lambda = 365$ nm) and/or evidenced with different TLC stains: a solution of KMnO_4 in 0.1 N NaOH, a 5% solution of phosphomolybdic acid in ethanol, Dragendorff reagent (a solution of KBiI_4 in CH_3COOH and H_2O) for amines and quaternary ammonium salts, and ninhydrin.

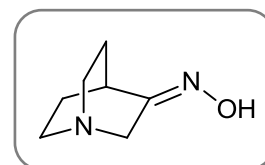
Column chromatographies were performed on silica gel Sigma-Aldrich (0.063-0.200 mesh) or neutral alumina as stationary phase; eluents have been specified time to time.

All reagents and organic solvents for the reactions were of analytical grade. Several reactions were carried out in anhydrous condition (flame-dried glassware) and under inert (argon or nitrogen) atmosphere; those conditions are implied whenever in the synthetic procedure dry solvents are listed.

7.1.2 Synthesis of NS6740 derivatives

7.1.2.1 Synthesis of 1,4- and 1,3-diazabicyclo[3.2.2]nonane dihydrochloride **16** and **44**

Quinuclidine-3-one oxime (41)



A water solution (100 mL) of commercially available quinuclidine-3-one hydrochloride (32.4 g, 200.5 mmol, 1 equiv) was added to a water solution of hydroxylamine hydrochloride (16 g, 230.5 mmol, 1.15 equiv) and sodium acetate (48.4 g, 589.4 mmol, 2.94 equiv). The mixture was stirred at 70 °C for 2 h and then cooled to r.t.; pH = 10 was reached by adding Na₂CO₃ portionwise and a white solid precipitate was obtained and filtered off under vacuum. Water phase was further extracted with a mixture of CH₂Cl₂/iPrOH 9:1. The organic layers were dried over anhydrous Na₂SO₄, filtered and concentrated in vacuum. Both fractions of **41** were obtained as white, amorphous solid (28 g, yield 100%).

R_f = 0.43 (DCM/MeOH, 4:1)

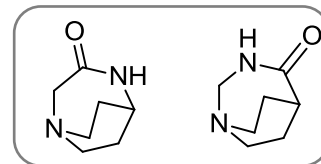
m.p. = 220.0 - 221.8 °C

¹H NMR ((CD₃)₂SO): δ 10.22 (s, 1H), 3.38 (s, 2H), 2.84 - 2.61 (m, 4H), 2.42 (p, J = 3.1 Hz, 1H), 1.78 - 1.56 (m, 4H).

¹³C NMR ((CD₃)₂SO): δ 162.21, 51.80, 46.73, 28.32, 26.38.

1,4-Diazabicyclo[3.2.2]nonan-3-one (42) and 1,3-diazabicyclo[3.2.2]nonan-4-one (43)

41 (38 g, 271.1 mmol, 1 equiv) was added portionwise to 130 °C preheated mechanically stirred polyphosphoric acid (95 mL) over 6 h, obtaining a light brown gummy mixture. The latter was stirred at 130 °C



overnight and the color turned into dark brown. 10 M NaOH (pH = 12-13) and ice were added to the acidic mixture. The water phase was saturated with NaCl and extracted by a mixture of DCM/iPrOH, 4:1. The combined organic layers were dried over anhydrous Na₂SO₄, filtered and concentrated in vacuo. The resulting crude was purified by silica gel column chromatography (DCM/MeOH, 4:1). Two regioisomers were isolated as light brown, amorphous solids.

42: light brown amorphous solid (9.23 g, yield 24%)

R_f = 0.39 (DCM/MeOH, 4:1)

m.p. = 211.2-213 °C

¹H NMR (CDCl₃): δ 6.91 (s, 1H), 3.69 (s, 2H), 3.47 – 3.37 (m, 1H), 3.09 (qdd, J = 14.5, 9.2, 5.6 Hz, 4H), 2.19 – 2.08 (m, 2H), 1.89 (dt, J = 14.0, 4.8 Hz, 2H).

¹³C NMR (CDCl₃): δ 178.67, 62.30, 46.25, 44.14, 30.20.

43: light brown amorphous solid (1.64 g, yield 4.3%)

R_f = 0.41 (DCM/MeOH, 95:5)

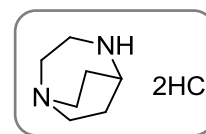
m.p. = 121.6 – 122.5 °C

¹H NMR (CDCl₃): δ 7.12 (br s, 1H), 5.82 – 5.61 (m, 2H), 5.44 (s, 1H), 3.12 – 3.00 (m, 4H), 2.66 (t, J = 5.7 Hz, 2H), 2.19 (s, 2H).

¹³C NMR (CDCl₃): δ 173.94, 125.20, 125.04, 61.56, 52.91, 50.59, 26.28.

1,4-Diazabicyclo[3.2.2]nonane dihydrochloride (16)

In anhydrous and inert atmosphere, to a suspension of **42** (5.59 g, 39.9 mmol, 1 equiv) in dry THF (70 mL) was added dropwise a 1 M solution of LiAlH₄ in THF (47.9 mL, 47.9 mmol, 1.2 equiv) at 0 °C. The reaction reached the refluxing temperature and a light-yellow solution was obtained. After 8h the reaction was complete and a white solid was crashed out. Excess LiAlH₄ was quenched with EtOAc (50 mL) and few drops of MeOH at 0 °C, giving an additional white precipitate that was filtered off. The obtained yellow solution was subsequently added to a 4 M solution of HCl in 1,4-dioxane (22.2 mL, 88.6 mmol, 2 equiv) and stirred at r.t. overnight. A brown precipitate was obtained and recrystallized from MeOH/Et₂O, affording **16** as light brown prisms (4.2g, yield 47.6%).



$R_f = 0.46$ (MeOH/H₂O/NH₃, 4:1:1)

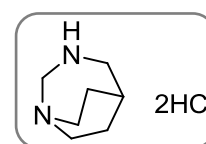
m.p. = 307 °C (dec.)

HRMS (ESI+) m/z calcd for C₇H₁₅N₂ 127.12297 [M + H]⁺, found 127.12304

¹H NMR (CD₃OD): δ 4.17 – 4.10 (m, 1H), 3.80 – 3.43 (m, 8H), 2.40 (td, $J = 8.0, 3.8$ Hz, 4H). ¹³C NMR (CD₃OD): δ 66.89, 51.76, 46.69, 38.77, 21.34.

1,3-Diazabicyclo[3.2.2]nonane dihydrochloride (44)

In anhydrous and inert atmosphere, to a suspension of **43** (700 mg, 4.99 mmol, 1 equiv) in dry THF (9 mL) was added dropwise a 1 M solution of LiAlH₄ in THF (5.98 mL, 5.98 mmol, 1.2 equiv) at 0 °C. The suspension was refluxed overnight. Excess LiAlH₄ was quenched with AcOEt (6.5 mL) and few drops of MeOH at 0 °C, giving a white precipitate that was filtered off under vacuum. The obtained yellow solution was subsequently added to a 4 M solution of HCl in 1,4-dioxane (2.8 mL, 11.1 mmol) and stirred at r.t. overnight. A brown precipitate was obtained and recrystallized from MeOH/Et₂O, affording **44** as light brown prisms (600 mg, yield 45%).



$R_f = 0.60$ (DCM/MeOH, 9:1)

m.p. = 117–119 °C

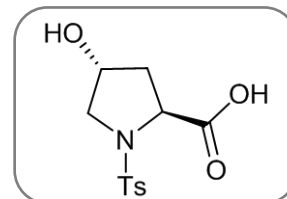
¹H NMR (CD₃OD): δ 6.08 – 5.71 (m, 2H), 3.91 (dd, $J = 12.3, 6.1$ Hz, 2H), 3.66 – 3.42 (m, 6H), 2.56 (br s, 2H).

^{13}C NMR (CD_3OD): δ 126.72, 120.57, 53.95, 52.23, 51.16, 35.57, 25.21, 23.57.

7.1.2.2 Synthesis of (1*S*,4*S*)-2-benzyl-2,5-diazabicyclo[2.2.1]heptane and (1*R*,4*R*)-2-benzyl-2,5-diazabicyclo[2.2.1]heptane

(2*S*,4*R*)-4-Hydroxy-1-tosylpyrrolidine-2-carboxylic acid (**45**)

To a commercially available 4-hydroxy-L-proline (5.0 g, 38.1 mmol, 1 equiv), solubilized in water (40 mL) and cooled down at 0 °C, Na_2CO_3 (8.5 g, 80.1 mmol, 2.10 equiv) and TsCl (8.7 g, 45.8 mmol, 1.20 equiv) were added portionwise. The white suspension obtained was warmed to r.t. and, after a while, the white solid dissolved giving a colorless solution. The reaction was stirred for 24 h. After addition of 12 M HCl at 0 °C to reach pH = 1-2, a solid precipitated and was filtered off. The filter cake was dried *in vacuo* to obtain **45** as a white crystalline solid (9.1 g, yield 84%).



R_f = 0.49 (DCM/MeOH, 1:1)

m.p. = 148.7 - 151.1 °C

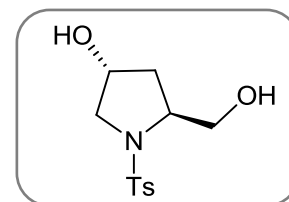
$[\alpha]_D$ = -116.2 (c = 1.85, ethanol)

^1H NMR (CD_3OD): δ 7.75 (d, J = 8.2 Hz, 2H), 7.39 (d, J = 8.2 Hz, 2H), 4.33 (m, 1H), 4.22 (t, J = 7.9 Hz, 1H), 3.57 (dd, J = 10.9, 4.2 Hz, 1H), 3.26 (m, 2H), 2.43 (s, 3H), 2.07 (dd, J = 8.0, 4.3 Hz, 2H).

^{13}C NMR ($(\text{CD}_3)_2\text{CO}$): δ 173.50, 144.23, 136.21, 130.29, 128.65, 70.13, 60.62, 57.31, 40.24, 21.42.

(3R,5S)-5-(Hydroxymethyl)-1-tosylpyrrolidin-3-ol (46)

Under anhydrous and inert atmosphere and at 0 °C, to compound **45** (9.1 g, 32 mmol, 1 equiv) solubilized in dry THF was added dropwise a solution of 1 M BH₃ in THF (94 mL, 94 mmol, 2.93 equiv). The mixture was stirred at r.t. overnight (TLC in EtOAc). The reaction was quenched with cool deionized water added at 0 °C; then THF was evaporated in vacuum. The water phase was extracted with EtOAc and the combined organic layers were dried over anhydrous Na₂SO₄, filtrated and concentrated *in vacuo* to afford the final product **46** as a white amorphous solid (8.1 g, yield 93%).



R_f = 0.36 (EtOAc)

m.p. = 132.4 - 134.5 °C

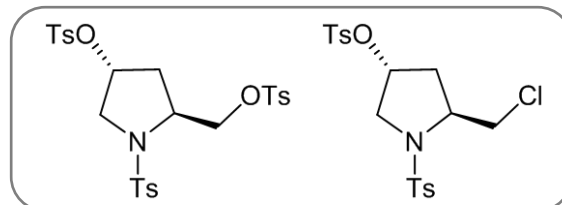
[α]_D = -43.3 (c = 1.85, ethanol)

¹H NMR (CDCl₃): δ 7.76 (d, J = 8.1 Hz, 2H), 7.33 (d, J = 7.9 Hz, 2H), 4.32 (bs, 1H), 3.93 - 3.84 (m, 1H), 3.79 (d, J = 7.6 Hz, 1H), 3.71 - 3.53 (m, 2H), 3.39 (d, J = 12.2 Hz, 1H), 2.43 (s, 3H), 2.04 - 1.78 (m, 2H).

¹³C NMR (CDCl₃): δ 143.96, 133.73, 129.69, 127.82, 69.43, 65.13, 62.70, 60.67, 57.78, 37.61, 21.55.

((2*S*,4*R*)-1-Tosyl-4-(tosyloxy)pyrrolidin-2-yl)methyl 4-methylbenzenesulfonate
(**47a**) and (3*R*,5*S*)-5-(chloromethyl)-1-tosylpyrrolidin-3-yl 4-
methylbenzenesulfonate (**47b**)

Under anhydrous and inert atmosphere, intermediate **46** (9.3 g, 34.3 mmol, 1 equiv) and DMAP (0.8 g, 6.9 mmol, 0.2 equiv) were suspended in dry DCM. At 0 °C



pyridine was added (13.3 mL, 164.5 mmol, 4.8 equiv), followed by a dropped solution of TsCl (32.7 g, 171.3 mmol, 5 equiv) in dry DCM. The mixture was stirred at r.t. for 30 h and then was heated to 45 °C for additional 3 days. The reaction was concentrated *in vacuo* and the resulting crude was purified by silica gel column chromatography, eluted by cyclohexane/EtOAc, (7:3). The tritosylated intermediate and the chloro-containing intermediate were isolated.

47a: white solid (8.9 g, yield 61%)

$R_f = 0.25$ (cyclohexane/EtOAc, 1:1)

m.p. = 131.7 - 133.5 °C

$[\alpha]_D = -56.0$ (c = 1.17, acetone)

$^1\text{H NMR}$ (CDCl_3): δ 7.73 (d, $J = 7.2$ Hz, 2H), 7.55 (dd, $J = 15.5, 7.7$ Hz, 4H), 7.36 - 7.14 (m, 6H), 4.71 (bs, 1H), 4.25 (m, 1H), 4.12 - 3.98 (m, 1H), 3.75 (bs, 1H), 3.46 (bs, 2H), 2.41 (s, 9H), 1.99 (s, 2H).

$^{13}\text{C NMR}$ (CDCl_3): δ 145.46, 144.53, 132.51, 130.18, 130.15, 130.01, 128.11, 127.86, 127.81, 78.09, 71.70, 56.87, 54.78, 35.85, 21.82, 21.74.

47b: light pink solid (3.7 g, yield 19%)

$R_f = 0.62$ (cyclohexane/EtOAc, 1:1)

m.p. = 144.9 - 147 °C

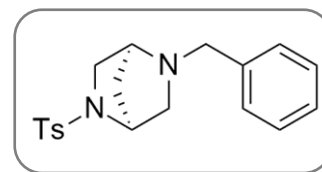
$[\alpha]_D = -34.1$ (c = 1.0 acetone)

$^1\text{H NMR}$ (CDCl_3): δ 7.70 (d, $J = 7.8$ Hz, 2H), 7.58 (d, $J = 8.0$ Hz, 2H), 7.32 (d, $J = 6.8$ Hz, 4H), 4.84 (bs, 1H), 4.01 - 3.68 (m, 2H), 3.60 (d, $J = 2.6$ Hz, 1H), 2.45 (s, 3H), 2.24 - 2.01 (m, 2H).

$^{13}\text{C NMR}$ (CDCl_3): δ 145.3, 144.3, 129.98, 129.86, 127.71, 127.67, 78.2, 58.8, 55.12, 47.67, 36.9, 21.68, 21.62.

(1S,4S)-2-Benzyl-5-tosyl-2,5-diazabicyclo[2.2.1]heptane (**48**)

To a suspension of **47a** (4 g, 6.9 mmol, 1 equiv) in MeOH (25 mL) under magnetic stirring in a flask, benzylamine (7.5 mL, 69 mmol, 10 equiv) was added dropwise at r.t. The mixture was then poured in a sealed



tube and heated at 90 °C for 22 h. Upon completion, the reaction was cooled down and MeOH was evaporated under reduced pressure. The resulting crude was purified by silica gel chromatography (cyclohexane/EtOAc, 3:2) to afford **48** as a light yellow solid (2.2 g, yield 91%).

$R_f = 0.44$ (cyclohexane/EtOAc, 1:1)

m.p. = 115.6 - 119.2 °C

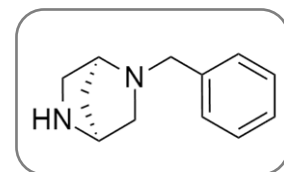
$[\alpha]_D = +18.0$ (c = 1.0, acetone)

$^1\text{H NMR}$ (CDCl_3): δ 7.73 (d, $J = 2.6$ Hz, 2H), 7.37 - 7.17 (m, 7H), 4.27 (bs, 1H), 3.66 (m, 2H), 3.42 (bs, 1H), 3.02 (d, $J = 9.4$ Hz, 1H), 2.84 (bs, 1H), 2.69 (m, 1H), 2.42 (s, 3H), 1.71 (s, 1H), 1.12 (m, 1H).

$^{13}\text{C NMR}$ (CDCl_3): δ 143.71, 135.77, 129.97, 128.64, 128.57, 127.68, 127.34, 61.26, 60.97, 59.69, 57.59, 50.67, 35.27, 21.75.

(1S,4S)-2-Benzyl-2,5-diazabicyclo[2.2.1]heptane (**49**)

Previous **48** (0.5 g, 1.5 mmol), suspended in a 33% hydrogen bromide solution in acetic acid (7.5 mL), was heated to 50 °C. After 5 h, the reaction was cooled at 0 °C



and EtOAc was added; the mixture was stirred for 15 min and the precipitated cake was filtered off. The filtrate was treated with a saturated aqueous solution of Na_2CO_3 and the resulting aqueous solution was extracted three times with a mixture of DCM/*i*-PrOH, 4:1. The combined organic layers were dried over anhydrous Na_2SO_4 , filtered and concentrated in vacuum to achieve **49** as a yellow oil (230 mg, yield 81%).

$R_f = 0.43$ (DCM/MeOH, 4:1)

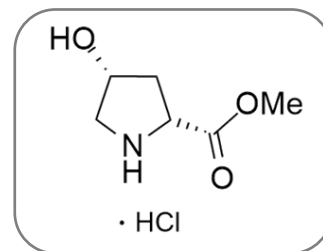
$[\alpha]_D = +37.7$ (c = 0.74, chloroform)

$^1\text{H NMR}$ (CD_3OD): δ 7.36 - 7.20 (m, 5H), 3.80 - 3.68 (m, 2H), 3.52 - 3.18 (m, 3H), 2.87 - 2.70 (m, 2H), 2.52 (d, $J = 10.5$ Hz, 1H), 1.72 (m, 2H).

$^{13}\text{C NMR}$ (CDCl_3): δ 139.51, 128.46, 128.45, 126.84, 61.49, 60.38, 58.27, 57.04, 48.1, 35.29.

(2R,4R)-Methyl-4-hydroxypyrrolidine-2-carboxylate hydrochloride (**50**)

Commercially available 4-*cis*-hydroxy-D-proline (5.42 g, 41.3 mmol, 1 equiv) was dissolved in the minimum amount of MeOH, cooled to 0 °C and added dropwise by a 1.25 M solution of HCl in MeOH (3 g, 82.6 mmol of HCl in 66 mL of MeOH). The mixture was firstly warmed ad r.t. and then refluxed for 6 h. The solvent was concentrated under reduced pressure and then Et₂O was added, providing a white precipitate. The cake was filtrated under vacuum and washed with Et₂O to afford **50** as a white solid (6 g, yield 80%).



R_f = 0.50 (*tert*-BuOH/H₂O/AcOH, 4:2:1)

m.p. = 151.7 – 153.4 °C

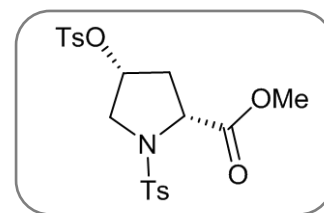
[α]_D = + 27.6 (c = 1.01, methanol)

¹H NMR (CD₃OD): δ 4.55 (ddd, *J* = 6.6, 5.0, 2.5 Hz, 2H), 3.85 (s, 3H), 3.39 – 3.29 (m, 2H), 2.54 – 2.41 (m, 1H), 2.40 – 2.32 (m, 1H).

¹³C NMR (CD₃OD): 171.15, 71.30, 54.89, 53.76, 51.90, 37.65.

(2R,4R)-Methyl 1-tosyl-4-(tosyloxy)pyrrolidine-2-carboxylate (**51**)

To 6 g (33 mmol, 1 equiv) of previous **50** were added pyridine (65 mL) and Et₃N (99 mmol, 13.8 mL, 3 equiv) at 0 °C and the mixture was allowed to stir for 10 min. TsCl (60.4 g, 317 mmol, 6.6 equiv) was added in small portions as to control the temperature between 0-5 °C.



After stirring at 0 °C for 15 h, to the reaction was added 40 mL of ice-cold water and allowed to stir at r.t. for one additional hour. The aqueous phase was extracted for three times with DCM and the combined organic layers were dried over anhydrous Na₂SO₄, filtered and concentrated *in vacuo*. The resulting crude was purified by silica gel chromatography (cyclohexane/EtOAc, 7:3), obtaining **51** as a white solid (13.2 g, yield 88%).

R_f = 0.61 (cyclohexane/EtOAc, 1:1)

m.p. = 86.7 – 88.4 °C

[α]_D = + 30.6 (c = 1.02, acetone)

¹H NMR (CDCl₃): δ 7.74 – 7.65 (m, 4H), 7.34 – 7.27 (m, 4H), 4.94 (tt, J = 5.4, 2.7 Hz, 1H), 4.50 (dd, J = 9.2, 3.0 Hz, 1H), 3.63 (s, 3H), 3.61 – 3.56 (m, 1H), 3.44 (ddd, J = 11.8, 2.5, 0.8 Hz, 1H), 2.42 (d, J = 2.7 Hz, 6H), 2.40 – 2.31 (m, 1H), 2.20 (ddd, J = 14.4, 9.2, 5.3 Hz, 1H).

¹³C NMR (CDCl₃): δ 171.16, 145.42, 144.19, 135.27, 133.42, 130.10, 129.88, 127.83, 127.66, 78.36, 59.04, 53.24, 52.72, 36.98, 21.80, 21.70.

(2R,4S)-Methyl 4-acetoxy-1-tosylpyrrolidine-2-carboxylate (**52**)

Under anhydrous and inert atmosphere, **51** (13 g, 28.7 mmol, 1 equiv) was dissolved in dry toluene (90 mL). Tetraethylammonium acetate (9.75 g, 37.3 mmol, 1.3 equiv) was added and the reaction was heated to reflux for 4 h. The reaction was cooled and washed twice with water and dried over anhydrous Na₂SO₄. Evaporation of the solvent provided a crude, which was purified by silica gel chromatography to give **52** as a light yellow solid (6.77 g, yield 73%).

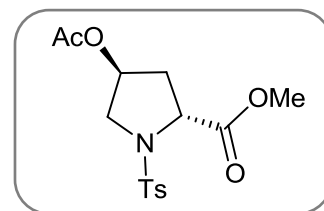
R_f = 0.38 (cyclohexane/EtOAc, 1:1)

m.p. = 80 – 82.9 °C

[α]_D = + 102.1 (c = 1.02, methanol)

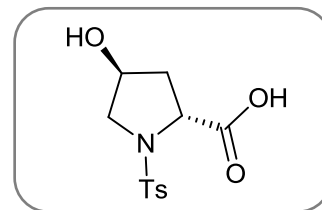
¹HNMR (CDCl₃): δ 7.76 (d, J = 8.3 Hz, 2H), 7.33 (d, J = 8.0 Hz, 2H), 5.13 (dt, J = 4.1, 2.3 Hz, 1H), 4.34 (dd, J = 8.7, 7.7 Hz, 1H), 3.77 (s, 3H), 3.70 (dd, J = 12.4, 4.0 Hz, 1H), 3.55 (dt, J = 12.4, 1.6 Hz, 1H), 2.43 (s, 3H), 2.37 – 2.27 (m, 1H), 2.20 (ddd, J = 13.7, 9.0, 4.7 Hz, 1H), 1.70 (s, 3H).

¹³CNMR (CDCl₃): δ 171.99, 169.99, 143.87, 134.75, 129.69, 127.83, 72.65, 59.73, 54.03, 52.70, 36.69, 21.54, 20.54.



(2R,4S)-4-Hydroxy-1-tosylpyrrolidine-2-carboxylic acid (53)

To **52** (6.6 g, 19.3 mmol, 1 equiv) in THF was added 0.5 M KOH in water (5.42 g, 96.7 mmol, 5 equiv) and the mixture was stirred at r.t. for 3 h. THF was evaporated under reduced pressure and 2 N HCl was added to achieve pH = 1. The water was removed *in vacuo*,



providing a white solid that was treated repetitively with DCM. The combined organic layers were evaporated to give **53** as a white solid (4.2 g, yield 76%).

$R_f = 0.49$ (DCM/MeOH, 1:1)

m.p. = 145.8 - 147.1 °C

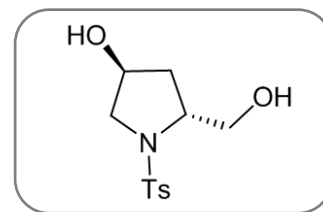
$[\alpha]_D = +100.1$ (c = 1.1, methanol)

$^1\text{H NMR}$ (CD_3OD): δ 7.71 (d, $J = 8.2$ Hz, 2H), 7.35 (d, $J = 8.1$ Hz, 2H), 4.33 - 4.26 (m, 1H), 4.19 (t, $J = 7.9$ Hz, 1H), 3.53 (dd, $J = 10.9, 4.1$ Hz, 1H), 3.24 (t, $J = 9.5$ Hz, 1H), 2.39 (s, 3H), 2.13 - 1.97 (m, 2H).

$^{13}\text{CNMR}$ (CD_3OD): δ 176.03, 145.20, 135.95, 130.64, 128.93, 70.50, 61.21, 57.52, 40.31, 21.48.

(3S,5R)-5-(Hydroxymethyl)-1-tosylpyrrolidin-3-ol (54)

Under anhydrous and inert conditions, **53** (4.2 g, 14.7 mmol, 1 equiv) was dissolved in dry THF (260 mL) and then cooled at 0 °C. A solution of 1 M BH₃ in THF (613 mg, 44.2 mL, 3 equiv) was added dropwise, then the reaction was warmed to r.t. and stirred for 6 h. Cool deionized water was added to quench the reaction at 0 °C and then THF was evaporated under reduced pressure. The water phase was extracted with EtOAc for three times. The combined organic layers were dried over anhydrous Na₂SO₄, filtrated and concentrated *in vacuo* to afford **54** as a white amorphous solid (3.27 g, yield 86%).



R_f = 0.42 (EtOAc)

m.p. = 129.8 - 133.5 °C

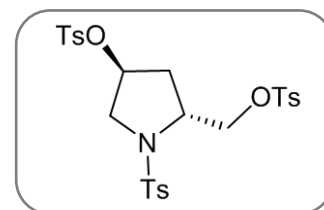
[α]_D = +43.1 (c = 1.85, ethanol)

¹H NMR (CDCl₃): δ 7.76 (d, J = 8.3 Hz, 2H), 7.33 (d, J = 8.0 Hz, 2H), 4.37 - 4.25 (m, 1H), 3.87 (dd, J = 11.6, 3.0 Hz, 1H), 3.78 (ddd, J = 7.9, 6.2, 3.8 Hz, 1H), 3.66 - 3.54 (m, 2H), 3.37 (dt, J = 12.1, 2.0 Hz, 1H), 2.43 (s, 3H), 1.98 - 1.79 (m, 2H).

¹³C NMR (CDCl₃): δ 144.14, 133.98, 129.86, 128.01, 69.73, 65.35, 60.87, 58.05, 37.89, 21.72.

((2R,4S)-1-Tosyl-4-(tosyloxy)pyrrolidin-2-yl)methyl 4-methylbenzenesulfonate (55)

Under anhydrous and inert conditions, **54** (1.33 g, 4.90 mmol, 1 equiv) and DMAP (120 mg, 0.98 mmol, 0.2 equiv) were suspended in dry DCM. Dry pyridine (1.90 mL, 23.5 mmol, 4.8 equiv) was added, followed by a dropped solution of TsCl (1.87 g, 9.80 mmol, 2 equiv) in dry DCM. The mixture stirred at 0 °C for 27 h. The reaction was concentrated *in vacuo* and the resulting crude was purified by silica gel column chromatography (cyclohexane/EtOAc, 7:3). Compound **55** was obtained as white solid (1.5 g, yield 53%).



$R_f = 0.25$ (cyclohexane/EtOAc, 1:1)

m.p. = 123.6 – 129.4 °C

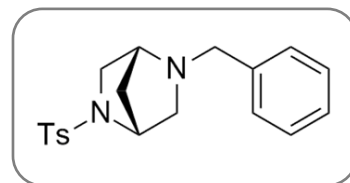
$[\alpha]_D = +55.5$ (c = 0.88, acetone)

$^1\text{H NMR}$ (CDCl_3): δ 7.78 (d, $J = 8.2$ Hz, 2H), 7.60 (dd, $J = 8.2, 16.4$ Hz, 4H), 7.38 – 7.26 (m, 6H), 4.77 (p, $J = 3.5$ Hz, 1H), 4.31 (dd, $J = 3.5, 10.5$ Hz, 1H), 4.11 (dd, $J = 6.5, 10.5$ Hz, 1H), 3.85 – 3.77 (m, 1H), 3.52 (d, $J = 2.9$ Hz, 2H), 2.46 – 2.43 (m, 9H), 2.07 – 2.04 (m, 2H).

$^{13}\text{C NMR}$ (CDCl_3): δ 145.37, 144.50, 133.14, 130.12, 130.00, 128.06, 127.81, 78.10, 71.63, 56.85, 54.78, 35.82, 21.78.

(1R,4R)-2-Benzyl-5-tosyl-2,5-diazabicyclo[2.2.1]heptane (**56**)

To a suspension of **55** (1.4 g, 2.42 mmol, 1 equiv) in MeOH (12.5 mL) under magnetic stirring in a flask, benzylamine (2.6 mL, 24.2 mmol, 10 equiv) was added dropwise at r.t. The mixture was then poured in a sealed tube and heated up to 90 °C overnight. Upon completion, the reaction was cooled and the solvent was evaporated under reduced pressure. The resulting crude was purified by silica gel chromatography (cyclohexane/EtOAc, 3:2) to give **56** as a light yellow solid (600 mg, yield 72%).



$R_f = 0.44$ (cyclohexane/EtOAc, 1:1)

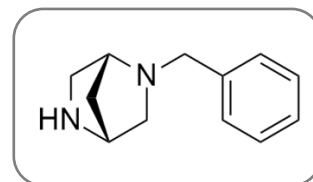
m.p. = 117.7 - 119.1 °C $[\alpha]_D = -18.5$ (c = 1.0, chloroform)

$^1\text{H NMR}$ (CDCl_3): δ 7.67 (d, $J = 8.2$ Hz, 2H), 7.27 - 7.15 (m, 7H), 4.25 - 4.17 (m, 1H), 3.58 - 3.55 (m, 3H), 3.34 (m, 1H), 2.96 (dd, $J = 2.3, 9.9$ Hz, 1H), 2.77 (dd, $J = 2.3, 9.9$ Hz, 1H), 2.61 - 2.58 (m, 1H), 2.37 (s, 3H), 1.64 (d, $J = 9.9$ Hz, 1H), 1.04 (d, $J = 9.9$ Hz, 1H).

$^{13}\text{C NMR}$ (CDCl_3): δ 143.56, 139.22, 135.81, 129.87, 128.48, 128.44, 127.61, 127.14, 61.14, 61.00, 59.61, 57.62, 50.77, 35.20, 21.66.

(1R,4R)-2-Benzyl-2,5-diazabicyclo[2.2.1]heptane (**57**)

A suspension of **56** (500 mg, 1.46 mmol) in 7.5 mL of 33% hydrogen bromide in acetic acid was heated to 50 °C and stirred for 5 h. Upon completion, EtOAc was added at 0°C and the mixture was stirred for 15 min; the resulting precipitated cake was filtered to afford the detosylated bicycle as dihydrobromide salt, which was added with a saturated aqueous solution of Na_2CO_3 and extracted three times with a mixture of DCM/*i*-PrOH, 4:1. The combined organic layers were dried over anhydrous Na_2SO_4 , filtered and concentrated *in vacuo* to afford **57** as a yellow oil (230 mg, yield 82%).



$R_f = 0.43$ (DCM/MeOH, 4:1)

$[\alpha]_D = -36.6$ (c = 0.73, chloroform)

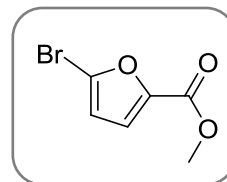
$^1\text{H NMR}$ (CD_3OD): δ 7.42 - 7.18 (m, 4H), 3.73 (q, $J = 13.0$ Hz, 2H), 3.60 - 2.67 (m, 1H), 3.45 - 3.33 (m, 1H), 3.20 (dd, $J = 10.6, 1.1$ Hz, 1H), 2.80 (ddd, $J = 37.4, 10.4, 2.5$ Hz, 2H), 2.53 (dd, $J = 10.1, 1.2$ Hz, 1H), 1.88 (d, $J = 9.9$ Hz, 1H), 1.58 (d, $J = 10.0$ Hz, 1H).

$^{13}\text{C NMR}$ (CD_3OD): δ 131.61, 128.61, 127.96, 126.77, 60.25, 60.01, 57.61, 56.48, 46.6, 34.6.

7.1.2.3 Synthesis of differently substituted acyl chlorides 97-110

Methyl 5-bromofuran-2-carboxylate (58)

To a solution of 5-bromofuran-2-carboxylic acid (8.7 g, 45.5 mmol, 1 equiv) in MeOH (150 mL), H₂SO₄ was added dropwise (0.2 mL/mmol) and the mixture was refluxed for 24 h. The solvent was then evaporated under vacuum. Deionized water was added to the resulting crude and the aqueous solution was extracted from DCM. The organic phase was finally washed once with a saturated aqueous solution of NaHCO₃, dried over anhydrous Na₂SO₄ and evaporated under reduced pressure. The final compound **58** was isolated as white solid without any further purification (8.85 g, yield 95%).



R_f = 0.55 (cyclohexane/EtOAc, 85:15), UV.

m.p. = 65.4 – 66.6 °C.

¹H NMR (CDCl₃): δ 7.13 (dd, *J* = 4.5, 2.3 Hz, 1H), 6.46 (dd, *J* = 4.6, 2.3 Hz, 1H), 3.89 (s, 3H).

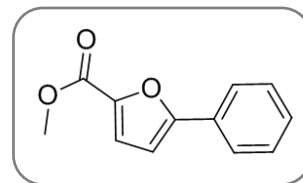
¹³C NMR (CDCl₃): δ 158.08, 146.28, 127.58, 120.18, 114.01, 52.17.

7.1.2.3.1 General procedure for the preparation of compounds 71-82 via Suzuki-Miyaura reaction between methyl 5-bromofuran-2-carboxylate and the appropriate boronic acid.

Under inert conditions, to a stirred degassed solution of methyl 5-bromofuran-2-carboxylate (**58**) (1 equiv) and Pd(PPh₃)₄ (0.05 equiv) in 1,2-dimethoxyethane (10 mL) (compound **59-69**) or DMF (compound **70**), the appropriate boronic acid (1.4 equiv) was added. Degassed aqueous solution of 2 M Na₂CO₃ (4.2 equiv) was added and the final mixture was refluxed for 12 h. Upon completion, the reaction was cooled down and deionized water was added; the organic solvent was evaporated and the water phase was extracted with DCM. The resulting organic phase was dried over anhydrous Na₂SO₄, filtered and concentrated under reduced pressure. The crude was purified by column chromatography, giving the pure cross-coupling compound.

Methyl 5-phenylfuran-2-carboxylate (71)

The title compound was prepared following the general procedure from methyl 5-bromofuran-2-carboxylate (**58**) (1.20 g, 5.86 mmol, 1 equiv), commercially available phenylboronic acid (**59**) (1 g, 8.43 mmol, 1.40 equiv), Pd(PPh₃)₄ (338 mg, 0.293 mmol, 0.05 equiv) and an aqueous solution of 2 M Na₂CO₃ (2.61 g, 24.6 mmol in 12.30 mL of H₂O, 4.20 equiv). After standard workup and purification through column chromatography eluted by cyclohexane/EtOAc (1:1), **71** was obtained as a white solid (990 mg, yield 84%).



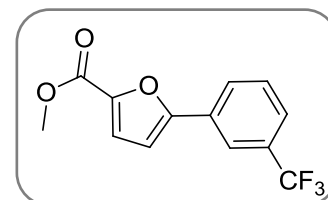
R_f = 0.55 (cyclohexane/EtOAc, 4:1)

m.p. = 63.2 - 64.4 °C

¹H NMR (CDCl₃): δ 7.81 - 7.75 (m, 2H), 7.46 - 7.31 (m, 3H), 7.25 (d, *J* = 3.6 Hz, 1H), 6.74 (d, *J* = 3.6 Hz, 1H), 3.92 (s, 3H). ¹³C NMR (CDCl₃): δ 159.35, 157.71, 143.70, 129.61, 129.07, 128.94, 124.97, 120.18, 106.97, 51.99.

Methyl 5-(3-(trifluoromethyl)phenyl)furan-2-carboxylate (72)

The title compound was prepared following the general procedure from methyl 5-bromofuran-2-carboxylate (**58**) (1.20 g, 15.8 mmol, 1 equiv), commercially available (3-(trifluoromethyl)phenyl)boronic acid (**60**) (3 g, 8.43 mmol, 1.40 equiv), Pd(PPh₃)₄ (652 mg, 0.56 mmol, 0.05 equiv) and an aqueous solution of 2 M Na₂CO₃ (5 g, 47.4 mmol in 24 mL of H₂O, 4.20 equiv). After standard workup and purification through column chromatography eluted by cyclohexane/EtOAc (8:2), **72** was obtained as a white solid (2.8 g, yield 92%).



R_f = 0.58 (cyclohexane/EtOAc, 4:1)

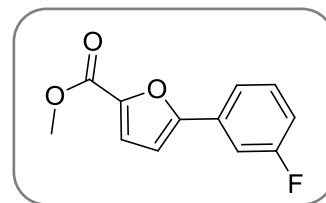
m.p. = 81.4 - 86.5 °C

¹H NMR ((CD₃)₂CO): δ 8.13 (t, *J* = 3.8 Hz, 2H), 7.77 - 7.72 (m, 2H), 7.36 (d, *J* = 3.6 Hz, 1H), 7.27 (d, *J* = 3.7 Hz, 1H), 3.89 (s, 3H).

¹³C NMR (CDCl₃): δ 159.33, 156.09, 144.61, 132.40, 131.97, 131.54, 131.11 (q, *J* = 32.53), 130.29, 128.50, 126.94, 125.31 (q, *J* = 271.47), 129.73, 128.17, 125.74, 125.70, 125.65, 125.60 (q, *J* = 3.4 Hz), 121.94, 121.89, 121.84, 121.79 (q, *J* = 3.4 Hz), 120.22, 118.98, 108.34, 52.31.

Methyl 5-(3-fluorophenyl)furan-2-carboxylate (73)

The title compound was prepared following the general procedure from methyl 5-bromofuran-2-carboxylate (**58**) (1.05 g, 5.10 mmol, 1 equiv), commercially available (3-fluorophenyl)boronic acid (**61**) (1 g, 7.15 mmol, 1.40 equiv), Pd(PPh₃)₄ (295 mg, 0.26 mmol, 0.05 equiv) and an aqueous solution of 2 M Na₂CO₃ (2.27 g, 21.44 mmol in 10.7 mL of H₂O, 4.20 equiv). After standard workup and purification through column chromatography eluted by cyclohexane/EtOAc (8:2), **73** was obtained as a yellow solid (974 mg, yield 87%).



R_f = 0.50 (cyclohexane/EtOAc, 4:1)

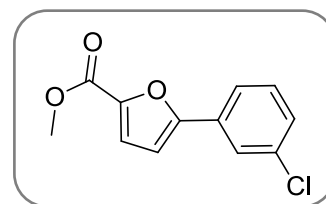
m.p. = 84.2 – 85.8 °C

¹H NMR (CDCl₃): δ 7.49 – 7.45 (m, 1H), 7.42 – 7.36 (m, 1H), 7.30 (td, *J* = 8.0, 5.8 Hz, 1H), 7.18 – 7.15 (m, 1H), 6.99 – 6.91 (m, 1H), 6.67 (dd, *J* = 3.5, 1.6 Hz, 1H), 3.84 (s, 3H).

¹³C NMR (CDCl₃): δ 165.05, 161.79 (d, *J* = 246.1 Hz), 159.41, 156.49, 144.32, 131.88, 131.77 (d, *J* = 8.5 Hz), 130.89, 130.78 (d, *J* = 8.3 Hz), 120.87, 120.83 (d, *J* = 3.0 Hz), 120.26, 116.28, 116.00 (d, *J* = 21.3 Hz), 112.23, 111.95 (d, *J* = 23.7 Hz), 108.09, 52.54.

Methyl 5-(3-chlorophenyl)furan-2-carboxylate (74)

The title compound was prepared following the general procedure from methyl 5-bromofuran-2-carboxylate (**58**) (1 g, 4.89 mmol, 1 equiv), commercially available (3-chlorophenyl)boronic acid (**62**) (1.07 g, 6.84 mmol, 1.40 equiv), Pd(PPh₃)₄ (282 mg, 0.24 mmol, 0.05 equiv) and an aqueous solution of 2 M Na₂CO₃ (2.18 g, 20.5 mmol in 10.30 mL of H₂O, 4.20 equiv). After standard workup and purification through column chromatography eluted by cyclohexane/EtOAc (4:1), **74** was obtained as a white solid (700 mg, yield 60%).



R_f = 0.55 (cyclohexane/EtOAc, 4:1)

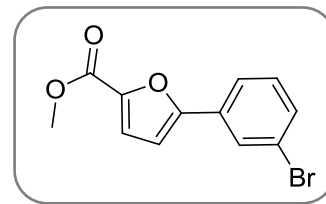
m.p. = 75.8 – 76.7 °C

¹H NMR (CDCl₃): δ 7.76 (s, 1H), 7.68 – 7.60 (m, 1H), 7.40 – 7.21 (m, 3H), 6.75 (t, *J* = 3.5 Hz, 1H), 3.91 (s, *J* = 1.7 Hz, 3H). ¹³C NMR ((CD₃)₂CO): δ 159.18, 156.25, 145.03, 135.39,

132.25, 131.59, 129.55, 125.07, 123.77, 120.62, 109.38, 52.11.

Methyl 5-(3-bromophenyl)furan-2-carboxylate (75)

The title compound was prepared following the general procedure from methyl 5-bromofuran-2-carboxylate (**58**) (1 g, 5 mmol, 1 equiv), commercially available (3-bromophenyl)boronic acid (**63**) (1 g, 5 mmol, 1 equiv), Pd(PPh₃)₄ (290 mg, 0.25 mmol, 0.05 equiv) and an aqueous solution of 2 M Na₂CO₃ (2.23 g, 21 mmol in 10.5 mL of H₂O, 4.20 equiv). After standard workup and purification through column chromatography eluted by cyclohexane/DCM (1:1), **75** was obtained as a yellow oil (1.01 g, yield 77%).



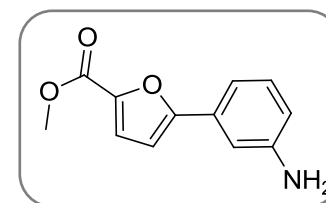
R_f = 0.48 (cyclohexane/EtOAc, 4:1)

¹H NMR (CDCl₃): δ 7.94 (s, 1H), 7.71 (dd, *J* = 7.8, 0.5 Hz, 1H), 7.48 (d, *J* = 7.9 Hz, 1H), 7.33 – 7.26 (m, 2H), 6.77 (d, *J* = 3.4 Hz, 1H), 3.95 (s, 3H).

¹³C NMR ((CD₃)₂CO): δ 159.16, 156.11, 145.06, 132.51, 131.82, 127.97, 124.19, 123.46, 120.62, 109.40, 52.12.

Methyl 5-(3-aminophenyl)furan-2-carboxylate (76)

The title compound was prepared following the general procedure from methyl 5-bromofuran-2-carboxylate (**58**) (945 mg, 4.61 mmol, 1 equiv), commercially available (3-aminophenyl)boronic acid monohydrate (**64**) (1 g, 6.45 mmol, 1.40 equiv), Pd(PPh₃)₄ (266 mg, 0.23 mmol, 0.05 equiv) and an aqueous solution of 2 M Na₂CO₃ (2.05 g, 19.4 mmol in 9.7 mL of H₂O, 4.20 equiv). After standard workup and purification through column chromatography eluted by cyclohexane/EtOAc (3:2), **76** was obtained as a brown solid (710 mg, yield 71%).



R_f = 0.44 (cyclohexane/EtOAc, 4:1)

m.p. = 103.6 – 104.9 °C

¹H NMR (CDCl₃): δ 7.24 – 7.12 (m, 4H), 6.68 (t, *J* = 4.2 Hz, 2H), 3.91 (s, 3H).

¹³C NMR ((CD₃)₂CO): δ 159.38, 158.97, 149.94, 144.09, 131.01, 130.45, 120.71, 115.98, 114.07, 110.76, 107.57, 51.92.

Methyl 5-(3-hydroxyphenyl)furan-2-carboxylate (77)

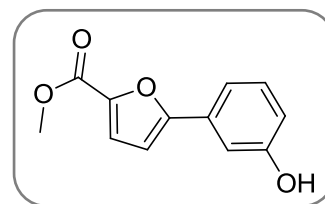
The title compound was prepared following the general procedure from methyl 5-bromofuran-2-carboxylate (**58**) (700 mg, 3.41 mmol, 1 equiv), commercially available (3-hydroxyphenyl)boronic acid (**65**) (660 mg, 4.78 mmol, 1.4 equiv), Pd(PPh₃)₄ (197 mg, 0.17 mmol, 0.05 equiv) and an aqueous solution of 2 M Na₂CO₃ (1.52 g, 14.34 mmol in 7.2 mL of H₂O, 4.20 equiv). After standard workup and purification through column chromatography eluted by cyclohexane/EtOAc (7:3), **77** was obtained as a brown solid (510 mg, yield 68%).

R_f = 0.50 (cyclohexane/EtOAc, 7:3)

m.p. = 142.6 – 144.3 °C

¹H NMR ((CD₃)₂CO): δ 8.53 (s, 1H), 7.36 – 7.23 (m, 3H), 6.99 – 6.94 (m, 1H), 6.92 – 6.82 (m, 1H), 3.86 (s, 3H).

¹³C NMR ((CD₃)₂CO): δ 159.35, 158.80, 158.13, 144.46, 131.71, 131.08, 120.68, 117.05, 116.91, 112.10, 108.17, 51.99.

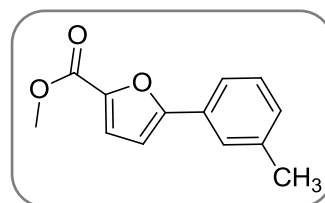
*Methyl 5-(m-tolyl)furan-2-carboxylate (78)*

The title compound was prepared following the general procedure from methyl 5-bromofuran-2-carboxylate (**58**) (800 mg, 3.9 mmol, 1 equiv), commercially available (3-(methyl)phenyl)boronic acid (**66**) (743 mg, 5.46 mmol, 1.40 equiv), Pd(PPh₃)₄ (225 mg, 0.20 mmol, 0.05 equiv) and an aqueous solution of 2 M Na₂CO₃ (1.74 g, 16.4 mmol in 8.2 mL of H₂O, 4.20 equiv). After standard workup and purification through column chromatography eluted by cyclohexane/EtOAc (9:1), **78** was obtained as a yellow solid (738 mg, yield 87%).

R_f = 0.58 (cyclohexane/EtOAc, 4:1)

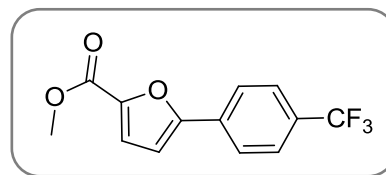
m.p. = 85.6 – 88.7 °C

¹H NMR ((CD₃)₂CO): δ 7.34 – 7.26 (m, 2H), 7.02 (td, J = 7.7, 1.7 Hz, 1H), 6.97 (dd, J = 3.6, 2.0 Hz, 1H), 6.88 (d, J = 7.6 Hz, 1H), 6.68 (dd, J = 3.6, 2.0 Hz, 1H), 3.53 (s, 3H), 2.05 (s, 3H). ¹³C NMR ((CD₃)₂CO): δ 158.80, 157.40, 144.12, 138.90, 131.20, 130.89, 129.46, 122.20, 113.56, 109.21, 52.10, 21.05.



Methyl 5-(4-trifluorophenyl)furan-2-carboxylate (79)

The title compound was prepared following the general procedure from methyl 5-bromofuran-2-carboxylate (**58**) (308.40 mg, 1.50 mmol, 1 equiv), commercially available (4-trifluoromethylphenyl)



boronic acid (**67**) (400 mg, 2.11 mmol, 1.40 equiv), Pd(PPh₃)₄ (166.92 mg, 0.15 mmol, 0.1 equiv) and an aqueous solution of 2 M Na₂CO₃ (1.34 g, 12.64 mmol in 6.32 mL of H₂O, 8.40 equiv). After standard workup and purification through column chromatography eluted by cyclohexane/EtOAc (9:1), **79** was obtained as a yellowish solid (240 mg, yield 60%).

R_f = 0.3 (cyclohexane/EtOAc, 85:15)

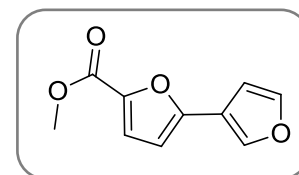
m.p. = 86 - 87 °C

¹HNMR (CDCl₃): δ 7.91 (d, J = 8.79 Hz, 2H), 7.69 (d, J = 8.24 Hz, 2H), 7.20 (d, J = 3.5 Hz, 1H), 7.11 (d, J = 3.51 Hz, 1H), 3.76 (s, 3H).

¹³CNMR ((CD₃)₂CO): δ 159.97, 156.99, 146.28, 134.71, 132.07, 131.64, 131.21, 130.78 (q, J = 32.25 Hz), 127.71, 127.66, 127.61, 127.25 (q, J = 3.42 Hz), 126.68, 131.28, 127.68, 124.09, 120.50 (q, J = 271.77), 111.07, 52.96.

Methyl [2,3'-bifuran]-5-carboxylate (80)

The title compound was prepared following the general procedure from methyl 5-bromofuran-2-carboxylate (**58**) (340.26 mg, 1.66 mmol, 1 equiv), commercially available 3-furanyl boronic acid (**68**) (260



mg, 2.32 mmol, 1.40 equiv), Pd(PPh₃)₄ (95.90 mg, 0.083 mmol, 0.05 equiv) and an aqueous solution of 2 M Na₂CO₃ (738.85 g, 6.97 mmol in 3.40 mL of H₂O, 4.20 equiv). After standard workup and purification through column chromatography eluted by cyclohexane/EtOAc (9:1), **80** was obtained as a yellow oil (358.35 mg, yield 81%).

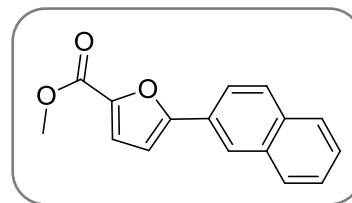
R_f = 0.40 (cyclohexane/EtOAc, 4:1)

¹HNMR ((CD₃)₂CO): δ 8.09 (s, 1H), 7.68 (d, J = 1.76 Hz, 1H), 7.27 (d, J = 3.51 Hz, 1H), 6.86 (d, J = 1.76 Hz, 1H), 6.65 (d, J = 3.51, 1H).

¹³C NMR ((CD₃)₂CO): δ 158.58, 151.80, 143.85, 142.88, 139.98, 119.49, 116.58, 107.90, 107.11, 50.89.

Methyl 5-(naphthalen-2-yl)furan-2-carboxylate (81)

The title compound was prepared following the general procedure from methyl 5-bromofuran-2-carboxylate (**58**) (340.56 mg, 1.66 mmol, 1 equiv), commercially available (1-naphthalen)boronic acid (**69**) (400 mg, 2.33 mmol, 1.40 equiv), Pd(PPh₃)₄ (95.98 mg, 0.083 mmol, 0.05 equiv) and an aqueous solution of 2 M Na₂CO₃ (739.50 mg, 6.98 mmol in 3.49 mL of H₂O, 4.20 equiv). After standard workup and purification through column chromatography eluted by cyclohexane/EtOAc (95:5), **81** was obtained as a brown oil (400 mg, yield 95%).



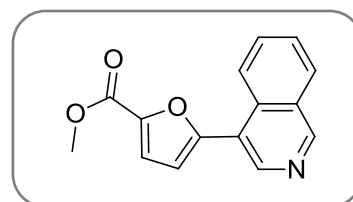
R_f = 0.37 (cyclohexane/EtOAc, 9:1)

¹H NMR ((CD₃)₂CO): δ 8.48 – 8.41 (m, *J* = 8.8 Hz, 1H), 8.03 – 7.91 (m, *J* = 8.2 Hz, 2H), 7.88 – 7.77 (m, *J* = 7.2 Hz, 1H), 7.66 – 7.50 (m, 3H), 7.40 (d, *J* = 3.6 Hz, 1H), 6.98 (d, *J* = 3.6 Hz, 1H).

¹³C NMR ((CD₃)₂CO): δ 158.58, 157.04, 144.20, 134.08, 130.11, 129.95, 128.74, 127.21, 127.10, 127.03, 126.28, 125.31, 124.98, 119.43, 111.29, 51.23.

Methyl 5-(isoquinulin-4-yl)furan-2-carboxylate (82)

The title compound was prepared following the general procedure from methyl 5-bromofuran-2-carboxylate (**58**) (270 mg, 1.31 mmol, 1 equiv), commercially available (3-isoquinulin)boronic acid (**70**) (250 mg, 1.45 mmol, 1.10 equiv), Pd(PPh₃)₄ (75.91 mg, 0.067 mmol, 0.05 equiv) and an aqueous solution of 2 M Na₂CO₃ (585 mg, 5.52 mmol in 2.76 mL of H₂O, 4.20 equiv). After standard workup and purification through column chromatography eluted by cyclohexane/EtOAc (1:1), **82** was obtained as an off-white solid (243 mg, yield 73%).



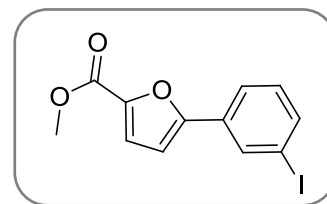
R_f = 0.50 (cyclohexane/EtOAc, 3:2) m.p. = 135 - 140 °C

¹H NMR ((CD₃)₂CO): δ 9.35 (s, 1H), 8.86 (s, 1H), 8.50 (d, *J* = 8.6 Hz, 1H), 8.21 (d, *J* = 8.2 Hz, 1H), 7.90 (t, *J* = 8.5 Hz, 1H), 7.78 (t, *J* = 8.5 Hz, 1H), 7.45 (d, *J* = 3.6 Hz, 1H), 7.18 (d, *J* = 3.6 Hz, 1H), 3.93 (s, 3H).

¹³C NMR ((CD₃)₂CO): δ 158.43, 154.72, 153.73, 144.91, 142.87, 131.96, 131.68, 128.48, 128.41, 127.81, 124.07, 120.70, 119.37, 111.79, 51.31.

Methyl 5-(3-iodophenyl)furan-2-carboxylate (83)

An aqueous solution of H₂SO₄ conc. (310 μL in 1.5 mL of H₂O) was added dropwise to a water suspension of **76** (330 mg, 1.52 mmol, 1 equiv) at 0 °C, giving a white suspension. An aqueous solution of NaNO₂ (111 mg, 1.60 mmol, 1.05 equiv) was added and a yellow suspension was obtained, which was stirred at 0 °C for 1 h. Then a solution of KI in water (378 mg, 2.28 mmol, 1.5 equiv) was dropped into the yellow suspension, giving a red thick precipitate. The mixture was stirred at 0 °C until completion of the reaction. Then water was added and extracted three times with DCM. The combined organic phases were dried over anhydrous Na₂SO₄, filtered and concentrated *in vacuo*, giving a brown crude. Cyclohexane was employed to treat the crude and the purple organic layers were combined and concentrated in vacuum to afford the pure compound **83** as a brown solid (270 mg, yield 54%).



R_f = 0.48 (cyclohexane/EtOAc, 4:1)

m.p. = 81.2 – 82.1 °C

¹H NMR (CDCl₃): δ 8.12 (s, 1H), 7.71 (dd, *J* = 18.0, 7.9 Hz, 2H), 7.24 (d, *J* = 3.6 Hz, 1H), 7.15 (t, *J* = 7.9 Hz, 1H), 6.75 (d, *J* = 3.5 Hz, 1H), 3.92 (s, 3H).

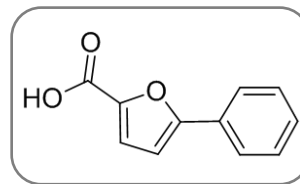
¹³C NMR ((CD₃)₂CO): δ 159.20, 156.03, 145.07, 138.63, 133.92, 132.48, 131.86, 124.73, 120.67, 109.31, 95.09, 52.12.

7.1.2.3.2 General procedure for the hydrolysis of methyl ester intermediates 71-83.

An aqueous 1.5 M NaOH solution of compounds **71-76** and **78-83** (1.5 equiv) or 1.5 M LiOH of compound **77** (4 equiv) was added dropwise to a solution of the appropriate methyl ester (1 equiv) in THF at 0 °C. The resulting mixture was stirred at room temperature overnight (derivatives **71-76** and **78-83**) or 48 h (derivative **77**). The reaction was concentrated under reduced pressure and the aqueous residue was cooled at 0 °C and acidified by an aqueous 2 M solution of HCl added dropwise (pH = 1-2). The corresponding carboxylic acid precipitated and was filtered under vacuum (compounds **84-88** and **90-96**); compound **89** was extracted from water phase by DCM/*i*-PrOH 4:1. All the afforded compounds were used for the next step without any further purification.

5-Phenylfuran-2-carboxylic acid (84)

The title compound was prepared following the general procedure from **71** (500 mg, 2.47 mmol, 1 equiv) and an aqueous 1.5 M solution of NaOH (148 mg, 3.71 mmol in 2.47 mL of H₂O, 1.50 equiv). After standard workup, **84** was obtained as a white solid.



84: white solid (419 mg, yield 90%)

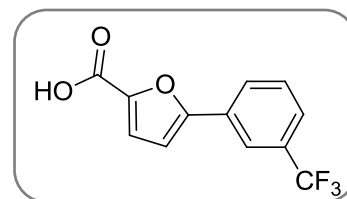
R_f = 0.54 (DCM/MeOH, 4:1) m.p. = 148.9 – 150.2 °C

¹H NMR (D₂O): δ 7.86 (d, *J* = 7.8 Hz, 2H), 7.54 – 7.38 (dt, 3H), 7.13 (d, *J* = 3.5 Hz, 1H), 6.92 (d, *J* = 3.4 Hz, 1H).

¹³C NMR ((CD₃)₂CO): δ 159.2, 157.6, 144.7, 130.2, 129.5, 129.4, 125.1, 120.4, 107.8.

5-(3-(Trifluoromethyl)phenyl)furan-2-carboxylic acid (85)

The title compound was prepared following the general procedure from **72** (760 mg, 2.81 mmol, 1 equiv) and an aqueous 1.5 M solution of NaOH (169 mg, 4.22 mmol in 2.8 mL of H₂O, 1.50 equiv). After standard workup, **85** was obtained as a white solid (432 mg, yield 60%).



R_f = 0.28 (DCM/MeOH, 4:1)

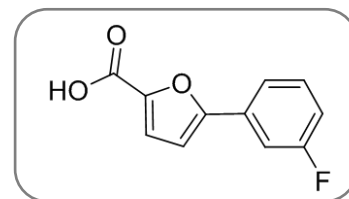
m.p. = 141.2 – 143.5 °C

¹H NMR ((CD₃)₂CO): δ 8.15 (dd, *J* = 4.4, 2.8 Hz, 2H), 7.77 – 7.72 (m, 2H), 7.37 (d, *J* = 3.6 Hz, 1H), 7.27 (d, *J* = 3.6 Hz, 1H).

¹³C NMR (75 MHz, acetone) δ 159.27, 156.12, 145.73, 132.43, 132.00, 131.57, 131.14 (q, *J* = 32.54 Hz), 131.54, 131.01, 130.46, 126.87, 123.27, 119.67 (q, *J* = 271.56 Hz), 129.00, 126.18, 126.13, 126.08, 126.03 (q, *J* = 3.57 Hz), 121.93, 121.89, 121.84, 121.79 (q, *J* = 3.75 Hz), 120.75, 109.79.

5-(3-Fluorophenyl)furan-2-carboxylic acid (**86**)

The title compound was prepared following the general procedure from **73** (930 mg, 4.22 mmol, 1 equiv) and an aqueous 1.5 M solution of NaOH (253 mg, 6.34 mmol in 4.22 mL of H₂O, 1.50 equiv). After standard workup, **86** was obtained as a white solid (780 mg, yield 90%).



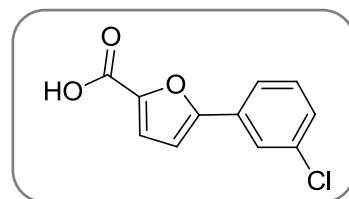
$R_f = 0.40$ (DCM/MeOH, 4:1) m.p. = 179.9 – 181.0 °C

¹H NMR ((CD₃)₂CO): δ 7.72 – 7.67 (m, 1H), 7.63 – 7.58 (m, 1H), 7.58 – 7.49 (m, 1H), 7.34 (d, $J = 3.7$ Hz, 1H), 7.22 – 7.17 (m, 1H), 7.15 (d, $J = 3.6$ Hz, 1H), 2.82 (br s, 1H).

¹³C NMR ((CD₃)₂CO): δ 165.65, 162.41 (d, $J = 244.2$ Hz), 159.32, 156.55, 145.43, 132.80, 132.69 (d, $J = 8.5$ Hz), 132.02, 131.91 (d, $J = 8.5$ Hz), 121.41, 121.37 (d, $J = 2.9$ Hz), 120.74, 116.56, 116.27 (d, $J = 21.5$ Hz), 112.21, 111.89 (d, $J = 24$ Hz), 109.38.

5-(3-Chlorophenyl)furan-2-carboxylic acid (**87**)

The title compound was prepared following the general procedure from **74** (600 mg, 2.54 mmol, 1 equiv) and an aqueous 1.5 M solution of NaOH (152 mg, 3.80 mmol in 2.5 mL of H₂O, 1.50 equiv). After standard workup, **87** was obtained as a white solid (530 mg, yield 94%).



$R_f = 0.40$ (DCM/MeOH, 4:1)

m.p. = 233.5 – 234.6 °C

¹H NMR (DMSO): δ 7.37 (t, $J = 1.7$ Hz, 1H), 7.29 (d, $J = 7.8$ Hz, 1H), 7.04 (t, $J = 7.8$ Hz, 1H), 6.96 (d, $J = 8.2$ Hz, 1H), 6.73 (d, $J = 3.5$ Hz, 1H), 6.66 (d, $J = 3.4$ Hz, 1H), 2.87 (s, 1H).

¹³C NMR (DMSO): δ 162.78, 160.00, 141.56, 133.83, 131.62, 130.93, 128.03, 123.61, 122.59, 117.48, 108.92.

5-(3-Bromophenyl)furan-2-carboxylic acid (88)

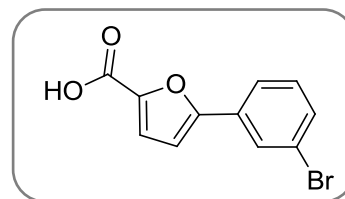
The title compound was prepared following the general procedure from **75** (1 g, 3.56 mmol, 1 equiv) and an aqueous 1.5 M solution of NaOH (213 mg, 5.34 mmol in 3.6 mL of H₂O, 1.50 equiv). After standard workup, **88** was obtained as a white solid (909 mg, yield 96%).

R_f = 0.40 (DCM/MeOH, 4:1)

m.p. = 180.0 – 183.8 °C

¹H NMR ((CD₃)₂CO): δ 11.37 (br s, 1H), 8.02 (t, *J* = 1.8 Hz, 1H), 7.87 – 7.82 (m, 1H), 7.58 (ddd, *J* = 7.9, 1.9, 1.0 Hz, 1H), 7.45 (t, *J* = 7.9 Hz, 1H), 7.34 (d, *J* = 3.6 Hz, 1H), 7.17 (d, *J* = 3.6 Hz, 1H).

¹³C NMR ((CD₃)₂CO): δ 159.29, 156.05, 145.46, 132.60, 132.46, 131.83, 127.96, 124.18, 123.46, 120.74, 109.45.

*5-(3-Aminophenyl)furan-2-carboxylic acid (89)*

The title compound was prepared following the general procedure from **76** (350 mg, 1.61 mmol, 1 equiv) and an aqueous 1.5 M solution of NaOH (97 mg, 2.42 mmol in 1.6 mL of H₂O, 1.50 equiv). Upon completion, an aqueous 2 M solution of HCl was

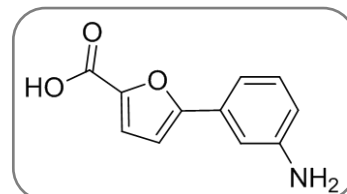
added to reach pH = 7 and the water phase was extracted with DCM. The organic layers were dried over anhydrous Na₂SO₄, filtered and concentrated under vacuum, affording **89** as a brown solid (270 mg, yield 83%).

R_f = 0.36 (DCM/MeOH, 4:1)

m.p. = 185.7 – 187.1 °C

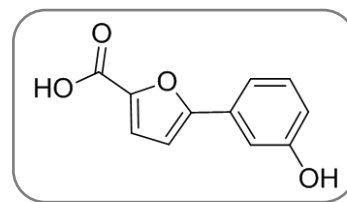
¹H NMR ((CD₃)₂CO): δ 7.34 (s, 1H), 7.30 (dd, *J* = 4.3, 3.8 Hz, 2H), 7.06 (d, *J* = 3.7 Hz, 2H), 6.93 (dt, *J* = 6.1, 2.2 Hz, 1H).

¹³C NMR ((CD₃)₂CO): δ 159.58, 149.86, 144.58, 132.66, 130.40, 129.51, 120.64, 115.89, 114.04, 110.79, 107.53.



5-(3-Hydroxyphenyl)furan-2-carboxylic acid (90)

The title compound was prepared following the general procedure from **77** (400 mg, 1.83 mmol, 1 equiv) and an aqueous 2.5 M solution of LiOH (176 mg, 7.34 mmol in 3 mL of H₂O, 4 equiv); the reaction took 2 days to reach completeness. After standard workup, **90** was obtained as a light brown solid (330 mg, yield 88%).



$R_f = 0.33$ (DCM/MeOH, 4:1)

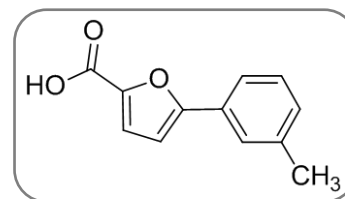
m.p. = 168.8 – 169.7 °C

¹H NMR ((CD₃)₂CO): δ 8.04 (br s, 2H), 7.38 – 7.19 (m, 4H), 6.90 (dd, $J = 9.0, 5.7$ Hz, 2H).

¹³C NMR ((CD₃)₂CO): δ 160.17, 158.54, 158.09, 144.53, 131.51, 130.84, 120.92, 116.93, 116.76, 112.05, 108.03.

*5-(*m*-Tolyl)furan-2-carboxylic acid (91)*

The title compound was prepared following the general procedure from **78** (688 mg, 3.18 mmol, 1 equiv) and an aqueous 1.5 M solution of NaOH (191 mg, 4.77 mmol in 3.2 mL of H₂O, 1.50 equiv). After standard workup, **91** was obtained as a white solid (564 mg, yield 88%).



$R_f = 0.60$ (cyclohexane/EtOAc, 1:1)

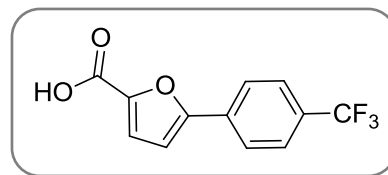
m.p.: 138.1 – 140.3 °C

¹H NMR ((CD₃)₂CO): δ 11.25 (br s, 1H), 7.66 (dd, $J = 11.0, 4.2$ Hz, 2H), 7.36 (t, $J = 7.7$ Hz, 1H), 7.31 (d, $J = 3.5$ Hz, 1H), 7.22 (d, $J = 7.6$ Hz, 1H), 7.02 (d, $J = 3.5$ Hz, 1H), 2.40 (s, 3H).

¹³C NMR ((CD₃)₂CO): δ 159.44, 158.24, 144.88, 139.55, 130.55, 129.79, 125.93, 122.66, 120.80, 108.06, 21.37.

5-(4-Trifluorophenyl)furan-2-carboxylic acid (92)

The title compound was prepared following the general procedure from **79** (220 mg, 0.814 mmol, 1 equiv) and an aqueous 1.5 M solution of NaOH (49 mg, 1.22 mmol in 0.814 mL of H₂O, 1.5 equiv).



After standard workup, **92** was obtained as a white solid (208 mg, yield 100%).

$R_f = 0.50$ (DCM/MeOH, 9:1)

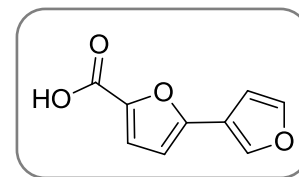
m.p. = 175 - 179 °C

¹H NMR ((CD₃)₂CO): δ 8.07 (d, $J = 8.3$ Hz, 2H), 7.84 (d, $J = 8.5$ Hz, 2H), 7.37 (d, $J = 3.6$ Hz, 1H), 7.25 (d, $J = 3.6$ Hz, 1H).

¹³C NMR ((CD₃)₂CO): δ 160.16, 156.92, 146.89, 134.94, 131.21, 127.80, 127.72, 127.67, 127.61 (q, $J = 3.4$ Hz), 126.74, 121.47, 111.16.

[2,3'-Bifuran]-5-carboxylic acid (93)

The title compound was prepared following the general procedure from **80** (250 mg, 1.3 mmol, 1 equiv) and an aqueous 1.5 M solution of NaOH (79 mg, 1.95 mmol in 1.3 mL of H₂O, 1.5 equiv). After standard workup, **93** was obtained as a white solid (208.6 mg, yield 90%).



$R_f = 0.55$ (EtOAc)

m.p. = 137-140 °C

¹H NMR ((CD₃)₂CO): δ 8.07 (d, $J = 8.3$ Hz, 2H), 7.84 (d, $J = 8.5$ Hz, 2H), 7.37 (d, $J = 3.6$ Hz, 1H), 7.25 (d, $J = 3.6$ Hz, 1H).

¹³C NMR ((CD₃)₂CO): δ 159.38, 152.46, 145.33, 144.36, 141.03, 120.50, 118.08, 108.67, 108.21.

5-(Naphthalen-2-yl)furan-2-carboxylic acid (94)

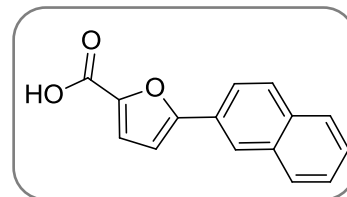
The title compound was prepared following the general procedure from **81** (400 mg, 1.59 mmol, 1 equiv) and an aqueous 1.5 M solution of NaOH (95 mg, 2.4 mmol in 1.6 mL of H₂O, 1.5 equiv). After standard workup, **94** was obtained as a white solid (337 mg, yield 90%).

R_f = 0.55 (EtOAc)

m.p. = 173 - 175 °C

¹H NMR ((CD₃)₂CO): δ 8.54 – 8.42 (m, 1H), 8.07 – 7.96 (m, 2H), 7.89 (dd, *J* = 7.2, 1.2 Hz, 1H), 7.68 – 7.55 (m, 3H), 7.43 (d, *J* = 3.5 Hz, 1H), 7.05 (d, *J* = 3.5 Hz, 1H).

¹³C NMR ((CD₃)₂CO): δ 158.87, 156.89, 144.80, 134.10, 130.14, 129.85, 128.70, 127.17, 127.05, 126.26, 125.32, 125.03, 124.50, 119.35, 111.27.

*5-(Isoquinolin-4-yl)furan-2-carboxylic acid (95)*

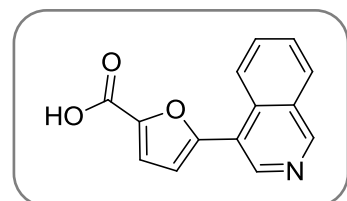
The title compound was prepared following the general procedure from **82** (240 mg, 0.950 mmol, 1 equiv) and an aqueous 1.5 M solution of NaOH (57 mg, 1.42 mmol in 0.950 mL of H₂O, 1.5 equiv). After standard workup, **95** was obtained as a white solid (175 mg, yield 77%).

R_f = 0.57 (DCM/MeOH, 1:1 and 3 drops of AcOH)

m.p. = 248 - 251 °C

¹H NMR ((DMSO-d₆) δ 9.55 (s, 1H), 8.73 (s, 1H), 8.39 (d, *J* = 8.6 Hz, 1H), 8.29 (d, *J* = 8.2 Hz, 1H), 7.96 (t, *J* = 7.7 Hz, 1H), 7.75 (t, *J* = 7.5 Hz, 1H).

¹³C NMR (DMSO-d₆): δ 159.48, 151.85, 149.24, 146.68, 136.39, 134.53, 133.47, 131.24, 130.41, 128.22, 125.00, 123.84, 119.78, 114.55.



5-(3-Iodophenyl)furan-2-carboxylic acid (96)

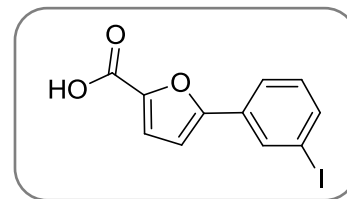
The title compound was prepared following the general procedure from **83** (270 mg, 0.8 mmol, 1 equiv) and an aqueous 1.5 M solution of NaOH (49 mg, 1.23 mmol in 0.8 mL of H₂O, 1.50 equiv). After standard workup, **96** was obtained as a brown solid (214 mg, yield 83%).

R_f = 0.42 (DCM/MeOH, 4:1)

m.p. = 190 – 194 °C

¹H NMR (CDCl₃): δ 8.15 (s, 1H), 7.74 (dd, *J* = 18.4, 7.5 Hz, 2H), 7.39 (d, *J* = 3.5 Hz, 1H), 7.17 (t, *J* = 7.9 Hz, 1H), 6.80 (d, *J* = 3.5 Hz, 1H).

¹³C NMR ((CD₃)₂CO): δ 159.32, 155.93, 145.51, 138.55, 133.91, 132.59, 131.83, 124.71, 120.70, 109.32, 95.08.

**7.1.2.3.3 General procedure for the chlorination of carboxylic acid intermediates **84-96** and the commercially available 5-(3-nitrophenyl)furan-2-carboxylic acid**

Thionyl chloride (2 mL/mmol carboxylic acid) was added dropwise to the appropriate carboxylic acid at 0 °C. The resulting mixture was stirred at reflux till complete consumption of the starting material. Thionyl chloride was distilled and the corresponding acyl chloride was used for the next step without any further purification.

5-Phenylfuran-2-carbonyl chloride (97)

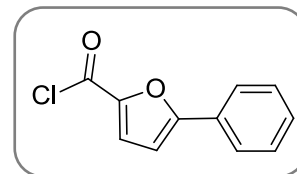
The title compound was prepared following the general procedure from **84** (420 mg, 2.23 mmol) and SOCl_2 (2 mL/mmol carboxylic acid, 4.46 mL). The reaction was completed after 6 h. After standard workup, **97** was obtained as a brown solid (453 mg, yield 100%).

$R_f = 0.56$ (cyclohexane/EtOAc, 4:1)

m.p. = 59.7 - 62.3 °C

$^1\text{H NMR}$ (CDCl_3): δ 7.84 - 7.79 (m, 2H), 7.57 (dd, $J = 3.8, 0.6$ Hz, 1H), 7.50 - 7.41 (m, 3H), 6.85 (dd, $J = 3.8, 0.6$ Hz, 1H).

$^{13}\text{C NMR}$ ($(\text{CD}_3)_2\text{CO}$): δ 165.63, 162.38, 155.11, 132.36, 132.24, 128.47, 122.23, 122.19, 118.01, 117.72, 113.04, 112.72, 110.99.

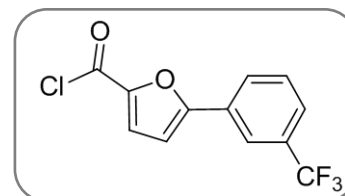
*5-(3-(Trifluoromethyl)phenyl)furan-2-carbonyl chloride (98)*

The title compound was prepared following the general procedure from **85** (786 mg, 2.47 mmol) and SOCl_2 (2 mL/mmol carboxylic acid, 4.94 mL). The reaction was completed after 3 h. After standard workup, **98** was obtained as a yellow solid (590 mg, yield 70%).

$R_f = 0.60$ (DCM/MeOH, 98:2) m.p. = 76.5 - 78.9 °C

$^1\text{H NMR}$ ($(\text{CD}_3)_2\text{CO}$): δ 8.24 - 8.18 (m, 2H), 7.87 - 7.83 (m, 2H), 7.83 - 7.75 (m, 1H), 7.48 (dd, $J = 3.1, 2.3$ Hz, 1H).

$^{13}\text{C NMR}$ ($(\text{CD}_3)_2\text{CO}$): δ 160.06, 155.11, 145.85, 132.59, 132.16, 131.72, 131.29 (q, $J = 32.5$ Hz), 131.15, 130.39, 130.28, 126.67, 123.07, 119.46 (q, $J = 271.77$ Hz), 129.65, 128.31, 127.42, 127.36, 127.31, 127.26 (q, $J = 3.9$ Hz), 122.74, 122.69, 122.64, 122.59 (q, $J = 4$ Hz), 111.20.



5-(3-Fluorophenyl)furan-2-carbonyl chloride (99)

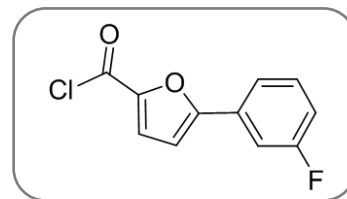
The title compound was prepared following the general procedure from **86** (400 mg, 1.9 mmol) and SOCl₂ (2 mL/mmol carboxylic acid, 3.8 mL). The reaction was completed after 4 h. After standard workup, **99** was obtained as a yellow solid (427 mg, yield 97%).

R_f = 0.55 (cyclohexane/EtOAc, 4:1)

m.p. = 85.6 – 87.4 °C

¹H NMR ((CD₃)₂CO): δ 7.82 (d, *J* = 4.0 Hz, 1H), 7.80 – 7.75 (m, 1H), 7.68 (ddd, *J* = 9.9, 2.5, 1.5 Hz, 1H), 7.60 (td, *J* = 8.1, 5.9 Hz, 1H), 7.35 (d, *J* = 3.9 Hz, 1H), 7.28 (ddd, *J* = 8.6, 2.5, 1.3 Hz, 1H).

¹³C NMR ((CD₃)₂CO): δ 164.7, 161.45, 159.6, 131.42, 131.31, 127.54, 121.3, 121.27, 117.09, 116.8, 111.79.

*5-(3-Chlorophenyl)furan-2-carbonyl chloride (100)*

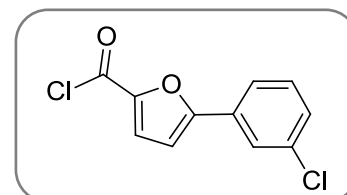
The title compound was prepared following the general procedure from **87** (515 mg, 2.31 mmol) and SOCl₂ (2 mL/mmol carboxylic acid, 4.62 mL). The reaction was completed after 4 h. After standard workup, **100** was isolated as a white solid (530 mg, yield 95%).

R_f = 0.56 (cyclohexane/EtOAc, 4:1)

m.p. = 100.7 – 102.5 °C

¹H NMR (DMSO): δ 7.88 – 7.85 (m, 1H), 7.80 – 7.74 (m, 1H), 7.55 – 7.42 (m, 3H), 7.34 (dd, *J* = 3.7, 1.8 Hz, 1H), 7.28 (dd, *J* = 3.6, 1.7 Hz, 1H).

¹³C NMR ((CD₃)₂CO): δ 178.18, 160.29, 145.73, 135.65, 131.90, 131.90, 131.37, 131.37, 130.90, 130.90, 128.42, 128.42, 125.90, 125.90, 124.62, 124.62, 111.04, 111.04.



5-(3-Bromophenyl)furan-2-carbonyl chloride (101)

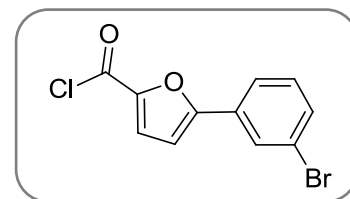
The title compound was prepared following the general procedure from **88** (850 mg, 3.18 mmol) and SOCl_2 (2 mL/mmol carboxylic acid, 6.36 mL). The reaction was completed after 2 h. After standard workup, **101** was obtained as a brown solid (870 mg, yield 96%).

R_f = 0.56 (cyclohexane/EtOAc, 4:1)

m.p. = 79.7 – 81.4 °C

^1H NMR ($(\text{CD}_3)_2\text{CO}$): δ 8.08 (s, 1H), 7.92 (d, J = 7.8 Hz, 1H), 7.81 (d, J = 3.9 Hz, 1H), 7.67 (d, J = 7.9 Hz, 1H), 7.50 (t, J = 8.0 Hz, 1H), 7.37 (d, J = 3.9 Hz, 1H).

^{13}C NMR ($(\text{CD}_3)_2\text{CO}$): δ 160.07, 155.02, 145.65, 133.77, 131.97, 131.46, 128.71, 128.32, 124.92, 123.60, 110.94.

*5-(3-Aminophenyl)furan-2-carbonyl chloride (102)*

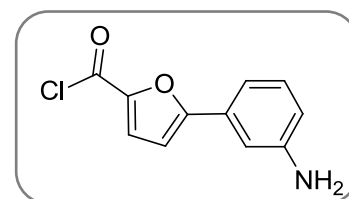
The title compound was prepared following the general procedure from **89** (270 mg, 1.33 mmol) and SOCl_2 (2 mL/mmol carboxylic acid, 2.66 mL). The reaction was completed after 4 h. After standard workup, **102** was obtained as a brown solid (290 mg, yield 98%).

R_f = 0.52 (cyclohexane/EtOAc, 4:1)

m.p. = 113.9 – 115.2 °C

^1H NMR ($(\text{CD}_3)_2\text{CO}$): δ 8.25 (s, 1H), 8.04 – 7.89 (m, 2H), 7.84 (t, J = 4.0 Hz, 1H), 7.68 (s, 1H), 7.39 – 7.30 (m, 1H).

^{13}C NMR ($(\text{CD}_3)_2\text{CO}$): δ 167.32, 160.47, 155.09, 143.72, 131.33, 130.66, 128.65, 128.46, 127.48, 123.49, 110.97.



5-(3-Hydroxyphenyl)furan-2-carbonyl chloride (103)

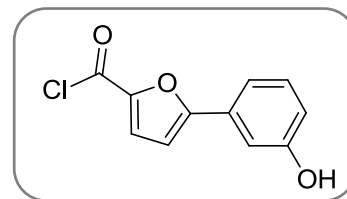
The title compound was prepared following the general procedure from **90** (330 mg, 1.62 mmol) and SOCl₂ (2 mL/mmol carboxylic acid, 3.24 mL). The reaction was completed after 6 h. After standard workup, **103** was obtained as a black solid (320 mg, yield 89%).

R_f = 0.41 (DCM/MeOH, 4:1)

m.p. = 168.8 – 169.7 °C

¹H NMR ((CD₃)₂CO): δ 7.77 (d, *J* = 3.9 Hz, 1H), 7.39 – 7.31 (m, 3H), 7.18 (d, *J* = 3.9 Hz, 1H), 6.98 (ddd, *J* = 7.4, 2.6, 1.7 Hz, 1H).

¹³C NMR ((CD₃)₂CO): δ 162.23, 158.83, 154.92, 145.07, 131.31, 130.64, 128.64, 118.32, 117.64, 112.64, 109.94.

*5-(m-Tolyl)furan-2-carbonyl chloride (104)*

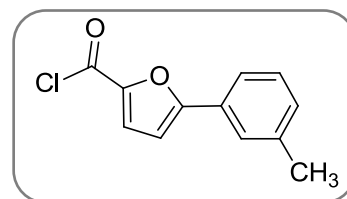
The title compound was prepared following the general procedure from **91** (500 mg, 2.47 mmol) and SOCl₂ (2 mL/mmol carboxylic acid, 4.94 mL). The reaction was completed after 2 h. After standard workup, **104** was obtained as yellow solid (540 mg, yield 99%).

R_f = 0.50 (cyclohexane/EtOAc, 7:3)

m.p. = 54.3 – 56.8 °C

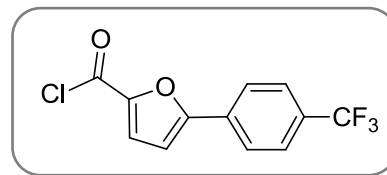
¹H NMR ((CD₃)₂CO): δ 7.79 (d, *J* = 3.9 Hz, 1H), 7.73 (dd, *J* = 10.1, 4.2 Hz, 2H), 7.42 (t, *J* = 7.6 Hz, 1H), 7.32 (d, *J* = 7.6 Hz, 1H), 7.23 (d, *J* = 3.9 Hz, 1H), 2.42 (s, 3H).

¹³C NMR ((CD₃)₂CO): δ 162.40, 162.40, 154.85, 145.05, 139.81, 131.90, 129.94, 129.33, 128.70, 126.60, 123.39, 109.74, 21.33.



5-(4-Trifluorophenyl)furan-2-carbonyl chloride (105)

The title compound was prepared following the general procedure from **92** (190 mg, 0.74 mmol) and SOCl₂ (2 mL/mmol carboxylic acid, 1.5 mL). The reaction was completed after 2 h. After standard workup, **105** was obtained as yellow oil (204 mg, yield 100%).



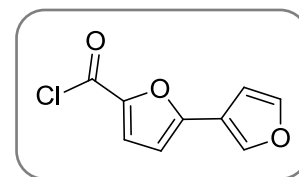
R_f = 0.38 (cyclohexane/EtOAc, 9:1)

¹H NMR ((CD₃)₂CO): δ 8.14 (d, J = 7.3), 7.88 (d, J = 7.3), 7.84 (d, J = 3.4), 7.44 (d, J = 3.4).

¹³C NMR ((CD₃)₂CO): 160.10, 155.24, 146.12, 128.33, 127.14, 127.09, 127.04, 126.99 (q, J = 3.4 Hz), 126.79, 120.70, 111.79.

[2,3'-Bifuran]-5-carbonyl chloride (106)

The title compound was prepared following the general procedure from **93** (190 mg, 1.07 mmol) and SOCl₂ (2 mL/mmol carboxylic acid, 2.15 mL). The reaction was completed after 2 h. After standard workup, **106** was obtained as a brown semi-solid (202 mg, yield 96%).



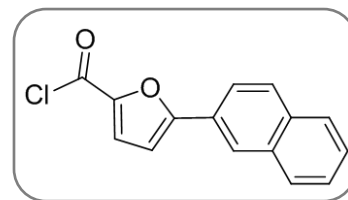
R_f = 0.55 (cyclohexane/EtOAc, 8:2)

¹H NMR ((CD₃)₂CO): δ 8.25 (m, 1H), 7.81 – 7.66 (m, 2H), 6.99 (d, J = 3.8 Hz, 1H), 6.96 – 6.92 (m, 1H).

¹³C NMR ((CD₃)₂CO): δ 147.55, 146.64, 143.60, 132.90, 129.66, 128.16, 115.80, 110.77, 109.44.

5-(Naphthalen-2-yl)furan-2-carbonyl chloride (107)

The title compound was prepared following the general procedure from **94** (300 mg, 1.26 mmol) and SOCl_2 (2 mL/mmol carboxylic acid, 2.50 mL). The reaction was completed after 4 h. After standard workup, **107** was obtained as a brown oil (220 mg, yield 100%).



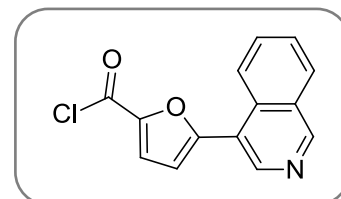
$R_f = 0.57$ (cyclohexane/EtOAc, 9:2)

$^1\text{H NMR}$ ($(\text{CD}_3)_2\text{CO}$): δ 8.48 – 8.38 (m, 1H), 8.07 – 7.94 (m, 2H), 7.88 (d, $J = 7.3$ Hz, 1H), 7.82 – 7.77 (m, 1H), 7.66 – 7.52 (m, 3H), 7.14 (d, $J = 3.8$ Hz, 1H).

$^{13}\text{C NMR}$ ($(\text{CD}_3)_2\text{CO}$): δ 161.33, 154.27, 144.77, 134.02, 131.06, 129.85, 128.88, 127.87, 127.63, 127.09, 126.48, 125.85, 125.26, 124.69, 112.80.

5-(Isoquinolin-4-yl)furan-2-carbonyl chloride (108)

The title compound was prepared following the general procedure but dissolving compound **95** (180 mg, 0.75 mmol) and SOCl_2 (2 mL/mmol carboxylic acid, 1.5 mL). The reaction was completed after 4 h. After standard workup, **108** was obtained as a brown oil (150 mg, yield 77%).



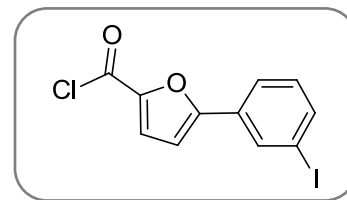
$R_f = 0.42$ (cyclohexane/EtOAc, 9:2)

$^1\text{H NMR}$ ($(\text{CD}_3)_2\text{SO}$): 9.77 (s, 1H), 8.99 (s, 1H), 8.66 (d, $J = 8.2$ Hz, 1H), 8.53 (d, $J = 8.1$ Hz, 1H), 8.22 (t, $J = 7.8$ Hz, 1H), 8.01 (t, $J = 7.6$ Hz, 1H), 7.51 (d, $J = 3.6$ Hz, 1H), 7.48 (d, $J = 3.6$ Hz, 1H).

$^{13}\text{C NMR}$ ($(\text{CD}_3)_2\text{SO}$): δ 159.1, 152.3, 150.8, 144.5, 143.4, 129, 129.2, 129.0, 127.8, 127.2, 125.1, 122.1, 117.2, 109.4.

5-(3-Iodophenyl)furan-2-carbonyl chloride (109)

The title compound was prepared following the general procedure from **96** (200 mg, 0.64 mmol) and SOCl₂ (2 mL/mmol carboxylic acid). The reaction was completed after 2 h. After standard workup, **109** was obtained as a dark brown solid (211 mg, yield 100%).



R_f = 0.61 (cyclohexane/EtOAc, 4:1)

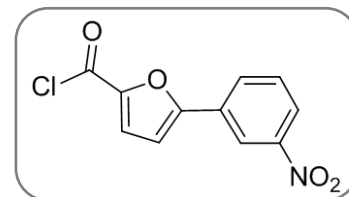
m.p. = 88.6 - 89.0 °C

¹H NMR (CDCl₃): δ 8.14 (s, *J* = 1.7 Hz, 1H), 7.79 - 7.73 (m, 2H), 7.56 (d, *J* = 3.8 Hz, 1H), 7.20 (t, *J* = 7.9 Hz, 1H), 6.85 (d, *J* = 3.8 Hz, 1H).

¹³C NMR ((CD₃)₂CO): δ 160.01, 155.01, 145.62, 139.85, 134.63, 131.94, 131.42, 128.39, 125.43, 110.84, 95.14.

5-(3-Nitrophenyl)furan-2-carbonyl chloride (110)

The title compound was prepared following the general procedure from commercially available 5-(3-nitrophenyl)furan-2-carboxylic acid (200 mg, 0.86 mmol) and SOCl₂ (2 mL/mmol carboxylic acid, 1.72 mL). The reaction was completed after 2.5 h. After standard workup, **110** was obtained as a brown solid (200 mg, yield 93%).



R_f = 0.4 (cyclohexane/EtOAc, 7:3)

m.p. = 111 - 113 °C

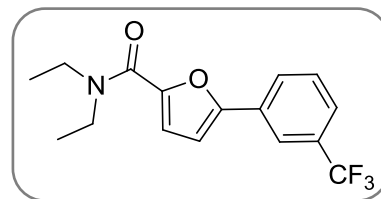
¹H NMR ((CD₃)₂CO): δ 8.69 (t, *J* = 1.8 Hz, 1H), 8.39 - 8.30 (m, 2H), 7.94 - 7.79 (m, 2H), 7.55 (d, *J* = 3.9 Hz, 1H).

¹³C NMR ((CD₃)₂CO): δ 158.40, 154.33, 145.21, 131.00, 130.82, 130.10, 127.43, 124.36, 123.10, 119.74, 110.97.

7.1.2.4 Synthesis of NS6740 fragments 11-15

N,N-Diethyl-5-(3-(trifluoromethyl)phenyl)furan-2-carboxamide (**11**)

Et₃N (0.19 mL, 1.88 mmol, 1 equiv) was added to a solution of 5-(3-(trifluoromethyl)phenyl)furan-2-carbonyl chloride **98** (515 mg 1.88 mmol, 1 equiv) in DCM, followed by dropwise addition of Et₂NH.



The reaction was stirred for 1.5 h at r.t. Upon completion, deionized water was added and the reaction mixture was extracted with EtOAc. The pooled organic layers were dried over anhydrous Na₂SO₄ and evaporated under reduced pressure. The crude was purified by silica gel column chromatography eluted by cyclohexane/EtOAc (7:3), giving the final compound **11** as a yellow solid (290 mg, yield 50%).

R_f = 0.45 (cyclohexane/EtOAc, 3:2)

m.p. = 45.2 – 47.9 °C

HRMS (ESI+) *m/z* calcd for C₁₆H₁₆NO₂F₃Na 334.10253 [M + Na]⁺, found 334.10209.

¹H NMR ((CD₃)₂CO): δ 8.11 – 8.05 (m, 1H), 7.76 – 7.66 (m, 1H), 7.20 (d, *J* = 3.6 Hz, 1H), 7.10 (d, *J* = 3.6 Hz, 1H), 3.63 (m, 4H), 1.29 (m, 6H).

¹³C NMR ((CD₃)₂CO): δ 160.13, 154.44, 150.75, 132.70, 132.36, 131.93, 131.59 (q, *J* = 32.24 Hz), 131.77, 131.33, 127.74, 124.13, 120.52 (q, *J* = 271.78 Hz), 129.31, 126.35, 126.30, 126.25, 126.20 (q, *J* = 3.46 Hz), 122.29, 122.25, 122.19, 122.15 (q, *J* = 3.34 Hz), 119.12, 109.99, 43.34, 14.90.

7.1.2.4.1 General procedure for the acylation reaction of 1,4-diazabicyclo[3.2.2]nonane dihydrochloride (**16**) and the appropriate acyl chloride

Under anhydrous and inert conditions, a suspension of 1,4-diazabicyclo[3.2.2]nonane dihydrochloride **16** (1 equiv) in dry DMF was warmed to 60 °C. After 40 minutes, the mixture was cooled to r.t. and Cs₂CO₃ (5 equiv) was added to achieve pH = 8-9. The mixture was cooled at 0 °C and the appropriate acyl chloride was added portionwise. The reaction was stirred at r.t. overnight. Upon completion, the mixture was diluted with deionized water and extracted repetitively with CHCl₃/*i*-PrOH. The combined organic layers were further washed with brine for three times, then dried over anhydrous Na₂SO₄, filtered and concentrated *in vacuo* to

afford the corresponding crude. To 1 equiv dissolved in MeOH (5 mL) fumaric acid (1 equiv) was added to obtain the corresponding fumaric salt. After stirring overnight at r.t., the solvent was removed at reduced pressure and the crude salt was recrystallized from a proper solvent.

1,4-Diazabicyclo[3.2.2]nonan-4-yl(5-phenylfuran-2-yl)methanone fumarate (12)

The title compound was prepared following the general procedure from 1,4-diazabicyclo[3.2.2]nonane dihydrochloride **16** (180 mg, 0.90 mmol, 1 equiv), **97** (224 mg, 1.08 mmol, 1.2 equiv) and Cs₂CO₃ (1.47 g, 4.52 mmol, 5 equiv). After standard workup and subsequent reaction with fumaric acid (66 mg, 0.57 mmol, 1 equiv), the final compound **12** was obtained through recrystallization from MeOH as a white solid (180mg, yield 53%).

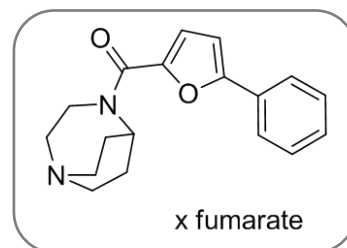
R_f = 0.33 (DCM/MeOH, 9:1)

m.p. = 174.4 - 176.3 °C

HRMS (ESI+) *m/z* calcd for C₁₈H₂₁N₂O₂ 297.15975 [M + H]⁺, found 297.15975; calcd for C₁₈H₂₀N₂O₂Na 319.14170 [M + Na]⁺, found 319.14182.

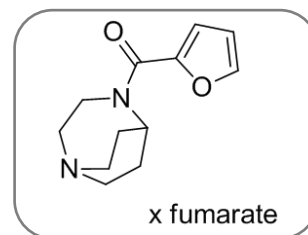
¹H NMR (CD₃OD): δ 7.82 - 7.75 (m, 2H), 7.48 - 7.33 (m, 3H), 7.21 (d, *J* = 3.6 Hz, 1H), 6.96 (d, *J* = 3.7 Hz, 1H), 6.71 (s, 2H), 5.01 - 4.81 (m, 1H), 4.35 - 4.21 (m, 2H), 3.58 - 3.43 (m, 6H), 2.50-2.14 (m, 4H).

¹³C NMR (CD₃OD): δ 170.45, 160.90, 157.61, 147.35, 135.89, 130.90, 130.08, 129.96, 125.56, 107.90, 47.14, 24.54.



1,4-Diazabicyclo[3.2.2]nonan-4-yl(furan-2-yl)methanone fumarate (13)

The title compound was prepared following the general procedure from 1,4-diazabicyclo[3.2.2]nonane dihydrochloride **16** (180 mg, 0.90 mmol, 1 equiv), commercially available furan-2-carbonyl chloride (148 mg, 1.1 mmol, 0.11 mL, 1.2 equiv) and Cs₂CO₃ (1.47 g, 4.50 mmol, 5 equiv). After standard workup and reaction with fumaric acid (65 mg, 0.56 mmol, 1 equiv), the final compound **13** was obtained through recrystallization from MeOH and Et₂O as a white solid (100 mg, yield 53%).
R_f = 0.60 (DCM/MeOH, 4:1 and 50 μL of aqueous NH₃)



m.p. = 180 – 182 °C

HRMS (ESI+) *m/z* calcd for C₁₂H₁₇N₂O₂ 221.12845 [M + H]⁺, found 221.12829; calcd for C₁₂H₁₆N₂O₂Na 243.11040 [M + Na]⁺, found 243.11053.

¹H NMR (CD₃OD): δ 7.72 (dd, *J* = 1.7, 0.7 Hz, 1H), 7.11 (d, *J* = 3.4 Hz, 1H), 6.69 (s, 2H), 6.61 (dd, *J* = 3.5, 1.8 Hz, 1H), 4.87 – 4.77 (m, 1H), 4.30 – 3.17 (m, 2H), 3.52 (dt, *J* = 15.9, 6.8 Hz, 6H), 2.42 – 2.12 (m, 4H).

¹³C NMR (CD₃OD): δ 171.27, 161.01, 148.34, 146.35, 136.10, 118.38, 112.63, 56.22, 46.96, 24.16.

1-(1,4-Diazabicyclo[3.2.2]nonan-4-yl)ethanone fumarate (14)

The title compound was prepared following the general procedure from 1,4-diazabicyclo[3.2.2]nonane dihydrochloride **16** (150 mg, 0.75 mmol, 1 equiv), commercially available acetyl chloride (200 mg, 1.50 mmol, 0.06 mL, 1.2 equiv) and Cs₂CO₃ (1.20 g, 3.80 mmol, 5 equiv). After standard workup and reaction with fumaric acid (54 mg, 0.46 mmol, 1 equiv), the final compound **14** was obtained through recrystallization from EtOH and Et₂O as a light brown solid (150 mg, yield 64%).

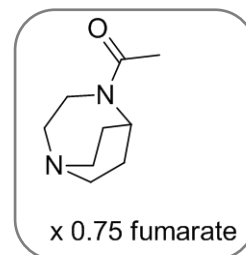
R_f = 0.35 (DCM/MeOH, 4:1 and 100 μL of aqueous NH₃)

m.p. = 168.9 – 169.9 °C

HRMS (ESI+) *m/z* calcd for C₉H₁₇N₂O 169.13354 [M + H]⁺, found 191.11548; calcd for C₉H₁₆N₂ONa 191.11548 [M + Na]⁺, found 191.11546.

¹H NMR (CD₃OD): δ 6.68 (s, 1.5H), 4.78 – 4.33 (m, 1H), 4.07 – 3.83 (m, 2H), 3.52 – 3.35 (m, 6H), 2.29 – 1.97 (m, 7H).

¹³C NMR (CD₃OD): δ 171.96, 171.86, 171.62, 136.21, 56.83, 55.90, 47.08, 46.82, 46.26, 41.73, 36.77, 24.74, 23.65, 22.03, 21.16.

*4-Ethyl-1,4-diazabicyclo[3.2.2]nonane fumarate (15)*

Under inert and anhydrous conditions, to **14** (300 mg, 1.78 mmol, 1 equiv) suspended in dry Et₂O a suspension of LiAlH₄ (152 mg, 4 mmol, 2.25 equiv) in dry Et₂O was added dropwise at 0 °C. After 3 h, the reaction was quenched with a saturated aqueous solution of Na₂SO₄ × 10 H₂O. The mixture was filtered and the organic solvent was evaporated under vacuum. The crude (1 eq) was reacted with fumaric acid (206 mg, 1.78 mmol, 1 equiv) and the final compound **15** was obtained through recrystallization from MeOH and Et₂O as a white solid (165 mg, yield 25%).

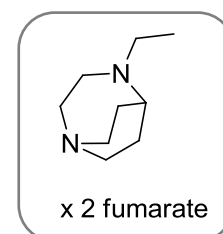
R_f = 0.33 (DCM/MeOH, 4:1 and 100 μL of aqueous NH₃)

m.p. = 134 – 135 °C

HRMS (ESI+) *m/z* calcd for C₉H₁₉N₂ 155.15428 [M + H]⁺, found 155.15426.

¹H NMR (CD₃OD): δ 6.71 (s, 4H), 3.73 – 3.66 (m, 1H), 3.51 – 3.43 (m, 2H), 3.37 – 3.23 (m, 8H), 3.10 (q, *J* = 7.2 Hz, 2H), 2.43 – 2.02 (m, 4H), 1.29 (t, *J* = 7.2 Hz, 3H).

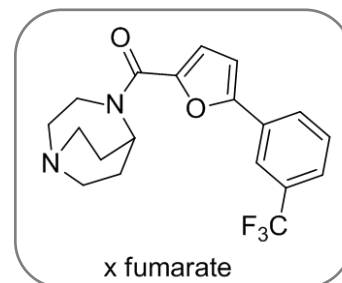
¹³C NMR (CD₃OD): δ 170.22, 135.82, 55.75, 52.29, 47.44, 46.42, 21.93, 11.25.



7.1.2.5 Synthesis of NS6740 positively charged derivatives

1,4-Diazabicyclo[3.2.2]nonan-4-yl(5-(3-trifluorophenyl)furan-2-yl)methanone fumarate (1)

The title compound was prepared following the general procedure reported in paragraph 7.1.2.4.1, from 1,4-diazabicyclo[3.2.2]nonane dihydrochloride **16** (425 mg, 2.13 mmol, 1 equiv), **98** (703 mg, 2.56 mmol, 1.2 equiv) and Cs₂CO₃ (3.48 g, 10.7 mmol, 5 equiv). Upon completion, standard work up was



applied giving the free amine as a yellow oil (404 mg, yield 52%). The corresponding free base was reacted with fumaric acid (76 mg, 0.66 mmol, 1 equiv) in MeOH. A precipitated was obtained and it was further recrystallized from EtOH, affording **1** as a white solid (100 mg, 30% yield).

R_f = 0.35 (DCM/MeOH, 9:1)

m.p.= 183 - 185 °C

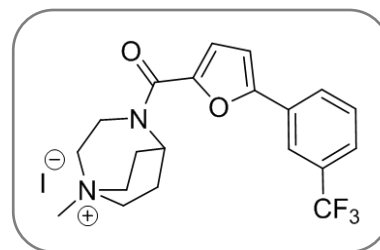
HRMS (ESI+) *m/z* calcd for C₁₉H₂₀N₂O₂F₃ 365.14714 [M + H]⁺, found 365.14658; calcd for C₁₉H₁₉N₂O₂F₃Na 387.12908 [M + Na]⁺, found 387.12908.

¹H NMR (CD₃OD): δ 8.17 – 7.99 (m, 2H), 7.77 – 7.59 (m, 2H), 7.25 (d, *J* = 3.6 Hz, 1H), 7.16 (d, *J* = 3.7 Hz, 1H), 6.73 (s, 2H) 4.34 (s, 1H), 3.77 - 3.37 (m, 6H), 2.54 – 2.13 (m, 2H).

¹³CNMR (CD₃OD): δ 172.01, 161.64, 156.51, 148.81, 136.95, 133.99, 133.57, 133.14, 132.72 (q, *J* = 32.42 Hz), 132.71, 131.94, 131.68, 128.07, 124.47, 120.87 (q, *J* = 271.78 Hz), 129.86, 127.14, 127.09, 127.03, 126.98 (q, *J* = 3.46 Hz), 122.97, 122.92, 122.87, 122.82 (q, *J* = 3.46 Hz), 121.27, 110.25, 59.18, 56.90, 47.87, 25.23, 19.19.

1-Methyl-4-(5-(3-(trifluoromethyl)phenyl)furan-2-carbonyl)-1,4-diazabicyclo[3.2.2]nonan-1-ium iodide (**17**)

To a solution of the corresponding free base **1** (150 mg, 0.41 mmol, 1 eq) in MeOH MeI (470 mg, 205 μ L, 3.3 mmol, 8 eq) was added dropwise by. The reaction was stirred overnight. After evaporation of the organic solvent and unreacted excess of MeI, the crude was recrystallized from *i*-PrOH and few drops of MeOH and the final compound **17** obtained as a white solid (85 mg, yield 40%).



$R_f = 0.2$ (EtOH/H₂O/NH₃, (4:2:2)) m.p. = 191 - 194 °C

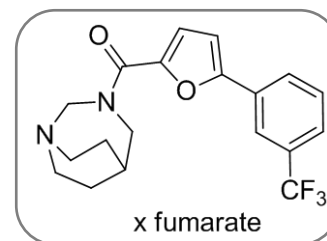
HRMS (ESI+) m/z calcd for C₂₀H₂₂N₂O₂F₃ 379.16279 [M + H]⁺, found 379.16262.

¹H NMR (CD₃OD) δ 8.13 - 7.96 (m, 1H), 7.76 - 7.56 (m, 1H), 7.24 (d, $J = 3.5$ Hz, 1H), 7.12 (d, $J = 3.6$ Hz, 1H), 5.00 - 4.87 (m, 1H), 4.55 - 4.09 (m, 2H), 4.03 - 3.52 (m, 6H), 2.65 - 2.23 (m, 4H).

¹³C NMR (CD₃OD): δ 160.36, 155.78, 147.64, 133.08, 132.65, 132.22, 131.79 ($J = 32$ Hz), 131.76, 131.12, 130.80, 127.20, 123.60, 119.99 ($J = 271.50$ Hz), 129.10, 126.28, 126.24, 126.19, 126.14 ($J = 3.4$ Hz), 122.13, 122.08, 122.02, 121.97 ($J = 3.4$ Hz), 120.73, 109.47, 65.97, 58.54, 57.95, 47.44, 25.56.

1,3-Diazabicyclo[3.2.2]nonan-3-yl(5-(3-(trifluoromethyl)phenyl)furan-2-yl)methanone (**18**)

Under anhydrous and inert conditions, a suspension of 1,3-diazabicyclo[3.2.2]nonane dihydrochloride **44** (120 mg, 0.95 mmol, 1 equiv) in dry DMF was warmed to 60 °C. After 40 min, the mixture was cooled to r.t. and Cs₂CO₃ (1.55 g, 4.75 mmol, 5 equiv) was added to achieve pH = 8-9. The mixture was cooled at 0 °C and 5-(3-(trifluoromethyl)phenyl)furan-2-carbonyl chloride **98** (313 mg, 1.14 mmol, 1.2 equiv) was added portionwise. The reaction was stirred at r.t. overnight. Upon completion, the mixture was diluted with deionized water and extracted repetitively with CHCl₃/*i*-PrOH. The combined organic layers were further washed with brine for three times, then dried over anhydrous Na₂SO₄, filtered and concentrated *in vacuo* to afford the corresponding crude. To the crude (1 equiv) dissolved in MeOH was added fumaric acid (50 mg, 0.43 mmol, 1 equiv). After stirring overnight at r.t., the solvent was removed at reduced pressure and the crude salt was recrystallized from EtOH and Et₂O, giving the final compound **18** as a light brown solid (105 mg, 50%).



R_f = 0.35 (DCM/MeOH, 95:5)

m.p. = 122.2 – 124 °C.

HRMS (ESI+) *m/z* calcd for C₁₉H₂₀N₂O₂F₃ 365.14714 [M + H]⁺, found 365.14739; calcd for C₁₉H₁₉N₂O₂F₃Na 387.12908 [M + Na]⁺, found 387.12929.

¹H NMR (CD₃OD): δ 8.27 – 8.06 (m, 2H), 7.78 – 7.57 (m 2H), 7.28 (d, *J* = 3.6 Hz, 1H), 7.13 (d, *J* = 3.6 Hz, 1H), 6.69 (s, 2H), 6.00 (d, *J* = 9.7 Hz, 1H), 5.78 (d, *J* = 10.0 Hz, 1H), 3.90 – 3.73 (m, 4H), 3.44 – 3.34 (m, 5H), 2.62 – 2.22 (m, 2H).

¹³CNMR (CD₃OD): 171.78, 162.29, 156.73, 149.16, 136.90, 134.01, 133.58, 133.15, 132.72 (q, *J* = 32.24 Hz), 132.74, 131.79, 131.74, 128.14, 124.54, 120.54 (q, *J* = 270.63 Hz), 130.02, 127.44, 127.10, 127.06, 127.00, 126.96, (q, *J* = 4.6 Hz), 1123.10, 123.05, 122.99, 122.94 (q, *J* = 3.45 Hz), 122.42, 118.83, 110.64, 57.91, 52.84, 51.31, 36.45, 24.71.

7.1.2.5.1 General procedure for the synthesis of intermediates 111 and 112

The reaction was conducted under anhydrous conditions. The appropriate benzyl diazabicyclo (**49** and **57**) was dissolved in dry 1,4-dioxane. The mixture was cooled at 0 °C and dry TEA was added giving a white precipitate; the reaction was stirred for 10 min. Finally, the acyl chloride **98** was added dropwise and the mixture was stirred at r.t. Upon completion, the reaction was filtered and the solvent was evaporated under vacuum. The resulting crude was treated repetitively with a mixture of cyclohexane/EtOAc (1:1); the combined organic layers were evaporated under reduced pressure, giving the desired semi-final products.

((1S,4S)-5-Benzyl-2,5-diazabicyclo[2.2.1]heptan-2-yl)(5-(3-(trifluoromethyl)phenyl)furan-2-yl)methanone (111)

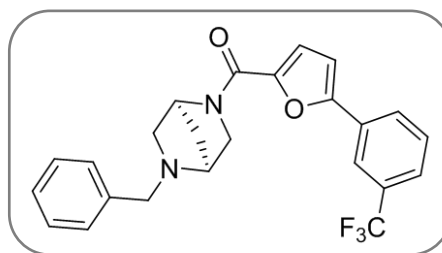
Benzyl derivative **111** was achieved employing the general procedure reported in 7.1.2.5.1 paragraph using **49** (206 mg, 0.59 mmol, 1 equiv), **98** (162 mg, 0.59 mmol, 1 equiv) and TEA (0.09 mL, 0.65 mmol, 1.10 equiv). Standard workup was applied and the desired product **111** was obtained as a pale yellow oil (450 mg, yield 96%).

$R_f = 0.39$ (cyclohexane/EtOAc, 3:2)

$[\alpha]_D = +11.0$ (c = 1.05, chloroform)

$^1\text{H NMR}$ (CDCl_3): δ 7.76 (t, $J = 18.0$ Hz, 2H), 7.49 – 7.06 (m, 8H), 6.80 – 6.67 (s, 1H), 4.95 (d, $J = 47.9$ Hz, 1H), 4.11 – 3.40 (m, 6H), 3.18 – 2.73 (m, 2H), 2.09 – 1.61 (m, 2H).

$^{13}\text{C NMR}$ (CDCl_3): δ 159.83, 155.56, 150.10, 140.58, 140.50, 133.81, 133.37, 132.93, 132.35 (q, $J = 32$ Hz), 132.30, 131.22, 131.16, 130.89, 127.29, 123.71, 120.09 (q, $J = 270$ Hz), 130.21, 130.12, 129.06, 128.87, 126.67, 126.62, 126.57, 126.52, (q, $J = 3.4$ Hz), 122.76, 122.71, 122.66, 122.61 (q, $J = 3.4$ Hz), 120.05, 119.77, 109.63, 62.67, 61.27, 60.52, 59.20, 54.70, 35.45.



(1*R*,4*R*)-5-Benzyl-2,5-diazabicyclo[2.2.1]heptan-2-yl(5-(3-(trifluoromethyl)phenyl)furan-2-yl)methanone (**112**)

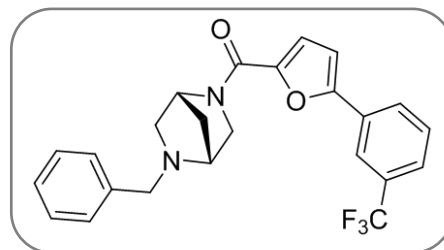
Benzyl derivative **112** was achieved employing the general procedure reported in 7.1.2.5.1 paragraph using **57** (120 mg, 0.64 mmol, 1 equiv), **98** (175 mg, 0.64 mmol, 1 equiv) and TEA (0.07 mL, 0.70 mmol, 1.10 equiv). Standard workup was applied and the desired product **112** was obtained as a yellow oil (220 mg, yield 81%).

$R_f = 0,39$ (cyclohexane/EtOAc 3:2)

$[\alpha]_D = -11.0$ ($c = 1.05$, chloroform)

$^1\text{H NMR}$ (CD_3OD): δ 8.04 (dd, $J = 19.0, 9.4$ Hz, 2H), 7.65 (d, $J = 4.0$ Hz, 2H), 7.46 – 7.17 (m, 6H), 7.12 (d, $J = 3.6$ Hz, 1H), 5.03 (d, $J = 81.7$ Hz, 1H), 4.18 – 3.48 (m, 5H), 3.18 – 2.83 (m, 2H), 1.99 (dt, $J = 22.8, 13.8$ Hz, 2H).

$^{13}\text{C NMR}$ (CD_3OD): δ 159.87, 156.63, 149.40, 140.52, 140.41, 133.93, 133.50, 133.07, 132.64 (q, $J = 32$ Hz), 132.70, 131.83, 131.59, 127.99, 124.39, 120.79 (q, $J = 270$ Hz), 130.76, 130.28, 129.80, 129.61, 129.18, 126.97, 126.93, 126.89, 126.85 (q, $J = 3.4$ Hz), 122.92, 122.87, 122.82, 122.77 (q, $J = 3.4$ Hz), 120.62, 120.26, 110.29, 63.31, 61.18, 60.64, 59.89, 55.37, 35.25.

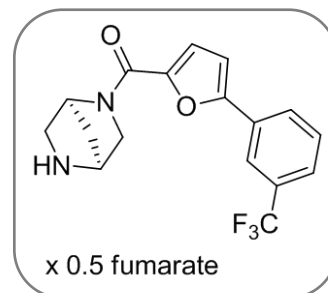


7.1.2.5.2 General procedure for the synthesis of compounds **19** and **20**

Palladium on activated carbon (10%) was added to a solution of the appropriate benzylated compound in MeOH. The reaction was stirred overnight at r. t. under hydrogen. Upon completion, the catalyst was filtered off and washed with MeOH. The filtrate was concentrated to give a crude, which was dissolved in the minimum amount of MeOH and reacted with fumaric acid; the pure final compound was obtained *via* recrystallization from an appropriate solvent.

(1S,4S)-2,5-Diazabicyclo[2.2.1]heptan-2-yl(5-(3-(trifluoromethyl)phenyl)furan-2-yl)methanone fumarate (19)

Benzylated compound **111** (300 mg, 0.7 mmol, 1 equiv) was deprotected following the procedure reported in 7.1.2.5.2 paragraph, using Pd/C (30 mg). The mixture was stirred overnight, and, upon hydrogenolysis completion, standard workup was applied. The resulting crude was reacted with fumaric acid (69 mg, 0.59 mmol, 1 equiv) in MeOH. The crude salt was recrystallized from EtOH/iPrOH/Et₂O and the final product **19** was achieved as a white solid (15 mg, yield 9%).



$R_f = 0.31$ (DCM/MeOH, 4:1)

m.p. = 119.7 - 121.4 °C

$[\alpha]_D = +24.0$ (c = 1.1, methanol)

HRMS (ESI+) m/z calcd for C₁₇H₁₆N₂O₂F₃ 337.11584 [M + H]⁺, found 337.11571; calcd for C₁₇H₁₅N₂O₂F₃Na 359.09778 [M + Na]⁺, found 359.09742.

¹H NMR (CD₃OD): δ 8.05 (s, 1H), 7.66 (d, $J = 4.3$ Hz, 1H), 7.30 (d, $J = 3.5$ Hz, 1H), 7.13 (d, $J = 3.4$ Hz, 1H), 6.64 (s, 1H), 5.45-5.11 (m, 1H), 4.44 - 4.39 (m, 1H), 3.80 - 3.76 (m, 1H), 3.56 - 3.50 (m, 1H), 2.25 - 2.10 (m, 1H).

¹³C NMR (CD₃OD): δ 173.60, 160.03, 156.92, 148.95, 137.34, 133.93, 133.50, 133.07, 132.64 (q, $J = 32$ Hz), 132.52, 131.90, 131.55, 127.95, 124.35, 120.74 (q, $J = 270$ Hz), 129.82, 127.15, 127.10, 127.05, 127.00 (q, $J = 3.4$ Hz), 122.95, 122.90, 122.85, 122.79 (q, $J = 3.4$ Hz), 121.27, 110.46, 60.26, 57.51, 54.65, 53.57, 36.34.

(1R,4R)-2,5-Diazabicyclo[2.2.1]heptan-2-yl(5-(3-(trifluoromethyl)phenyl)furan-2-yl)methanone fumarate (**20**)

Benzylated compound **112** (140 mg, 0.32 mmol, 1 equiv) was deprotected following the procedure reported in 7.1.2.5.2 paragraph, using Pd/C (14 mg, 10%). The mixture was stirred overnight, and, upon hydrogenolysis completion, standard workup was applied. The resulting crude was reacted with fumaric acid (69 mg, 0.59 mmol) in MeOH. The crude salt was recrystallized from EtOH/*i*-PrOH/Et₂O, and the final product **20** was achieved as a white solid (11 mg, yield 10%).

$R_f = 0.31$ (DCM/MeOH, 4:1)

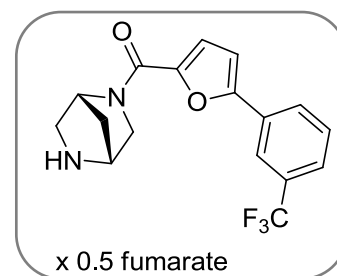
m.p. = 118.5 - 120.1 °C

$[\alpha]_D = -24.3$ (c = 1.05, methanol)

HRMS (ESI+) m/z calcd for C₁₇H₁₆N₂O₂F₃ 337.11584 [M + H]⁺, found 337.11586; calcd for C₁₇H₁₅N₂O₂F₃Na 319.14170 [M + Na]⁺, found 359.09778.

¹H NMR (CD₃OD): δ 8.06 (m, 2H), 7.66 (m, 2H), 7.30 (d, $J = 3.5$ Hz, 1H), 7.13 (d, $J = 3.5$ Hz, 1H), 6.65 (s, 1H), 5.45 - 5.09 (m, 1H), 4.55 - 4.49 (m, 1H), 4.21 - 4.17 (m, 1H), 3.64 - 3.60 (m, 3H), 2.22 - 2.09 (m, 2H).

¹³C NMR (CD₃OD): δ 173.56, 160.07, 156.93, 148.97, 137.41, 133.94, 133.51, 133.08, 132.65 (q, $J = 32$ Hz), 132.53, 131.90, 131.56, 127.96, 124.36, 120.72 (q, $J = 270$ Hz), 129.83, 127.16, 127.11, 127.06, 127.01 (q, $J = 3.4$ Hz), 122.96, 122.90, 122.85, 122.80 (q, $J = 3.4$ Hz), 121.20, 110.46, 60.17, 57.51, 54.72, 53.50, 36.35.



7.1.2.6 Synthesis of compound 21

4-((5-(3-(Trifluoromethyl)phenyl)furan-2-yl)methyl)-1,4 diazabicyclo[3.2.2]nonane fumarate (**21**)

Under anhydrous conditions, a suspension of LiAlH_4 (39.8 mg, 1.05 mmol, 2.25 equiv) in dry Et_2O was dropped into a solution of **1** (170 mg, 0.47 mmol, 1 equiv) in dry Et_2O at 0 °C. The mixture was refluxed for 2 h, then quenched with a saturated aqueous solution of sodium tartrate and extracted with DCM. The pooled organic layers were dried over anhydrous Na_2SO_4 , filtered, and concentrated under vacuum. The corresponding crude was dissolved in MeOH and reacted with fumaric acid (27 mg, 0.23 mmol) at r.t. overnight. After recrystallization from EtOH and Et_2O , the final compound **21** was obtained as a white solid (30 mg, yield 11%).

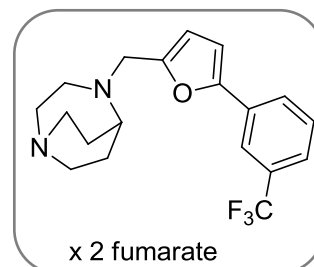
$R_f = 0.45$ (DCM/MeOH, 9:1)

m.p. = 105.7 – 108.1 °C

HRMS (ESI+) m/z calcd for $\text{C}_{19}\text{H}_{22}\text{N}_2\text{OF}_3$ 351.16787 $[\text{M} + \text{H}]^+$, found 351.16821.

^1H NMR (CD_3OD): δ 8.16 (d, $J = 7.4$ Hz, 2H), 7.79 (t, $J = 7.8$ Hz, 2H), 7.13 (d, $J = 3.3$ Hz, 1H), 6.95 (s, 3.6H), 6.71 (d, $J = 3.3$ Hz, 1H), 4.13 (s, 2H), 3.65 (dt, $J = 34.1, 7.5$ Hz, 6H), 3.56 – 3.51 (m, 2H), 2.49 – 2.13 (m, 4H).

^{13}C NMR (CD_3OD): δ 169.86, 153.72, 153.47, 135.72, 132.97, 132.91, 132.48, 132.06, 131.63 (q, $J = 32.13$ Hz), 130.96, 127.36, 123.76, 120.16 (q, $J = 271.73$ Hz), 130.76, 128.02, 124.82, 124.77, 124.72, 124.67 (q, $J = 3.95$ Hz), 120.98, 120.93, 120.88, 120.83 (q, $J = 3.95$ Hz), 112.69, 108.61, 65.01, 54.86, 54.05, 52.85, 47.47, 46.64, 22.91.



7.1.2.7 Synthesis of NS6740 derivatives 22-33

1,4-Diazabicyclo[3.2.2]nonan-4-yl(5-(3-fluorophenyl)furan-2-yl)methanone fumarate (22)

The title compound was prepared following the general procedure (paragraph 7.1.2.4.1) from 1,4-diazabicyclo[3.2.2]nonane dihydrochloride **16** (250 mg, 1.26 mmol, 1 equiv), **99** (363 mg, 1.50 mmol, 1.2 equiv) and Cs₂CO₃ (2.05 g, 6.28 mmol, 5 equiv). After standard workup and reaction with fumaric acid (92 mg, 0.79 mmol, 1 equiv), the final compound **22** was obtained through recrystallization from *i*-PrOH as a light brown solid (180 mg, yield 46%).

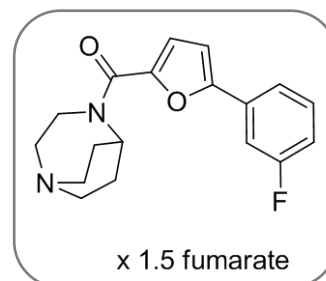
R_f = 0.33 (DCM/MeOH, 9:1)

m.p. = 180.5 - 181.5 °C

HRMS (ESI+) *m/z* calcd for C₁₈H₂₀N₂O₂F 315.15033 [M + H]⁺, found 315.15059; calcd for C₁₈H₁₉N₂O₂FNa 337.13228 [M + Na]⁺, found 337.13275.

¹H NMR (CD₃OD): δ 7.60 (dd, *J* = 7.9, 1.1 Hz, 1H), 7.55 – 7.42 (m, 2H), 7.21 (d, *J* = 3.6 Hz, 1H), 7.14 – 7.07 (m, 1H), 7.03 (d, *J* = 3.6 Hz, 1H), 6.71 (s, 3H), 4.95 - 4.83 (m, 1H), 4.40 - 4.20 (m, 2H), 3.56 (dt, *J* = 15.9, 7.4 Hz, 6H), 2.49 - 2.22 (m, 4H).

¹³C NMR (CD₃OD): δ 170.46, 166.16, 162.91(d, *J* = 244.89 Hz), 160.68, 158.06, 156.06, 147.62, 135.89, 133.04, 132.92 (d, *J* = 9.56 Hz), 132.11, 132.00 (d, *J* = 8.48 Hz), 121.45, 121.41 (d, *J* = 2.87 Hz), 120.69, 116.64, 116.36 (d, *J* = 21.49 Hz), 112.32, 112.00 (d, *J* = 24.06 Hz), 109.05, 46.93, 25.25, 23.70.



1,4-Diazabicyclo[3.2.2]nonan-4-yl(5-(3-chlorophenyl)furan-2-yl)methanone fumarate (23)

The title compound was prepared following the general procedure (paragraph 7.1.2.4.1) from 1,4-diazabicyclo[3.2.2]nonane dihydrochloride **16** (250 mg, 1.26 mmol, 1 equiv), **100** (338 mg, 1.51 mmol, 1.2 equiv) and Cs₂CO₃ (2.05 g, 6.28 mmol, 5 equiv). After standard workup and reaction with fumaric acid (104 mg, 0.90 mmol, 1 equiv), the final compound **23** was obtained through recrystallization from *i*-PrOH as a light brown solid (320 mg, yield 80%).

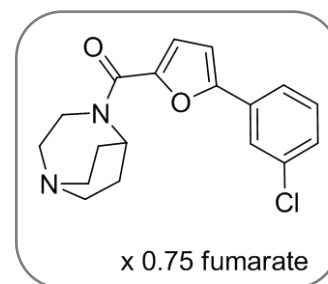
R_f = 0.33 (DCM/MeOH, 9:1)

m.p. = 185.8 - 187.5 °C

HRMS (ESI+) *m/z* calcd for C₁₈H₂₀N₂O₂Cl 331.12078 [M + H]⁺, found 331.12062; calcd for C₁₈H₁₉N₂O₂ClNa 353.10273 [M + Na]⁺, found 353.10254.

¹H NMR (CD₃OD): δ 7.80 (s, 1H), 7.72 (d, *J* = 7.7 Hz, 1H), 7.44 (t, *J* = 7.9 Hz, 1H), 7.37 (ddd, *J* = 8.1, 1.9, 1.1 Hz, 1H), 7.20 (d, *J* = 3.6 Hz, 1H), 7.04 (d, *J* = 3.7 Hz, 1H), 6.70 (s, 1.5H), 4.38 - 4.18 (m, 2H), 3.61 - 3.45 (m, 6H), 2.45 - 2.20 (m, 4H).

¹³C NMR (CD₃OD): δ 170.99, 160.73, 155.80, 147.79, 136.08, 136.04, 132.71, 131.70, 129.71, 125.31, 123.86, 120.56, 109.11, 56.07, 47.00, 23.92.

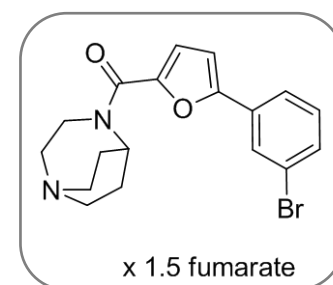


1,4-Diazabicyclo[3.2.2]nonan-4-yl(5-(3-bromophenyl)furan-2-yl)methanone fumarate (24)

The title compound was prepared following the general procedure (paragraph 7.1.2.4.1) from 1,4-diazabicyclo[3.2.2]nonane dihydrochloride **16** (200 mg, 1.0 mmol, 1 equiv), **101** (344 mg, 1.21 mmol, 1.2 equiv) and Cs₂CO₃ (1.64 g, 5.02 mmol, 5 equiv). After standard workup and reaction with fumaric acid (63 mg, 0.54 mmol, 1 equiv), the final compound **24** was obtained through recrystallization from MeOH and Et₂O as a light brown solid (161 mg, yield 43%).

R_f = 0.33 (DCM/MeOH, 9:1)

m.p. = 203.7 - 205 °C



HRMS (ESI+) m/z calcd for $C_{18}H_{20}N_2O_2Br$ 375.07027 $[M + H]^+$, found 375.07052; calcd for $C_{18}H_{19}N_2O_2BrNa$ 397.05221 $[M + Na]^+$, found 397.05225.

1H NMR (CD_3OD): δ 7.92 (s, 1H), 7.73 (d, $J = 7.8$ Hz, 1H), 7.50 (d, $J = 8.2$ Hz, 1H), 7.35 (t, $J = 7.9$ Hz, 1H), 7.19 (d, $J = 3.5$ Hz, 1H), 7.01 (d, $J = 3.6$ Hz, 1H), 6.71 (s, 3H), 4.95 - 4.81 (m, 1H), 4.40 - 4.20 (m, 2H), 3.57 (dt, $J = 15.1, 6.7$ Hz, 6H), 2.50 - 2.22 (m, 4H).

^{13}C NMR (CD_3OD): δ 170.48, 160.74, 155.68, 147.78, 135.91, 132.93, 132.71, 131.91, 128.25, 124.28, 124.03, 120.55, 109.12, 56.04, 47.05, 24.20.

1,4-Diazabicyclo[3.2.2]nonan-4-yl(5-(3-aminophenyl)furan-2-yl)methanone fumarate (25)

The title compound was prepared following the general procedure (paragraph 7.1.2.4.1) from 1,4-diazabicyclo[3.2.2]nonane dihydrochloride **16** (180 mg, 0.90 mmol, 1 equiv), **102** (240 mg, 1.08 mmol, 1.2 equiv) and Cs_2CO_3 (1.47 g, 4.52 mmol, 5 equiv). After standard workup and reaction with fumaric acid (65 mg, 0.56 mmol, 1 equiv), the final compound **25** was obtained through recrystallization from MeOH and Et₂O as a light brown solid (100 mg, yield 42%).

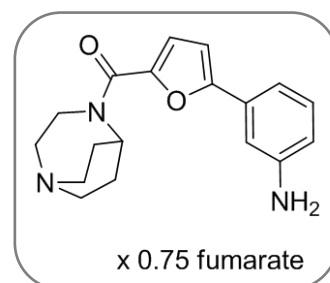
$R_f = 0.54$ (DCM/MeOH, 9:1 and 3 drops of aqueous NH_3)

m.p. = 217.3 - 219.4 °C

HRMS (ESI+) m/z calcd for $C_{18}H_{22}N_3O_2$ 312.17065 $[M + H]^+$, found 312.17087; calcd for $C_{18}H_{21}N_3O_2Na$ 334.15260 $[M + Na]^+$, found 334.15250.

1H NMR (CD_3OD): δ 7.20 - 7.04 (m, 4H), 6.84 (d, $J = 3.6$ Hz, 1H), 6.75 - 6.70 (m, 1H), 6.69 (s, 1.5H), 4.35 - 4.13 (m, 2H), 3.57 - 3.37 (m, 6H), 2.46 - 2.16 (m, 4H).

^{13}C NMR (CD_3OD): δ 170.00, 159.51, 156.78, 148.21, 145.60, 134.74, 130.09, 129.31, 119.50, 115.56, 113.79, 110.46, 106.05, 55.07, 45.66, 23.70.



1,4-Diazabicyclo[3.2.2]nonan-4-yl(5-(3-hydroxyphenyl)furan-2-yl)methanone fumarate (26)

The title compound was prepared following the general procedure (paragraph 7.1.2.4.1) from 1,4-diazabicyclo[3.2.2]nonane dihydrochloride **16** (200 mg, 1.0 mmol, 1 equiv), **103** (268 mg, 1.21 mmol, 1.2 equiv) and Cs₂CO₃ (1.64 g, 5.02 mmol, 5 equiv). After standard workup and reaction with fumaric acid (67 mg, 0.58 mmol, 1 equiv), the final compound **26** was obtained through recrystallization from MeOH and Et₂O as a light brown solid (100mg, yield 40%).

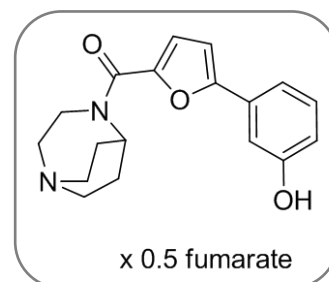
R_f = 0.35 (DCM/MeOH, 4:1)

m.p. = 231 - 233.2 °C

HRMS (ESI+) *m/z* calcd for C₁₈H₂₁N₂O₃ 313.15467 [M + H]⁺, found 313.15474; calcd for C₁₈H₂₀N₂O₃Na 335.13661 [M + Na]⁺, found 335.13646.

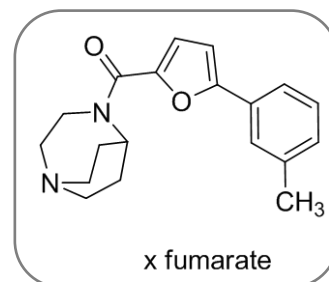
¹H NMR (CD₃OD): δ 7.29 - 7.21 (m, 2H), 7.20 - 7.15 (m, 2H), 6.88 (d, *J* = 3.6 Hz, 1H), 6.82 - 6.76 (m, 1H), 6.69 (s, 1H), 4.32 - 4.12 (m, 2H), 3.48 - 3.34 (m, 6H), 2.50 - 2.00 (m, 4H)

¹³C NMR (CD₃OD): δ 171.76, 160.95, 159.18, 157.56, 147.38, 136.28, 132.10, 131.18, 116.98, 116.89, 112.12, 107.80, 47.10, 42.69.



*1,4-Diazabicyclo[3.2.2]nonan-4-yl(5-(*m*-tolyl)furan-2-yl)methanone fumarate (27)*

The title compound was prepared following the general procedure (paragraph 7.1.2.4.1) from 1,4-diazabicyclo[3.2.2]nonane dihydrochloride **16** (150 mg, 0.75 mmol, 1 equiv), **104** (200 mg, 1.50 mmol, 1.2 equiv) and Cs₂CO₃ (1.23 g, 3.77 mmol, 5 equiv). After standard workup and subsequent reaction with fumaric acid (59 mg, 0.50 mmol, 1 equiv), the final compound **27** was obtained through recrystallization from EtOH/Et₂O as a brown solid (150mg, yield 64%).



R_f = 0.50 (DCM/MeOH, 9:1)

m.p. = 157.2 - 158.8 °C

HRMS (ESI+) *m/z* calcd for C₁₉H₂₃N₂O₂ 311.17540 [M + H]⁺, found 311.17531; calcd for C₁₉H₂₂N₂O₂Na 333.15735 [M + Na]⁺, found 333.15743.

¹H NMR (CD₃OD): δ 7.63 - 7.52 (m, 2H), 7.32 (t, *J* = 7.6 Hz, 1H), 7.23 - 7.15 (m, 2H), 6.92 (d, *J* = 3.6 Hz, 1H), 6.70 (s, 2H), 4.38 - 4.18 (m, 2H), 3.53 (dt, *J* = 15.5, 6.9 Hz, 6H), 2.47 - 2.21 (m, 4H).

¹³C NMR (CD₃OD): δ 171.12, 160.91, 157.77, 147.19, 139.98, 136.07, 130.82, 130.70, 129.99, 126.06, 122.74, 120.84, 107.78, 55.94, 47.03, 24.67, 21.45.

1,4-Diazabicyclo[3.2.2]nonan-4-yl(5-(4-trifluorophenyl)furan-2-yl)methanone fumarate (28)

The title compound was prepared following the general procedure (paragraph 7.1.2.4.1) from 1,4-diazabicyclo[3.2.2]nonane dihydrochloride **16** (105 mg, 0.53 mmol, 1 equiv), **105** (175 mg, 0.64 mmol, 1.2 equiv) and Cs₂CO₃ (865 mg, 2.65 mmol, 5 equiv). After standard workup and reaction with fumaric acid (48 mg, 0.41 mmol, 1 equiv), the final compound **28** was obtained through recrystallization from EtOH as an off-white solid (100 mg, yield 50%).

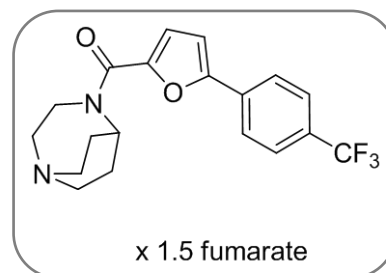
R_f = 0.34 (DCM/MeOH, 9:1)

m.p. = 167 – 169 °C

HRMS (ESI+) *m/z* calcd for C₁₉H₂₀N₂O₂F₃ 365.14714 [M + H]⁺, found 365.14701; calcd for C₁₉H₁₉N₂O₂F₃Na 387.12908 [M + Na]⁺, found 387.12924.

¹H NMR (CD₃OD): δ 7.97 (d, *J* = 8.3 Hz, 2H), 7.75 (d, *J* = 8.4 Hz, 2H), 7.24 (d, *J* = 3.6 Hz, 1H), 7.14 (d, *J* = 3.7 Hz, 1H), 6.71 (s, 3H), 4.93 – 4.67 (m, 1H), 4.45 – 4.12 (m, 2H), 3.76 – 3.41 (m, 6H), 2.52 – 2.11 (m, 4H).

¹³C NMR (CD₃OD): δ 170.30, 160.73, 155.72, 148.29, 135.87, 134.37, 131.94, 131.51, 131.08, 130.65 (*J* = 32 Hz) 130.92, 127.33, 123.74, 120.14 (*J* = 3.5 Hz), 127.14, 127.09, 127.04, 126.99 (*J* = 3.5 Hz), 125.98, 120.62, 110.04, 58.36, 56.02, 47.08, 24.21, 18.41.



[2,3'-Bifuran]-5-yl(1,4-diazabicyclo[3.2.2]nonan-4-yl)methanone fumarate (29)

The title compound was prepared following the general procedure (paragraph 7.1.2.4.1) from 1,4-diazabicyclo[3.2.2]nonane dihydrochloride **16** (150 mg, 0.75 mmol, 1 equiv), **106** (175 mg, 0.89 mmol, 1.2 equiv) and Cs₂CO₃ (1.20 g, 3.7 mmol, 5 equiv). After standard workup and reaction with fumaric acid (40 mg, 0.35 mmol, 1 equiv), the final compound **29** was obtained through recrystallization from MeOH, EtOH, Et₂O as a white solid (80 mg, yield 57%).

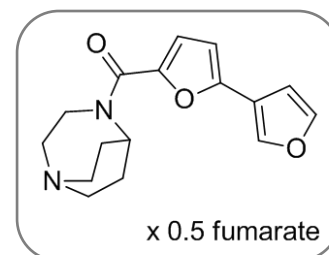
R_f = 0.33 (DCM/MeOH, 9:1);

m.p. = 176 - 178 °C

HRMS (ESI+) *m/z* calcd for C₁₆H₁₉N₂O₃ 287.13902 [M + H]⁺, found 287.13926; calcd for C₁₆H₁₈N₂O₃Na 309.12096 [M + Na]⁺, found 309.12118.

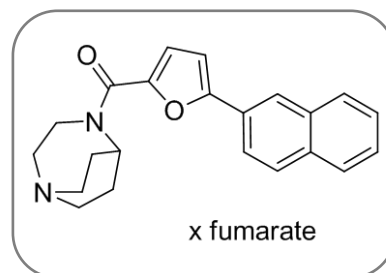
¹H NMR (CD₃OD): δ 7.99 (s, 1H), 7.64 - 7.56 (m, 1H), 7.15 (d, *J* = 3.5 Hz, 1H), 6.80 - 6.76 (m, 1H), 6.67 (d, *J* = 3.6 Hz, 1H), 4.90 - 4.73 (m, 1H), 4.51 - 4.00 (m, 2H), 3.54 (dt, *J* = 15.7, 6.8 Hz, 6H), 2.49 - 2.12 (m, 4H).

¹³C NMR (CD₃OD): δ 171.34, 160.75, 151.78, 146.49, 145.53, 141.15, 136.12, 120.50, 118.30, 108.73, 107.87, 66.85, 55.66, 46.92, 24.28, 15.44.



1,4-Diazabicyclo[3.2.2]nonan-4-yl(5-(naphthalen-2-yl)furan-2-yl)methanone fumarate (30)

The title compound was prepared following the general procedure (paragraph 7.1.2.4.1) from 1,4-diazabicyclo[3.2.2]nonane dihydrochloride **16** (160 mg, 0.80 mmol, 1 equiv), **107** (250 mg, 0.97 mmol, 1.2 equiv) and Cs₂CO₃ (1.30 g, 4 mmol, 5 equiv). After standard workup and reaction with fumaric acid (54 mg, 0.46 mmol, 1 equiv), the final compound **30** was obtained through recrystallization from MeOH as a white solid (95 mg, yield 45%).



R_f = 0.34 (DCM/MeOH, 9:1)

m.p. = 179 – 181 °C

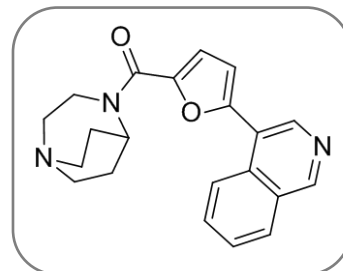
HRMS (ESI+) *m/z* calcd for C₂₂H₂₃N₂O₂ 347.17540 [M + H]⁺, found 347.17569; calcd for C₂₂H₂₂N₂O₂Na 369.15735 [M + Na]⁺, found 369.15719.

¹H NMR (CD₃OD): δ 8.37 – 8.30 (m, 1H), 8.00 – 7.92 (m, 2H), 7.82 (dd, *J* = 7.2, 0.9 Hz, 1H), 7.66 – 7.52 (m, 3H), 7.33 (d, *J* = 3.4 Hz, 1H), 6.98 (d, *J* = 3.6 Hz, 1H), 6.69 (s, 2H), 5.05 – 4.90 (m, 1H), 4.47 – 4.09 (m, 2H), 3.48 (dt, *J* = 15.7, 7.4 Hz, 6H), 2.57 – 2.03 (m, 4H).

¹³C NMR (CD₃OD): δ 170.77, 160.97, 157.06, 148.00, 136.00, 135.49, 131.56, 130.96, 129.86, 128.46, 128.22, 128.17, 127.39, 126.39, 125.93, 112.11, 47.17.

1,4-Diazabicyclo[3.2.2]nonan-4-yl(5-(isoquinolin-4-yl)furan-2-yl)methanone fumarate (31)

The title compound was prepared following the general procedure (paragraph 7.1.2.4.1) from 1,4-diazabicyclo[3.2.2]nonane dihydrochloride **16** (84 mg, 0.42 mmol, 1 equiv), **108** (130 mg, 0.50 mmol, 1.2 equiv) and Cs₂CO₃ (700 mg, 2 mmol, 5 equiv). After standard workup and reaction with fumaric acid (20 mg, 0.17 mmol, 1 equiv), several recrystallization attempts with different combinations of solvents failed. Thus the crude salt was treated with a saturated solution of Na₂CO₃ and the water phase was extracted with DCM. The solvent was concentrated and hexane was added, providing the precipitation of **31** as the free base (light brown semi-solid, 20 mg, yield 30%).



R_f = 0.41 (DCM/MeOH, 98:2)

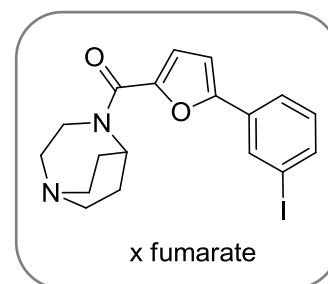
HRMS (ESI+) *m/z* calcd for C₂₁H₂₂N₃O₂ 348.17065 [M + H]⁺, found 348.17076; calcd for C₂₁H₂₁N₃O₂Na 370.15260 [M + Na]⁺, found 370.15292.

¹H NMR (CD₃OD): δ 9.33 (s, 1H), 8.85 (s, 1H), 8.48 (d, *J* = 8.6 Hz, 1H), 8.20 (d, *J* = 8.2 Hz, 1H), 7.88 (t, *J* = 7.5 Hz, 1H), 7.76 (t, *J* = 7.5 Hz, 1H), 7.44 (d, *J* = 3.6 Hz, 1H), 7.17 (d, *J* = 3.6 Hz, 1H), 4.76 - 4.70 (m, 1H), 4.02 - 3.95 (m, 2H), 3.10 - 2.97 (m, 6H) 2.13 - 2.07 (m, 2H), 1.80 - 1.68 (m, 2H).

¹³C NMR (CD₃OD): δ 159.52, 152.67, 151.95, 147.97, 141.17, 132.25, 128.55, 128.43, 127.95, 127.2, 123.81, 127.71, 117.71, 109.56, 57.05, 56.02, 46.20, 23.21, 14.41.

1,4-Diazabicyclo[3.2.2]nonan-4-yl(5-(3-iodophenyl)furan-2-yl)methanone fumarate
(32)

The title compound was prepared following the general procedure (paragraph 7.1.2.4.1) from 1,4-diazabicyclo[3.2.2]nonane dihydrochloride **16** (90 mg, 0.45 mmol, 1 equiv), **109** (180 mg, 0.54 mmol, 1.2 equiv) and Cs₂CO₃ (736 mg, 2.26 mmol, 5 equiv). After standard workup and reaction with fumaric acid (92



mg, 0.79 mmol, 1 equiv), the final compound **32** was obtained through recrystallization from MeOH and Et₂O as a light brown solid (150 mg, yield 53%).

R_f = 0.33 (DCM/MeOH, 9:1)

m.p. = 184.2–186.7 °C

HRMS (ESI+) *m/z* calcd for C₁₈H₂₀N₂O₂I 423.05640 [M + H]⁺, found 423.05698; calcd for C₁₈H₁₉N₂O₂INa 445.03834 [M + Na]⁺, found 445.03820.

¹H NMR (CD₃OD): δ 8.15 (d, *J* = 1.4 Hz, 1H), 7.75 (dd, *J* = 20.0, 7.9 Hz, 2H), 7.28 – 7.15 (m, 2H), 7.02 (d, *J* = 3.6 Hz, 1H), 6.71 (s, 2H), 4.38 – 4.18 (m, 2H), 3.62 – 3.42 (m, 6H), 2.46 – 2.19 (m, 4H).

¹³C NMR (CD₃OD): δ 170.54, 160.78, 155.56, 147.77, 138.83, 135.91, 134.25, 132.86, 131.85, 124.78, 120.58, 108.96, 95.30, 55.47, 47.07, 24.06.

1,4-Diazabicyclo[3.2.2]nonan-4-yl(5-(3-nitrophenyl)furan-2-yl)methanone fumarate
(**33**)

The title compound was prepared following the general procedure (paragraph 7.1.2.4.1) from 1,4-diazabicyclo[3.2.2]nonane dihydrochloride **16** (120 mg, 0.6 mmol, 1 equiv), **110** (180 mg, 0.75 mmol, 1.2 equiv) and Cs₂CO₃ (970 mg, 3 mmol, 5 equiv). After standard workup and reaction with fumaric acid (50 mg, 0.40 mmol, 1 equiv), the final compound **33** was obtained through recrystallization from MeOH as a yellow solid (100 mg, yield 50%).

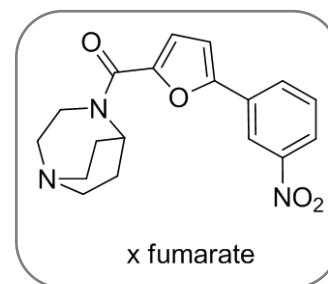
R_f = 0.33 (DCM/MeOH, 9:1)

m.p. = 202–205 °C

HRMS (ESI+) *m/z* calcd for C₁₈H₂₀N₃O₄ 342.14483 [M + H]⁺, found 342.14493; calcd for C₁₈H₁₉N₃O₄Na 364.12678 [M + Na]⁺, found 364.12655.

¹H NMR (CD₃OD): δ 8.60 (s, 1H), 8.18 (dd, *J* = 12.9, 9.1 Hz, 2H), 7.70 (t, *J* = 8.0 Hz, 1H), 7.22 (d, *J* = 3.3 Hz, 1H), 7.18 (d, *J* = 3.6 Hz, 1H), 6.53 (s, 2H), 4.86 – 4.72 (m, 1H), 4.38 – 4.18 (m, 2H), 3.50 (dt, *J* = 14.2, 6.2 Hz, 6H), 2.50 – 2.06 (m, 4H).

¹³C NMR ((CD₃)₂SO): δ 167.08, 158.01, 151.68, 148.45, 147.73, 134.54, 130.86, 130.79, 130.11, 122.79, 118.32, 117.32, 109.54, 48.59, 45.23, 26.07, 24.67.

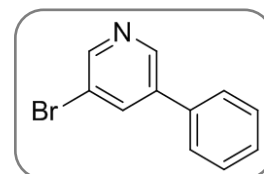


7.1.3 Synthesis of KC-1 derivatives

7.1.3.1 Synthesis of the positively charged KC-1 derivatives 34-37

3-Bromo-5-phenylpyridine (113)

Under inert conditions, to a degassed solution of the commercially available 2,6-dibromopyridine (2 g, 8.45 mmol, 1.18 equiv) in 1,2-dimethoxyethane was added Pd(PPh₃)₄ (0.250 g, 0.160 mmol, 0.02 equiv) and the mixture was stirred at r.t. for 15 min. A degassed aqueous solution of 2 M K₂CO₃ (3.50 g, 25.4 mmol in 12.7 mL of H₂O, 3.35 equiv) was added and the mixture was stirred for additional 5 min. Finally, the commercially available phenyl boronic acid (930 mg, 7.6 mmol, 1 equiv) was added and the reaction was refluxed for 6 h. Upon completion, the reaction was cooled down and 1 M NaOH was added; the water phase was extracted using Et₂O. The resulting organic phase was dried over anhydrous Na₂SO₄, filtered and concentrated under reduced pressure. The crude was purified by column chromatography eluted with hexane/EtOAc (4:1), and **113** was obtained as a hygroscopic white solid (1.40 g, yield 77%).



R_f = 0.50 (DCM)

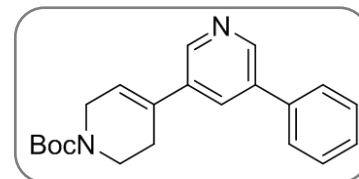
m.p. = 35–38 °C

¹H NMR (CDCl₃): δ 8.73 (d, *J* = 1.8 Hz, 1H), 8.63 (d, *J* = 2.0 Hz, 1H), 7.97 (t, *J* = 2.0 Hz, 1H), 7.57 – 7.35 (m, 5H).

¹³C NMR (CDCl₃): δ 149.53, 146.55, 138.37, 136.98, 136.44, 129.39, 128.89, 127.35, 121.11.

tert-Butyl 5-phenyl-5',6'-dihydro-[3,4'-bipyridine]-1'(2'H)-carboxylate (**114**)

Under inert conditions, to a degassed solution of previously prepared **113** (1.5 g, 6.4 mmol, 1 equiv) in DMF, Pd(PPh₃)₄ (370 mg, 0.32 mmol, 0.05 equiv) was added and the mixture stirred at r.t. for 15 min. Then, *tert*-butyl 4-(4,4,5,5-tetramethyl-1,3,2-dioxaborolan-2-yl)-5,6-dihydropyridine-1(2H)-carboxylate (2.4 g, 7.6 mmol, 1.2 equiv) was added, followed by addition of a degassed aqueous solution of 2 M Na₂CO₃ (2.85 g, 27 mmol, 13.5 mL). Initially, a precipitate was obtained and then the reaction turned into a dark mixture, which was refluxed overnight. Upon completion, DMF was evaporated, deionized water was added and the mixture was extracted with DCM. The organic phase was dried over anhydrous Na₂SO₄, filtered and concentrated under reduced pressure. The crude brown oil was purified by column chromatography eluted with hexane/EtOAc (7:3). Compound **114** was obtained as a light yellow oil (1.70 g, yield 80%).



R_f = 0.50 (DCM/MeOH, 95:5)

¹H NMR (CDCl₃): δ 8.72 (d, *J* = 2.0 Hz, 1H), 8.62 (d, *J* = 2.0 Hz, 1H), 7.81 (t, *J* = 2.0 Hz, 1H), 7.66 – 7.35 (m, 5H), 6.16 (s, 1H), 4.12 (d, *J* = 2.6 Hz, 2H), 3.68 (t, *J* = 5.6 Hz, 2H), 2.58 (m, 2H), 1.50 (s, 9H).

¹³C NMR (CDCl₃): δ 146.91, 145.29, 137.76, 136.28, 136.02, 130.72, 129.06, 128.15, 127.18, 79.86, 28.46, 28.34, 27.22, 24.84.

5-Phenyl-1',2',3',6'-tetrahydro-3,4'-bipyridinium dichloride (34)

A solution of previously synthesized compound **114** (860 mg, 2.5 mmol, 1 equiv) in methanol was reacted with 38% HCl (1.60 mL, 25 mmol, 10 equiv), which was added dropwise at 0 °C. The reaction was stirred at r.t. for 72 h. A yellowish solid formed and was recovered by filtration, then washed with Et₂O to afford 540 mg of light yellow solid. 220 mg were recrystallized from EtOH and the final compound **33** was obtained as a light yellow solid (140 mg, yield 60%).

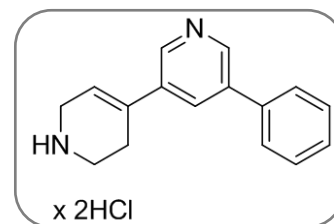
R_f = 0.50 (DCM/MeOH/0.5NH₄OH, 6:4:0.5)

m.p. = 213-216 °C

MS [M]⁺ (C₁₆ H₁₆ N₂⁺) Calcd [M+H]⁺ 237.1386 and [M+Na]⁺ 259.1206 Found [M+H]⁺ 237.1394 and [M+Na]⁺ 259.1206.

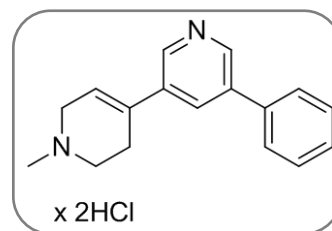
¹H NMR (D₂O): δ 8.86 (s, 1H), 8.71 (s, 1H), 8.70 (s, 1H), 7.67 (dd, J = 7.7, 1.7 Hz, 2H), 7.56 – 7.42 (m, 3H), 6.42 (s, 1H), 3.98 – 3.78 (m, 2H), 3.47 (t, J = 6.1 Hz, 2H), 2.88 – 2.75 (m, 2H).

¹³C NMR (CDCl₃): δ 140.3, 138.5, 138.3, 136.4, 133.5, 130.1, 130.0, 129.5, 127.4, 122.4, 42.1, 40.4, 22.7.



1'-Methyl-5-phenyl-1',2',3',6'-tetrahydro-3,4'-bipyridinium dichloride (35)

To the corresponding free base of **34** (240 mg, 1.02 mmol, 1 equiv), solubilized in deionized water/MeOH (4:1), formaldehyde (0.76 mL, 10.2 mmol, 10 equiv) and 38% HCl (to reach pH = 6-7) were added. The reaction



was stirred at r.t. for 10 min. and then NaCNBH₃ (96 mg, 1.52 mmol, 1.5 equiv) was added. The mixture was then stirred at r.t. for 18 h. The reaction was quenched by addition of 1 M NaOH; the water phase was extracted with DCM and the resulting organic phase was dried over anhydrous Na₂SO₄, filtered and concentrated under reduced pressure. The obtained crude yellow oil (200 mg, 0.795 mmol, 1 equiv) was dissolved in MeOH and 38% HCl (0.133 mL, 1.6 mmol, 2 equiv) was added dropwise at 0 °C; the solution was then stirred at r.t. Upon completion, the solvent was evaporated and the crude was recrystallized from MeOH/EtOH, obtaining the final compound **35** as a very light yellow solid (100 mg, yield 40%).

R_f = 0.38 (DCM/MeOH, 7:3)

m.p. = 226-228 °C

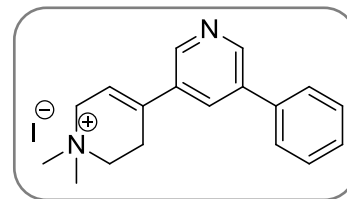
MS [M]⁺ (C₁₇ H₁₈ N₂⁺) Calcd [M+H]⁺ 251.1543 and [M+Na]⁺ 273.1362 Found [M+H]⁺ 251.1544 and [M+Na]⁺ 273.135.

¹H NMR (CD₃OD) δ 9.14 (s, 1H), 9.01 (s, 1H), 8.97 (s, 1H), 7.90 (d, J = 7.2 Hz, 2H), 7.69 – 7.54 (m, 3H), 6.66 (s, 1H), 4.22 (d, J = 17.1 Hz, 1H), 3.97 (d, J = 17.3 Hz, 1H), 3.92 – 3.77 (m, 1H), 3.55 – 3.43 (m, 1H), 3.23 – 2.96 (m, 6H).

¹³C NMR (CD₃OD): δ 140.1, 138.6, 136.9, 130.0, 129.4, 127.3, 122.6, 51.8, 50.0, 41.6, 23.7.

1',1'-Dimethyl-5-phenyl-1',2',3',6'-tetrahydro-[3,4'-bipyridin]-1'-ium iodide (36)

The corresponding free base of **33** (250 mg, 1.06 mmol, 1 equiv) and NaHCO₃ (90 mg, 1.06 mmol, 1 equiv) was solubilized in MeOH and cooled down to 0 °C. Slow addition of MeI (0.05 mL, 0.74 mmol, 0.7 equiv) was carried out and then the reaction was stirred at 0 °C for 7 h. Additional 0.3, 0.5 and 0.5 equivalents of MeI were added after 7, 15 and 25 h, respectively. After 20 h, a white precipitate was observed and after total 33 h at 0 °C the reaction was complete. The white solid was filtered off and the organic solvent was evaporated. Both solids obtained were recrystallized from MeOH/EtOH, giving the final compound **36** as a white solid (0.200 g, yield 47%).



$R_f = 0.25$ (EtOH / H₂O / NH₃, 4:2:1)

m.p. = 243-245 °C

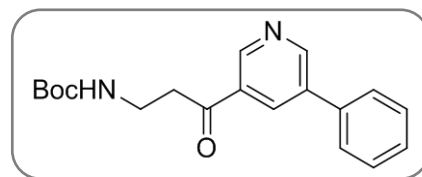
MS [M]⁺ (C₁₈ H₂₁ N₂⁺) Calcd [M+H]⁺ 265.1699 Found [M+H]⁺ 265.1705.

¹H NMR (DMSO): δ 8.83 (s, 1H), 8.73 (s, 1H), 8.16 (s, 1H), 7.78 (d, *J* = 7.3 Hz, 2H), 7.57 – 7.36 (m, 3H), 6.50 – 4.34 (m, 1H), 4.23 – 4.06 (m, 2H), 3.74 – 3.56 (m, 2H), 3.17 (s, 7H), 3.06 – 2.89 (m, 2H).

¹³C NMR (DMSO): δ 47.48, 145.73, 137.20, 135.70, 134.03, 131.23, 131.10, 129.56, 128.79, 127.52, 117.88, 60.61, 58.15, 51.28, 22.76.

tert-Butyl (3-oxo-3-(5-phenylpyridin-3-yl)propyl)carbamate (**115**)

Under anhydrous and inert conditions, 1.6 M *n*BuLi in hexane (2.6 mL, 4.2 mmol, 1 equiv) was dissolved in dry Et₂O (20 mL) and cooled down at -78 °C. A solution of 3-bromo-5-phenylpyridine **113** (1 g, 4.2 mmol, 1 equiv) in dry Et₂O was slowly added dropwise giving an orange suspension, which was stirred at -78 °C for 20 min. Finally, the addition of commercially available *tert*-butyl 2-oxopyrrolidine-1-carboxylate (780 mg, 4.2 mmol, 1 equiv) solubilized in dry Et₂O (8 mL) was carried out, slowly obtaining an orange solution. The mixture was stirred at -78 °C for 3.5 h, then warmed up to r.t. and quenched by addition of 1 M HCl (8 mL, pH = 1-2). The following extraction was made using Et₂O and the organic phase was dried over anhydrous Na₂SO₄, filtered and concentrated *in vacuo*. The crude was purified by column chromatography eluted with hexane/EtOAc (3:2), obtaining **115** as a white solid (0.900 g, yield 63%)



R_f = 0.55 (DCM/MeOH, 95:5)

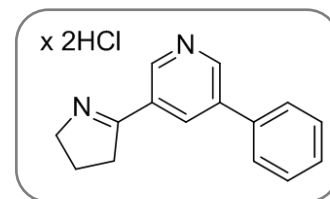
m.p. = 84-87 °C

¹H NMR (CDCl₃): δ 9.12 (d, *J* = 1.8 Hz, 1H), 8.99 (d, *J* = 2.1 Hz, 1H), 8.40 (t, *J* = 2.0 Hz, 1H), 7.61 (d, *J* = 7.2 Hz, 2H), 7.56 – 7.39 (m, 3H), 4.90 (br s, 1H), 3.36 – 3.16 (m, 2H), 3.11 (t, *J* = 7.0 Hz, 2H), 1.99 (p, *J* = 6.7 Hz, 2H), 1.42 (s, 9H).

¹³C NMR (CDCl₃): δ 198.49, 156.11, 151.77, 147.99, 136.74, 136.63, 133.46, 131.98, 129.20, 128.60, 127.16, 79.18, 39.87, 36.10, 28.34, 24.28.

3-(3,4-Dihydro-2H-pyrrol-1-ium-5-yl)-5-phenylpyridin-1-ium dichloride (37)

Previously prepared **115** (500 mg, 1.5 mmol) was solubilized in DCM (10 mL) and added dropwise by TFA (5 mL, 3.4 mL/mmol of starting material) at 0 °C. The reaction was stirred for 2 h at 0-5 °C and then quenched with 5 M NaOH (20 mL, pH = 10-12). The



water phase was extracted with DCM/*i*-PrOH (9:1) and the resulting organic phase was dried over anhydrous Na₂SO₄, filtered and concentrated in vacuum. The crude free base was obtained as a yellowish semi-solid (0.320 g, yield 98%). The free base (0.240 g, 1.08 mmol, 1 equiv) was dissolved in MeOH and 38% HCl (0.18 mL, 2.16 mmol, 2 equiv) was added dropwise at 0 °C. The crude was recrystallized with EtOH and the final compound **37** was obtained as colorless crystals (0.100 g, yield 30%)

R_f = 0.55 (DCM/MeOH, 98:2)

m.p. = 224-225 °C

MS [M]⁺ (C₁₅ H₁₄ N₂⁺) Calcd [M+H]⁺ 223.1230 and [M+Na]⁺ 245.1049 Found [M+H]⁺ 223.1240 and [M+Na]⁺ 245.1046.

¹H NMR (CD₃OD): δ 9.24 (d, *J* = 1.9 Hz, 1H), 9.15 (d, *J* = 2.0 Hz, 1H), 8.71 (t, *J* = 2.1 Hz, 1H), 7.81 (d, *J* = 7.5 Hz, 2H), 7.59 (t, *J* = 7.5 Hz, 2H), 7.53 (t, *J* = 7.4 Hz, 1H), 4.34 (t, *J* = 7.8 Hz, 2H), 3.77 (t, *J* = 8.2 Hz, 2H), 2.55 – 2.48 (m, 2H).

¹³C NMR (CD₃OD): 153.31, 148.33, 137.71, 135.55, 135.43, 129.20, 129.10, 127.10, 123.31, 54.42, 35.23, 24.82, 19.71.

7.1.3.2 Synthesis of *meta*-CF₃ phenyl substituted KC-1 derivative 39*3-Bromo-5-(3-(trifluoromethyl)phenyl)pyridine (116)*

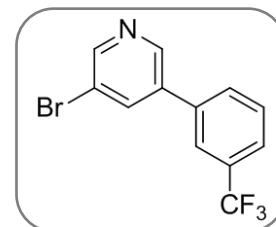
Under inert conditions, to a degassed solution of the commercially available 2,6-dibromopyridine (2 g, 8.4 mmol, 1.18 equiv), in 1,2-dimethoxyethane, Pd(PPh₃)₄ (0.165 g, 0.143 mmol, 0.02 equiv) was added and the mixture was stirred at r.t. for 15 min. A degassed aqueous solution of 2 M K₂CO₃ (3.30 g, 24 mmol in 12 mL of H₂O, 3.35 equiv) was added and the mixture was stirred for additional 5 min. Finally, the commercially available (3-(trifluoromethyl)phenyl)boronic acid (1.35 g, 7.15 mmol, 1 equiv) was added and the reaction was refluxed for 6 h. Upon completion, the reaction was cooled down and 1 M NaOH was added; the water phase was extracted using Et₂O. The resulting organic phase was dried over anhydrous Na₂SO₄, filtered and concentrated under reduced pressure. The crude was purified by column chromatography eluted with hexane/EtOAc (4:1) and **116** was obtained as a hygroscopic white solid (1.14 g, yield 50%).

R_f = 0.55 (DCM/MeOH, 95:5)

m.p. = 39-40 °C

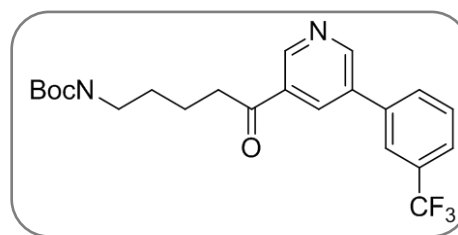
¹H NMR (CDCl₃): δ 8.77 (s, 1H), 8.73 (s, 1H), 8.05 (s, 1H), 7.81 (s, 1H), 7.79 – 7.58 (m, 3H).

¹³C NMR (CDCl₃): δ 150.03, 148.92, 146.11, 140.62, 136.66, 132.05, 131.73, 131.30, 130.87, 130.28, 129.64, 129.16, 125.55, 121.94, 118.32, 125.31, 125.26, 125.21, 125.16, 123.88, 123.83, 123.78, 123.73, 120.61.



tert-Butyl (5-oxo-5-(5-(3-(trifluoromethyl)phenyl)pyridin-3-yl)pentyl)carbamate
(117)

Under anhydrous and inert conditions, 1.5 M *n*BuLi in hexane (1.1 mL, 1.62 mmol, 1 equiv) was dissolved in dry Et₂O (10 mL) and cooled down at -78 °C. A solution of 3-bromo-5-(3-trifluoromethyl)phenyl)pyridine **116** (500 mg, 1.62 mmol, 1 equiv) in dry Et₂O (5



mL) was slowly added dropwise giving a red-orange solution, which was stirred at r.t. for 45 min., darkening after 30 min. Finally, the mixture was cooled down to -78 °C again and the addition of *tert*-butyl 2-oxopiperidine-1-carboxylate (0.322 g, 1.62 mmol, 1 equiv) solubilized in dry Et₂O (4 mL) was carried out, slowly obtaining an orange solution. The mixture was stirred at -78 °C for 1 h, then warmed up to 0 °C and quenched by addition of 1 M HCl (8 mL, pH = 6-7). The following extraction was made using Et₂O and the organic phase was dried over anhydrous Na₂SO₄, filtered and concentrated in vacuum. The crude was purified by column chromatography eluted by hexane/EtOAc (3:2), giving **117** as a yellowish solid (380 mg, yield 55%).

R_f = 0.41 (DCM/MeOH, 95:5)

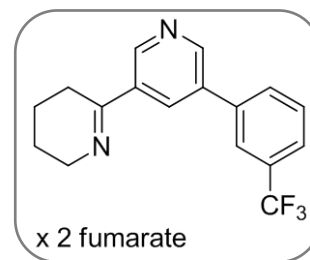
m.p. = 74-76 °C

¹H NMR (CDCl₃): δ 9.17 (s, 1H), 9.00 (s, 1H), 8.40 (s, 1H), 7.89 – 7.57 (m, 5H), 4.62 (br s, 1H), 3.28 – 2.99 (m, 4H), 1.90 – 1.73 (m, 2H), 1.67 – 1.51 (m, 2H), 1.42 (s, 9H).

¹³C NMR (CDCl₃): δ 198.40, 156.04, 151.46, 148.58, 137.49, 135.27, 133.46, 131.11, 131.69, 131.26, 130.83, 132.06, 130.46, 129.70, 129.16, 125.56, 121.94, 118.33, 125.22, 125.17, 125.12, 125.07, 123.90, 123.85, 123.80, 123.75, 78.76, 39.86, 38.37, 29.40, 28.23, 20.78.

5'-(3-(Trifluoromethyl)phenyl)-3,4,5,6-tetrahydro-2,3'-bipyridinium fumarate (39)

Previously prepared **117** (250 mg, 0.56 mmol) was solubilized in DCM (4 mL) and added dropwise by TFA (2 mL, 3.4 mL/mmol of starting material) at 0 °C. The cloudy orange solution was stirred for 3.5 h at 0-5 °C and then quenched with 5 M NaOH (20 mL, pH = 10-12). The water phase was extracted from DCM and the resulting organic phase was dried over anhydrous Na₂SO₄, filtered and concentrated in vacuum. The crude free base was obtained as a yellow semi-solid (0.150 g, yield 88%). The free base (145 mg, 0.50 mmol, 1 equiv) was dissolved in MeOH and fumaric acid (14 mg, 0.125 mmol, 1 equiv) was added portionwise at 0 °C. MeOH was evaporated, the orangish semi-solid crude was washed with Et₂O and a yellowish solid crashed out. The latter was recrystallized from Et₂O and the final compound **39** was obtained as a light yellow solid (30 mg, 12% yield).



R_f = 0.48 (DCM/MeOH, 95:5)

m.p. = 145-147 °C

MS [M]⁺ (C₁₇ H₁₅ F₃ N₂⁺) Calcd [M+H]⁺ 305.1260 Found [M+H]⁺ 305.1265.

¹H NMR (CD₃OD): δ 8.43 (s, 1H), 8.20 – 7.84 (m, 2H), 7.74 (m, 2H), 6.72 (s, 4H), 3.84 (t, *J* = 6.5 Hz, 2H), 1.99 – 1.61 (m, 3H), (H⁺ in position 2 and 6 of pyridine ring and H⁺ on C3 position of cyclic imine are exchanged with deuterium).

¹³C NMR (CD₃OD): δ 162.21, 148.56, 146.23, 138, 132.91, 131.34, 130.74, 129.98, 125, 123.70, 49, 26.84, 20.81, 18.50.

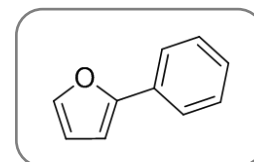
7.1.3.3 Synthesis of KC-1 derivatives 38 and 40

7.1.3.3.1 General procedure for the preparation of intermediates 118 and 119 via Suzuki-Miyaura reaction between 2-bromofuran and differently substituted phenyl boronic acids.

Under inert conditions, a sealed vial was loaded with a degassed solution of 2-bromofuran (1.10 equiv) in 1,2-dimethoxyethane. Pd(PPh₃)₄ (0.03 equiv) was added and an orange suspension was obtained, which turned into an orange solution after few minutes. The mixture was stirred at r.t. for 15 min and the appropriate boronic acid (1 equiv) and a degassed aqueous solution of 2 M Na₂CO₃ (4 equiv) were added, obtaining a yellow solution. The reaction was stirred at 50-60 °C for 6 h. Upon completion, the reaction was cooled down and DME was evaporated; deionized water was added and extracted by DCM. The resulting organic phase was dried over anhydrous Na₂SO₄, filtered and concentrated under reduced pressure. The crude was purified by column chromatography eluted with hexane.

2-Phenylfuran (**118**)

The starting intermediate 2-phenylfuran was prepared following the general procedure from commercially available 2-bromofuran (3 g, 20.4 mmol, 1.10 equiv), commercially available phenyl boronic acid (2.25 g, 18.5 mmol, 1 equiv),



Pd(PPh₃)₄ (0.715 g, 0.62 mmol, 0.03 equiv), 2 M Na₂CO₃ (8.20 g, 78 mmol in 39 mL of H₂O, 4 equiv). After standard work-up and purification by column chromatography eluted with hexane, **118** was obtained as a yellowish oil (1.60 g, yield 62%).

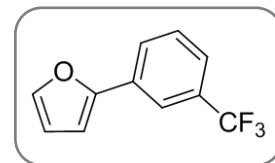
R_f = 0.52 (hexane)

¹H NMR (CDCl₃): 7.67 (d, *J* = 7.8 Hz, 1H), 7.45 (s, 1H), 7.37 (t, *J* = 7.6 Hz, 1H), 7.24 (t, *J* = 7.6 Hz, 1H), 6.63 (d, *J* = 3.2 Hz, 1H), 6.45 (t, *J* = 3.2 Hz, 1H).

¹³C NMR (CDCl₃): δ 149.53, 146.55, 138.37, 136.98, 136.44, 129.39, 128.89, 127.35, 121.11.

2-(3-(Trifluoromethyl)phenyl)furan (**119**)

The starting intermediate 2-(3-(trifluoromethyl)phenyl)furan **119** was prepared following the general procedure from commercially available 2-bromofuran (3 g, 20.4 mmol, 1.10 equiv), commercially available (3-trifluoromethyl)phenyl boronic acid (3.5 g, 18.5 mmol, 1 equiv), Pd(PPh₃)₄ (0.715 g, 0.62 mmol, 0.03 equiv), 2 M Na₂CO₃ (8.20 g, 78 mmol in 39 mL of H₂O, 4 equiv). After standard workup and purification by column chromatography eluted with hexane, **119** was obtained as a colorless oil (3 g, yield 77%).



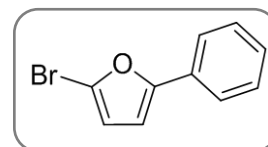
R_f = 0.58 (hexane)

¹H NMR (CDCl₃): δ 7.93 (s, 1H), 7.87 – 7.80 (m, 1H), 7.53 – 7.47 (m, 3H), 6.75 (d, *J* = 3.1 Hz, 1H), 6.51 (t, *J* = 3.1 Hz, 1H).

¹³C NMR (CDCl₃): δ 148.70, 147.02, 137.94, 137.16, 135.62, 129.54, 128.43, 128.02, 127.28, 124.10, 120.89.

2-Bromo-5-phenylfuran (**120**)

118 (1 g, 6.9 mmol, 1 equiv) was dissolved in DMF (6 mL) and *N*-bromosuccinimide (1.4 g, 7.6 mmol, 1.1 equiv) was added portionwise at 0 °C. During the addition, the solution turned into orange, green and orange again after addition of a small amount of DMF. The reaction was stirred at 0 °C for 1 h and then poured into deionized water/ice. The extraction was carried out using the minimum amount of DCM; the organic phase was additionally washed with brine. The organic solution was dried over anhydrous Na₂SO₄, filtered and concentrated *in vacuo*; the crude was purified by column chromatography eluted by hexane. Compound **120** was obtained as an orange oil (0.750 g, yield 52%).



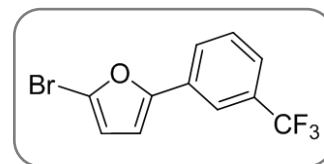
R_f = 0.55 (hexane)

¹H NMR (CDCl₃): δ 7.63 (dd, *J* = 8.4, 1.2 Hz, 2H), 7.44 – 7.33 (m, 2H), 7.33 – 7.22 (m, 1H), 6.60 (d, *J* = 3.4 Hz, 1H), 6.39 (d, *J* = 3.4 Hz, 1H).

¹³C NMR (CDCl₃): δ 156.06, 130.01, 128.89, 127.89, 123.62, 121.58, 113.57, 107.50.

2-Bromo-5-(3-(trifluoromethyl)phenyl)furan (121)

119 (2 g, 9.4 mmol, 1 equiv) was dissolved in DMF (6 mL) and *N*-bromosuccinimide (1.7 g, 9.4 mmol, 1 equiv) was added portionwise at 0 °C. The reaction was stirred at 0 °C for 1 h and then poured into deionized water/ice. The extraction was carried out using the minimum amount of DCM; the organic phase was additionally washed with brine. The organic solution was dried over anhydrous Na₂SO₄, filtered and concentrated in vacuum, then purified by column chromatography eluted by hexane. Compound **121** was obtained as an orange oil (2.4 g, yield 89%).



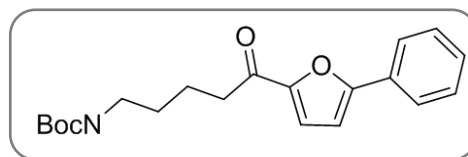
R_f = 0.57 (hexane)

¹H NMR (CDCl₃): δ 7.86 (s, 1H), 7.80 – 7.74 (m, 1H), 7.52 – 7.47 (m, 2H), 6.69 (d, *J* = 3.4 Hz, 1H), 6.42 (d, *J* = 3.4 Hz, 1H).

¹³C NMR (CDCl₃): δ 157.01, 131.79, 131.23, 129.72, 128.66, 127.20, 126.50, 124.03, 120.50, 112.13, 107.68.

tert-Butyl (5-oxo-5-(5-phenylfuran-2-yl)pentyl)carbamate (**122**)

Under inert and anhydrous conditions, 1.5 M *n*BuLi in dry hexane (2.1 mL, 3.14 mmol, 1 equiv) was dissolved in dry Et₂O and cooled down at -78 °C. A solution of previously prepared 2-bromo-5-phenylfuran **120** (0.700 g, 3.14 mmol, 1 equiv) in dry Et₂O (14 mL) was slowly added dropwise, obtaining an initial yellow solution that turned into orange during the addition. The reaction was slowly warmed up at r.t. and darkened during stirring for 1 h. The mixture was cooled down at -78 °C again, added dropwise by a dry solution of commercially available *tert*-butyl 2-oxopiperidine-1-carboxylate (0.625 g, 3.14 mmol, 1 equiv) in Et₂O (5.5 mL) and stirred for 1 h. The reaction was warmed up to 0 °C and quenched by addition of deionized water and 1 N HCl (pH = 2). The two phases were separated, the organic solvent was dried over anhydrous Na₂SO₄, filtered and concentrated under vacuum. The crude was partially purified by column chromatography, eluted with DCM/MeOH (96:4) and the dark oil obtained was kept at low temperature overnight. The brownish semi-solid obtained was triturated with hexane, obtaining the off-white solid **122** that was separated and additionally washed with fresh hexane (0.600 g, yield 56%).



R_f = 0.53 (DCM/MeOH, 95:5)

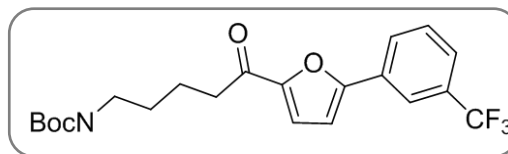
m.p. = 68-70 °C

¹H NMR (CDCl₃): δ 7.79 (dd, *J* = 8.3, 1.4 Hz, 2H), 7.49 – 7.31 (m, 3H), 7.27 (d, *J* = 3.8 Hz, 1H), 6.78 (d, *J* = 3.6 Hz, 1H), 4.60 (br s, 1H), 3.22 – 3.13 (m, 2H), 2.91 (t, *J* = 7.3 Hz, 2H), 1.79 (p, *J* = 6.8 Hz, 2H), 1.65 – 1.51 (m, 2H), 1.44 (s, 9H).

¹³C NMR (CDCl₃): δ 188.81, 157.49, 155.98, 151.70, 132.16, 129.33, 129.15, 128.84, 124.90, 119.17, 107.33, 79.02, 40.14, 37.72, 29.61, 28.39, 21.34.

tert-Butyl (5-oxo-5-(5-(3-(trifluoromethyl)phenyl)furan-2-yl)pentyl)carbamate (**123**)

Under inert and anhydrous conditions, 1.5 M *n*BuLi in dry hexane (2.15 mL, 3.23 mmol, 1 equiv) was dissolved in dry Et₂O (6 mL) and cooled



down at -78 °C. A solution of previously prepared 2-bromo-5-(3-(trifluoromethyl)phenyl)furan **121** (1 g, 3.23 mmol, 1 equiv) in dry Et₂O (14 mL) was slowly added dropwise, obtaining a green solution. The reaction mixture slowly warmed up at r.t. and darkened during stirring for 1 h. The mixture was cooled down at -78 °C again, added dropwise by a dry solution of *tert*-butyl 2-oxopiperidine-1-carboxylate (0.644 g, 3.23 mmol, 1 equiv) in Et₂O and stirred for 1 h. The reaction was warmed up to r.t. and quenched by addition of deionized water and 1 N HCl (pH = 2). The two phases were separated, the organic solvent dried over anhydrous Na₂SO₄, filtered and concentrated under vacuum. The crude was partially purified by column chromatography, eluted with DCM/MeOH (95:5); the dark oil obtained was dissolved in hexane/Et₂O and kept at low temperature overnight. A brownish semi-solid precipitated and, after the separation of the organic solvent, it was additionally washed with fresh hexane to afford compound **123** as an off-white solid (0.500 g, yield 40%).

R_f = 0.50 (DCM/MeOH, 95:5)

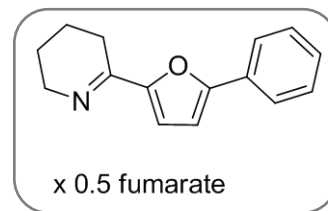
m.p. = 91-93 °C

¹H NMR (CDCl₃): δ 8.08 – 7.88 (m, 2H), 7.71 – 7.45 (m, 2H), 7.29 (d, *J* = 3.7 Hz, 1H), 6.86 (d, *J* = 3.6 Hz, 1H), 4.59 (br s, 1H), 3.23 – 3.10 (m, 2H), 2.92 (t, *J* = 7.2 Hz, 2H), 1.80 (p, *J* = 6.8 Hz, 2H), 1.67 – 1.55 (m, 2H), 1.44 (s, 5H).

¹³C NMR (CDCl₃): δ 188.83, 156.00, 155.69, 152.17, 132.11, 131.67, 131.24, 130.81, 130.11, 129.47, 129.17, 127.93, 128.56, 121.95, 118.34, 125.61, 125.56, 125.51, 125.46, 121.67, 121.62, 121.57, 121.52, 119.04, 108.45, 79.08, 40.11, 37.79, 29.59, 28.37, 21.21.

6-(5-Phenylfuran-2-yl)-2,3,4,5-tetrahydropyridinium fumarate (38)

Previously prepared **122** (0.500 g, 1.46 mmol) was solubilized in DCM (4 mL) and added dropwise by TFA (5.25 mL, 3.6 mL/mmol of starting material) at 0 °C. The initial orange solution turned into dark green and finally into dark brown; the mixture was stirred for 1 h at 0-5 °C and then quenched with 5 M NaOH (pH = 10-12). The water phase was extracted from DCM and the resulting organic phase was dried over Na₂SO₄, filtered and concentrated *in vacuo*. The crude free base was obtained as a brown oil (0.300 g, yield 91%). The free base (0.300 g, 1.33 mmol, 1 equiv) was dissolved in MeOH and fumaric acid (0.077 g, 0.665 mmol, 1 equiv) was added portionwise at 0 °C. MeOH was evaporated, the red solid crude was recrystallized by MeOH/EtOH and the final compound **38** was obtained as red crystals (0.300 g, yield 50%).



R_f = 0.38 (DCM/MeOH, 95:5)

m.p. = 177-180 °C

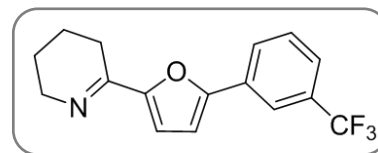
MS [M]⁺ (C₁₅ H₁₅ O N₂⁺) Calcd [M+H]⁺ 226.1226 Found [M+H]⁺ 226.1219.

¹H NMR (CD₃OD): δ 7.98 (dd, *J* = 7.8, 1.8 Hz, 2H), 7.80 (d, *J* = 4.0 Hz, 1H), 7.64 – 7.38 (m, 3H), 7.22 (d, *J* = 4.0 Hz, 1H), 6.71 (s, 1H), 3.80 (t, *J* = 5.6 Hz, 2H), 2.13 – 1.82 (m, 2H) (protons on C3 position of cyclic imine were exchanged with deuterium).

¹³C NMR (CD₃OD): δ 168.76, 161.66, 144.96, 134.42, 130.24, 128.86, 128.14, 125.64, 125.31, 109.12, 44.12, 19.72, 16.44.

6-(5-(3-(Trifluoromethyl)phenyl)furan-2-yl)-2,3,4,5-tetrahydropyridinium fumarate
(40)

Previously prepared **123** (0.400 g, 0.972 mmol) was solubilized in DCM and added dropwise by TFA (3.5 mL, 3.6 mL/mmol of starting material) at 0 °C, obtaining a green solution. The mixture was stirred for 1 h at 0-5 °C and then quenched with 5 M NaOH (pH = 10-12). The water phase was extracted with DCM and the resulting organic phase was dried over anhydrous Na₂SO₄, filtered and concentrated *in vacuo*. The crude free base was obtained as a brown semi-solid (0.280 g, yield 98%).



The free base (0.260 g, 0.89 mmol, 1 equiv) was dissolved in MeOH and fumaric acid (0.052 g, 0.45 mmol, 0.5 equiv) was added portionwise at 0 °C. MeOH was evaporated and several recrystallization attempts were carried out with different combinations of solvents; a precipitate was obtained which was treated with 1 M NaOH and the corresponding free base of **40** was provided as red oil (0.050 g, yield 14%).

R_f = 0.50 (DCM/MeOH, 95:5)

MS [M]⁺ (C₁₆H₁₄F₃NO) Calcd [M+H]⁺ 294.1100 Found [M+H]⁺ 294.1090.

¹H NMR (CDCl₃): δ 8.03 – 7.86 (m, 2H), 7.57 – 7.44 (m, 2H), 6.85 (d, *J* = 3.5 Hz, 1H), 6.79 (d, *J* = 3.6 Hz, 1H), 3.85 (t, *J* = 4.0 Hz, 2H), 2.61 (t, *J* = 6.4 Hz, 2H), 1.92 – 1.62 (m, 4H).

¹³C NMR (CDCl₃): 158.01, 153.72, 153.20, 131.01, 129.25, 127.43, 125.10, 124.31, 121.05, 121.00, 119.95, 108.01, 49.62, 26.12, 22.13, 19.15.

7.2 Electrophysiological studies

7.2.1 Materials and methods

Human $\alpha 7$ nAChR was expressed in *Xenopus laevis* and electrophysiological recordings were conducted using OpusXpress 6000A (two-voltage clamping) (Molecular Devices, Union City, CA). The voltage and current electrodes were filled with 3 M KCl and continuous Ringer-s solution flux (115 mM NaCl, 2.5 mM KCl, 1.8 mM CaCl₂, 10 mM HEPES, and 1 μ M atropine, pH = 7.2) at 2 ml/min was used during the experiment. Oocytes were voltage-clamped at -60 mV. The average of two initial application of ACh was used as control response and considered to normalize the following responses.

The drug solution was obtained either in deionized water or DMSO and the drug application was carried out in 12 seconds, followed by 181 seconds of washout.

The control ACh was purchased from Sigma-Aldrich Chemical Company (St. Louis, MO) and concentration used was 60 μ M. The responses were calculated as both peak current amplitudes and net charge. Data were analyzed by Clampfit 10.3 and were expressed as means \pm SEM from at least four oocytes for each experiment.

Experiment on $\alpha 4\beta 2$ and $\alpha 3\beta 4$ were run employing similar conditions; the ACh control concentration was 100 μ M for $\alpha 4\beta 2$ and 30 μ M for $\alpha 3\beta 4$.

Data were collected at 50 Hz, filtered at 20 Hz, and analyzed by Clampfit 10.3 (Molecular Devices) and Excel (Microsoft, Redmond, WA). Data were expressed as means \pm SEM from at least five oocytes for each experiment, unless otherwise stated, and plotted by Kaleidagraph 4.1 (Abelbeck Software, Reading, PA).

Comparisons of results were made using t-tests between the groups of experimental values. A value of $P < 0.05$ was used to constitute the level of significance.

NS6740 and its derivatives investigation on $\alpha 7$:

Two-shot experiment: application of two initial 60 μ M ACh pre-controls, followed by test drug application at different concentrations (1, 3, 10, 30 μ M test drug). Then, 60 μ M ACh post-control was delivered to determine the receptor desensitization, followed by 10 μ M type II PAM PNU-120596 to determine the residual receptor potentiation. Finally, 60 μ M ACh post-control determine the desensitization or rundown of the receptors.

One-shot experiment: application of two initial 60 μM ACh pre-controls, followed by test drug application at different concentrations (1, 3, 10, 30 μM test drug) co-applied with 10 μM type II PAM PNU-120596, to determine the receptor potentiation. Finally, 60 μM ACh post-control determine the desensitization or rundown of the receptors.

Investigation of 13 and 17 on $\alpha 4\beta 2$: application of two initial 30 μM ACh pre-controls, followed by 100 μM test drug application to determine the agonist activity. Finally, 30 μM ACh post-control is delivered.

Investigation of agonist activity of 12, 22-24, 27 and 32 on $\alpha 4\beta 2$ and $\alpha 3\beta 4$: application of two initial 100 ($\alpha 3\beta 4$) or 30 ($\alpha 4\beta 2$) μM ACh pre-controls, followed by 30 μM test drug to determine the agonist activity. Finally, 100 ($\alpha 3\beta 4$) or 30 ($\alpha 4\beta 2$) μM ACh post-control is delivered, to determine the receptor desensitization.

Investigation of competitive antagonist activity of 12, 22-24, 27 and 32 on $\alpha 4\beta 2$ and $\alpha 3\beta 4$: application of two initial 100 ($\alpha 3\beta 4$) or 30 ($\alpha 4\beta 2$) μM ACh pre-controls, followed by 30 μM test drug co-applied with 100 ($\alpha 3\beta 4$) or 30 ($\alpha 4\beta 2$) μM ACh control to determine the competitive antagonist activity. Finally, 100 ($\alpha 3\beta 4$) or 30 ($\alpha 4\beta 2$) μM ACh post-control is delivered, to determine the receptor desensitization.

Recovery study of NS6740 and 27: application of two initial 60 μM ACh pre-controls, followed by 10 μM test drug. Then, six applications of 60 μM ACh post-control are applied at increasing time points to determine the sustained receptor desensitization. Finally, 10 μM type II PAM PNU-120596 is applied to determine the residual receptor potentiation.

CRCs curves for 13 and 17: after two initial 60 μM ACh pre-controls, increasing concentrations (0.1, 0.3, 1, 3, 10, 30 μM) of test drug are applied. Each application is followed by 60 μM ACh pre-control to determine the receptor desensitization.

KC-1 and its derivatives investigation on $\alpha 7$:

Investigation of agonist activity: application of two initial 60 μM ACh pre-controls, followed by 100 μM of test drug and final 60 μM ACh post-control to determine the receptor desensitization.

Investigation of competitive antagonist activity: application of two initial 60 μM ACh pre-controls, followed by 100 μM of test drug co-applied with 60 μM ACh control and final 60 μM ACh post-control to determine the receptor desensitization.

Investigation of receptor potentiation: application of two initial 60 μM ACh pre-controls, followed by 100 μM test drug co-applied with 10 μM type II PAM PNU-120596 and final 60 μM ACh post-control to determine the receptor desensitization.

Investigation of agonist activity of KC-1 and 34-37 on $\alpha 4\beta 2$: application of two initial 30 μM ACh pre-controls, followed by 100 μM test drug to determine the agonist activity. Finally, 30 μM ACh post-control is delivered, to determine the receptor desensitization.

Investigation of competitive antagonist activity of KC-1 and 34-37 on $\alpha 4\beta 2$: application of two initial 30 μM ACh pre-controls, followed by 100 μM test drug co-applied with 30 μM ACh control to determine the competitive antagonist activity. Finally, 30 μM ACh post-control is delivered, to determine the receptor desensitization.

Investigation of NS6740, 28 and 33 on h $\alpha 7\text{S}36\text{V}$ and h $\alpha 7\text{S}36\text{A}$: two-shot and one shot experiments were carried out employing the same protocols already described for the WT, using 30 μM test drug, 60 μM ACh control and 10 μM type II PAM PNU-120596.

7.3 *In silico* studies

7.3.1 Materials and methods

Ligand molecules investigated were hand-drawn with MolView and structurally adjusted and protonated using Molden 5.0.

HF/6-31G* optimization followed by a B3LYP/6-31G** optimization were employed. Generated potential output files were converted to .mol2. Employing Schrödinger Suite 2004-2, ligand preparation was carried out with Lig-Prep program: the possible states were generated at target pH = 7 ± 2 using Epik and for each compound three low energy ring conformations were generated. Upon preparation, the ligands were docked on each interface of Homology Model 2 (HM2). Extra-precision Glide was used and the following parameters were employed:

- Flexible ligand sampling
- Addition of Epik state penalties to docking score
- Intramolecular hydrogen bond were rewarded
- Planarity of conjugated pi atom was enhanced
- Post-docking minimization was applied

All poses were ranked based on GlideScore and only protonated forms were considered for the analysis.

Abbreviations

Abbreviations

General Abbreviations

ACh: Acetylcholine; CNS: central nervous system; PNS: peripheral nervous system; nAChR: nicotinic acetylcholine receptor; LGIC: ligand gated ion channel; GABA_AR: gamma aminobutyric acid receptor A; GlyR: glycine receptor; ECD: extracellular domain; MIR: main immunogenic region; TM: transmembrane; TMD: transmembrane domain; ICD: intracellular domain; CICR: calcium-induced calcium release; VGCC: voltage gated calcium channel; ADHD: attention deficit hyperactivity disorder, cryo-EM: cryogenic electron microscopy; ACh-BP: acetylcholine-binding protein; LBS: ligand binding site; HM2: homology model 2; PAM: positive allosteric modulation; DAA: direct allosteric activation; ER: endoplasmic reticulum; GPBC: G-protein binding cluster; PLC: phospholipase C; IP₃: inositol-3-phosphate; IL-: interleukin; TNF- α : tumor necrosis factor alpha; JAK/STAT: Janus kinase/Signal Transducer and Activator of Transcription protein; NF- κ B: nuclear factor kappa-light-chain-enhancer of activated B cells; (PI3K)/Akt/Nrf-2: phosphatidylinositol 3'-kinase/protein kinase B/nuclear factor erythroid 2-related factor 2; I- κ B: IkappaB kinase; HO-1: heme-oxygenase-1; diEdiMA: diethyldimethylammonium; triEMA: triethylammonium; IA: inhibitory avoidance; LPS: lipopolysaccharide; CCI: chronic constrictive nerve injury; Δ PD: ipsilateral paw diameter; MLA: methyllycaconitine; KO: knock out; i.p.: intraperitoneally; CRC: concentration-response curve; WT: wild type.

Solvents

DCM or CH₂Cl₂: dichloromethane; CHCl₃: chloroform; MeOH: methanol; EtOH: ethanol; EtOAc: ethyl acetate; THF: tetrahydrofuran; Et₂O: diethyl ether; H₂O: water; DMSO: dimethyl sulfoxide; DMF: dimethylformamide; CDCl₃: deuterated chloroform; CD₃OD: deuterated methanol; (CD₃)₂SO: deuterated dimethyl sulfoxide; (CD₃)₂CO: deuterated acetone. DMF: *N,N*-Dimethylformamide; DME: dimethoxyethane; THF: tetrahydrofuran; *iPr*-OH: isopropanol; DME/H₂O: dimethoxyethane/water; CH₃CN: acetonitrile.

Reagents

Na₂SO₄: sodium sulfate, NaHCO₃: sodium bicarbonate; Na₂CO₃: sodium carbonate; K₂CO₃: potassium carbonate; HCl: hydrochloric acid; H₂: hydrogen; Pd/C: palladium on carbon; BH₃ in THF: borane tetrahydrofuran complex; *n*BuLi: *n*-butyl lithium; Et₃N: trimethylamine; Boc: *tert*-butoxycarbonyl; DMAP: 4-(Dimethylamino)pyridine; Cs₂CO₃: cesium carbonate; MeI: iodomethane; NH₂OH·HCl: hydroxylamine hydrochloride; CH₃COONa: sodium acetate; H_{*n*+2}P_{*n*}O_{*3n*+1}: poliphosphoric acid;

LiAlH₄: lithium aluminum hydride; TsCl: tosyl chloride; HBr/AcOH: bromidic acid/acetic acid; KOH: potassium hydroxide; H₂SO₄: sulfuric acid; Pd(PPh₃)₄: tetrakis(triphenylphosphine)palladium(0); NaNO₂: sodium nitrite; KI: potassium iodide; NaOH: sodium hydroxide; LiOH: lithium hydroxide; SOCl₂: thionyl chloride; TEA: triethylamine; HCl/MeOH: hydrochloric acid in methanol; HCHO: formaldehyde; NaBH₃CN: sodium cyanoborohydride; NBS: N-bromo succinimide.

Analytical characteristics:

GENERAL – m.p.: melting point; °C: Celsius degree; r.t: room temperature; h: hours; min: minutes; equiv.: equivalents;

NMR Spectroscopy – MHz: megaHertz; δ : chemical shift (ppm); ppm: parts per million; *J*: NMR coupling constant; Hz: Hertz; s: singlet; br s: broad singlet; d: doublet; dd: double of doublets; ddd: double of doublet of doublet; dt: double of triplets; t: triplet; q: quartet; m: multiplet.

MASS Spectroscopy – *m/z*: mass to charge ratio; M⁺: molecular ion.

CHROMATOGRAPHY – *R_f* : retention factor.

References

-
- [1] C. Gotti and F. Clementi, "Neuronal nicotinic receptors: from structure to pathology" *Prog. Neurobiol.* 74, 363–396, 2004.
- [2] A. A. Jensen, B. Frølund, T. Liljefors and P. Krosgaard-Larsen, "Neuronal Nicotinic Acetylcholine Receptors: Structural Revelations, Target Identifications, and Therapeutic Inspirations" *J. Med. Chem.* 48, 4705-4744, 2005.
- [3] N. R. Romanelli and F. Gualtieri, "Cholinergic Nicotinic Receptors: Competitive Ligands, Allosteric Modulators, and their potential applications" *Med. Res. Rev.* 23, 393-426, 2003.
- [4] R. L. Papke, "Merging old and new perspectives on nicotinic acetylcholine receptors" *Biochem. Pharmacol.* 89, 1-11, 2014.
- [5] D. Manetti, C. Bellucci, N. Chiaramonte, S. Dei, E. Teodori and M. Romanelli, "Designing selective modulators for the nicotinic receptor subtypes: challenges and opportunities" *Fut. Med. Chem.* 10, 4, 433-459, 2018.
- [6] J.P. Changeux, "Nicotine addiction and nicotinic receptors: lessons from genetically modified mice" *Nat. Rev. Neurosci.* 11, 389-401, 2010.
- [7] R. Exley and S. Cragg, "Presynaptic nicotinic receptors: a dynamic and diverse cholinergic filters of striatal dopamine neurotransmission" *Br. J. Pharm.* 153, S283-S297, 2008.
- [8] J. Corradi and C. Bouzat, "Understanding the Bases of Function and Modulation of $\alpha 7$ Nicotinic Receptors: Implications for Drug Discovery" *Mol. Pharmacol.* 90, 288-299, 2016.
- [9] I. B. Levitan, "MODULATION OF ION CHANNELS BY PROTEIN PHOSPHORYLATION AND DEPHOSPHORYLATION" *Annu. Rev. Physiol.* 56, 193-212, 1994.
- [10] S. L. Swope, T. C. Moss, C. D. Blackstone and R. D. Huganir, "Phosphorylation of ligand-gated ion channels: a possible mode of synaptic plasticity" *FASEB J.* 6, 2514-2523, 1992.
- [11] X. Cheng, I. Ivanov, H. Wang, S. M. Sine and J. A. McCammon, "Nanosecond-Timescale Conformational Dynamics of the Human $\alpha 7$ Nicotinic Acetylcholine Receptor" *Biophys. J.* 93, 2622–2634, 2007.
- [12] G. Sharma and S. Vijayaraghavan, "Modulation of presynaptic store calcium induces releases of glutamate and postsynaptic firing," *Neuron.* 38, 929-939, 2003.
- [13] D. A. Rusakov, "Ca²⁺-dependent mechanism of presynaptic control at central synapses," *Neuroscience*, 12, 317-326, 2006.

- [14] P. Newhouse, A. Singh and A. Potter, "Nicotine and nicotinic receptor involvement in neuropsychiatric disorders" *Curr. Top. Med. Chem.* 4, 3, 267-282, 2004.
- [15] R. Shytle, A. Silver, M. B. Newman, D. V. Sheehan and P. R. Sanberg, "The Nicotinic Acetylcholine Receptor as a target for Antidepressant Drug development," *Mol. Psychiatr.* 7, 525-535, 2002.
- [16] N. Ripoll, M. Bronnec and M. Bourin, "Nicotinic receptors and schizophrenia" *Curr. Med. Res. Opin.* 20, 1057-1074, 2004.
- [17] S. Wonnacott, "Presynaptic nicotinic ACh receptors" *Trends in Neurosci.* 20, 2, 92-98, 1997.
- [18] J. A. Dani and D. Bertrand, "Nicotinic acetylcholine receptors and nicotinic cholinergic mechanisms of the central nervous system" *Annu. Rev. Pharmacol.* 47, 699-729, 2007.
- [19] M. Rosas-Ballina and K. J. Tracey, "Cholinergic control of inflammation" *J. Intern. Med.* 265, 6, 663-679, 2009.
- [20] C. Toyoshima and N. Unwin, "Ion channel of acetylcholine receptor reconstructed from images of post-synaptic membranes" *Nature* 336, 6169, 247-250, 1988.
- [21] N. Unwin, "Nicotinic Acetylcholine Receptor an 9 Å Resolution" *J. Mol. Biol.* 229, 4, 1101-1124, 1993.
- [22] N. Unwin, "Refined Structure of Nicotinic Acetylcholine Receptor at 4Å Resolution," *J. Mol. Biol.* 346, 967-989, 2005.
- [23] K. Brejc, W. J. van Dijk, R. V. Klaassen, M. Schuurmans, J. van der Oost, A. B. Smit and T. K. Sixma, "Crystal structure of an ACh-binding protein reveals the ligand-binding domain of nicotinic receptors" *Nature* 411, 269-276, 2001.
- [24] S. B. Hanse, G. Sulzenbacher, T. Huxford, P. Marchot, P. Taylor and Y. Bourne, "Structures of Aplysia AChBP complexes with nicotinic agonists and antagonists reveal distinctive binding interfaces and conformations" *EMBO J.* 346, 967-989, 2005.
- [25] S.-X. Li, S. Huang, N. Bren, K. Noridomi, C. . D. Dellisanti, S. M. Sine and L. Chen, "Ligand-binding domain of an $\alpha 7$ -nicotinic receptor chimera and its complex with agonist" *Nature Neurosci.* 14, 1253-1259, 2011.
- [26] N. Tabassum, Q. Ma, G. Wu, T. Jiang and R. Yu, "Exploring the binding energy profiles of full agonists, partial agonists, and antagonists of the $\alpha 7$ nicotinic acetylcholine receptor" *J. Mol. Model.* 23, 251-256, 2017.

- [27] K. Pesti, A. K. Szabo, A. Mike and E. S. Vizi, "Kinetic properties and open probability of $\alpha 7$ nicotinic acetylcholine receptors" *Neuropharmacology* 81, 111-115, 2014.
- [28] R. L. Papke and J. S. Thinschmidt, "The correction of alpha7 nicotinic acetylcholine receptor concentration-response relationships in *Xenopus* oocytes," *Neurosci. Lett.* 256, 163-166, 1998.
- [29] R. L. Papke and J. K. Porter Papke, "Comparative pharmacology of rat and human $\alpha 7$ nAChR conducted with net charge analysis" *Br. J. Pharmacol.* 137, 49-61, 2002.
- [30] D. K. Williams, C. Peng, M. R. Kimbrell and R. L. Papke, "Intrinsically Low Open Probability of alpha7 Nicotinic Acetylcholine Receptors Can Be Overcome by Positive Allosteric Modulation and Serum Factors Leading to the Generation of Excitotoxic Currents at Physiological Temperature," *Mol. Pharmacol.* 89, 746-759, 2012.
- [31] D. Bertrand and M. Gopalakrishnan, "Allosteric modulation of nicotinic acetylcholine receptors" *Biochem. Pharmacol.* 74, 8, 1155-1163, 2007.
- [32] M. D. Isaacson, N. A. Horenstein, C. Stokes, W. R. Kem and R. L. Papke, "Point-to-point ligand-receptor interactions across the subunit interface modulate the insulation and stabilization of conformational states of alpha7 nAChR by benzylidene anabaseines" *Biochem. Pharmacol.* 85, 6, 817-828, 2013.
- [33] D. K. Williams, J. Wang and R. L. Papke, "Investigation of the Molecular Mechanism of the $\alpha 7$ Nicotinic Acetylcholine Receptor Positive Allosteric Modulator PNU-120596 Provides Evidence for Two Distinct Desensitized States" *Mol. Pharmacol.* 80, 1013-1032, 2011.
- [34] B. J. Melancon, C. R. Hopkins, M. R. Mood, K. A. Emmitte, C. M. Niswender, A. Christopoulos, J. Conn and C. W. Lindsley, "Allosteric Modulation of Seven Transmembrane Spanning Receptors: Theory, Practice and Opportunities for Central Nervous System Drug Discovery" *J. Med. Chem.* 55, 4, 1445-1464, 2012.
- [35] J. H. Gronlien, M. Hakerud, H. Ween, K. Thorin-Hagene, C. A. Briggs, M. Gopalakrishnan and J. Malysz, "Distinct profiles of alpha 7 nAChR positive allosteric modulation revealed by structurally diverse chemotypes" *Mol. Pharmacol.* 72, 715-724, 2007.
- [36] A. Chatzidaki and N. S. Millar, "Allosteric modulation of nicotinic acetylcholine receptors" *Biochem. Pharmacol.* 97, 408-417, 2015.
- [37] R. L. Papke, C. Stokes, M. I. Damaj, G. A. Thaku, K. Manther, M. Treinin, D. Bagdas, A. R. Kulkarni and N. A. Horenstein, "Persistent Activation of $\alpha 7$ nicotinic ACh receptors associated with stable induction of different desensitized states" *Br. J. Pharmacol.* 175, 1838-1854, 2018.

- [38] N. A. Horenstein, R. L. Papke, A. R. Kulkarni, G. U. Chaturbhuj, C. Stokes, K. Manther and G. A. Takhur, "Critical Molecular Determinants of $\alpha 7$ Nicotinic Acetylcholine Receptor Allosteric Activation: separation of direct allosteric activation and positive allosteric modulation" *J. Biol. Chem.* 291, 5049-5067, 2016.
- [39] R. L. Papke, N. A. Horenstein, A. R. Kulkarni, C. Stokes, L. W. Corrie, C. Y. Maeng and G. A. Thakur, "The activity of GAT107, an allosteric activator and positive modulator of $\alpha 7$ nicotinic acetylcholine receptors (nAChR), is regulated by aromatic amino acids that span the subunit interface" *J. Biol. Chem.* 289, 7, 4515-4531, 2014.
- [40] R. L. Papke, K. Chojnacka and N. A. Horenstein, "The minimal pharmacophore for silent agonism of alpha7 nAChR," *J. Pharm. Exp. Ther.* 350, 665-680, 2014.
- [41] D. K. Williams, J. Wang and R. L. Papke, "Positive allosteric modulators as an approach to nicotinic acetylcholine receptor-targeted therapeutics: advantages and limitations" *Biochem. Pharmacol.* 82, 8, 915-930, 2011.
- [42] R. Lape, D. Colquhoun and L. G. Sivilotti, "On the nature of partial agonism in the nicotinic receptor superfamily" *Nature* 454, 722-727, 2008.
- [43] L. Chiodo, T. E. Malliavin, L. Maragliano and G. Cottone, "A possible desensitized state conformation of the human $\alpha 7$ nicotinic receptor: A molecular dynamic study" *Biophys Chem.* 229, 99-109, 2017.
- [44] N. Kabbani and R. A. Nichols, "Beyond the Channel: Metabotropic Signaling by Nicotinic Receptors" *Trends Pharmacol. Sci.* 39, 4, 354-366, 2018.
- [45] N. Kabbani, J. C. Nordman, B. A. Corgiat, D. P. Veltri, A. Shehu, V. A. Seymour and D. J. Adams, "Are nicotinic acetylcholine receptors coupled to G proteins?" *Bioessays* 35, 1025-1034, 2013.
- [46] N. Kabbani, "Proteomics of membrane receptors and signaling" *Proteomics* 8, 855-865, 2008.
- [47] S. G. Grant and W. P. Blackstock, "Proteomics in neuroscience: from protein to network" *J. Neurosci.* 21, 8315-8318, 2001.
- [48] J. A. Paulo, W. J. Brucker and E. Hawrot, "Proteomic Analysis of an $\alpha 7$ Nicotinic Acetylcholine Receptor Interactome" *J. Proteom. Res.* 8, 1849-1858, 2009.
- [49] N. Kabbani, M. P. Woll, R. Levenson, J. M. Lindstrom and J. Changeux, "Intracellular complexes of the beta 2 subunit of the nicotinic acetylcholine receptor in brain identified by proteomics" *PNAS* 105, 51, 20570-20575, 2007.

- [50] T. D. McClure-Begley, I. Esterlis, K. L. Stone, T. T. Lam, S. R. Grady, C. M. Colangelo, J. M. Lindstrom, M. J. Marks and M. R. Picciotto, "Evaluation of the Nicotinic Acetylcholine Receptor-Associated Proteome at Baseline and Following Nicotine Exposure in Human and Mouse Cortex" *eNeuro* 3, 4, 1-20, 2016.
- [51] J. C. Nordman, W. S. Philips, N. Kodama, S. G. Clark, C. Del Negro and N. Kabbani, "Axon Targeting of the Alpha 7 Nicotinic Receptor in Developing Hippocampal Neurons by Gpr116 Regulates Growth," *J. Neurochem.* 129, 4, 649-662, 2014.
- [52] J. R. King, J. C. Nordman, S. P. Bridges, M. Lin and N. Kabbani, "Identification and Characterization of a G Protein-binding Cluster in alpha 7 Nicotinic Acetylcholine Receptors" *J. Biol. Chem.* 290, 33, 20060-20070, 2015.
- [53] C. Stokes, M. Treinin and R. L. Papke, "Looking below the surface of nicotinic acetylcholine receptor" *Trends Pharmacol.* 36, 8, 514-523, 2015.
- [54] C. Zhong, D. A. Talmage and L. W. Role, "Nicotine Elicits Prolonged Calcium Signaling along Ventral Hippocampal Axons" *PLOS ONE* 8, 12, 1-14, 2013.
- [55] L. V. Borovikova, S. Ivanova, M. Zhang, H. Yang, G. I. Botchkina, L. R. Watkin, H. Wang, N. Abumrad, J. W. Eaton and K. J. Tracey, "Vagus nerve stimulation attenuates the systemic inflammatory response to endotoxin" *Nature* 405, 458-462, 2000.
- [56] H. Wang, M. Yu, M. Ochari, C. A. Amella, M. Tanovic, S. Susarla, J. H. Li, H. Wang, H. Yang, L. Ulloa, Y. Al-Abed, C. J. Czura and K. J. Tracey, "Nicotinic acetylcholine receptor alpha7 subunit is an essential regulator of inflammation" *Nature* 421, 384-388, 2003.
- [57] G. Vida, G. Pena, E. A. Deitch and L. Ulloa, "Alpha7-cholinergic receptor mediates vagal induction of splenic norepinephrine" *J. Immunol.* 186, 4340-4346, 2014.
- [58] D. Martelli, M. J. McKinley and R. M. McAllen, "The cholinergic anti-inflammatory pathway: A critical review" *Auton. Neurosci-Basic* 182, 65-69, 2014.
- [59] M. Bencherif, P. M. Lippiello, R. Lucas and M. B. Marrero, "Alpha7 nicotinic receptors as novel therapeutic targets for inflammation-based diseases" *Cell. Mol. Life Sci.*, 68, 931-949, 2011.
- [60] W. J. de Jong and L. Ulloa, "The alpha7 nicotinic acetylcholine receptor as a pharmacological target for inflammation" *Br. J. Pharmacol.* 151, 915-929, 2007.
- [61] C. A. Baez-Pagán, M. Delgado-Vélez and J. A. Lasalde-Dominicci, "Activation of the Macrophage $\alpha 7$ Nicotinic Acetylcholine Receptor and Control of Inflammation" *J. Neuroimmune Pharmacol.* 10, 3, 468-476, 2015.

- [62] W. de Jonge, E. P. van der Zanden, F. O. The, M. F. Bijlsma, D. J. van Westerloo, R. J. Bennink, H. Berthoud, S. Uematsu, S. Akira, R. M. van den Wijngaard and G. E. Boeckxstaens, "Stimulation of the vagus nerve attenuates macrophage activation by activating the Jak2-STAT3 signaling pathway" *Nat. Immunol.* 6, 8, 844-851, 2005.
- [63] K. Tsoyi, H. J. Jang, J. W. Kim, H. K. Chang, Y. S. Lee, H. Pae, H. J. Kim, H. G. Seo, J. H. Lee, H. Chung and K. C. Chang, "Stimulation of Alpha7 Nicotinic Acetylcholine Receptor by Nicotine Attenuates Inflammatory Response in Macrophages and Improves Survival in Experimental Model of Sepsis Through Heme Oxygenase-1 Induction" *Antiox. Redox Signal.* 14, 11, 2057-2070, 2011.
- [64] J. Egea, I. Buendia, E. Parada, E. Navarro, R. León and M. G. Lopez, "Anti-inflammatory role of microglial alpha7 nAChRs and its role in neuroprotection" *Biochem. Pharmacol.* 97, 463-472, 2015.
- [65] N. A. Horenstein and R. L. Papke, "Anti-inflammatory Silent Agonists" *ACS Med. Chem. Lett.* 8, 989-991, 2017.
- [66] R. L. Papke, D. Bagdas, A. R. Kulkarni, T. Gould, S. D. AlSharari, G. A. Thakur and M. I. Damaj, "The analgesic-like properties of the alpha7 nAChR silent agonist NS6740 is associated with non-conducting conformations of the receptor" *Neuropharmacology* 91, 34-42, 2015.
- [67] M. Quadri, D. Bagdas, W. Toma, C. Stokes, N. A. Horenstein, M. I. Damaj and R. L. Papke, "The Antinociceptive and Anti-Inflammatory Properties of the $\alpha 7$ nAChR Weak Partial Agonist p-CF3 N,N-diethyl-N'-phenylpiperazine" *J. Pharmacol. Exp. Ther.* 367, 203-214, 2018.
- [68] L. Boulet, G. M. Gauvreau, D. W. Cockcroft, B. David, L. Vachon, Y. Cormier and P. M. O'Byrne, "Effects of ASM-024, a modulator of acetylcholine receptor function, on airway responsiveness and allergen-induced responses in patients with mild asthma" *Can. Respir. J.* 22, 4, 230-234, 2015.
- [69] D. A. Bagdas, J. L. Wilkerson, A. Kulkarni, W. Toma, S. AlSharari, Z. Gul, A. H. Lichtman, R. L. Papke, G. A. Thakur and M. I. Damaj, "The $\alpha 7$ nicotinic receptor dual allosteric agonist and positive allosteric modulator GAT107 reverses nociception in mouse models of inflammatory and neuropathic pain" *Br. J. Pharmacol.* 173, 2506-2520, 2016.
- [70] M. Quadri, R. L. Papke and N. A. Horenstein, "Dissection of N,N-diethyl-N'-phenylpiperazines as $\alpha 7$ nicotinic receptor silent agonists" *Bioorg. Med. Chem.* 24, 2, 286-293, 2016.
- [71] M. Quadri, C. Stokes, A. Gulsevin, A. C. Felts, K. A. Abboud, R. L. Papke and N. A. Horenstein, "Sulfonium as a Surrogate for Ammonium: A New $\alpha 7$ Nicotinic Acetylcholine Receptor Partial Agonist with Desensitizing Activity" *J. Med. Chem.* 60, 18, 7928-7934, 2017.

- [72] M. Quadri, C. Matera, A. Silnovic, M. Pismataro, N. A. Horenstein, C. Stokes, R. L. Papke and C. Dallanoce, "Identification of $\alpha 7$ Nicotinic Acetylcholine Receptor Silent Agonists Based on the Spirocyclic Quinuclidine- $\Delta 2$ -Isoxazoline Scaffold: Synthesis and Electrophysiological Evaluation" *ChemMedChem* 12, 1335-1348, 2017.
- [73] M. Quadri, A. Silnovic, C. Matera, N. A. Horenstein, C. Stokes, M. De Amici, R. L. Papke and C. Dallanoce, "Novel 5-(quinuclidin-3-ylmethyl)-1,2,4-oxadiazoles to investigate the activation of the $\alpha 7$ nicotinic acetylcholine receptor subtype: Synthesis and electrophysiological evaluation" *Eur. J. Med. Chem.* 160, 207-228, 2018.
- [74] C. A. Briggs, J. H. Grønlien, P. Curzon, D. B. Timmermann, H. Ween, K. Thorin-Hagene, P. Kerr, D. J. Anderson, J. Malysz, T. Dyhring, G. M. Olsen, D. Peters, W. H. Bunnelle and M. Gopalakrishnan, "Role of channel activation in cognitive enhancement mediated by $\alpha 7$ nicotinic acetylcholine receptors" *Br. J. Pharmacol.* 158, 1486-1494, 2009.
- [75] R. L. Papke and C. Stokes, "Working with OpusXpress: methods for high volume oocyte experiments" *Methods*, 51, 1, 121-133, 2010.
- [76] M. S. Thomsen and J. D. Mikkelsen, "The $\alpha 7$ nicotinic acetylcholine receptor ligands methyllycaconitine, NS6740 and GTS-21 reduce lipopolysaccharide-induced TNF- α release from microglia" *J. Neuroimmunol.* 251, 65-72, 2012.
- [77] M. V. Skok, "Editorial: To channel or not to channel? Functioning of nicotinic acetylcholine receptors in leukocytes" *J. Leuk. Biol.* 86, 1-3, 2009.
- [78] K. Chojnacka, R. L. Papke and N. A. Horenstein, "Synthesis and evaluation of a conditionally-silent agonist for the $\alpha 7$ nicotinic acetylcholine receptor" *Bioorg. Med. Chem. Lett.* 23, 4145-4149, 2013.
- [79] D. Peters, G. M. Olsen, E. O. Nielsen, T. D. Jorgensen and P. K. Ahring, "NOVEL DIAZABICYCLIC ARYL DERIVATIVES" Patent WO 2004/076453 A1, 2004.
- [80] T. F. Braish and D. E. Fox, "Synthesis of (S,S)- and (R,R)-2-Alkyl-2,5-diazabicyclo[2.2.1]heptanes" *J. Org. Chem.* 55, 1684-1687, 1990.
- [81] A. Giovannini, D. Savoia and A. Umanironchi, "Organometallic ring-opening reactions of N-acyl and N-alkoxycarbonyl lactams- synthesis of cyclic imines" *J. Org. Chem.* 54, 228-234, 1989.
- [82] R. L. Papke, "Estimation of both the potency and efficacy of $\alpha 7$ nAChR agonists from single-concentration response" *Life Sci.* 78, 2812-2819, 2006.
- [83] G. Schaftenaar and J. H. Noordik, "Molden: a pre- and post-processing program for molecular and electronic structures" *J. Comp. Aid. Mol. Design* 14, 123-134, 2000.

- [84] R. A. Friesner, R.B. Murphy, M. P. Repasky, L. L. Frye, J. R. Greenwood, T. A. Halgren, P. C. Sanschagrín and D. T. Mainz, "Extra Precision Glide: Docking and Scoring Incorporating a Model of Hydrophobic Enclosure for Protein-Ligand Complexes" *J. Med. Chem.* 6177-6196, 2006.
- [85] R. E. Hibbs, G. Sulzenbacher, J. Shi, T. T. Talley, S. Conrod, W. R. Kem, P. Taylor, P. Marchot and Y. Bourne, "Structural determinants for interaction of partial agonists with acetylcholine binding protein and neuronal $\alpha 7$ nicotinic acetylcholine receptor" *EMBO J.* 28, 3040-3051, 2009.